UNIVERSITY OF SOUTHAMPTON

FACULTY OF ENGINEERING, SCIENCE AND MATHMATICS

INSTITUTE OF SOUND AND VIBRATION RESEARCH

ACTIVE VIBRATION ISOLATION WITH A DISTRIBUTED PARAMETER ISOLATOR

by

Bo Yan

Thesis submitted for the degree of
Doctor of Philosophy

November 2007

UNIVERSITY OF SOUTHAMPTON

ABSTRACT

FACULTY OF ENGINEERING, SCIENCE AND MATHMATICS
INSTITUTE OF SOUND AND VIBRATION RESEARCH

DOCTOR OF PHILOSOPHY

Active Vibration Isolation with a Distributed Parameter Isolator

by Bo Yan

Conventional vibration isolators are usually assumed to be massless for the purpose of modelling. This simplification tends to overestimate the isolator performance because of neglecting the internal resonances (IRs) due to the distributed mass effects in the isolator, which is especially important for lightly damped metallic isolators. Previous research on the problem of IRs is not particularly comprehensive, because it does not clarify the characteristics of the distributed parameter isolator. Furthermore, with the development of active vibration isolation, there is a need to investigate the effects of isolator IRs on the control performance and stability for commonly used control strategies. Effective ways to attenuate these effects are also required.

This thesis concerns the active vibration isolation of a piece of delicate equipment mounted on a distributed parameter isolator, which is modelled as different idealised configurations under various types of deformation. The model is first developed to determine the effects of IRs on a single-degree-of-freedom system with a distributed parameter isolator. This analysis is then extended to include the resonance behaviour of the supporting structure. Simple expressions are derived which describe the behaviour of various types of distributed parameter isolator. The parameters which control the isolator performance at various frequencies are clarified theoretically and experimentally. The effects of IRs on control performance and stability of several control strategies are determined and compared. Absolute Velocity Feedback (AVF) control is shown to be the optimal solution to minimise the mean square velocity of the equipment mass supported by a distributed parameter isolator. A stability condition for an AVF control system containing a distributed parameter isolator is proposed. Based on this condition, different approaches to stabilize such a control system are presented. Experimental work is carried out to validate the theoretical results.

Based on the improved knowledge of the characteristics of IRs in the distributed parameter isolator, different approaches which can suppress the IRs are proposed. AVF control with more damping in the isolator is demonstrated to be effective in attenuating the IRs theoretically and experimentally. Absolute velocity plus acceleration feedback control and AVF control on a fraction of the isolator length are also shown theoretically to be effective ways to attenuate the IRs and improve the isolation performance over a broad range of frequencies.

Acknowledgements

I would like to express my most sincere gratitude to my supervisors, Prof. Mike Brennan, Prof. Steve Elliott and Dr. Neil Ferguson, not only for their numerous guidance, constant support and kind encouragement throughout this research, but also for their precious advice which is invaluable for my future development.

Many constructive suggestions from Prof. Paolo Gardonio and Prof. Brian Mace to improve the quality of this work are gratefully acknowledged.

Many thanks also go to Mrs. Maureen Mew, Miss Anne-Marie McDonnell, Miss Joanne Hazell and other ISVR administrative stuff for their kind assistance and care during my study; to the workshop technicians for their effective assistance in my experimental work; to my friends and colleagues in the ISVR for their constant support and generous friendship; and to those I cannot all mention here, whose kindness and help makes my life in the UK more enjoyable.

Finally, but most importantly, my most heartfelt gratitude are reserved for my parents, my wife and my brother, for their constant and unconditional love, support and encouragement.

Contents

List of Figures

List of Tables

Nomenclature

Abbreviations

APF	Acceleration-Position Feedback
AVF	Absolute Velocity Feedback
IFF	Integral Force Feedback
IR	Internal Resonance
LPF	Low-Pass Filter
PPF	Positive Position Feedback
RVF	Relative Velocity Feedback
SDOF	Single-degree-of-freedom

Symbols

$\mathbf{A}$, $\mathbf{D}$	Coefficient matrix
A, B, U, V	Complex wave amplitude
C	Capacitor
D	Mean diameter of the coil of a helical spring
$D(j\omega)$	Primary disturbance
E, E^*	Young's modulus and complex Young's modulus
F	Force
$F_s(j\omega)$	Secondary actuator force
G, G^*	Shear modulus and complex shear modulus
$G(j\omega)$	Plant frequency response function
$G(j\omega)H(j\omega)$	Open-loop frequency response function
$G'(j\omega)$	Plant frequency response function from actuator force to absolute equipment velocity for the stabilized system
G_{lag}	Frequency response function of a lag compensator
G_{lead}	Frequency response function of a lead compensator

$H(j\omega)$	Frequency response function of a feedback controller
$H_{\mathrm{APF}}(j\omega)$	Frequency response function of the APF controller
$H_{\mathrm{IFF}}(j\omega)$	Frequency response function of the IFF controller
$H_{\mathrm{LPF}}(j\omega)$	Frequency response function of a first order low-pass filter
$H_{\mathrm{PPF}}(j\omega)$	Frequency response function of the PPF controller
I	Second moment of area
$\mathbf{J}$	Quadratic performance index
J_e	Polar moment of inertia of the equipment
J_s	Polar second moment of area of the isolator
K_B	Static bending stiffness
K_b, K_b^*	Stiffness and complex stiffness of the base
K_g	Gain margin
K_j	Modal stiffness of the j^{th} mode
K_L	Static longitudinal stiffness
K_S	Static shear stiffness
K_s	Static stiffness of a helical spring
K_T	Static torsional stiffness
L	Length
ΔL	Deflection of a helical spring
M_j	Modal mass of the j^{th} mode
N	Number of total coils of a helical spring
$\mathbf{P}$	Positive-definite real symmetric matrix
P_{f_a}	Time averaged power generated by the active control force
$\mathbf{Q}$	Positive-definite or positive-semidefinite real symmetric matrix
Q_b	Internal force applied to the base from the isolator
Q_e	Internal force or moment applied to the equipment from the isolator
Q_{x1}, Q_{x2}	Internal force applied to one end of the upper part of the isolator
Q_{y1} , Q_{y2}	Internal force applied to one end of the lower part of the isolator
Q_1, Q_2	Internal force or moment applied to one end of the isolator
$\mathbf{R}$	Positive-definite real symmetric matrix

R_1, R_2	Resistor
S	Cross-sectional area
S_b	Power spectral densities of the base disturbance
S_e	Power spectral densities of the equipment response
T	Transmissibility
T_a	Force transmissibility
T_F	Torsion moment
T_1	Coefficient of a lead compensator
T_2	Coefficient of a lag compensator
$\lvert T\rvert_{\text{massless}}$	Modulus of the transmissibility for the massless isolator
$\lvert T\rvert_{\max}$	Maximum modulus of the transmissibility
$\lvert T\rvert_{\min}$	Minimum modulus of the transmissibility
U_F	Shear force strain energy
U_T	Torsion strain energy
U_{total}	Total strain energy
$W(j\omega)$	Response of the system
Y_{bb}	Input mobility of the base when coupled to the rest of the system
Y_{eb}	Transfer mobility from the force on the base to the equipment velocity when the system is coupled
$Y_{eb}^{'}$	Transfer mobility from the force on the base to the equipment velocity when the stabilized system is coupled
Y_{ee}	Input mobility of the equipment when coupled to the rest of the system
$Y_{ee}^{'}$	Input mobility of the equipment when coupled to the rest of the stabilized system
Y_{er}	Transfer mobility from the force applied to the point *r* to the equipment velocity when the system is coupled
Y_{rr}	Point mobility from the force applied to the point *r* to the velocity at point *r* when the system is coupled
Y_{rb}	Transfer mobility from the force applied to the base to the velocity at point *r* when the system is coupled

Y_{ts}	Mobility from the excitation point *s* to the response point *t* in a multi-degree-of freedom system
Z_a	Total impedance of the additional SDOF system
$\mathbf{Z_B}$	Impedance matrix of a finite sliding-free Euler-Bernoulli beam under lateral vibration
Z_b	Impedance of the base
Z_e	Impedance of the equipment
$\mathbf{Z_I}$	Impedance matrix of a distributed parameter isolator
Z_i	Impedance of the massless isolator
Z_{ia}	Impedance of the combined suspension of the additional SDOF system
$\mathbf{Z_L}$	Impedance matrix of a finite rod under longitudinal vibration
Z_{ma}	Impedance of the mass in the additional SDOF system
$\mathbf{Z_S}$	Impedance matrix of a finite shear beam under lateral vibration
$\mathbf{Z_T}$	Impedance matrix of a finite rod under torsional vibration
$\mathbf{Z_x}$	Impedance matrix of the upper part of the isolator
$\mathbf{Z_y}$	Impedance matrix of the lower part of the isolator
Z_t, Z_{te}, Z_{tb}	Total impedance
Z_{x11}, Z_{x22}	Point impedance of the upper part of the isolator
Z_{x12}, Z_{x21}	Transfer impedance of the upper part of the isolator
Z_{y11}, Z_{y22}	Point impedance of the lower part of the isolator
Z_{y12}, Z_{y21}	Transfer impedance of the lower part of the isolator
Z_{11}, Z_{22}	Point impedance of the isolator
Z_{12}, Z_{21}	Transfer impedance of the isolator
$\mathbf{b}$, $\mathbf{d}$	Coefficient vector
c	Damping coefficient
c_a	Damping coefficient of an additional SDOF system
c_{eq}	Equivalent damping coefficient
c_i	Complex wave speed in the distributed parameter isolator
c_l	Complex wave speed for the finite rod undergoing longitudinal vibration

c_s	Complex wave speed for the finite rod undergoing torsional vibration and the shear beam undergoing lateral vibration
d	Wire diameter of the coil of a helical spring
e_i	Input of an electrical circuit for a lead compensator
e_o	Output of an electrical circuit for a lead compensator
f	Primary force applied to the base
f_a, f_{a1}, f_{a2}	Active control force
$f_a^{'}$	Force transmitted to the base through the additional SDOF system
f_B, f_{B1}, f_{B2}	Blocked force
f_b	External force applied to the base
f_e	External force applied to the equipment
f_T	Transmitted force
f_1	Corner frequency of the frequency response function $1+j\omega\lambda$ in Hz
f_2	Corner frequency of a first order low-pass filter in Hz
h, h_1, h_2, g	Constant gain
$h_{\max}$	Maximum control gain
k^*	Complex wavenumber
k_a	Stiffness of an additional SDOF system
k_b, k_b^*	Bending wavenumber and complex bending wavenumber
k_l, k_l^*	Longitudinal wavenumber and complex longitudinal wavenumber
k_s, k_s^*	Shear wavenumber and complex shear wavenumber
m	Mass
m_a	Mass of an additional SDOF system
m_b	Mass of the base
m_e	Mass of the equipment
m_i	Mass of the isolator
m_s	Mass of a helical spring
n	Number of active coils of a helical spring
q	Weighting on the mean square velocity of the equipment mass
r	Weighting on the mean square control effort applied

$u(L)$	Displacement or angle at one end of the isolator
$\dot{u}(L)$	Velocity or angular velocity at one end of the isolator
$u(x,t)$	Displacement or angle of an element along the isolator
$u(0)$	Displacement or angle at one end of the isolator
$\dot{u}(0)$	Velocity or angular velocity at one end of the isolator
u_b	Displacement of the base
$\dot{u}_b$	Velocity of the base
u_e	Displacement of the equipment
u_e/δ_{st}	Amplitude ratio
$(u_e/\delta_{st})_{massless}$	Modulus of the amplitude ratio for the massless isolator
$\lvert u_e/\delta_{st}\rvert_{\max}$	Maximum modulus of the amplitude ratio
$\lvert u_e/\delta_{st}\rvert_{\min}$	Minimum modulus of the amplitude ratio
$\dot{u}_e$	Velocity of the equipment
$\overline{\dot{u}_e^2}$	Mean square velocity of the equipment
$\ddot{u}_e$	Acceleration of the equipment
u_l	Displacement of the middle mass of the mass-spring-mass-spring-mass system
$\ddot{u}_l$	Acceleration of the middle mass of the mass-spring-mass-spring-mass system
$\dot{u}_r$	Velocity of the point r along the isolator where the active force applied
$\mathbf{x}$, $\dot{\mathbf{x}}$	State vector
x	Length of the upper part of the isolator
$\mathbf{y}$	Disturbance vector
y	Length of the lower part of the isolator
Ω, Ω_a, Ω_j	Frequency ratio
Γ_b	Ratio of the base resonance frequency to the equipment resonance frequency
Γ_f	Ratio of the corner frequency of the low-pass filter to the system fundamental resonance frequency
α	Coefficient of a lead compensator

β	Coefficient of a lag compensator
δ_{st}	Static deflection of the base
ε_F	Strain due to the shear force
ε_T	Strain due to the torsion
ϕ, φ	Phase angle (degree)
$\phi_b^{(a)}$	Modal amplitude evaluated at the base at the natural frequency of the additional SDOF system
$\phi_b^{(j)}$	j^{th} modal amplitude evaluated at the base
$\phi_e^{(a)}$	Modal amplitude evaluated at the equipment at the natural frequency of the additional SDOF system
$\phi_e^{(j)}$	j^{th} modal amplitude evaluated at the equipment
$\phi_r^{(j)}$	j^{th} modal amplitude evaluated at the control point *r*
$\phi_s^{(j)}$	j^{th} modal amplitude evaluated at the excitation point *s*;
$\phi_t^{(j)}$	j^{th} modal amplitude evaluated at the response point *t*
$\varphi_{\max}$	Maximum phase lead or phases lag
γ, γ^*	Real coefficient and complex coefficient
γ_g	Phase margin (degree)
η_b	Loss factor in the base
η_i	Loss factor in a distributed parameter isolator
η_l	Loss factor in a finite rod under longitudinal vibration
η_s	Loss factor in a finite rod under torsional vibration
κ	Longitudinal, torsional or shear rigidity
λ, λ'	Real coefficient in the absolute velocity plus acceleration feedback controller
μ_b	Ratio of the mass of the base to the mass of the equipment
μ_i	Ratio of the mass or the rotational inertia of the isolator to the mass or the rotational inertia of the equipment
μ_k	Ratio of static stiffness of the isolator to the stiffness of the base
μ_s	Ratio of the mass of a helical spring to the mass of the equipment
θ_{low}, θ_1, θ_2	Phase angle (degree)

ρ	Density
τ_F	Stress due to the shear force
τ_T	Stress due to the torsion moment
ω	Frequency (rad/s)
ω_a	Natural frequency of the additional SDOF system
ω_b	Natural frequency of the base
ω_c	Frequency where the maximum phases lead or phase lag occurs
ω_e	Natural frequency of the equipment
ω_f	Corner frequency of the filter
ω_l	Longitudinal internal resonance frequencies in a fixed-fixed finite rod
ω_{low}, ω_1, ω_2	Frequency (rad/s)
ω_j	Natural frequency of the j^{th} mode
ω_s	Longitudinal internal resonance frequencies in a helical spring
ω_x	Longitudinal internal resonance frequencies in the upper part of the isolator
ω_y	Longitudinal internal resonance frequencies in the lower part of the isolator
ξ, $\dot{\xi}$, $\ddot{\xi}$	Response of the filter
ζ	Viscous damping ratio
ζ_a, ζ_{a1}, ζ_{a2}	Active damping ratio
ζ_f	Damping ratio of the filter
ζ_j	Modal damping ratio of the j^{th} mode
ζ_s	Damping ratio of the additional SDOF system

Chapter 1

Introduction

1.1 Background

Vibration is a physical phenomenon of oscillation of objects with respect to a equilibrium position [1]. Although in some cases vibration can be useful and desirable (e.g. ultrasonic vibrations, vibration conveyers, impactors and music), in most cases it is detrimental and undesirable. It can cause fatigue, discomfort, noise, etc. Excessive vibration amplitude can, for example, lead to damage of mechanical systems or even destruction of buildings (e.g. the collapse of Tacoma Narrows bridge due to wind-induced vibration). Vibration due to the engine and from uneven road may cause discomfort to passengers in vehicles. Structural vibration (e.g. surface vibration) can be transmitted to surfaces that radiate noise to the surrounding environment, which is referred to as structure-borne noise. These potentially detrimental effects motivate engineers to find approaches to control vibration levels.

1.1.1 Vibration control

Vibration control measures can be classified as follows: passive vibration control, semi-active vibration control and active vibration control.

Passive vibration control involves the modification of the stiffness, mass and damping of a vibrating system to make the system less responsive to its vibratory environment [2]. The modification may take the form of basic structural changes or the addition of passive elements which requires no external assistance apart from their immediate passive neighbours or structural components that interact with them. In general, passive vibration control involves the use of reactive or resistive devices that either load the transmission path of the disturbing vibration or absorb vibrational energy [3]. Passive vibration control is usually simple to implement, reliable and cost efficient, but its successful application requires a thorough understanding of the vibration problem in hand. It often has limited capability to control the structural response. Also it has limitations such as lack of versatility, and potentially large size and weight. There are significant limitations in structural applications where broadband disturbances of highly uncertain nature are encountered [3-5].

Semi-active vibration control can be broadly defined as a passive vibration control measure in which the systems mechanical properties, such as stiffness and damping, can be adjusted in real time by the application of a control signal [3, 6]. Adaptive-passive vibration control can be categorized as semi-active vibration control. In an adaptive-passive system, the properties are changed relatively slowly, but in a semi-active system, the properties are changed within a cycle of vibration [7]. Although semi-active devices behave in a strongly nonlinear way, they are inherently passive and can not destabilize the system [8]. Semi-active vibration control strategies can maintain the reliability of passive devices using a small amount of energy to tune the system, yet provide versatility, adaptability and better performance at high frequencies [3, 9]. Its main disadvantage is its inherent nonlinearity and complicated engineering design.

Active vibration control augments the system with actuators, sensors and some form of electronic controller together with signal conditioning devices to achieve the modification of the characteristics of the vibrating system [6, 10]. In contrast to passive vibration control, active vibration control systems do require external energy to drive

active devices continuously. Active vibration control can provide superior performance over a wide frequency range and has the advantage of reducing the volume and weight of the structure, although its practical applications are limited due to the cost, stability and energy consumption [6, 11]. The active vibration system is usually integrated with a passive approach to form a hybrid vibration control, intended to improve the reliability and reduce the amount of external power necessary to achieve control performance.

1.1.2 Vibration isolation

A generic vibration control problem can be separated into three components: the source, the transmission path and the receiver as shown in Figure 1.1 [1, 12]. There are three approaches to control vibration levels. Firstly, it is preferable to reduce the vibrational excitation at source, but this is often impractical because of technical or economic reasons. Secondly, the vibration levels can be controlled by modifying the dynamic characteristics of the receiver to reduce the ability of the structure to respond to the input energy, which can be achieved by localised additions, i.e. absorbers and neutralisers, addition of damping or structural modification. Finally, the vibration levels can be controlled by isolating the receiver from the vibrating source through the transmission path. The last approach is called vibration isolation, which is the dynamic decoupling of the receiver and the source. It is usually achieved by placing a resilient element in the transmission path [12]. Such resilient interconnections constitute the vibration isolators or “anti-vibration mounts”. For a given source and receiver, an isolator can reduce the vibrations of the receiver to acceptable levels [13].

In practice, there are two common situations for vibration isolation: a) isolation of a vibrating machine from its surroundings and b) isolation of a delicate piece of equipment from a vibrating host structure [12]. It is the second from of vibration isolation which is concentrated on in the thesis. One of the most commonly used performance measures of an isolator is the transmissibility. The transmissibility is defined as the ratio of the amplitude of the transmitted motion or force at the receiver to

the amplitude of the input motion or force at the source [2]. Clearly, a good isolator results in a low receiver response for a given excitation and thus has a low transmissibility over the frequency range of interest.

In a similar way to the classification of vibration control, there are three classes of vibration isolation: passive vibration isolation, semi-active vibration isolation and active vibration isolation. The following sections briefly review the passive and active systems, as the former will be used as a benchmark for comparison in this study against the active configurations presented later.

1.1.2.1 Passive vibration isolation

The conventional passive vibration isolation system consists of compliant mounts positioned between the vibration source and the receiver to be protected. Passive isolation devices impart forces that are developed in response to the motion of the vibration source by means of their resilience and their energy dissipation properties [14]. These passive devices cannot supply energy to the system, so it cannot destabilize a conservative system [15]. However, simple passive vibration isolation systems have limited performance, which provides good isolation only at frequencies well above the resonance caused by the mass of the equipment and stiffness of the mount [12, 14].

A traditional passive vibration isolation model is the single-degree-of-freedom (SDOF) system model shown in Figure 1.2, which is normally adopted on mechanical vibrations [2, 16-19]. It consists of a rigid mass, representing the equipment, mounted on a rigid supporting structure through an isolator. For the purpose of modelling, the isolator is considered to be massless and modelled as an elastic spring in parallel with a viscous damper. The values of the spring stiffness and the damping coefficient are assumed to be constant in the frequency range of interest.

The magnitude of the transmissibility of this SDOF system is shown in Figure 1.3.

There is only one resonance peak corresponding to the equipment mass resonant on the stiffness of the isolator. At frequencies less than $\sqrt{2}$ times the resonance frequency, the transmissibility is equal to or greater than unity, i.e. the isolator is ineffective or amplifies the transmitted force or motion. At frequencies close to the resonance, the amplitude of the transmissibility is determined by the value of the damping ratio. The larger the damping ratio, the smaller the transmissibility. At frequencies greater than $\sqrt{2}$ times of the resonance frequency, the magnitude of the transmitted force or motion is smaller than the magnitude of the input excitation force or motion. This region is usually referred to as the isolation region. If the damping in the isolator is small, the transmissibility decreases at a rate of 40 dB per decade at frequencies well above the system resonance frequency [20, 21]. The viscous damping effect is reversed in the isolation region compared to that around the resonance frequency. Increasing damping in the isolator is detrimental to its performance in the isolation region. Thus there is a trade-off in the choice of damping for passive vibration isolation between good high frequency performance and good control at resonance.

Whilst viscous damping shown in Figure 1.2 receives the most attention in basic vibration texts, the massless isolator can also be modelled with a hysteretic damping, which leads to the concept of a complex stiffness [12]. If the massless isolator shown in Figure 1.2 is modelled as a spring with a complex stiffness, increasing damping in the isolator can reduce the transmissibility at the resonance frequency without degrading the high frequency isolation performance [19, 22]

Although the traditional passive vibration isolation model, in which the mass of isolator is assumed to be negligible, offers a wealth of information about vibration isolation and basic guidelines for isolator design, it is only valid at relatively low frequencies, for which the wavelength in the isolator is long compared to its dimension [12, 20]. At higher frequencies, realistic isolators, which have distributed mass, stiffness and damping, do not behave like the idealized massless models. Therefore the predictions

from this massless model are no longer accurate and may be misleading due to the internal mass effects of the isolator that are ignored.

1.1.2.2 Active vibration isolation

The compromise in the choice of damping for passive vibration isolation can be avoided by coupling an active system to a passive isolation system. The active control system reduces the overall response of a system by destructive interference using an external secondary vibration source [6]. With the development of computers fast enough to run control algorithms in real-time and more 'smart' materials such as piezo ceramics and shape memory alloys, active vibration isolation has become prevalent in the last few decades to achieve superior performance.

Active vibration isolation has been widely considered for applications to space structures [23-25], aircraft [26-28], automobiles [29-34], ships and marine machinery rafts [35, 36], buildings [37-39], etc. Spanos et al. [23] carried out vibration isolation experiments on a flexible structure utilizing a proof-mass shaker as the disturbance source and an active member as the isolator to investigate the active isolation of precision space structures from noisy space machinery. They concluded that an active stage can significantly reduce the transmissibility of a passive isolator both below and above its characteristic corner frequency. Vaillon et al. [24] investigated active isolation of sensitive payloads undergoing microvibration generated by some noisy equipment (such as reaction wheels or cryocoolers) and propagated though the primary structure of the satellite. Impressive isolation performance was achieved by incorporating active elements as isolators in all the struts. Schulz [26] investigated the application of active vibration isolation for compensation of vibrations generated by the rotor of a helicopter and transmitted to the cabin which is of great importance for rotorcraft design. Pearson et al. [27] identified that active vibration isolation in a helicopter can be applied at the main gear box to the fuselage interface. Elbeheiry and Karnopp [29] studied active suspension for a car. They investigated five types of suspension systems and concluded

the fully active suspension system provides much better body isolation than the other types. Karnopp [34] analyzed the benefits of road vehicle suspension systems incorporating generalized velocity feedback compared with conventional passive suspensions. A simple criterion is developed which indicates whether or not the introduction of active damping forces will result in significant benefit for pneumatic tired vehicles. Winberg et al. [35] showed that the sound level in the cabin of a ship could be minimized by actively isolating the hull from the engine. Loh and Ma [38] demonstrated that a combination of the active variable damper system with a passive base-isolation system is the most effective form of control of the building response when subjected to seismic excitation even under different site conditions. From this incomplete review, it is clear that there is a wide range of applications available for active vibration isolation.

However, stability is always an issue which may limit the performance and application of active vibration isolation. Although Balas [40] concluded that for collocated and dual actuators and sensors, a multi-input and multi-output system is unconditionally stable, such stability guarantees are not always valid in practice. The presence of real hardware and non-negligible dynamics of actuators and sensors, the unavoidable time delays, unmodelled dynamic characteristics, component failure and other uncertainties may destabilize active control systems. For example, Elliott et al. [41, 42] analyzed the stability and performance of an active vibration isolation system under absolute velocity feedback control, practically realised using either reactive or inertial actuators. It was concluded that such control systems are conditionally stable and thus the control performance was constrained due to the potential instability at high controller gains. Brennan et al. [43] and Ananthaganeshan [15] investigated both high frequency and low frequency dynamic behaviour of the system that limits controller gain. It was found that the phase advance due to the high-pass filters, which are necessary in vibration control systems to remove the DC signal in the feedback loop, may destabilize the control system, and thus is detrimental to the control performance. Due to the undesirable effects of the instability, great efforts should be expended on stability issues.

In active vibration isolation, the control forces generated by the external source are applied to the structure in a prescribed manner, which is defined as the control strategy. These strategies are applied to a physical system with the objectives of keeping the output (force, motion, etc) at a specified set of locations within the structure, below a specified level in the presence of any disturbances [3, 15]. There are two fundamental different strategies which have been used in the past for implementing active vibration isolation systems: feedforward and feedback control [44]. Feedforward control involves feeding a signal related to the disturbance input into the controller which then generates a control signal to drive actuators in order to cancel the disturbance. Feedforward control has generally been used for periodic disturbances, where a reference signal well correlated with the disturbance input is available to the controller [15, 44]. On the other hand, feedback control involves feeding a signal derived from the system response into the controller which then generates a control signal to drive actuators to attenuate the system response. Feedback control is generally used for random disturbances where a suitable reference signal is not available [44, 45]. Because base vibration typically has an unpredictable waveform with broadband random excitation spectra [46, 47], feedback control is widely used in isolating delicate equipment from base vibration.

In active vibration isolation, the output of the system can be fed into the controller directly to generate the control signal, which is simple and straightforward to implement [8, 48]. The output can be velocity, displacement, acceleration, force, etc. Benassi and Elliott [49, 50] investigated the design of inertial actuators with either local displacement feedback or local force feedback control and their use in active vibration isolation systems. Preumont [51] compares the acceleration feedback and force feedback implementation of the sky-hook damper when it is used to isolate a flexible structure from a disturbance source. Although active vibration isolation has been investigated by many researchers using displacement, acceleration or force feedback control, most of the work of this kind prefers velocity feedback control [40, 52, 53]. The advantage of using velocity feedback control is that the control system is proven to be unconditionally stable for collocated ideal force actuators and sensors, irrespective of

structural modelling errors [40, 54].

A traditional active vibration isolation model under output feedback control for a SDOF system is shown in Figure 1.4, which is widely used by researchers [6, 8, 55]. It is similar to its passive counterpart, and consists of a rigid mass, representing the equipment, mounted on a rigid supporting structure through an isolator. For the purpose of modelling, the isolator is also considered to be massless and modelled as an elastic spring in parallel with a viscous damper. The response of the equipment (velocity, acceleration, displacement, force, etc.) is fed into a controller to generate a control force in parallel with the passive isolator. If absolute velocity feedback control (AVF) is applied, i.e. the velocity of the equipment fed through a controller with a constant gain, the AVF control for such a system is equivalent as a 'sky-hook' damper [11]. The transmissibility for this SDOF active vibration isolation model is attenuated at the resonance frequency by the AVF control without compromising high-frequency performance. At frequencies well above the system resonance frequency, the transmissibility decreases at a rate of 40 dB per decade provided the passive damping in the isolator is small. The trade-off in passive vibration isolation between damping low-frequency resonances and achieving good high-frequency isolation is thus overcome by using active vibration isolation.

Similar to the conventional passive vibration isolation model, the traditional active vibration isolation model, in which the mass of isolator is also ignored, offers a good prediction tool and provides design guidelines at relatively low frequencies. However, at relatively high frequencies, the predictions based on this massless model may be wrong and misleading due to the internal mass effects of the isolator that are ignored.

1.1.3 Internal resonances in vibration isolators

1.1.3.1 Introduction

In practice, all realistic vibration isolators have distributed mass, stiffness and damping, which introduce dynamics into the isolators. These dynamics are associated with the resonance behaviour of the elastic motion of the isolator. Thus there are numerous frequencies associated with the natural modes, i.e. resonances, of the isolator. These resonances are referred to as internal resonances (IRs), or wave effects, in the isolators [13, 20, 21].

The IRs in the isolator are determined by various factors. It is found that the IRs in the isolator are dependent on the shape, material properties, dimensions, and boundary conditions of the isolators [20], as well as the type of deformation (e.g. compression, shear, flexure) [56]. Ungar and Dietrich [13] noted that the wave effects are more important in a heavier and larger isolator than those in a lighter and smaller isolator of equal static stiffness. It is also observed that the IRs occur in certain frequency ranges, when the wavelength of the exciting vibration in the isolator is comparable with the isolator's length [57]. Because the wavelength is inversely proportional to the frequency, the IRs in the isolator typically occur at high frequencies.

Given the trend in many segments of industry towards more complex equipment and machines, which are lighter and more compact, operating at greater speeds and higher power ratings, more problems associated with high frequency vibrations have become important. As a consequence, it is necessary to provide vibration isolation systems that will remain effective at high frequencies. However, due to the presence of the IRs in the isolator, the prediction based on the traditional massless isolator model, as discussed in last section for passive and active vibration isolation, holds true only at relatively low frequencies when wavelength in the isolator is long compared to its dimension. Therefore the traditional massless isolator model fails to perform satisfactorily at high

frequencies. A model with distributed mass, stiffness and damping is thus necessary to demonstrate the dynamic behaviour of many practical vibration isolators.

1.1.3.2 Distributed parameter isolator models

The idealized 'long-rod' model for helical springs and cylindrical rubber isolators, which have simple geometries and deformation behaviours, has been widely used by many researchers to investigate the wave effects in the isolator [13, 20, 21]. In this 'long-rod' theory, the isolator is modelled as a continuous elastic finite rod with internal damping, which has mass characterized by the material density. If such a distributed parameter isolator model is applied in the traditional SDOF passive vibration isolation system, the transmissibility of the system has the same peak at the system fundamental resonance as that for the massless isolator model. However, due to the effect of IRs at high frequencies, the transmissibility for the distributed parameter isolator does not decrease monotonically with frequency after the system resonance. It is found that the minimum of the transmissibility for the distributed parameter isolator decreases at about 20 dB per decade rather than 40 dB predicted from the massless isolator model [20]. This reveals that the traditional vibration isolation model, in which the isolator is assumed to be massless, significantly overestimates the isolation performance at high frequencies due to the effect of IRs.

Moreover, based on the idealized 'long-rod' model in which the lateral deformation of the isolator under the longitudinal excitation is ignored, it has been found that the amplitudes of the higher order IRs decrease rapidly with the frequency, i.e. the higher order IRs are effectively damped out by the isolator material damping [13, 20, 21]. A more complex model based on the Love's theory [58] that accounts for the effect of the lateral deformation in the isolator shows that the magnitude of the higher order IRs decreases even more rapidly [59]. Therefore, it can be concluded that only the first several IRs have the most practical significance in the isolator performance.

Other distributed parameter models for the realistic isolators have also been studied by previous researchers [56, 60]. Ungar [56] presented a simple SDOF model to show the IRs in leaf springs, which work on their flexural elasticity so that their IRs are associated with the resonant behavior in flexural vibration. The leaf spring was modeled as a continuous uniform beam rather than a rod. The damping effects were also included by considering a complex modulus of elasticity in the beam. It was also shown that the IRs are detrimental to the isolation performance in a certain frequency range. Ungar concluded that, given the same system frequency and mass ratio (isolator mass to equipment mass), vibration isolators that deform primarily in flexure may work better than isolators that deform primarily in compression or tension. The IRs in flexural springs have lower density with respect to frequency and occur at higher frequencies, which may not be excited in practice. Although the amplitude at an IR for a flexural spring is greater than that for a comparable compression spring, the IRs can be attenuated to a large extent since more damping can be incorporated more easily in practical flexural springs than in compression springs.

1.1.3.3 IRs in different types of isolators

Since the 1950s, many researchers have investigated the IR problem in both rubber isolators [59, 61, 62] and metal springs [63, 64] based on the idealized 'long-rod' model. Metal springs have a wide application in industries because of their attractive features, such as wide range of natural frequencies, more freedom in isolation design, and long service life. They can also be used under severe conditions, e.g. at temperatures far in excess of that permissible with non-metallic resilient materials, under strong corrosions of oil, dust water, ozone or atmospheric pressure, and in sizes to carry the heaviest loads [65]. However, compared to practical rubber isolators, in which the IRs can be more easily alleviated by the high internal damping of elastomer materials [21, 59], metal springs are more commonly involved in IR problems in practice due to the low damping of metal materials.

The IRs in metal springs generally occur at lower frequencies (a few hundred Hertz) with higher amplitude. Lee and Thompson [64] showed that the IRs lead to significant dynamic stiffening for helical springs above a certain frequency. This occurs at frequencies as low as about 40 Hz for an automotive suspension spring. Tomlinson [63] pointed out that it is especially necessary to consider the wave effects in the metal springs for high frequency isolation design. It was shown experimentally that the IRs in metal helical springs due to the longitudinal vibrations are more significant than those due to torsional vibrations, although these two different IRs tend to be equally important with the increasing spring size. Tomlinson [63] also shows analytically and experimentally that, in some situations, the first IR in metal springs appears below 200 Hz and has almost the same amplitude as the system resonance. As a consequence, the IR problem in metal springs has greater importance in practice than rubber isolators.

1.1.3.4 Control of IRs

Due to the significant effects of IRs in isolators on their high frequency isolation performance, much effort has been expended by previous researchers in the suppression of IRs. It was shown that the IRs can be simply attenuated by increasing the damping in the isolator [66]. A polymeric damping material can also be applied in parallel with the original isolator [63]. The polymeric material, which has a high loss factor, helps dissipate the energy at the IRs while the original isolator maintains the capability of supporting heavy components. However, it is not always practical to use high damping materials to suppress the IRs since typically such materials exhibit poor returnability and great creep, which degrade the load capacity of isolators and the performance of the system [57, 67]. Compound mounting systems, in which concentrated masses (referred to as intermediate masses) were inserted into isolators, have been used to achieve lower transmissibility at high frequencies [59]. However, the penalty is that the isolator performance at low frequencies is degraded. Snowdon [68] presented a method of using a dynamic vibration absorber, which efficiently attenuates the first IR peak in the isolator. Du et al [67] improved the high frequency isolation performance by applying a

dynamic vibration absorber (DVA) enhanced isolator. The modified isolator consisted of a cylindrical isolator made of rubberlike material with two embedded dynamic vibration absorbers. These were placed in the cylindrical cavity inside the isolator and each of them was connected to the isolator at the 'one-quarter-length' position through a thin plate that acted as an intermediate mass. However, introducing dynamic vibration absorbers into the isolator dramatically increases the complexity of the isolator and the resulting isolation system lacks versatility.

1.2 Motivation and objectives of the thesis

Among the various issues associated with vibration, the isolation of a delicate piece of equipment from a vibrating host base structure is a common situation in a number of engineering fields [12, 14, 41]. Due to design constraints and complex dynamics of the host structure, very little can often be done to reduce the vibration of the base [46]. Traditionally passive vibration isolation, consisting of vibration isolators made of compliant materials, is often used to provide dynamic decoupling between the delicate equipment and the host structure [2]. Base vibration typically has an unpredictable waveform and the vibration isolator has to deal with broadband excitation spectra [46, 47]. However, as presented in last section, conventional passive vibration isolation systems suffer from an inherent trade-off in the choice of damping between high frequency isolation, which requires a low level of damping, and isolation at the fundamental mounted resonance frequency, which requires a high level of damping [19, 22, 69, 70]. This inherent compromise can be overcome by applying active vibration isolation to a passive isolation system, which has been widely used to improve the performance of an isolator over a broad range of frequencies [6, 11, 71].

In conventional research methodologies for vibration isolation presented in last section, vibration isolators are usually considered as simple lumped parameter elements, which are assumed to be massless for the purpose of modelling. It has been shown that this simplification is only valid at relatively low frequencies when the wavelength in the isolator is long compared to its dimension [12]. At higher frequencies, realistic isolators, which have distributed mass, stiffness and damping, do not behave like the idealized

massless models. Therefore in an active/passive vibration isolation system there are several problems that should be addressed:

i. Firstly, the massless models for isolators tend to overestimate the isolator performance because the IRs due to the distributed mass in the isolator are neglected [13, 20]. The presence and importance of IRs in practical isolators has been identified by many researchers. The degradation in performance due to the IRs on vibration isolation is especially important for lightly damped metallic isolators, since the smaller the loss factor of the isolator the more significant are the resonances caused by the wave effects [20, 72, 73]. For a better description of the dynamic behaviour of vibration isolators at high frequencies, different distributed parameter models have been investigated and some factors, which affect the IRs in the isolator, have been presented in previous studies. However, previous research on the IR problem is not particularly comprehensive, because it does not clarify all the characteristics of vibration isolators. The parameters which control the isolator performance at various frequencies need to be clarified.
ii. Secondly, performance and stability are two crucial issues in active vibration isolation systems. Many electronic and mechanical factors introduce limitations on the control systems, which have been investigated in previous work, for example [15, 42, 43]. However, few investigations have been carried out to relate the way in which the IRs affect the performance and stability of the control systems for an isolator. Therefore, there is a need to quantify the effects of IRs on the control performance and stability for commonly used control strategies in active vibration isolation.
iii. Finally, due to the significant degradation effects of IRs on the isolator performance at relatively high frequencies, approaches need to be investigated to attenuate the IR peaks in order to improve the isolation performance over a broad range of frequencies. Although some methods to control IRs have been proposed in previous research [59, 63, 66-68], they all have inherent limitations either on the performance, or the practical complexity in design and implementation. Therefore, based on the understanding of isolator IRs, effective approaches are required to improve the isolation performance over a broad range of frequencies.

Motivated by the importance of IRs in vibration isolation and limitations in previous studies, there are four main objectives of this thesis:

i. To determine the effects of IRs in a realistic isolator on the passive isolation of a delicate piece of equipment from a vibrating host structure.
ii. To investigate theoretically and experimentally the effects of IRs on the hybrid active/passive isolation of a piece of equipment supported by a realistic isolator.
iii. To compare the control performance and analyze the stability of different control strategies in hybrid active/passive isolation of a piece of equipment supported by a realistic isolator.
iv. To investigate and implement an effective approach to suppress IRs in realistic isolators, and further improve the isolation performance over a broad range of frequencies.

1.3 Contributions of the thesis

The three main contributions of this thesis are as follows:

i. Simple expressions which describe the behaviour for various types of distributed parameter models for isolators have been derived. The parameters which control the isolator performance at various frequencies have been clarified.
ii. The effects of IRs on the control performance and stability of several control strategies have been determined. A stability condition for an absolute velocity feedback (AVF) control system has been identified. Based on this condition, ways in which an AVF control system can be stabilized have been presented.
iii. Different strategies to suppress IRs and improve the isolation performance of realistic isolators over a broad range of frequencies have been proposed.

1.4 Overview of the thesis

This study is concerned with the active vibration isolation of a piece of delicate equipment supported by a distributed parameter isolator. The structure of the thesis is organized as three parts. The first part (Chapter 1 and 2) reviews the previous research and introduces methodologies used in this study. The second part (Chapter 3, 4 and 5) investigates the characteristics of various types of distributed parameter isolator, and the effects of IRs in the isolator on the control performance and stability for several control strategies. The third part (Chapter 6 and 7) investigates strategies to attenuate IRs to improve the isolation performance over a broad range of frequencies. The detailed overview of the thesis is as follows:

Chapter 1 introduced the background of the study on vibration control, vibration isolation and IR problem in vibration isolators. The motivations of the thesis were outlined based on the problems summarized. It was followed by the main contributions.

Chapter 2 introduces concepts and methodologies used in the thesis by reviewing and summarizing the previous research on vibration isolation systems containing a massless isolator.

Chapter 3 investigates theoretically and experimentally the characteristics of passive vibration isolation systems containing a distributed parameter isolator, which is modelled as different idealised configurations under various deformations. Simple expressions which describe the behaviour for various types of isolator are derived. The parameters which control the isolator performance at various frequencies are clarified.

Chapter 4 investigates and compares the control performance and stability of active vibration isolation systems containing a distributed parameter isolator under various control strategies theoretically. Such systems either are undergoing base motion or have a base structure, which is allowed to have its own resonances. Absolute Velocity

Feedback (AVF) control is shown to be the optimal solution to minimise the mean square velocity of the equipment mass supported by a distributed parameter isolator

Chapter 5 examines approaches which can stabilize the active vibration isolation system containing a distributed parameter isolator on a flexible base under AVF control. These stabilizing approaches together with the control performance and stability of such a system are investigated experimentally on a four-spring active vibration isolation system.

Chapter 6 and 7 investigates theoretically and experimentally the strategies which can attenuate IRs in the isolator, in order to improve the isolation performance of a distributed parameter isolator over a broad range of frequencies, respectively.

Chapter 8 summarizes the overall conclusions, along with suggestions for future work.

Figure 1.1 *Schematic diagram of a general vibration control problem.*

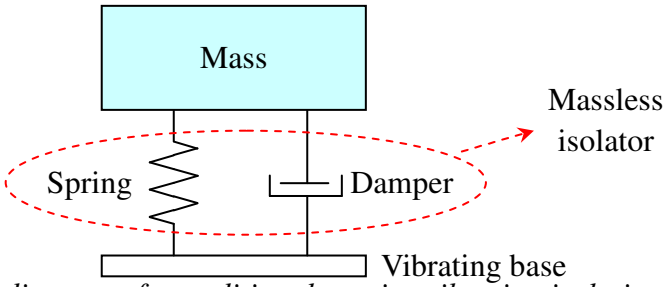

Figure 1.2 *Schematic diagram of a traditional passive vibration isolation model.*

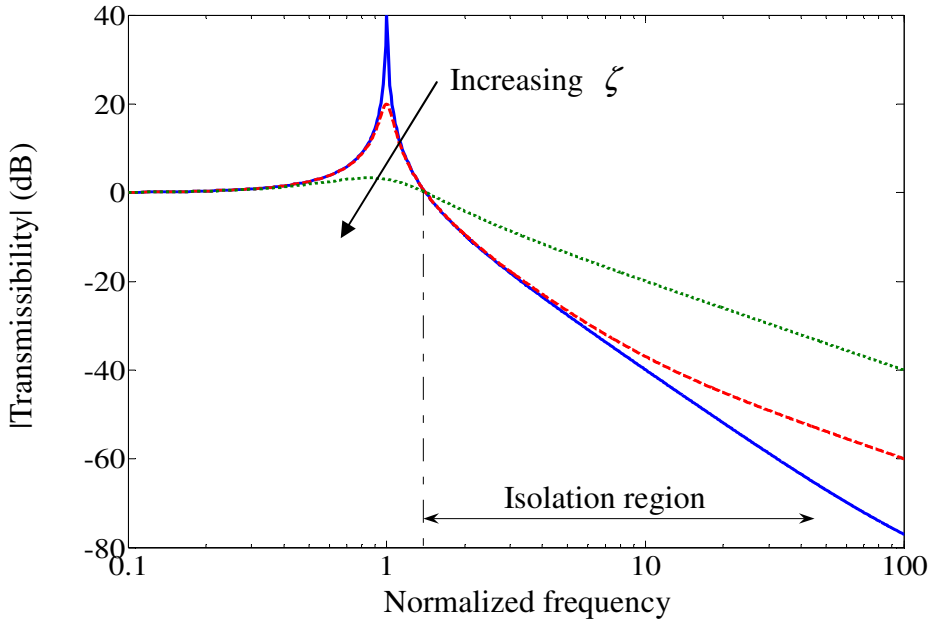

Figure 1.3 *Transmissibility of the traditional SDOF passive isolation model with different damping in the isolator.*

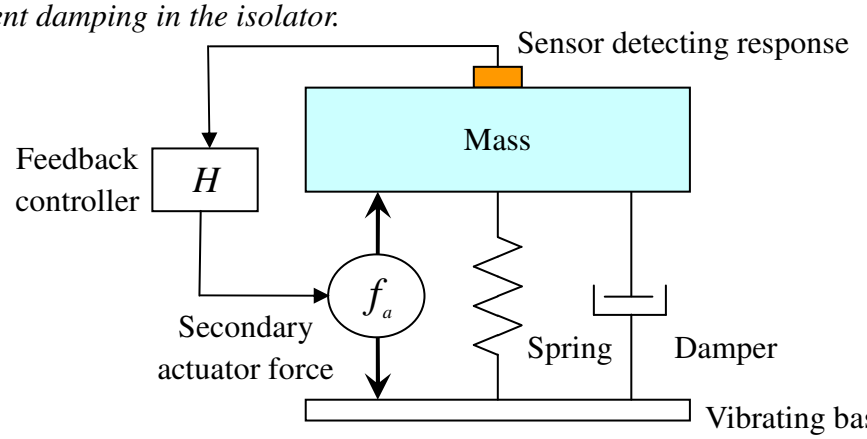

Figure 1.4 *Schematic diagram of a traditional active vibration isolation model.*

Chapter 2

Review of Active Vibration Isolation with a Massless Isolator

2.1 Introduction

Vibration isolation systems containing a massless isolator have been discussed in many books and papers, for example [2, 16, 18, 19]. In these studies, the massless isolator is usually modelled as a parallel combination of an elastic spring and a viscous damper. The dynamics of such systems has been extensively studied and analyzed by many researchers. The mobility and impedance approach is one of widely used methods for this analysis [41, 42]. To overcome the compromise in the choice of damping in passive vibration isolation, active components have been incorporated into passive systems to form active vibration isolators. The performance and stability of such active vibration isolation systems containing a massless isolator under different control strategies has been reported extensively in the literature.

The aim of this chapter is to introduce the concepts and methodologies used in this thesis by reviewing and summarizing the previous research on vibration isolation systems containing a massless isolator. The dynamics of a passive vibration isolation system containing such an isolator is first discussed. Then, concepts of single channel

feedback control and the Nyquist stability criteria are introduced. This is followed by an investigation and comparison of the performance and stability of different active control strategies, based on the massless isolator model.

2.2 Passive vibration isolation with a massless isolator

Figure 2.1 depicts a piece of equipment, represented by its impedance Z_e, mounted on a massless isolator undergoing base motion. The isolator is modelled as an elastic spring with stiffness *k* in parallel with a viscous damper with damping coefficient *c*. The dynamics of such a system are described in frequency domain by [52]

$$\left(Z_e + Z_i\right)\dot{u}_e - Z_i\dot{u}_b = 0 \tag{2.1}$$

where $\dot{u}_e$ and $\dot{u}_b$ are the velocities of the equipment and the base respectively, and $Z_i = k/j\omega + c$ is the impedance of the massless isolator. Therefore, the transmissibility of the system is given by

$$T = \frac{\dot{u}_e}{\dot{u}_b} = \frac{Z_i}{Z_e + Z_i} \tag{2.2}$$

If the equipment is modelled as a mass, i.e. $Z_e = j\omega m_e$, then the system becomes the traditional SDOF passive vibration isolation system discussed in Chapter 1. The transmissibility of such a system can be written in terms of non-dimensional parameters as [19]

$$T = \frac{1 + j2\zeta\Omega}{1 - \Omega^2 + j2\zeta\Omega} \tag{2.3}$$

where $\Omega = \omega/\omega_e$ is the ratio of the driving frequency ω to the system fundamental natural frequency $\omega_e = \sqrt{k/m_e}$ due to the interaction of the equipment mass and the stiffness of the isolator, and $\zeta = c/2\sqrt{km_e}$ is the viscous damping ratio. The magnitude of the transmissibility of this system is shown in Figure 1.3. Also the trade-off in the choice of damping between good high frequency performance and good control at resonance for passive vibration isolation has been discussed in Chapter 1.

2.3 Introduction to single channel feedback control

A single channel feedback control system with a control sensor and a secondary actuator is shown in Figure 2.2. Typically the response of the mechanical system is measured by a sensor, and then fed back through the controller defined by its frequency response $H(j\omega)$, to the secondary actuator [6]. Figure 2.3 depicts the equivalent block diagram for such a single channel feedback control system. The response of the system is given by

$$W(j\omega) = D(j\omega) + G(j\omega) F_s(j\omega) \tag{2.4}$$

where $G(j\omega)$ is defined as the 'plant response' of the mechanical system, which is the frequency response from the secondary actuator force $F_s(j\omega)$ in the absence of any primary disturbance (i.e. $D(j\omega) = 0$) to the sensor output $W(j\omega)$. The secondary actuator force is given by

$$F_s(j\omega) = -H(j\omega) W(j\omega) \tag{2.5}$$

The negative sign in the feedback controller accounts for the negative feedback. Combining equations (2.4) and (2.5), the closed-loop performance of such a feedback control system can be described by the ratio between the control system response, $W(j\omega)$ and the primary disturbance, $D(j\omega)$, which is given by [6, 74]

$$\frac{W(j\omega)}{D(j\omega)} = \frac{1}{1 + G(j\omega) H(j\omega)} \tag{2.6}$$

where the product of $G(j\omega) H(j\omega)$ is defined as the open-loop frequency response of the control system.

As discussed in many books on control [6, 48, 74-76], if at some frequency the open-loop frequency response $G(j\omega) H(j\omega)$ has little phase shift but simultaneously has a gain much greater than unity, so that

$$\left|1 + G(j\omega) H(j\omega)\right| >> 1 \tag{2.7}$$

Then one has

$$W(j\omega) << D(j\omega) \tag{2.8}$$

The response of the mechanical system is thus significantly reduced at this frequency. However, it may not be possible to ensure that the phase shift of the open-loop frequency response is always small. If the phase shift of the open-loop frequency response is 180º while its gain is unity at that frequency so that $1+G(j\omega)H(j\omega)=0$, then the response of the system becomes infinite, i.e. the control system becomes unstable. Therefore, the design of a practical feedback control system generally involves a compromise between a high open-loop gain for good performance and a low open-loop gain for stability [6].

The above discussion demonstrates that study of the open-loop frequency response of the system gives insight into the stability and performance of a feedback control system. The Nyquist stability criterion using the open-loop frequency response is therefore a powerful experimental tool to assess the characteristics of a control system. The Nyquist stability criterion states that a closed-loop control system is stable only if the polar plot of the open-loop frequency response (generally referred to as the Nyquist plot) does not enclose the unstable point (-1, 0j) [6, 76]. More practically, the Nyquist stability criterion provides not only the prediction for the absolute stability of a control system, but also its relative stability by looking at the proximity of the open-loop frequency response to the unstable point [6]. The proximity of the open-loop frequency response locus to the unstable point, which is generally represented in terms of gain margin and phase margin, can be used as a measure of the margin of stability [74]. If the phase shift of the open-loop frequency response is -180º at a frequency ω_1, the gain margin can be defined as the gain increase (in dB) necessary to cause instability and is given by [74]

$$K_g(\text{in dB}) = 20\log_{10}\left|\frac{1}{G(\omega_1)H(\omega_1)}\right| = -20\log_{10}\left|G(\omega_1)H(\omega_1)\right| \qquad (2.9)$$

If the magnitude of the open-loop frequency response is unity at a frequency ω_2, the phase margin can be defined as the amount of additional phase lag required to bring the system to the verge of instability, which is given by [74]

$$\gamma_g = 180^\circ + \phi(\omega_2) \qquad (2.10)$$

where $\phi(\omega_2)$ is the phase angle of the open-loop frequency response at ω_2.

2.4 Active vibration isolation with a massless isolator

In this section, active vibration isolation systems containing a massless isolator under various control strategies are reviewed and discussed. The control performance and stability for various control methods that can introduce active damping into the system are analyzed and compared, as well as acceleration feedback control, which can add mass to the system electronically. The optimal control is then discussed to find the best solution to isolate the equipment.

2.4.1 Absolute Velocity Feedback (AVF) control

AVF control applied to a vibration isolation system containing a massless isolator has been extensively investigated by many researchers [6, 11, 40-42, 46, 52, 53]. Figure 2.4(a) shows a base excited vibration isolation system containing a massless isolator under AVF control. An active control force f_a, which is in parallel with the isolator, reacts between the equipment and the base. The control force f_a is proportional to the velocity of the equipment $\dot{u}_e$, and fed back to the system through a feedback controller with a constant gain -*h*, so that

$$f_a = -h\dot{u}_e \tag{2.11}$$

2.4.1.1 Control performance

The relationship between the control force and the velocities of the equipment and the base for the active vibration isolation system in Figure 2.4(a) can be written as

$$(Z_e + Z_i)\dot{u}_e - Z_i\dot{u}_b = f_a \tag{2.12}$$

Substituting equation (2.11) into (2.12), the transmissibility of the system under AVF control is given by

$$T = \frac{Z_i}{Z_e + Z_i + h} \tag{2.13}$$

If the equipment is modelled as a mass, the transmissibility under AVF control can be written in terms of non-dimensional parameters as

$$T = \frac{1 + j2\zeta\Omega}{1 - \Omega^2 + j2(\zeta + \zeta_a)\Omega} \tag{2.14}$$

where $\zeta_a = h/2\sqrt{km_e}$ is the active damping ratio due to AVF control. It can be seen from the transmissibility in equation (2.14) that the AVF control adds a damping term to the denominator but leaves the numerator unchanged. The action of AVF control for this base excited system is thus the same as a skyhook damper [11]. Figure 2.4(b) shows the mechanical representation of the system under AVF control, which is equivalent to a viscous damper with damping coefficient *h* acting between the equipment and the inertial ground [11].

The transmissibility for the active vibration isolation system containing a massless isolator under AVF control is plotted in Figure 2.5, where the transmissibility of the system without control is also plotted for comparison. It can be seen that the transmissibility is attenuated at the resonance frequency by the AVF control without compromising the high frequency isolation performance. The trade-off in the choice of damping for passive vibration isolation is thus overcome by introducing active vibration isolation. Moreover, the higher the control gains, the better the isolation performance around the resonance frequency.

2.4.1.2 Stability analysis

The stability of the AVF control system has been discussed in several books and papers, for example [8, 41, 42]. Because the controller is a constant gain, the Nyquist analysis of the open-loop frequency response for AVF control can be simplified to the consideration of the plant response with unitary control gain (h=1). The plant response from the active force to the equipment velocity is given by

$$G = \left.\frac{\dot{u}_e}{f_a}\right|_{\dot{u}_b=0} = \frac{1}{Z_e + Z_i} \tag{2.15}$$

As discussed by Elliott et al. [41], the phase shift of Z_e is between -90º and 90º because it is an input impedance. The phase shift of Z_i is -90º if the isolator is dominated by its stiffness, reducing to 0º if it is dominated by its damping. Therefore

the overall phase shift of the plant response G is between -90º and 90º and is thus completely passive. Its Nyquist plot is then entirely on the right-hand side of the complex plane and the feedback system has an infinite gain margin and a phase margin of at least 90º. Based on the Nyquist stability criterion, the AVF control system containing a massless isolator undergoing base motion is unconditionally stable.

From another point of view, because the base motion is prescribed which is not affected by the active control force, the actuator and the sensor are thus collocated, so that such a system under AVF control is unconditionally stable [8, 40]. However, if the system is extended so that the base is not rigid but has its own resonance behaviour which will be affected by the active control force, the AVF control system becomes conditionally stable because the actuator and the sensor are no longer collocated. Under some conditions such an AVF control system on a flexible base will be unstable at high control gains [41].

2.4.2 Relative Velocity Feedback (RVF) control

Figure 2.6(a) shows a base excited vibration isolation system containing a massless isolator under RVF control. An active control force f_a, which is in parallel with the isolator, reacts between the equipment and the base. The control force f_a here is proportional to the difference between the velocity of the equipment $\dot{u}_e$ and the velocity of the base $\dot{u}_b$, and fed back to the system through a feedback controller with a constant gain $-h$, so that

$$f_a = -h\left(\dot{u}_e - \dot{u}_b\right) \tag{2.16}$$

2.4.2.1 Control performance

The relationship between the control force and the velocities of the equipment and the base for the active vibration isolation system under RVF control shown in Figure 2.6(a) is also given by equation (2.12). Substituting equation (2.16) into (2.12), the transmissibility of the system under RVF control is given by

$$T = \frac{Z_i + h}{Z_e + Z_i + h} \tag{2.17}$$

If the equipment is modelled as a mass, the transmissibility under RVF control can be written in terms of non-dimensional parameters as

$$T = \frac{1 + j2(\zeta + \zeta_a)\Omega}{1 - \Omega^2 + j2(\zeta + \zeta_a)\Omega} \tag{2.18}$$

It can be seen that a damping term is added to both the denominator and the numerator. The action of RVF control is thus the same as a passive viscous damper. Figure 2.6(b) shows the mechanical representation of the system under RVF control, which is equivalent to a viscous damper with damping coefficient h acting between the equipment and the base. Therefore, similar to the transmissibility for the passive vibration isolation system shown in Figure 1.3, the transmissibility for the system under RVF control is attenuated around the resonance frequency, while it is amplified at high frequencies above the resonance frequency due to RVF control. Thus, the same compromise in the choice of damping for passive vibration isolation also occurs in the system under RVF control.

2.4.2.2 Stability analysis

Because the controller is also a constant gain for RVF control, the plant response of the system can be used for the stability analysis. The plant response from the active force to the difference between the velocity of the equipment and the velocity of the base is also given by equation (2.15). Therefore the overall phase shift of the plant response is between -90º and 90º and is thus completely passive, so that the RVF control system containing a massless isolator undergoing base motion is unconditionally stable based on the Nyquist stability criterion. The unconditional stability of the RVF control system undergoing base motion can also be concluded due to the collocation of the actuator and sensor. Furthermore, even if the base is not rigid and has its own resonance behaviour, the RVF control system is still completely passive and thus unconditionally stable [72] because the actuator and the sensor remain collocated. The unconditional stability is the main advantage of RVF control compared to AVF control, although its control performance is worse than that of AVF control.

2.4.3 Integral Force Feedback (IFF) control

IFF control applied to a vibration isolation system containing a massless isolator has been presented in several books and papers, for example [8, 41, 50, 51]. Figure 2.7 shows a base excited vibration isolation system containing a massless isolator under IFF control. The control force f_a, which is in parallel with the isolator, reacts between the equipment and the base. The control force f_a is generated by feeding the transmitted force to the equipment through a controller with frequency response $H_{\text{IFF}}(j\omega)$ negatively, which is given by

$$H_{\text{IFF}}(j\omega) = \frac{h}{j\omega} \tag{2.19}$$

The transmitted force to the equipment f_T, which consists of the transmitted force from the isolator Q_e and the active force applied on the equipment f_a, generates the motion of the equipment and can be written as

$$f_T = Q_i + f_a = Z_e \dot{u}_e \tag{2.20}$$

The control force is thus given by

$$f_a = -H_{\text{IFF}}(j\omega) f_T = -\frac{h}{j\omega} Z_e \dot{u}_e \tag{2.21}$$

2.4.3.1 Control performance

The relationship between the control force and the velocities of the equipment and the base for the active vibration isolation system under IFF control shown in Figure 2.7 is also given by equation (2.12). Substituting equation (2.21) into (2.12), the transmissibility of the system under IFF control is given by

$$T = \frac{Z_i}{Z_e + Z_i + \frac{h}{j\omega} Z_e} \tag{2.22}$$

If the equipment is modelled as a mass, i.e. $Z_e = j\omega m_e$, the transmissibility under IFF control can be written as

$$T = \frac{Z_i}{Z_e + Z_i + h m_e} \tag{2.23}$$

Comparing equation (2.23) with equation (2.13) (the transmissibility of such a system under AVF control), the action of IFF control is also the same as a skyhook damper. The only difference is that the IFF control applied to a system containing a mass-like equipment is equivalent to a viscous damper with damping coefficient hm_e (rather than h for AVF control) acting between the equipment and the inertial ground.

2.4.3.2 Stability analysis

The stability of the IFF control system has been investigated by several researchers, for example [8, 41, 51]. Combining equations (2.15) and (2.20), the plant response from the active force to the transmitted force to the equipment is given by

$$G = \left.\frac{f_T}{f_a}\right|_{\dot{u}_b=0} = \frac{Z_e}{Z_e + Z_i} \tag{2.24}$$

Because the IFF controller is not a constant gain, the open-loop frequency response is used to analyze the stability, which is given by

$$GH_{\text{IFF}} = \frac{h}{j\omega}\frac{Z_e}{Z_e + Z_i} \tag{2.25}$$

The stability of the IFF control system can be investigated by examining the reciprocal of the open-loop frequency response, which is given by

$$\left(GH_{\text{IFF}}\right)^{-1} = \left(hZ_e\right)^{-1} j\omega\left(Z_e + Z_i\right) = \frac{1}{h} j\omega\left(1 + Z_e^{-1}Z_i\right) \tag{2.26}$$

Z_e^{-1} is passive since Z_e is an input impedance, so that Z_e^{-1} has a phase shift of between -90º and 90º. The phase shift of Z_i is -90º if the isolator is dominated by its stiffness, reducing to 0º if it is dominated by its damping. The phase shift of $1 + Z_e^{-1}Z_i$ can thus potentially vary between -180º and 90º. Therefore the overall phase shift of $\left(GH_{\text{IFF}}\right)^{-1}$ is between -90º and 180º. The phase limitations on the open-loop frequency response are thus between -180º and 90º. In the Nyquist plot of the open-loop frequency response, there is no loop on the left half of the complex plane crossing the negative real axis, and thus the IFF control system containing a massless isolator undergoing base motion is unconditionally stable based on the Nyquist stability criterion. However, such an IFF control system is not completely passive, and thus not robustly stable as an AVF

control system undergoing base motion. But if the equipment is rigid and has a mass-like impedance, i.e. $Z_e = j\omega m_e$, the open-loop frequency response can be reduced as $hm_e/(Z_e + Z_i)$, so that the overall phase shift of the open-loop frequency response is limited between -90º and 90º. The IFF control system is thus completely passive. The advantage of the IFF control system compared to AVF control is that it remains unconditionally stable for any combination of base and equipment dynamics [41], even if the base has its own resonance behaviour.

2.4.4 Positive Position Feedback (PPF) control

PPF control has been presented in several books and papers, for example [8, 77-80]. Figure 2.8 shows a base excited vibration isolation system containing a massless isolator under PPF control. The control force f_a, which is in parallel with the isolator, reacts between the equipment and the base. The control force f_a is generated by feeding the displacement of the equipment u_e through a controller with frequency response $H_{\mathrm{PPF}}(j\omega)$ in a positive sense. The PPF control is implemented using an auxiliary dynamic system, which is basically a second-order filter of the form [55, 77]

$$\ddot{\xi} + 2\zeta_f \omega_f \dot{\xi} + \omega_f^2 \xi = \omega_f^2 u_e \tag{2.27}$$

where u_e is the displacement of the equipment, and ξ, ω_f, ζ_f are the response, the natural frequency and the damping ratio of the filter respectively. The output from the filter is then multiplied by $g\omega_f^2$, where g is a constant gain, to give the secondary force f_a. If the signal is time harmonic, the filter output is given by

$$\xi = \frac{\omega_f^2}{\omega_f^2 + j2\zeta_f \omega_f \omega - \omega^2} u_e = \frac{1}{1 - \left(\omega/\omega_f\right)^2 + j2\zeta_f \, \omega/\omega_f} u_e \tag{2.28}$$

The control force is thus given by

$$f_a = g\omega_f^2 \xi = H_{\mathrm{PPF}}(j\omega) u_e = \frac{1}{j\omega} H_{\mathrm{PPF}}(j\omega) \dot{u}_e \tag{2.29}$$

where

$$H_{\mathrm{PPF}}(j\omega) = \frac{g\omega_f^2}{1-\left(\omega/\omega_f\right)^2 + j2\zeta_f\,\omega/\omega_f} \tag{2.30}$$

is the frequency response of the PPF controller which acts as a second order compensator.

Figure 2.9 shows the frequency response of the PPF controller. It can be seen that the PPF controller has -90º phase shift at its cut-off frequency with high magnitude, which is why the PPF control can act as an active damping for the specific frequency and needs fine-tuning [81]. Therefore, to attenuate a mode in the system, the cut-off frequency of the PPF controller should be closely matched to the mode. Furthermore, because the magnitude of the frequency response rolls off rapidly above the cut-off frequency, the PPF controller has less spillover to higher frequency modes. This inherent robustness to spillover to high frequency modes, i.e. insensitivity to the un-modelled high frequency dynamics, is the main advantage of PPF control [77]. However, the PPF controller may lead to spillover problem to lower frequency modes when the feedback gain is high.

2.4.4.1 Control performance

The relationship between the control force and the velocities of the equipment and the base for the active vibration isolation system under PPF control shown in Figure 2.8 is given by equation (2.12). Substituting equation (2.29) into (2.12), the transmissibility of the system under PPF control is given by

$$T = \frac{Z_i}{Z_e + Z_i - \dfrac{1}{j\omega}\dfrac{g\omega_f^2}{1-\left(\omega/\omega_f\right)^2 + j2\zeta_f\,\omega/\omega_f}} \tag{2.31}$$

If the equipment is modelled as a mass, i.e. $Z_e = j\omega m_e$, and the undamped natural frequency of the PPF controller ω_f is tuned to the system fundamental resonance frequency $\omega_e = \sqrt{k/m_e}$, the transmissibility of the system under PPF control can be written as

$$T = \frac{1 + j2\zeta\Omega}{1-\Omega^2 + j2\zeta\Omega - \dfrac{g}{m_e}\dfrac{1}{1-\Omega^2 + j2\zeta_f\Omega}} \tag{2.32}$$

At frequencies much lower than the system fundamental resonance frequency, i.e. $\Omega << 1$, and assuming the damping in the isolator is small, the transmissibility can be reduced to

$$T_{\Omega<<1} \approx \frac{1}{1-\frac{g}{m_e}} \tag{2.33}$$

It can be seen that PPF control adds a negative stiffness term $-g/m_e$ to the system, which may amplify the transmissibility of the system depending on the values of g and m_e. At the system fundamental resonance frequency, i.e. $\Omega = 1$, the transmissibility can be reduced to

$$T_{\Omega=1} \approx \frac{1+j2\zeta}{j\left(2\zeta + \frac{g}{m_e}\frac{1}{2\zeta_f}\right)} \tag{2.34}$$

Thus PPF control is equivalent to a skyhook damper with damping ratio $g/\left(2\zeta_f m_e\right)$ around the system fundamental resonance frequency, so that the resonance peak can be effectively attenuated. At high frequencies, well above the system fundamental resonance frequency, i.e. $\Omega >> 1$, the frequency response of the PPF controller rolls off rapidly, and thus the effect of PPF control is negligible.

Figure 2.10 shows the transmissibility for the active vibration isolation system containing a massless isolator under PPF control with various values for control gain g, where the transmissibility of the system without control is also plotted for comparison. It can be seen that the resonance peak is attenuated by PPF control without compromising the high frequency isolation performance, because the frequency response of the PPF controller rolls off very quickly at high frequencies. However, the transmissibility is amplified at frequencies lower than the resonance frequency due to the negative stiffness determined by the specific values of g and m_e.

2.4.4.2 Stability analysis

The equation of motion for the system shown in Figure 2.8 is given by

$$m_e\ddot{u}_e + c\left(\dot{u}_e - \dot{u}_b\right) + k\left(u_e - u_b\right) = f_a = g\omega_f^2\xi \tag{2.35}$$

It can be rearranged as

$$\ddot{u}_e + 2\zeta\omega_e\dot{u}_e + \omega_e^2 u_e - \frac{g\omega_f^2}{m_e}\xi = 2\zeta\omega_e\dot{u}_b + \omega_e^2 u_b \tag{2.36}$$

Combining equations (2.27) and (2.36) gives

$$\begin{bmatrix}\ddot{u}_e \\ \ddot{\xi}\end{bmatrix} + \begin{bmatrix}2\zeta\omega_e & 0 \\ 0 & 2\zeta_f\omega_f\end{bmatrix}\begin{bmatrix}\dot{u}_e \\ \dot{\xi}\end{bmatrix} + \begin{bmatrix}\omega_e^2 & -\dfrac{g\omega_f^2}{m_e} \\ -\omega_f^2 & \omega_f^2\end{bmatrix}\begin{bmatrix}u_e \\ \xi\end{bmatrix} = \begin{bmatrix}2\zeta\omega_e\dot{u}_b + \omega_e^2 u_b \\ 0\end{bmatrix} \tag{2.37}$$

To guarantee the stability of such a closed-loop system, the 'stiffness' matrix in equation (2.37) should be positive definite, that is the eigenvalues of this matrix are all positive [77]. Therefore, the stability condition is then given by

$$\frac{g}{m_e}\omega_f^2 < \omega_e^2 \tag{2.38}$$

In the earlier discussion, to control the system fundamental resonance mode, the natural frequency of the PPF controller ω_f was tuned to the system fundamental resonance frequency ω_e. So the stability condition given by equation (2.38) can be simplified so that the control gain g should be less than the mass of the equipment, i.e. $g < m_e$.

2.4.5 Acceleration-Position Feedback (APF) control

APF control was first introduced as an electrical dynamic vibration absorber by Kim et al. [82]. Figure 2.11 shows a base excited vibration isolation system containing a massless isolator under APF control. The control force f_a, which is in parallel with the isolator, reacts between the equipment and the base. The control force f_a is generated by feeding the acceleration of the equipment $\ddot{u}_e$ through a second order low-pass filter in a negative sense with frequency response $H_{\mathrm{APF}}(j\omega)$, which is given by

$$H_{\mathrm{APF}}(j\omega) = h\frac{2\zeta_f/\omega_f}{1-\left(\omega/\omega_f\right)^2 + j2\zeta_f\,\omega/\omega_f} \tag{2.39}$$

where ω_f and ζ_f are the natural frequency and the damping ratio of the filter respectively, and *h* is a constant control gain. The control force is then given by

$$f_a = -H_{\text{APF}}(j\omega)\ddot{u}_e = -h\frac{j2\zeta_f\,\omega/\omega_f}{1-(\omega/\omega_f)^2 + j2\zeta_f\,\omega/\omega_f}\dot{u}_e \tag{2.40}$$

It can be seen that, around the natural frequency of the APF controller, i.e. $\omega = \omega_f$, the control force can be reduced to equation (2.11), which is the active control force under AVF control. But at frequencies much lower or higher than its natural frequency, the active control force rolls off rapidly, i.e. the APF control is not sensitive to the dynamics in those frequency ranges. Therefore, the natural frequency of the APF controller should be closely matched to the mode that is required to be attenuated.

2.4.5.1 Control performance

The relationship between the control force and the velocities of the equipment and the base for the active vibration isolation system under APF control shown in Figure 2.11 is given by equation (2.12). Substituting equation (2.40) into (2.12), the transmissibility of the system under APF control is given by [82]

$$T = \frac{Z_i}{Z_e + Z_i + h\dfrac{j2\zeta_f\,\omega/\omega_f}{1-(\omega/\omega_f)^2 + j2\zeta_f\,\omega/\omega_f}} \tag{2.41}$$

It can be seen that, around the natural frequency of the APF controller, i.e. $\omega = \omega_f$, the transmissibility can be reduced to equation (2.13), which is the transmissibility of the system under AVF control, so that APF control is equivalent to a skyhook damper around its natural frequency. However, at frequencies much lower or higher than its natural frequency, the effects of APF control are negligible. If the equipment is modelled as a mass, i.e. $Z_e = j\omega m_e$, and the natural frequency of the APF controller ω_f is tuned to the system fundamental resonance frequency ω_e, the transmissibility of the system under APF control can be written as

$$T = \frac{1 + j2\zeta\Omega}{1-\Omega^2 + j2\zeta\Omega + j2\zeta_a\dfrac{j2\zeta_f\Omega}{1-\Omega^2 + j2\zeta_f\Omega}} \tag{2.42}$$

Figure 2.12 shows the transmissibility for the active vibration isolation system

containing a massless isolator under APF control with various values for active damping ratio ζ_a, where the transmissibility of the system without control is also plotted for comparison. It can be seen that the transmissibility is attenuated around the system fundamental resonance frequency with an increase in the active damping ratio due to APF control. However, the transmissibility close to the system fundamental resonance frequency is amplified due to APF control, since the APF controller is equivalent to a dynamic vibration absorber. While at frequencies much lower or higher than the system fundamental resonance frequency, the effects of APF control are negligible, because the active APF control force rolls off rapidly.

2.4.5.2 Stability analysis

From equation (2.15), the plant response from the active force to the acceleration of the equipment is given by

$$G = \left.\frac{\ddot{u}_e}{f_a}\right|_{\dot{u}_b=0} = \left.\frac{j\omega\dot{u}_e}{f_a}\right|_{\dot{u}_b=0} = \frac{j\omega}{Z_e + Z_i} \tag{2.43}$$

Because the APF controller is not a constant gain, the open-loop frequency response is used to analyze the stability, which is given by

$$GH_{\text{APF}} = \frac{j\omega}{Z_e + Z_i} \cdot \left(\frac{h}{\omega_f} \frac{2\zeta_f}{1 - \left(\omega/\omega_f\right)^2 + j2\zeta_f \, \omega/\omega_f} \right) \tag{2.44}$$

The phase shift of $1/\left(Z_e + Z_i\right)$ is between -90º and 90º, so that the phase shift of the first term $j\omega/\left(Z_e + Z_i\right)$ is between 0º and 180º. Because the APF controller is a second order low-pass filter, its phase shift can thus potentially vary between -180º and 0º. Therefore the overall phase shift of the open-loop frequency response is between -180º and 180º. The APF control system containing a massless isolator undergoing base motion is thus unconditionally stable based on the Nyquist stability criterion. However, such an APF control system is not passive, and thus not robustly stable. It is sensitive to the unmodelled actuator dynamics and other uncertainties in the system which might destabilize the control system.

2.4.6 Comparison of the control performance

In the above discussion, AVF, RVF, IFF, PPF and APF control can all bring active damping into the system around the system fundamental resonance. The comparison of the overall control performance for the active vibration isolation systems under these different control strategies can be realized by looking at their change in mean square response compared to the original passive system. The relationship between the power spectral densities of the base disturbance and equipment response can be written as [83]

$$S_e = |T|^2 S_b \tag{2.45}$$

where S_e and S_b are the power spectral densities of the equipment response and the base disturbance, respectively. The mean square velocity of the equipment is thus given by [83]

$$\overline{\dot{u}_e^2} = \int_{-\infty}^{+\infty} S_e d\Omega = \int_{-\infty}^{+\infty} |T|^2 S_b d\Omega \tag{2.46}$$

Substituting the corresponding transmissibility into equation (2.46), the change in mean square velocity for the system under different control strategies compared to the passive system can be calculated. For AVF, RVF, IFF and APF control, they all have the active damping ratio ζ_a in the transmissibility. However, the PPF control has an equivalent active damping ratio $g/(2\zeta_f m_e)$ around the system fundamental resonance peak. In order to plot the change in mean square velocity against active damping ratio ζ_a, the equivalent active damping ratio for PPF control is set to be $\zeta_a = g/(2\zeta_f m_e)$. Therefore, the range of the control gain *g* can be calculated according to the active damping ratio.

Figure 2.13 depicts the change in mean square velocity within the range $0.1 < \Omega < 1000$ when $\zeta = 0.005$, $m_e = 0.5$, $\zeta_f = 0.5$ and $\omega_f = \omega_e$. At high active damping ratios, AVF and IFF control provides increasing reduction in the mean square response. The performance of IFF control is determined by the mass of the equipment. In this case the mass of the equipment is 0.5, which is less than unity, the control performance of IFF

control is therefore worse than AVF control. The RVF, PPF and APF control do not produce monotonically reducing mean square response for an increase in active damping ratio. Furthermore, at $\zeta_a = 1$, i.e. the control gain $g = 2\zeta_f m_e \times \zeta_a = m_e$, the change in mean square velocity for PPF control is infinite, i.e. the PPF control system becomes unstable. The stability condition for PPF control given in equation (2.38) is thus validated.

2.4.7 Acceleration feedback control

Acceleration feedback control applied to a vibration isolation system containing a massless isolator has been investigated in several papers, for example [43, 47, 51]. Figure 2.14(a) shows a base excited vibration isolation system containing a massless isolator under acceleration feedback control. The control force f_a, which is in parallel with the isolator, reacts between the equipment and the base. The control force f_a is proportional to the acceleration of the equipment, and fed back to the system through a feedback controller with a constant gain $-h$, so that

$$f_a = -h\ddot{u}_e = -j\omega h\dot{u}_e \tag{2.47}$$

2.4.7.1 Control performance

The equation of motion for the active vibration isolation system under acceleration feedback control shown in Figure 2.14(a) is given by equation (2.12). Substituting equation (2.47) into (2.12), the transmissibility of the system under acceleration feedback control is given by

$$T = \frac{Z_i}{Z_e + Z_i + j\omega h} \tag{2.48}$$

If the equipment is modelled as a mass, the transmissibility can be written as [47]

$$T = \frac{1 + j2\zeta\Omega}{1 - \left(1 + \dfrac{h}{m_e}\right)\Omega^2 + j2\zeta\Omega} \tag{2.49}$$

Different from the aforementioned control strategies that all introduce active damping to the system, the action of acceleration feedback control for this base excited system is

equivalent to adding a mass h on top of the equipment as shown in Figure 2.14(b).

The magnitude of the transmissibility for the active vibration isolation system containing a massless isolator under acceleration feedback control is plotted in Figure 2.15, where the transmissibility of the system without control is also plotted for comparison. It can be seen that the system fundamental resonance peak moves to a lower frequency due to the acceleration feedback control, and thus the transmissibility at high frequencies is reduced.

2.4.7.2 Stability analysis

For acceleration feedback control, because the controller is a constant gain, the plant response of the system from the active force to the equipment acceleration can be used for the stability analysis, which is given by equation (2.43). The overall phase shift of the plant response is between 0º and 180º, and thus the acceleration feedback control system containing a massless isolator undergoing base motion is unconditionally stable. However, such a control system is not completely passive, and thus not robustly stable.

2.4.8 Optimal control

To find the best control strategy in attenuating the equipment response, the optimal control for active vibration isolation system containing a massless isolator undergoing base motion has been investigated [6]. Figure 2.16 shows a base excited system containing a massless isolator under optimal control. The equipment is modelled as a rigid mass. The massless isolator is modelled as an elastic spring in parallel with a viscous damper. The dynamics of such a system is described by

$$m_e\ddot{u}_e + c\left(\dot{u}_e - \dot{u}_b\right) + k\left(u_e - u_b\right) = f_a \tag{2.50}$$

which can be rearranged as

$$\ddot{u}_e = -\frac{c}{m_e}\dot{u}_e - \frac{k}{m_e}u_e + \frac{1}{m_e}f_a + \frac{c}{m_e}\dot{u}_b + \frac{k}{m_e}u_b \tag{2.51}$$

The state space representation for such a system has the form

$$\dot{\mathbf{x}}=\mathbf{A}\mathbf{x}+\mathbf{b}f_a+\mathbf{D}\mathbf{y} \tag{2.52}$$

where

$$\mathbf{x}=\begin{bmatrix} u_e \\ \dot{u}_e \end{bmatrix},\ \mathbf{A}=\begin{bmatrix} 0 & 1 \\ -\dfrac{k}{m_e} & -\dfrac{c}{m_e} \end{bmatrix},\ \mathbf{b}=\begin{bmatrix} 0 \\ \dfrac{1}{m_e} \end{bmatrix},\ \mathbf{D}=\begin{bmatrix} 0 & 0 \\ \dfrac{k}{m_e} & \dfrac{c}{m_e} \end{bmatrix},\ \mathbf{y}=\begin{bmatrix} u_b \\ \dot{u}_b \end{bmatrix} \tag{2.53a,b,c,d,e}$$

The general quadratic performance index which is to be minimized is given by [6, 74]

$$J=\int_0^\infty \left(\mathbf{x}'\mathbf{Q}\mathbf{x}+f_a'\mathbf{R}f_a\right)dt \tag{2.54}$$

where the prime denotes the transpose of the matrix, $\mathbf{Q}$ is a positive-definite or positive-semidefinite real symmetric matrix and $\mathbf{R}$ is a positive-definite real symmetric matrix. If one chooses

$$\mathbf{Q}=\begin{bmatrix} 0 & 0 \\ 0 & q \end{bmatrix}\ (q\geq 0),\ \mathbf{R}=[r]\ (r>0) \tag{2.55a,b}$$

The performance index can be written as

$$J=\int_0^\infty \left(q\dot{u}_e^2+rf_a^2\right)dt \tag{2.56}$$

where q is a weighting on the mean square velocity of the equipment mass and r is a weighting on the mean square control effort applied. The control force required to minimize the performance index is given by [6, 74]

$$f_a=-\mathbf{R}^{-1}\mathbf{b}'\mathbf{P}\mathbf{x} \tag{2.57}$$

where

$$\mathbf{P}=\begin{bmatrix} p_{11} & p_{12} \\ p_{12} & p_{22} \end{bmatrix} \tag{2.58}$$

is a positive-definite real symmetric matrix to ensure the control is stable, and satisfies the reduced-matrix Riccati equation

$$\mathbf{A}'\mathbf{P}+\mathbf{P}\mathbf{A}-\mathbf{P}\mathbf{b}\mathbf{R}^{-1}\mathbf{b}'\mathbf{P}+\mathbf{Q}=0 \tag{2.59}$$

Substituting the appropriate matrices into the reduced-matrix Riccati equation, three equations in terms of the unknown elements p_{11}, p_{12} and p_{22} result. They are given by

$$
\begin{aligned}
&-2\frac{k}{m_e}p_{12}-\frac{1}{rm_e^2}p_{12}^2=0\\
&p_{11}-\frac{c}{m_e}p_{12}-\frac{k}{m_e}p_{22}-\frac{1}{rm_e^2}p_{12}p_{22}=0\\
&2p_{12}-2\frac{c}{m_e}p_{22}-\frac{1}{rm_e^2}p_{22}^2+q=0
\end{aligned}
\tag{2.60a,b,c}
$$

There are two solutions to equation (2.60a) given by

$$p_{12}=0,\ \ p_{12}=-2rkm_e \tag{2.61a,b}$$

The solution to equation (2.60c) can be written as

$$p_{22}=rm_e\left(\pm\sqrt{c^2+\frac{2p_{12}+q}{r}}-c\right) \tag{2.62}$$

Finally equation (2.60b) shows that

$$p_{11}=\frac{c}{m_e}p_{12}+\frac{k}{m_e}p_{22}+\frac{1}{rm_e^2}p_{12}p_{22} \tag{2.63}$$

Because the matrix **P** is positive-definite, one has

$$p_{11}>0,\ \begin{vmatrix}p_{11} & p_{12}\\ p_{12} & p_{22}\end{vmatrix}=p_{11}p_{22}-p_{12}^2>0 \tag{2.64a,b}$$

Combining equations (2.61-2.64), the only solution that ensures the matrix **P** is positive-definite is given by

$$\mathbf{P}=\begin{bmatrix}p_{11} & p_{12}\\ p_{12} & p_{22}\end{bmatrix}=\begin{bmatrix}rk\left(\sqrt{c^2+\frac{q}{r}}-c\right) & 0\\ 0 & rm_e\left(\sqrt{c^2+\frac{q}{r}}-c\right)\end{bmatrix} \tag{2.65}$$

Substituting appropriate matrices into equation (2.57), the control force is thus given by

$$f_a=-\frac{1}{rm_e}\left(p_{12}u_e+p_{22}\dot{u}_e\right)=-\left(\sqrt{c^2+\frac{q}{r}}-c\right)\dot{u}_e \tag{2.66}$$

It can be seen that the optimal control strategy to minimise the mean square velocity of the equipment mass is precisely the AVF control, which results in skyhook damping of the controlled system [6]. If the damping in the system is negligible, i.e. $c<<1$, the control force given by equation (2.66) can be reduced to

$$f_a = -\sqrt{\frac{q}{r}}\dot{u}_e \tag{2.67}$$

which is identical to the result derived by Fuller et al. [6]. The feedback control gain for optimal control is thus given by $\sqrt{q/r}$, which is a simple function of the ratio of the relative penalty on minimising mean square equipment velocity response and mean square control effort. The smaller the control effort weighting *r*, the higher the feedback control gain, and thus the better the control performance.

2.4.9 Summary

The control performance and stability of active vibration isolation systems containing a massless isolator under different control strategies have been reviewed and compared. AVF control introduces skyhook damping to the system, which is effective in attenuating the resonance peak. Also AVF control has shown to be robustly stable for a base excited system, while it becomes conditionally stable if both the equipment and base dynamics are included. RVF control is equivalent to a viscous damper between the equipment and the base. Thus in this case there is a trade-off between the isolation performance at the resonance frequency and the isolation performance at high frequency, although RVF control is always unconditionally stable. If the equipment is a rigid mass, IFF control also introduces skyhook damping to the system. Although IFF control is not robustly stable for a base excited system, it remains unconditionally stable even if the base has its own resonance behaviour. Both PPF and APF controllers are second order filters that introduce active damping at the system fundamental resonance frequency, and then roll off rapidly at high frequencies, so that they are not sensitive to spillover at high frequencies. However, the PPF controller needs to be carefully designed to control a specific mode, and it may cause amplification at low frequencies due to the negative stiffness introduced. APF control is not robustly stable and thus very sensitive to the unmodelled actuator dynamics and other uncertainties in the system which might destabilize the control system. Different from other control methods, acceleration feedback control is equivalent to adding a mass onto the equipment, so that the

resonance peak moves to a lower frequency and the equipment response at high frequencies is reduced. Finally the study for optimal control shows that, to minimise the mean square velocity of the equipment mass, AVF control is the optimal solution.

2.5 Conclusions

Previous research on vibration isolation systems containing a massless isolator, which is modelled as an elastic spring in parallel with a viscous damper, has been reviewed and summarized. The compromise in the choice of damping in passive vibration isolation has been demonstrated. The concepts of single channel feedback control have been introduced together with the Nyquist stability criterion. The control performance and stability of active vibration isolation systems containing a massless isolator under various control strategies have been analyzed and compared. The different control strategies have their own advantages and disadvantages in isolating a piece of equipment undergoing base excitation based on the massless isolator model. It is shown that AVF control is an optimal solution to minimise the mean square velocity of the equipment mass.

The concepts and methodologies introduced in this chapter are applied to the vibration isolation systems containing a distributed parameter isolator discussed in the following chapters.

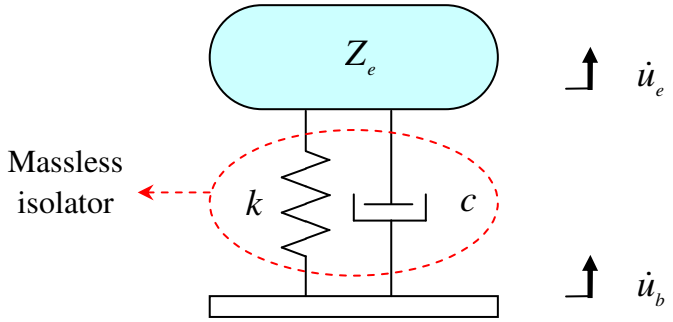

Figure 2.1 *Schematic diagram of a vibration isolation system containing a massless isolator undergoing base motion, where* $\dot{u}_e$ *and* $\dot{u}_b$ *are velocities of the equipment and the base respectively;* Z_e *is the input impedance of the unconnected equipment at the location of the isolator connection; k is the spring stiffness and c is the damping coefficient of the viscous damper.*

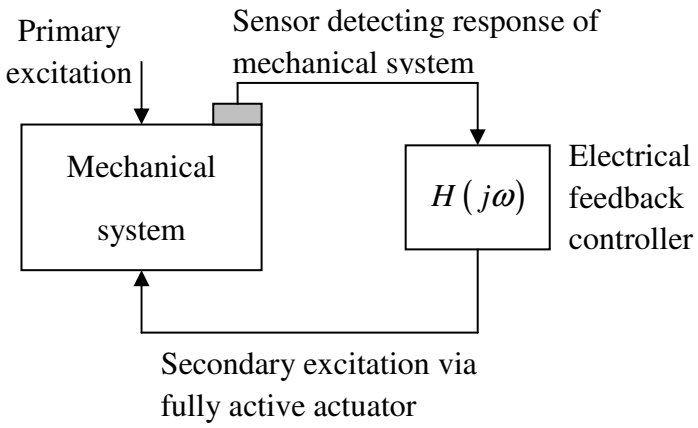

Figure 2.2 *Schematic diagram of a single channel feedback control system.*

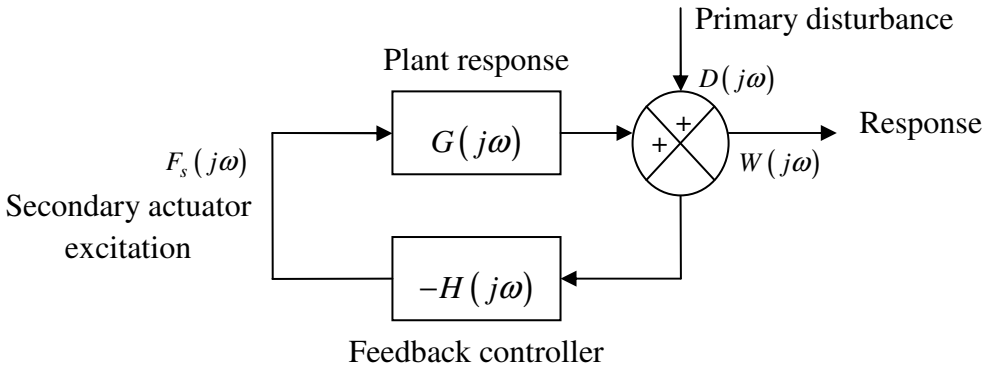

Figure 2.3 *Equivalent block diagram of the single channel feedback control system shown in Figure 2.2.*

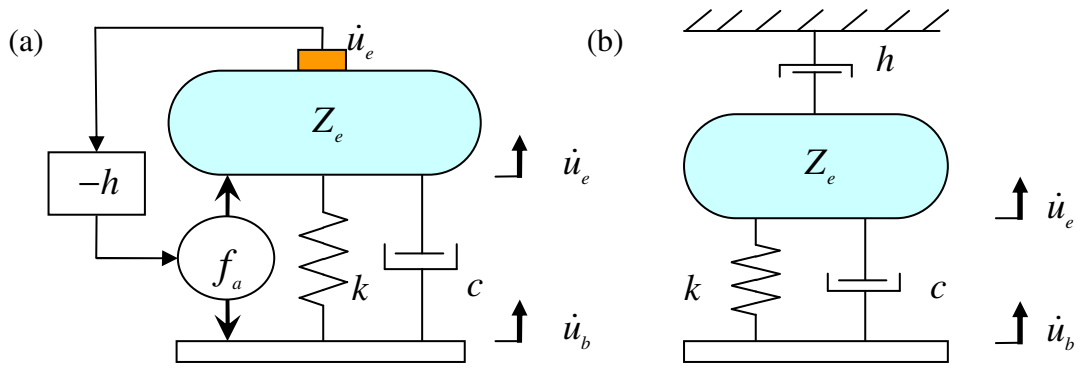

Figure 2.4 *(a) schematic diagram and (b) mechanical representation of a base excited system containing a massless isolator under AVF control, where h is the constant feedback control gain and* f_a *is the active control force.*

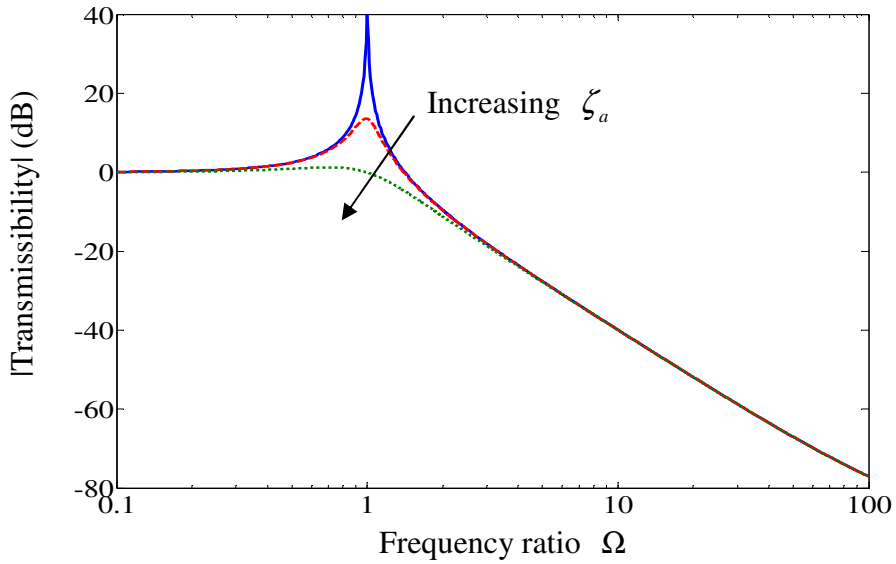

Figure 2.5 *Transmissibility of the active vibration isolation system under AVF control with* $\zeta = 0.005$ *and the active damping ratio* $\zeta_a = 0$ *(solid line),* $\zeta_a = 0.1$ *(dashed line) or* $\zeta_a = 0.5$ *(dotted line).*

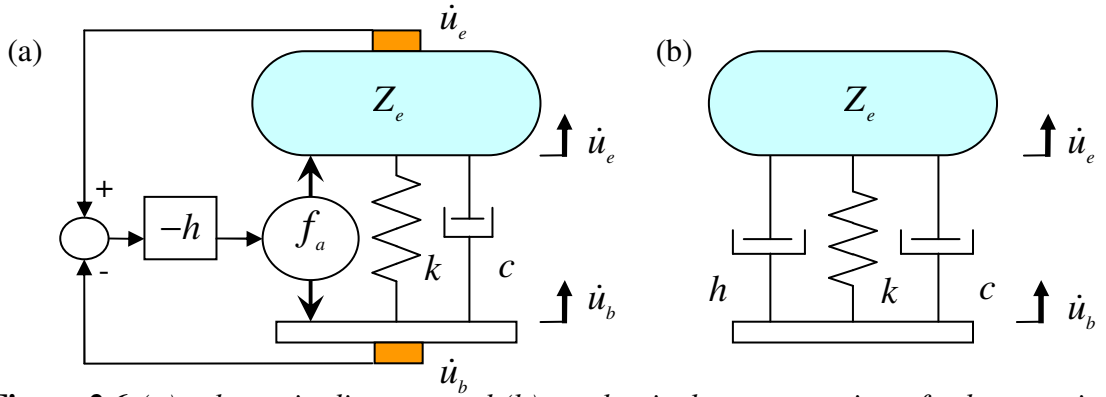

Figure 2.6 *(a) schematic diagram and (b) mechanical representation of a base excited system containing a massless isolator under RVF control.*

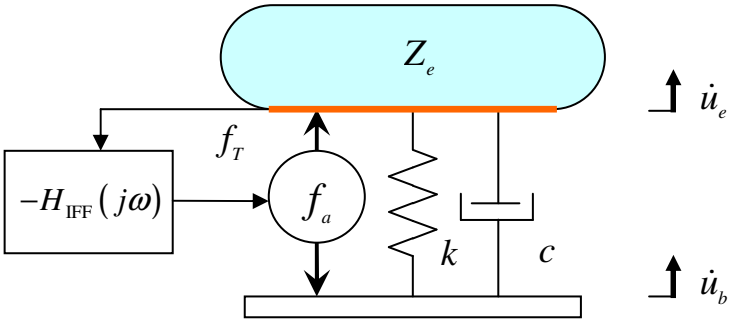

Figure 2.7 *Schematic diagram of a base excited system containing a massless isolator under IFF control, where* $H_{\text{IFF}}(j\omega)$ *is the frequency response of the IFF controller and* f_T *is the transmitted force to the equipment.*

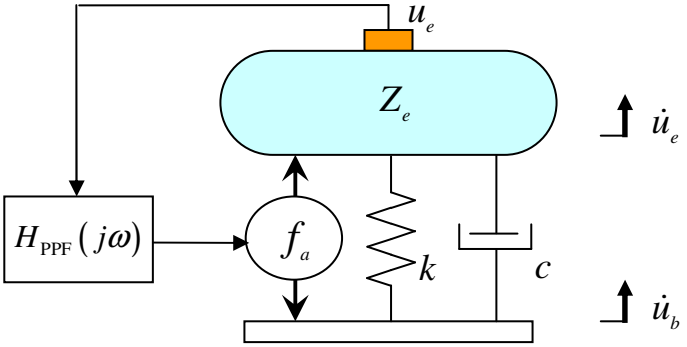

Figure 2.8 *Schematic diagram of a base excited system containing a massless isolator under PPF control, where* u_e *is the displacement of the equipment and* $H_{\text{PPF}}(j\omega)$ *is the frequency response of the PPF controller.*

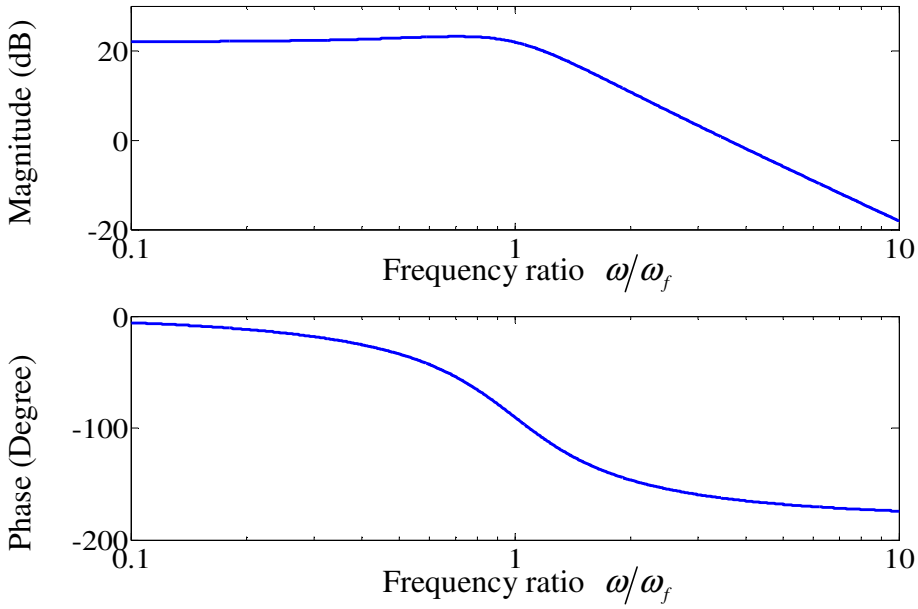

Figure 2.9 *Frequency response of the PPF controller when the natural frequency of the filter* $\omega_f = 5$*, the damping ratio of the filter* $\zeta_f = 0.5$ *and the gain* $g = 0.5$*.*

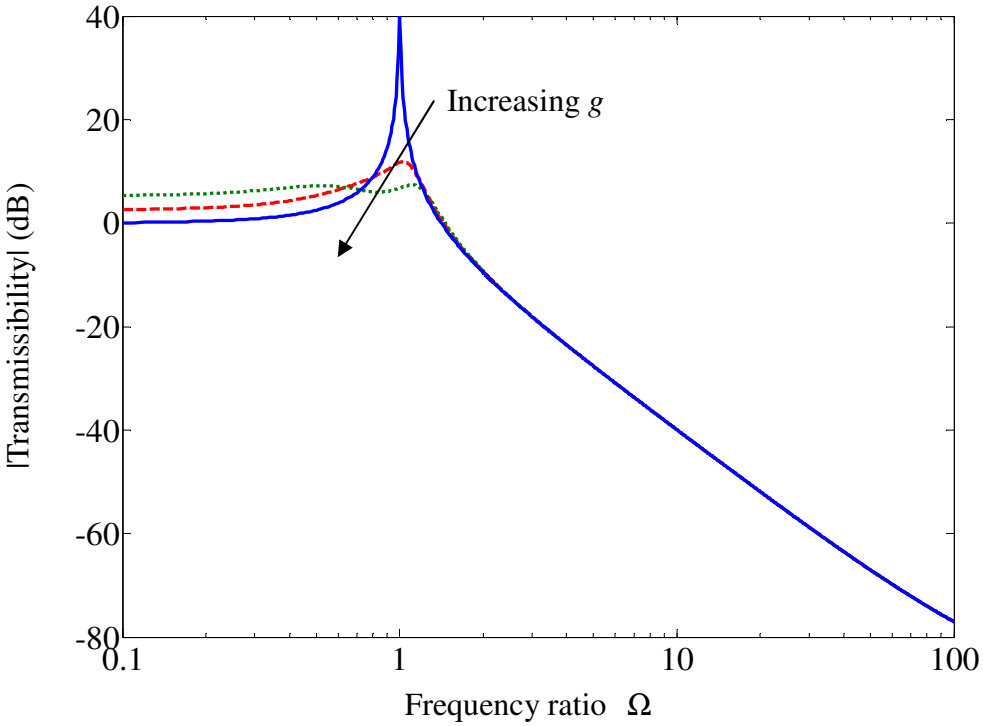

Figure 2.10 *Transmissibility of the active vibration isolation system under PPF control when* $\zeta = 0.005$, $\omega_f = \omega_e$, $\zeta_f = 0.5$, *the mass of the equipment* $m_e = 2$ *and* $g = 0$ *(solid line),* $g = 0.5$ *(dashed line) or* $g = 0.9$ *(dotted line).*

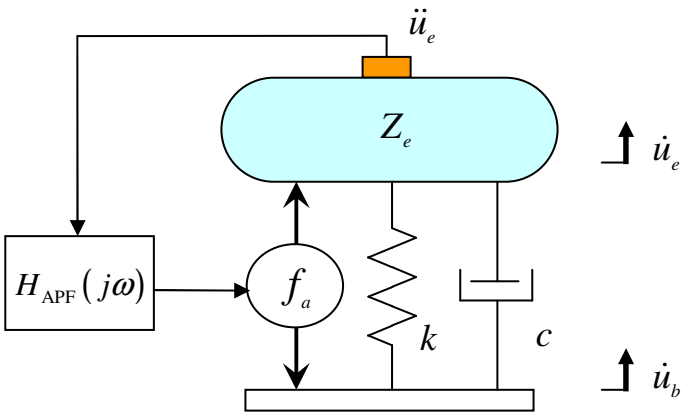

Figure 2.11 *Schematic diagram of a base excited system containing a massless isolator under APF control, where* $\ddot{u}_e$ *is the acceleration of the equipment and* $H_{\mathrm{APF}}(j\omega)$ *is the frequency response of the APF controller.*

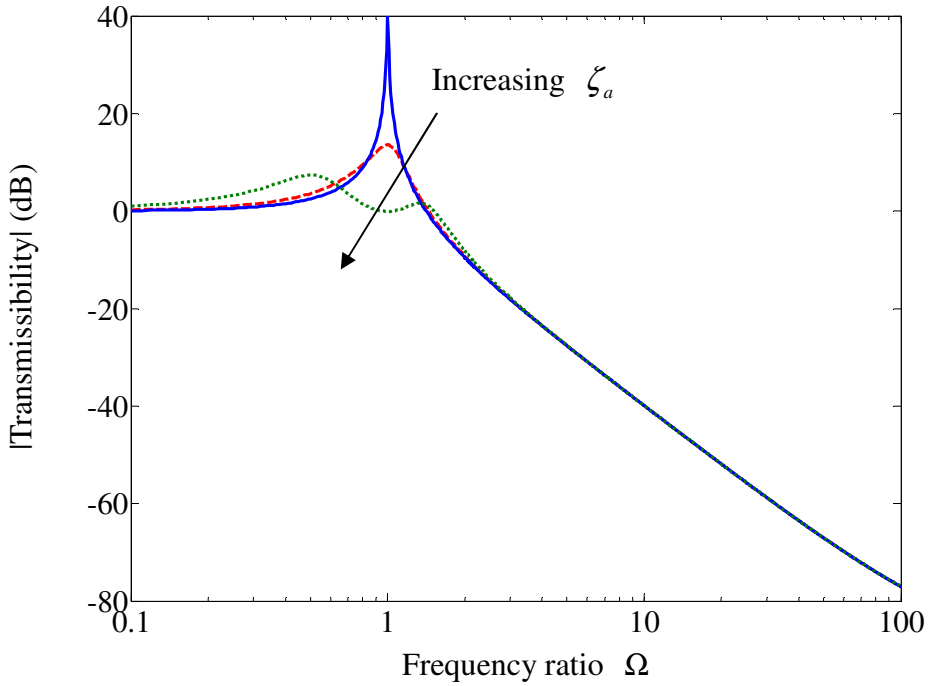

Figure 2.12 *Transmissibility of the active vibration isolation system under APF control with* $\zeta = 0.005$, $\omega_f = \omega_e$, $\zeta_f = 0.5$ *and* $\zeta_a = 0$ *(solid line),* $\zeta_a = 0.1$ *(dashed line) or* $\zeta_a = 0.5$ *(dotted line).*

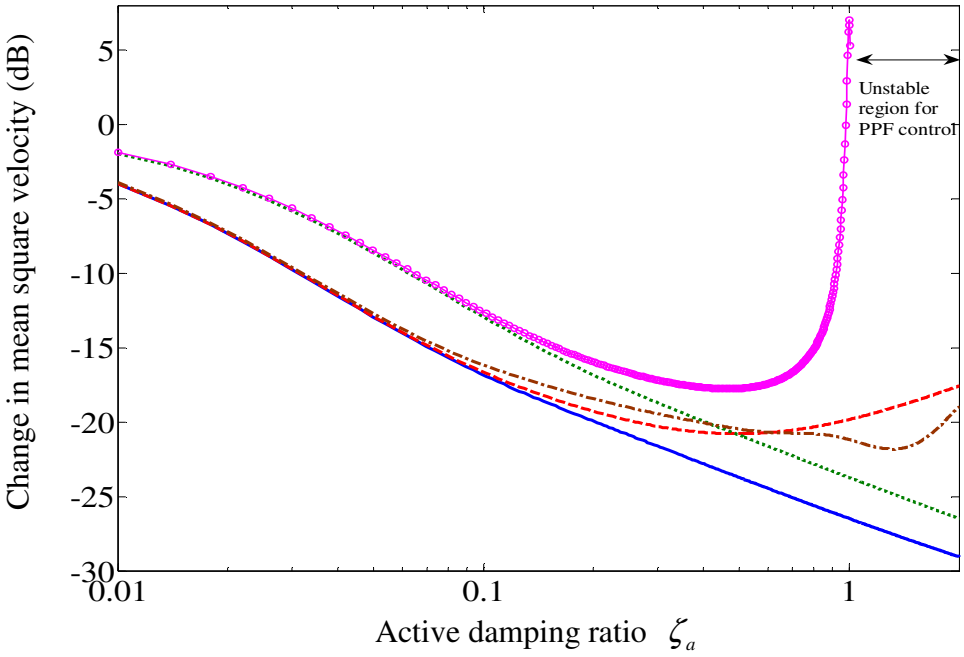

Figure 2.13 *Normalized change in mean square velocity for the system under AVF (solid line), RVF (dashed line), IFF (dotted line), PPF (line with circle) and APF (dashed-dotted line) control compared to the passive system when* $\zeta = 0.005$, $m_e = 0.5$, $\omega_f = \omega_e$ *and* $\zeta_f = 0.5$.

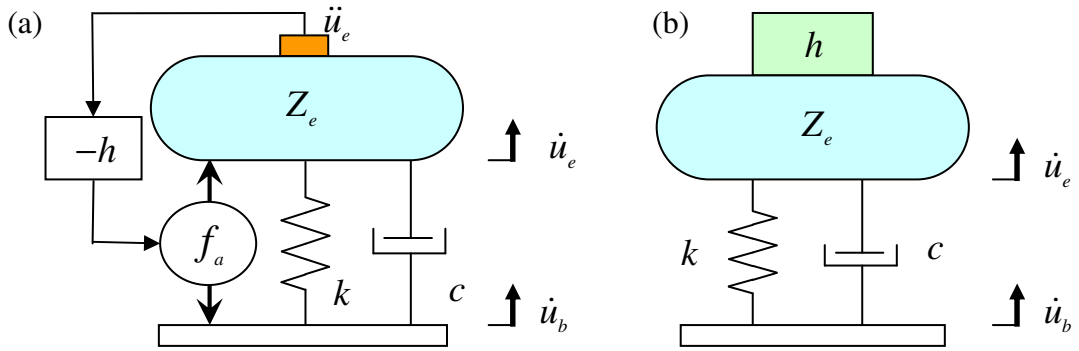

Figure 2.14 *(a) schematic diagram and (b) mechanical representation of a base excited system containing a massless isolator under acceleration feedback control.*

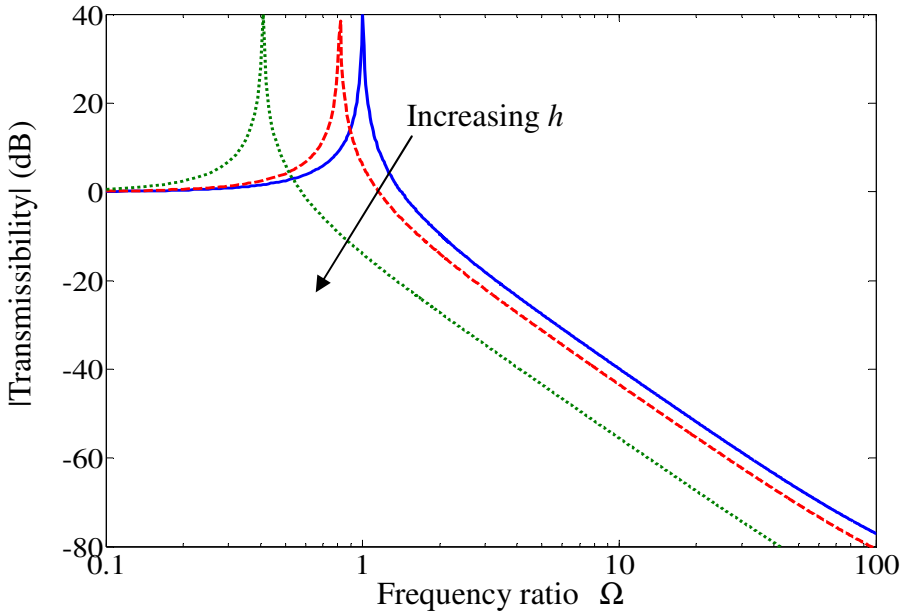

Figure 2.15 *Transmissibility of the vibration isolation system under acceleration feedback control when* $\zeta = 0.005$ *and* $h = 0$ *(solid line),* $h/m_e = 0.5$ *(dashed line) or* $h/m_e = 5$ *(dotted line).*

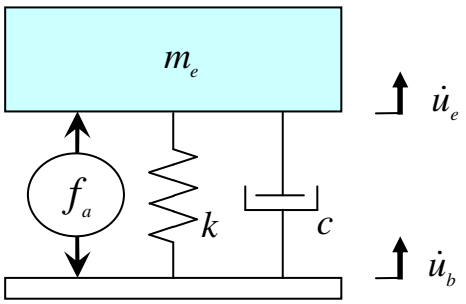

Figure 2.16 *Schematic diagram of a base excited system containing a massless isolator under optimal control.*

Chapter 3

Passive Vibration Isolation with a Distributed Parameter Isolator

3.1 Introduction

As described in Chapter 2, traditional vibration isolation models, in which the mass of isolator is assumed to be negligible, offer a wealth of information about vibration isolation and basic guidelines for isolation design. However, this assumption is only valid at frequencies which are low enough that the wavelength in the isolator is long compared to its size, as discussed in Chapter 1 [12, 20]. At higher frequencies, the predictions based on a massless isolator model are no longer accurate, and may be misleading due to the internal mass effects of the isolator that are ignored. Due to industrial trends towards more complex equipment and machines, greater operating speeds and higher power ratings, vibration isolation is becoming important at high frequencies, where traditional massless isolator models fail to perform satisfactorily. A model incorporating a distributed parameter isolator is thus necessary for high frequency isolation analysis.

The aim of this chapter is to investigate, theoretically and experimentally, the characteristics of a passive vibration isolation system containing a distributed parameter

isolator. First, different distributed parameter models for the isolator are presented. Their characteristics in isolating a piece of equipment (a rigid mass) from base motion are investigated. The way in which various system parameters affect the response of the system at various frequencies is then discussed. Experimental work on a mass supported by a helical spring is presented to support and validate the theoretical results. Finally, the characteristics of a passive vibration isolation system containing a distributed parameter isolator on a flexible base are investigated.

3.2 System undergoing base motion

Passive vibration isolation systems containing a distributed parameter isolator undergoing base motion are investigated in this section.

3.2.1 Theoretical analysis

As mentioned in Chapter 1, the various types of realistic isolator (for example the compression and leaf springs in automotive suspension, viscoelastic engine mounts, etc...) can be modelled as different idealised configurations under various types of deformation. Figure 3.1 depicts the passive vibration isolation systems containing a piece of equipment supported by a distributed parameter isolator under different types of excitation (e.g. longitudinal, torsional, or lateral vibration). These distributed parameter models for a realistic isolator can be categorized into two types for the purpose of dynamic analysis. One type can be modelled using a second order partial differential equation, and is called a non-dispersive isolator, since the wave speed is independent of frequency. The other type can be modelled using a fourth or higher order partial differential equation, and is called a dispersive isolator, since the wave speed is dependent on frequency. In Figure 3.1 the distributed parameter isolator is modelled as a finite elastic rod under longitudinal vibration (Figure 3.1(a)) or torsional vibration (Figure 3.1(c)), or a beam under lateral vibration (Figure 3.1(e)), respectively. The rod in Figure 3.1(a, c) can be categorized as a non-dispersive isolator. The beam in Figure

3.1(e) can be categorized either as a non-dispersive isolator if it is represented as a shear beam, or a dispersive isolator if it is represented as an Euler-Bernoulli beam dominated by bending.

The generalized dynamics of the systems containing a distributed parameter isolator shown in Figure 3.1 are described by

$$Q_e = -Q_2 = Z_e \dot{u}_e$$
$$\begin{bmatrix} Q_1 \\ Q_2 \end{bmatrix} = \mathbf{Z_I} \begin{bmatrix} \dot{u}_b \\ \dot{u}_e \end{bmatrix} = \begin{bmatrix} Z_{11} & Z_{12} \\ Z_{21} & Z_{22} \end{bmatrix} \begin{bmatrix} \dot{u}_b \\ \dot{u}_e \end{bmatrix} \quad (3.1a,b)$$

where Q_e, Q_1 and Q_2 are the internal forces shown in Figure 3.1(b) and (f), or moments shown in Figure 3.1(d); $\dot{u}_e$ and $\dot{u}_b$ are velocity in Figure 3.1(b) and (f), or angular velocity in Figure 3.1(d) of the equipment and the base respectively; Z_e is the input impedance of the unconnected equipment at the location of the isolator connection; $\mathbf{Z_I} = \mathbf{Z_L}$, $\mathbf{Z_T}$, $\mathbf{Z_S}$ (for shear beam) or $\mathbf{Z_B}$ (for Euler-Bernoulli beam) is the impedance matrix for the different isolator models and is discussed further below; and the subscripts 1 and 2 in the impedance matrix refer to the positions at the base and equipment respectively. From equations (3.1a, b), the transmissibility for all the systems shown in Figure 3.1 has the same form and can be written as [72]

$$T = \frac{\dot{u}_e}{\dot{u}_b} = \frac{-Z_{21}}{Z_e + Z_{22}} \quad (3.2)$$

The performance of passive vibration isolation systems containing such isolators is investigated and compared in the following sections.

3.2.1.1 Non-dispersive isolator

For the rod isolator under longitudinal vibration shown in Figure 3.1(a), the impedance matrix is given by [84, 85] (the detailed derivation can be found in Appendix A)

$$\mathbf{Z_L} = \begin{bmatrix} Z_{11} & Z_{12} \\ Z_{21} & Z_{22} \end{bmatrix} = \frac{S\sqrt{E^*\rho}}{j\sin\left(k_l^* L\right)} \begin{bmatrix} \cos\left(k_l^* L\right) & -1 \\ -1 & \cos\left(k_l^* L\right) \end{bmatrix} \quad (3.3)$$

where L, S, E^*, ρ are the length, cross-sectional area, Young's modulus and density of the isolator respectively; to account for damping in the isolator, the Young's modulus

is assumed to be complex, i.e. $E^* = E(1+j\eta_l)$, where η_l is the loss factor; $k_l^* \approx k_l(1-j\eta_l/2)$, where $k_l = \sqrt{\rho/E}\omega$ is the longitudinal wavenumber in the undamped isolator, and ω is angular frequency.

For the rod isolator under torsional vibration shown in Figure 3.1(c), the impedance matrix is given by [84, 85] (the detailed derivation can be found in Appendix A)

$$\mathbf{Z_T} = \begin{bmatrix} Z_{11} & Z_{12} \\ Z_{21} & Z_{22} \end{bmatrix} = \frac{J_s\sqrt{G^*\rho}}{j\sin\left(k_s^* L\right)} \begin{bmatrix} \cos\left(k_s^* L\right) & -1 \\ -1 & \cos\left(k_s^* L\right) \end{bmatrix} \tag{3.4}$$

where J_s is the polar second moment of area of the isolator; $G^* = G(1+j\eta_s)$ is the complex shear modulus, where η_s is the loss factor; $k_s^* \approx k_s(1-j\eta_s/2)$, where $k_s = \sqrt{\rho/G}\omega$ is the shear wavenumber in the undamped isolator.

Similarly for the shear beam isolator under lateral vibration in Figure 1(e), the impedance matrix is given by [86] (the detailed derivation can be found in Appendix A)

$$\mathbf{Z_S} = \begin{bmatrix} Z_{11} & Z_{12} \\ Z_{21} & Z_{22} \end{bmatrix} = \frac{S\sqrt{G^*\rho}}{j\sin\left(k_s^* L\right)} \begin{bmatrix} \cos\left(k_s^* L\right) & -1 \\ -1 & \cos\left(k_s^* L\right) \end{bmatrix} \tag{3.5}$$

Substituting the appropriate impedances in equations (3.3-3.5) into (3.2), and letting $Z_e = j\omega m_e$, where m_e is the mass of the equipment in Figures 3.1(a) and (e); $Z_e = j\omega J_e$, where J_e is the polar moment of inertia of the equipment in Figure 3.1(c); $\eta_i = \eta_l = \eta_s$, where the subscript *i* refers to the isolator; the generalized transmissibility can be written in non-dimensional form as

$$T = \frac{1}{\cos\left[\sqrt{\mu_i}\left(1-j\frac{\eta_i}{2}\right)\Omega\right] - \frac{\Omega}{\sqrt{\mu_i}}\left(1-j\frac{\eta_i}{2}\right)\sin\left[\sqrt{\mu_i}\left(1-j\frac{\eta_i}{2}\right)\Omega\right]} \tag{3.6}$$

where $\Omega = \omega/\omega_e$ is the ratio of the driving frequency ω to the system fundamental natural frequency ω_e due to the interaction of the equipment mass and the static stiffness of the isolator. For the rod isolator, $\omega_e = \sqrt{K_L/m_e}$ where $K_L = ES/L$ is the static longitudinal stiffness of the isolator; $\mu_i = \rho SL/m_e$ is the ratio of the mass of the

isolator to the mass of the equipment. For the torsional isolator, $\omega_e = \sqrt{K_T / J_e}$ where $K_T = GJ_s / L$ is the static torsional stiffness of the isolator; $\mu_i = \rho J_s L / J_e$ is the ratio of the polar moment of inertia of the isolator to the polar moment of inertia of the equipment. For the shear beam isolator, $\omega_e = \sqrt{K_S / m_e}$ where $K_S = GS / L$ is the static shear stiffness of the isolator and $\mu_i = \rho SL / m_e$ is also the ratio of the mass of the isolator to the mass of the equipment.

The transmissibility for the passive vibration isolation systems with a non-dispersive isolator is plotted in Figure 3.2 for the case in which $\mu_i = 0.1$ and $\eta_i = 0.01$. For comparison, the transmissibility of a system containing a massless isolator is also plotted. The transmissibility for a non-dispersive isolator has a peak at a frequency close to that of the fundamental resonance when the isolator is massless. The transmissibility for a non-dispersive isolator, however, is greater than that for the massless isolator, at high frequencies ($\Omega >> 1$), due to the effects of the IRs. Some characteristic lines are also plotted and identified. The dashed line called the 'maximum' line is through the IR peaks in the transmissibility. The dotted line is the 'minimum' line of the transmissibility across the isolator. The point circled corresponds to the frequency at which the transmissibility of a system with a non-dispersive isolator and a system with a massless isolator start to deviate, i.e. the wave effects in the isolator becomes detrimental to the isolator performance. The characteristic lines and point are determined below:

- Maximum line

The natural frequencies of a fixed-fixed rod occur when $\sin\left(\sqrt{\mu_i}\Omega\right) = 0$. At relatively low frequencies, assuming light damping in the isolator, i.e. $\eta_i << 1$ and light isolator compared to the equipment mass, i.e. $\mu_i << 1$, gives

$$\frac{1}{2}\eta_i \sqrt{\mu_i}\Omega << 1 \tag{3.7}$$

So using small angle approximations and considering $\sin\left(\sqrt{\mu_i}\Omega\right) = 0$, one has

$$\cos\left[\sqrt{\mu_i}\left(1-j\frac{\eta_i}{2}\right)\Omega\right]\approx\pm 1$$
$$\sin\left[\sqrt{\mu_i}\left(1-j\frac{\eta_i}{2}\right)\Omega\right]\approx\mp j\frac{1}{2}\eta_i\sqrt{\mu_i}\Omega \quad (3.8a,b)$$

Substituting equations (3.8a, b) into (3.6) gives

$$|T|=\frac{1}{\left|1+\frac{\Omega}{\sqrt{\mu_i}}\left(1-j\frac{\eta_i}{2}\right)j\frac{1}{2}\eta_i\sqrt{\mu_i}\Omega\right|} \quad (3.9)$$

Assuming that the imaginary part of equation (3.9) dominates around the IR frequencies in the isolator, the maximum line is given by

$$|T|_{\max}\approx\frac{2}{\eta_i}\frac{1}{\Omega^2} \quad (3.10)$$

This equation is a function of the loss factor η_i and frequency ratio Ω. It decreases at a rate of 40 dB per decade. From this equation, it should be noted that increasing damping in the isolator or decreasing the system fundamental resonance frequency are effective in attenuating the IR peaks.

The maximum line can also been derived from another point of view. The equations of motion described in equations (3.1a, b) can be rearranged as

$$\left(Z_e+Z_{22}\right)\dot{u}_e=-Z_{21}\dot{u}_b=f_B \quad (3.11)$$

where the blocked force f_B is the force transmitted from the base excitation by the attachment point between the equipment and the isolator to an infinitely rigid fixed point [87]. Based on this equation, the Thevenin equivalent system [87] is shown in Figure 3.3.

At IR frequencies in the lightly damped rod isolator under longitudinal vibration, assuming $\sin\left(k_l L\right)=0$ and $\eta_i<<1$, one has

$$\cos\left(k_l^* L\right)\approx\pm 1,\ \sin\left(k_l^* L\right)\approx\mp j\frac{1}{2}\eta_i k_l L \quad (3.12a,b)$$

Substituting equations (3.12a, b) into the point and transfer impedances of the finite rod shown in equation (3.3) gives

$$Z_{21} = \pm\frac{2K_L}{\eta_i\omega},\ Z_{22} = \frac{2K_L}{\eta_i\omega} \tag{3.13a,b}$$

Now, the impedance for a viscous damper is real and independent of frequency, so the non-dispersive isolator behaves as a frequency dependent damper with equivalent damping coefficient $c_{eq} = 2K_L/\eta_i\omega$ at its IR frequencies. The blocked force in Figure 3.3 at the IR frequencies is thus given by

$$f_B = -Z_{21}\dot{u}_b = \mp\frac{2K_L}{\eta_i\omega}\dot{u}_b \tag{3.14}$$

So the blocked force is determined by the loss factor η_i and static stiffness K_L of the isolator. A high loss factor η_i or low static stiffness K_L means smaller forces transmitted to the equipment and the isolator. Therefore, increasing η_i or decreasing K_L, which is equivalent to a decrease in the system fundamental resonance frequency, is effective in attenuating the effects of the IRs in the isolator. This solution is the same as that concluded from equation (3.10).

In Figure 3.3 it is clear that the equipment response is governed by the total impedance of the system, which is given by

$$Z_t = Z_e + Z_{22} \tag{3.15}$$

At relatively high frequencies, if the equipment has a mass-like impedance (i.e. $Z_e = j\omega m_e$ which increases with frequency), the point impedance Z_{22} can be ignored in equation (3.15) because even its maxima (which occurs at IR frequencies given by equation (3.13b), and decreases with frequency) is small compared to the equipment impedance. Therefore, the equipment mass dominates the response at relatively high frequencies. Equation (3.15) can thus be rewritten as

$$Z_t \approx Z_e = j\omega m_e \tag{3.16}$$

Therefore, at relatively high frequencies, the transmissibility of the system can be simplified and given by

$$T \approx \frac{-Z_{21}}{Z_e} \tag{3.17}$$

Substituting equation (3.13a), which describes the transfer impedance Z_{21} at IR

frequencies in the isolator, into (3.17), and noting that $Z_e = j\omega m_e$, the maximum line is given by

$$|T|_{\max} \approx \frac{2K_L}{\eta_i \omega^2 m_e} = \frac{2}{\eta_i}\frac{1}{\Omega^2} \tag{3.18}$$

which is identical to the maximum line given by equation (3.10).

- Minimum line

Assuming light damping in the isolator, i.e. $\eta_i << 1$, and considering $\sin\left(\sqrt{\mu_i}\Omega\right) = \pm 1$ gives

$$\begin{aligned} \sin\left[\sqrt{\mu_i}\left(1 - j\frac{\eta_i}{2}\right)\Omega\right] &\approx \pm 1 \\ \cos\left[\sqrt{\mu_i}\left(1 - j\frac{\eta_i}{2}\right)\Omega\right] &\approx \pm j\frac{1}{2}\eta_i\sqrt{\mu_i}\Omega \end{aligned} \tag{3.19a,b}$$

Substituting equations (3.19a, b) into (3.6)**,** the minimum line can be approximated by

$$|T|_{\min} \approx \sqrt{\mu_i}\frac{1}{\Omega} \tag{3.20}$$

which is a function of the mass (or polar moment of inertia) ratio μ_i and frequency ratio Ω. The minimum line decreases at a rate of 20 dB per decade, compared to the roll-off rate of 40 dB per decade for the massless isolator. It shows that the transmissibility for the non-dispersive isolator rolls off at a lower rate than that for the massless isolator at relatively high frequencies due to the IR effects. Substituting the appropriate μ_i and Ω into equation (3.20) gives

$$|T|_{\min} \approx \frac{S\sqrt{E\rho}}{\omega m_e} \text{ or } \frac{J_s\sqrt{G\rho}}{\omega J_e} \text{ or } \frac{S\sqrt{G\rho}}{\omega m_e} \tag{3.21}$$

It can be seen that the minimum line is independent of the isolator length. Therefore, to improve the performance of the isolator its mass, polar moment of inertia or natural frequency can be adjusted by changing the isolator parameters except for the length.

The minimum line can also be derived based on the Thevenin equivalent system shown in Figure 3.3. Substituting $\sin(k_l L) = \pm 1$ into the transfer impedance in equation (3.3), the minimum of the transfer impedance Z_{21}, i.e. the minimum of the blocked force f_B is determined by

$$Z_{21} = \pm j\sqrt{K_L m_i} \tag{3.22}$$

where $m_i = \rho SL$ is the mass of the isolator. Substituting equation (3.22) into (3.17), which describes the transmissibility of the system at relatively high frequencies, the minimum line can be determined to give

$$|T|_{\min} \approx \frac{\sqrt{K_L m_i}}{\omega m_e} = \sqrt{\mu_i}\,\frac{1}{\Omega} \tag{3.23}$$

which is identical to the minimum line given by equation (3.20).

- Crossing point

If the isolator mass is negligible, i.e. $\mu_i << 1$ and its damping is small, the expression for the transmissibility reduces to

$$|T|_{\text{massless}} \approx \left|\frac{1}{1-\Omega^2}\right| \tag{3.24}$$

Because the crossing point corresponds to the frequency at which the transmissibility for a non-dispersive isolator starts to differ from that for a massless isolator, one can assume $|T|_{\min} = |T|_{\text{massless}}$. By setting equations (3.20) and (3.24) to be equal and assuming that $\mu_i << 1$, the crossing point is given by

$$\Omega \approx \frac{1}{\sqrt{\mu_i}},\ |T| \approx \mu_i \tag{3.25}$$

which is only a function of the mass (or polar moment of inertia) ratio μ_i. This shows that, for a specific fixed equipment, the mass or the polar moment of inertia of the isolator is crucial to the isolator performance. The lighter the isolator, the higher the frequency at which the transmissibility for a non-dispersive isolator starts to differ from that for a massless isolator, i.e. the better the isolator performance.

3.2.1.2 Dispersive isolator

Distributed parameter isolators, where bending motion is dominant, may be represented by a dispersive system, which can be modelled using a fourth or higher order differential equation. In Figure 3.1(e), the distributed parameter isolator can be represented by an Euler-Bernoulli beam undergoing lateral vibration as an example of a dispersive isolator. One end of the isolator is sliding under external excitation. The

equipment represented by impedance Z_e is supported by the other end of the isolator. It is assumed that the equipment connects to the isolator by an internal force only (any internal moments are assumed to be negligible).

For a finite sliding-free Euler-Bernoulli beam, assuming there is no rotation at the sliding end and there is no bending moment at the free end, the impedance matrix is given by (the detailed derivation can be found in Appendix A)

$$\mathbf{Z_B} = \begin{bmatrix} Z_{11} & Z_{12} \\ Z_{21} & Z_{22} \end{bmatrix} \tag{3.26}$$

$$\begin{aligned} Z_{11} &= \frac{2E^*Ik_b^{*3}\cos\left(k_b^*L\right)\cosh\left(k_b^*L\right)}{j\omega\left(\sin\left(k_b^*L\right)\cosh\left(k_b^*L\right)-\cos\left(k_b^*L\right)\sinh\left(k_b^*L\right)\right)} \\ Z_{22} &= \frac{E^*Ik_b^{*3}\left(1+\cos\left(k_b^*L\right)\cosh\left(k_b^*L\right)\right)}{j\omega\left(\sin\left(k_b^*L\right)\cosh\left(k_b^*L\right)-\cos\left(k_b^*L\right)\sinh\left(k_b^*L\right)\right)} \\ Z_{12} = Z_{21} &= -\frac{E^*Ik_b^{*3}\left(\cos\left(k_b^*L\right)+\cosh\left(k_b^*L\right)\right)}{j\omega\left(\sin\left(k_b^*L\right)\cosh\left(k_b^*L\right)-\cos\left(k_b^*L\right)\sinh\left(k_b^*L\right)\right)} \end{aligned} \tag{3.27a,b,c}$$

where I is the second moment of area about the neutral axis of the isolator, $k_b^* \approx k_b(1-j\eta_i/4)$, where $k_b = \sqrt[4]{\rho S/EI}\sqrt{\omega}$ is the bending wavenumber in the undamped isolator.

If the equipment has a mass-like impedance, i.e. $Z_e = j\omega m_e$, and the appropriate impedances in equations (3.27b, c) are substituted into equation (3.2), the non-dimensional transmissibility can be written as

$$T = \frac{1}{\dfrac{1+\cos\gamma^*\cosh\gamma^*}{\cos\gamma^*+\cosh\gamma^*} - \sqrt[4]{\dfrac{3\Omega^2}{\mu_i^3}}\left(1-j\dfrac{\eta_i}{4}\right)\dfrac{\sin\gamma^*\cosh\gamma^*-\cos\gamma^*\sinh\gamma^*}{\cos\gamma^*+\cosh\gamma^*}} \tag{3.28}$$

$$\gamma^* = \gamma\left(1-j\frac{\eta_i}{4}\right) = \sqrt[4]{3\mu_i\Omega^2}\left(1-j\frac{\eta_i}{4}\right) \tag{3.29}$$

where $\Omega = \omega/\omega_e$ is the ratio of the driving frequency ω to the system fundamental natural frequency ω_e; $\omega_e = \sqrt{K_B/m_e}$ where $K_B = 3EI/L^3$ is the static bending stiffness of the isolator; $\mu_i = \rho SL/m_e$ is the ratio of the mass of the isolator to the mass of the equipment.

The transmissibility of the passive isolation system with a dispersive isolator is plotted in Figure 3.4 for $\mu_i = 0.1$ and $\eta_i = 0.01$. The transmissibility of such a system containing a massless isolator is also plotted for comparison. The transmissibility for a dispersive isolator has a peak at a frequency close to that of the fundamental resonance when the isolator is massless. The transmissibility for a dispersive isolator, however, is greater than that for the massless isolator, at high frequencies ($\Omega >> 1$), due to the effects of the IRs. Similar characteristic lines and point to those plotted in Figure 3.2 are also depicted in Figure 3.4 to describe the transmissibility. The characteristic lines and point are determined in a similar way to those for the non-dispersive isolator. The detailed procedure is as follows:

- Maximum line

At relatively high frequencies, i.e. $\gamma >> 1$, assuming that the damping in the isolator is very small, i.e. $\eta_i << 1$, one has

$$\sinh \gamma^* \approx \cosh \gamma^* >> 1 \tag{3.30}$$

Applying the conditions given in equation (3.30) to (3.28), the transmissibility can be simplified for $\Omega >> 1$ and is given by

$$T \approx \frac{1}{\cos \gamma^* - \sqrt[4]{\frac{3\Omega^2}{\mu_i^3}} \left(\sin \gamma^* - \cos \gamma^* \right)} \tag{3.31}$$

The natural frequencies of the sliding-free beam occur when

$$\sin \gamma \cosh \gamma - \cos \gamma \sinh \gamma = 0 \tag{3.32}$$

So, at relatively high frequencies, one has

$$\tan \gamma = \tanh \gamma \approx 1 \tag{3.33}$$

Therefore at IRs in the sliding-free beam which occur at relatively high frequencies, one has

$$\sin \gamma \approx \cos \gamma = \pm \frac{1}{\sqrt{2}} \tag{3.34}$$

Using small angle approximations and equation (3.34) gives

$$\sin\gamma^* \approx \pm\frac{1}{\sqrt{2}}\left(1 - j\frac{\eta_i}{4}\sqrt[4]{3\mu_i\Omega^2}\right)$$
$$\cos\gamma^* \approx \pm\frac{1}{\sqrt{2}}\left(1 + j\frac{\eta_i}{4}\sqrt[4]{3\mu_i\Omega^2}\right) \quad (3.35a,b)$$

Therefore, applying the conditions given in equations (3.35a, b) to (3.31), and assuming that the imaginary part of equation (3.31) dominates around the IR frequencies, the maximum line is given by

$$|T|_{\max} \approx \sqrt{\frac{2\mu_i}{3}}\frac{2}{\eta_i}\frac{1}{\Omega} \quad (3.36)$$

Different from the maximum line for the non-dispersive isolator, it is a function of not only the loss factor η_i and frequency ratio Ω, but the mass ratio μ_i as well. Increasing damping in the isolator or decreasing the system fundamental resonance frequency are again effective in attenuating these peaks. Substituting the appropriate μ_i and Ω into equation (3.36) gives

$$|T|_{\max} \approx \frac{\sqrt{2EI\rho S}}{m_e L}\frac{2}{\eta_i}\frac{1}{\omega} \quad (3.37)$$

It can be seen that, to suppress the IR peaks, the isolator mass can be adjusted by reducing its density or cross-section area, but increasing its length. It should be noted that the IR peaks decrease at a rate of 20 dB per decade, rather than 40 dB per decade for the non-dispersive isolator.

- Minimum line

As shown in equation (3.31), the transmissibility of the system at relatively high frequencies achieves its minima when $\left(\sin\gamma^* - \cos\gamma^*\right)$ is maximum, which is given by

$$\left|\sin\gamma^* - \cos\gamma^*\right|_{\max} = \sqrt{2} \quad (3.38)$$

Substituting equation (3.38) into (3.31), the minimum line is approximately given by

$$|T|_{\min} \approx \sqrt[4]{\frac{\mu_i^3}{12}}\frac{1}{\sqrt{\Omega}} \quad (3.39)$$

which is a function of the mass ratio μ_i and frequency ratio Ω. It decreases at a rate of 10 dB per decade, compared to the rate of 40 dB per decade for the massless isolator and 20 dB per decade for the non-dispersive isolator. Substituting the appropriate μ_i and Ω into equation (3.39) gives

$$|T|_{\min} \approx \sqrt[4]{\frac{EI(\rho S)^3}{4}} \frac{1}{m_e} \frac{1}{\sqrt{\omega}} \tag{3.40}$$

It can be seen that the minimum line is independent of the isolator length. Therefore, to improve the performance of the isolator its mass or natural frequency can be adjusted by changing the isolator parameters except for the length.

- Crossing point

By setting equations (3.39) and (3.24) to be equal, i.e. $|T|_{\min} = |T|_{\text{massless}}$ and assuming that $\mu_i << 1$, the crossing point is given by

$$\Omega \approx \sqrt[6]{12} \frac{1}{\sqrt{\mu_i}}, \quad |T| \approx \frac{1}{\sqrt[3]{12}} \mu_i \tag{3.41}$$

which is only a function of the mass ratio μ_i. Similar to the non-dispersive isolator, it shows that the lighter the isolator, the better the isolator performance.

3.2.1.3 Summary

From the discussion of passive vibration isolation systems containing either a non-dispersive isolator or a dispersive isolator, the characteristics of the distributed parameter isolators are summarized in Table 3.1. It shows that three factors are crucial in the isolation performance of the distributed parameter isolator, namely the mass (or polar moment of inertia) ratio μ_i, the loss factor in the isolator η_i and frequency ratio Ω. The IR peaks can be suppressed effectively by increasing the damping in the isolator or decreasing the system fundamental resonance frequency. Also, it shows that the lighter the isolator the better the isolation performance. However, it should be noted that the minimum line of the transmissibility is independent of the isolator length.

It can be seen that, compared to the non-dispersive isolator, the IRs for the dispersive isolator have a lower density with respect to frequency and occur at much higher non-dimensional frequencies. Generally, in practice, the IRs in the dispersive isolator can be attenuated to a large extent compared to those in the non-dispersive isolator, since more damping can be incorporated more easily into dispersive isolators, e.g. flexural springs [56]. Therefore, in practice the undesirable effects of IRs on the isolation performance for the non-dispersive isolator are more significant than that for

the dispersive isolator. The distributed parameter isolator is thus modelled as a finite elastic rod under longitudinal vibration in the following analysis

3.2.2 Experimental validation on a helical spring

A helical spring can be modelled theoretically as an equivalent finite elastic rod under longitudinal vibration for simplicity [20, 21]. Both objects can be modelled as distributed parameter elements, because their stiffness and mass are spread uniformly throughout their length. Therefore, an experiment using a helical spring, as an example of a non-dispersive isolator, was conducted to validate the theoretical findings for the distributed parameter isolator.

3.2.2.1 Experimental setup

An experimental rig was built as illustrated in Figure 3.5, which consisted of a rigid equipment mass supported by a helical spring. The equipment mass was excited by an electromagnetic shaker (LDS V201) along the centre axis of the helical spring. The shaker was driven with broadband noise. The characteristic properties of the equipment and the spring are listed in Table 3.2. Three accelerometers (PCB type 352C22) symmetrically attached to the top of the equipment were used to measure the acceleration response of the equipment. The outputs of these three accelerometers were averaged to eliminate the effect of any rotation. One accelerometer attached to the centre of the bottom of the helical spring was used to sense the acceleration response of the inelastic base, so that the transmissibility of the equipment to the base motion can be calculated. A dynamic signal analyser (Data Physics-Signalcalc Mobilyzer II) was used to both drive the system through a power amplifier (Ariston AX-910) and acquire the acceleration data above and below the isolator.

3.2.2.2 Experimental validation

As presented theoretically, the non-dimensional transmissibility of the passive vibration isolation system containing a rod isolator and its characteristics are given by equations (3.6), (3.10), (3.20), (3.24) and (3.25), respectively, in which $\Omega = \omega / \omega_e$,

$\omega_e = \sqrt{K_L / m_e}$, K_L is the static stiffness of the isolator, and μ_i is the ratio of the mass of the isolator to the mass of the equipment. The predicted results for the transmissibility of the experimental system can be obtained by substituting for the static stiffness of the helical spring and the ratio of the mass of the spring to the mass of the equipment into the corresponding equations. The static stiffness of a helical spring is given by [88]

$$K_s = \frac{Gd^4}{8nD^3} \tag{3.42}$$

where *G* is the shear modulus, *d* and *D* are wire diameter and mean diameter of the coil respectively and *n* is the number of active coils of the helical spring. The detailed derivation of the static stiffness of a helical spring is presented in Appendix B. The mass of the helical spring is given by

$$m_s = \frac{\pi^2 \rho N D d^2}{4} \tag{3.43}$$

where ρ and *N* are the density and the number of complete coils of the spring respectively. So the ratio of the mass of the helical spring to the mass of the equipment is given by

$$\mu_s = \frac{\pi^2 \rho N D d^2}{4 m_e} \tag{3.44}$$

Furthermore, the longitudinal IR frequencies in a helical spring can be predicted by

$$\omega_s = n\pi \sqrt{\frac{K_s}{m_s}} \text{ (in } rad/s) \ (n = 1, 2, 3...) \tag{3.45}$$

The detailed derivation can be found in Appendix B.

According to the parameters of the helical spring listed in Table 3.2, the appropriate static stiffness K_s was calculated as 5851 N/m and the mass ratio μ_s used in the experiment was calculated as 0.125.

Figure 3.6 shows the measured and predicted transmissibility with the characteristic lines and point of intersection. The first three IRs in the helical spring can clearly be observed between 200 and 800 Hz, which are well predicted (with less than 3% error) by equation (3.45) to be at 246.7 Hz, 493.4 Hz and 740.1 Hz. The experimental results

agree reasonably well with the prediction, although there are some small measured peaks between the resonance peaks possibly due to effects of rotational response. The undesirable effects of IRs in the distributed parameter isolator on the isolation performance compared to a massless isolator are clearly shown in the experimental results, with the transmissibility being greater than unity at the first IR as well as at the fundamental mounted resonance frequency. In addition, this result demonstrates that an equivalent elastic finite rod is a good representation for the distributed parameter model for a helical spring. The simple characteristic expressions shown in equations (3.10), (3.20) and (3.25) predict and describe the isolation performance of a distributed parameter isolator fairly accurately in the experiment.

3.3 System on a flexible base

In practice, the base structure is not usually rigid. Typically it possesses its own dynamics. Therefore, the performance and characteristics of a passive vibration isolation system containing a distributed parameter isolator on a flexible base are discussed in this section.

Figure 3.7 shows an isolated equipment represented by its impedance Z_e mounted on a structure that possesses its own dynamics and is represented by a base impedance Z_b under excitation of primary force f applied to the base. The distributed parameter isolator is modelled as a finite elastic rod. The equations of motion of such system are given by equations (3.1a, b) and

$$Z_b \dot{u}_b = f + Q_b = f - Q_1 \tag{3.46}$$

where Q_b is an internal force. The velocity of the equipment is thus given by [72]

$$\dot{u}_e = Y_{eb} f \tag{3.47}$$

where

$$Y_{eb} = \frac{-Z_{21}}{(Z_e + Z_{22})(Z_b + Z_{11}) - Z_{12}Z_{21}} \tag{3.48}$$

is the transfer mobility from the force, f on the base to the equipment velocity, $\dot{u}_e$ when the system is connected (the detailed derivation can be found in Appendix C).

If the equipment has a mass-like impedance, i.e. $Z_e = j\omega m_e$ and the base structure is modelled as a mass m_b on a complex spring, i.e. $K_b^* = K_b(1+j\eta_b)$, where η_b is the loss factor, the non-dimensional amplitude ratio of system can be written as

$$\frac{u_e}{\delta_{st}} = \frac{1}{\left[(1+j\eta_b)-\left(1+\frac{1}{\mu_b}\right)\frac{\Omega^2}{\Gamma^2}\right]\cos\left[\sqrt{\mu_i}\left(1-j\frac{\eta_i}{2}\right)\Omega\right]...}$$

$$...-\left[(1+j\eta_b)+\mu_k\mu_i(1+j\eta_i)-\frac{\Omega^2}{\Gamma^2}\right]\frac{\Omega}{\sqrt{\mu_i}}\left(1-j\frac{\eta_i}{2}\right)\sin\left[\sqrt{\mu_i}\left(1-j\frac{\eta_i}{2}\right)\Omega\right] \quad (3.49)$$

where u_e is the displacement of the equipment, $\delta_{st} = f/K_b$ is the static deflection of the base, $\Gamma = \omega_b/\omega_e = 1/\sqrt{\mu_k\mu_b}$ is the natural frequency ratio with $\omega_b = \sqrt{K_b/m_b}$ is the natural frequency of the base, $\mu_k = K_L/K_b$ is the stiffness ratio, and $\mu_b = m_b/m_e$ is the ratio of the mass of the supporting base structure to the mass of the mounted equipment.

Figure 3.8 depicts the amplitude ratio of the passive vibration isolation systems on a flexible base with a non-dispersive isolator. For comparison, the amplitude ratio of such a system containing a massless isolator is also plotted, where the first peak is the equipment resonance and the second peak is the base resonance. In order to exhibit the base resonance effects on the isolator IRs, the parameters of the system are chosen so that the base resonance occurs among the isolator IRs. It can be seen that the amplitude ratio for the distributed parameter isolator has the same peak at the equipment resonance as that for the massless isolator, but it is increased at relatively high frequencies due to the effects of IRs. The characteristic lines and point defined in the earlier discussion are also plotted to describe the amplitude ratio and included in Table 3.1, which are presented as follows:

- Maximum line

Similar to the derivation for the system undergoing base motion discussed in section 3.2.1.1, assuming light damping in the isolator and base, i.e. $\eta_i << 1$, $\eta_b << 1$ and considering the response when $\sin\left(\sqrt{\mu_i}\Omega\right) = 0$, the maximum line is given by

$$\left|\frac{u_e}{\delta_{st}}\right|_{\max} \approx \frac{2}{\eta_i}\frac{1}{\Omega^2}\frac{1}{\left|\left(1+\mu_k\mu_i-\frac{\Omega^2}{\Gamma^2}\right)\right|} \tag{3.50}$$

In practice, if $\mu_k = K_L / K_b << 1$ (flexible isolator compared to the base), and $\mu_i = \rho SL / m_e << 1$ (light isolator compared to the equipment), equation (3.50) can be written as

$$\left|\frac{u_e}{\delta_{st}}\right|_{\max} \approx \frac{2}{\eta_i}\frac{1}{\Omega^2}\frac{1}{\left|\left(1-\frac{\Omega^2}{\Gamma^2}\right)\right|} \tag{3.51}$$

This equation is a function of the loss factor η_i, frequency ratio Ω and natural frequency ratio Γ. Increasing damping in the isolator or decreasing the system fundamental resonance frequency are effective in attenuating the IR peaks. It should be also noted that, at frequencies much lower than the base resonance, i.e. $\Omega/\Gamma << 1$ the IR peaks in the isolator decrease at a rate of 40 dB per decade, while at frequencies much higher than the base resonance such that $\Omega/\Gamma >> 1$, the amplitude of IR peaks decrease at a rate of 80 dB per decade.

- Minimum line

Similar to the derivation for the system undergoing base motion discussed in section 3.2.1.1, assuming light damping in the isolator and base, i.e. $\eta_i << 1$, $\eta_b << 1$ and considering $\sin\left(\sqrt{\mu_i}\Omega\right) = \pm 1$, the minimum line is given by

$$\left|\frac{u_e}{\delta_{st}}\right|_{\min} \approx \sqrt{\mu_i}\frac{1}{\Omega}\frac{1}{\left|\left(1+\mu_k\mu_i-\frac{\Omega^2}{\Gamma^2}\right)\right|} \tag{3.52}$$

In practice, if $\mu_k << 1$ and $\mu_i << 1$, equation (3.52) can be written as

$$\left|\frac{u_e}{\delta_{st}}\right|_{\min} \approx \sqrt{\mu_i}\frac{1}{\Omega}\frac{1}{\left|\left(1-\frac{\Omega^2}{\Gamma^2}\right)\right|} \tag{3.53}$$

which is a function of the mass ratio μ_i, the frequency ratio Ω and the natural frequency ratio Γ. It can be seen that the minimum line tends to reduce at a rate of 20 dB per decade at frequencies much lower than the base resonance, rather than 40 dB per decade for the massless isolator. It reduces at a rate of 60 dB per decade at frequencies much higher than the base resonance, rather than 80 dB per decade for the massless isolator. It shows that the isolation performance for the distributed parameter isolator is much worse than that of the massless isolator at relatively high frequencies due to the IR effects. The minimum line is again independent of the isolator length. Therefore, to improve the performance of the isolator its mass or natural frequency can be adjusted by changing the isolator parameters except for the length.

- Crossing point for $\Gamma >> 1$

Assuming light damping in the isolator and base, i.e. $\eta_i << 1$, $\eta_b << 1$, also considering that the isolator mass is light compared to the equipment mass, i.e. $\mu_i << 1$, the amplitude ratio for a massless isolator can be written as

$$\left(\frac{u_e}{\delta_{st}}\right)_{massless} = \frac{1}{1-\left[1+\left(1+\frac{1}{\mu_b}-\Omega^2\right)\frac{1}{\Gamma_b^2}\right]\Omega^2} \tag{3.54}$$

which is identical to the amplitude ratio of a traditional two-stage isolation system containing massless isolators [2, 72]

If the base resonance frequency is much greater than the equipment resonance frequency, i.e. $\omega_b >> \omega_e$ so that $\Gamma >> 1$, the minimum line shown in equation (3.53) for the system on a flexible base can be reduced to the minimum line shown in equation (3.20) for the system undergoing base motion. Also, the amplitude ratio for a massless isolator shown in equation (3.54) can be reduced to the transmissibility for a massless isolator shown in equation (3.24) at frequencies much lower than the natural frequency of the base ω_b. Therefore, when $\Gamma >> 1$, the crossing point for the system on a flexible base is thus the same as that for the system undergoing base motion shown in equation (3.25).

3.4 Conclusions

Passive vibration isolation systems containing a distributed parameter isolator have been investigated theoretically and experimentally. A distributed parameter isolator has been modelled using different idealised configurations under various deformations. The isolators can be categorized into two types for the purpose of dynamic analysis, namely a non-dispersive isolator and a dispersive isolator. It has been shown that the isolation performance is significantly affected by IRs in both isolator types. Simple expressions which describe the behaviour for distributed parameter isolators have been derived. It has been shown that the damping in the isolator, the ratio of the isolator mass (or polar moment of inertia) to the equipment mass (or polar moment of inertia) and the system fundamental resonance frequency are all crucial to the isolation performance. Therefore, more efforts should be expended on lightly damped isolators, e.g. metallic isolators that have inherently low damping, in which the IRs may cause more significant detrimental effects. Also, it is concluded that, in general for the examples considered here, the IR effects in the non-dispersive isolator on the isolation performance are more significant than that for the dispersive isolator. The experiment on a helical spring has supported and validated the theoretical analysis and some of the predictions. Such models describe the isolation performance of a distributed parameter isolator fairly accurately.

The dynamic models developed in this chapter containing a non-dispersive isolator, which is modelled as finite elastic rod, will be used in the following discussion for the active vibration isolation with a distributed parameter isolator. The expressions for the maximum line, the minimum line and the crossing point reveal the parameters that dominate the isolation performance of the distributed parameter isolator at various frequencies. This offers basic guidelines for the isolation design of a distributed parameter isolator, which directs effective ways to improve the isolator performance. It is also beneficial to understanding the performance of active vibration isolation systems containing a distributed parameter isolator discussed in following chapters.

Isolator type	$\lvert T\rvert_{\max}$	$\lvert T\rvert_{\min}$	Crossing point $\left(\Omega,\ \lvert T\rvert\right)$
Non-dispersive isolator	$\frac{2}{\eta_i}\frac{1}{\Omega^2}$	$\sqrt{\mu_i}\frac{1}{\Omega}$	$\left(\frac{1}{\sqrt{\mu_i}},\ \mu_i\right)$
Dispersive isolator	$\sqrt{\frac{2\mu_i}{3}}\frac{2}{\eta_i}\frac{1}{\Omega}$	$\sqrt{\frac{\mu_i^3}{12}}\frac{1}{\sqrt{\Omega}}$	$\left(\sqrt[6]{12}\frac{1}{\sqrt{\mu_i}},\ \frac{1}{\sqrt[3]{12}}\mu_i\right)$

Table 3.1 *Characteristics of distributed parameter isolators undergoing base motion, where* Ω *is the non-dimensional frequency ratio,* η_i *is the loss factor in the isolator and* μ_i *is the ratio of the mass (or polar moment of inertia) of the isolator to the mass (or polar moment of inertia) of the equipment.*

Mass of the equipment	193.1 g (measured)
Shear modulus of the spring	7.93×10^{10} N / m^2 (supplier data)
Density of the spring	7900 kg / m^3 (supplier data)
Wire diameter of the spring	2.6 mm (supplier data)
Mean diameter of the coil of the spring	24 mm (supplier data)
Number of complete coils of the spring	7.6 (supplier data)
Number of active coils of the spring	5.6 (supplier data)

Table 3.2 *Characteristic properties of the experimental rig on a helical spring.*

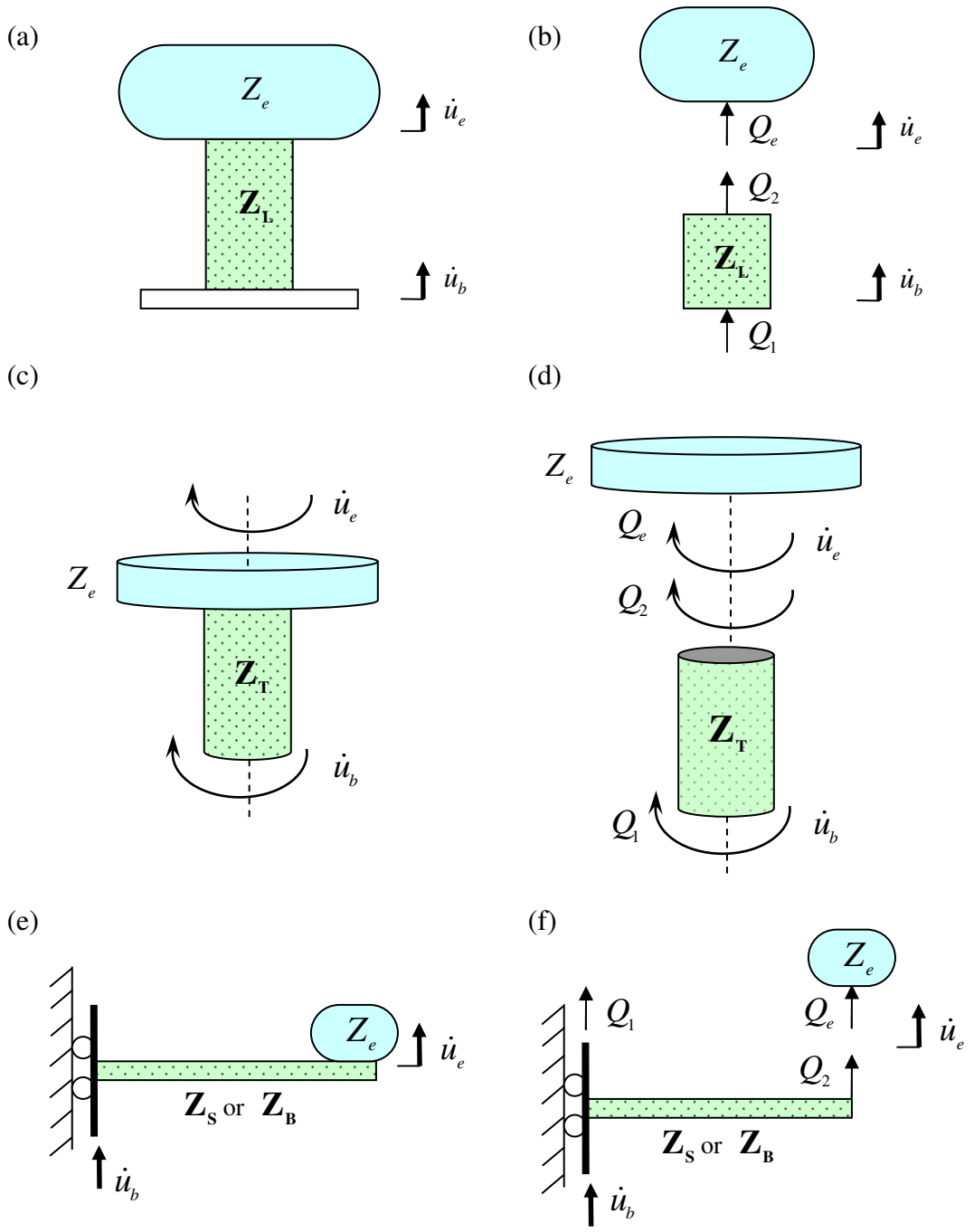

Figure 3.1 *Schematic diagrams of passive vibration isolation systems containing a distributed parameter isolator under (a) longitudinal, (c) torsional or (e) lateral vibration. (b), (d) and (f) are respectively free body diagrams.* Q_e, Q_1 *and* Q_2 *are the internal forces in (b) and (f), or moments in (d);* $\dot{u}_e$ *and* $\dot{u}_b$ *are velocities in (b) and (f), or angular velocities (d) of the equipment and the base respectively;* Z_e *is the input impedance of the equipment;* $\mathbf{Z_L}$ *and* $\mathbf{Z_T}$ *are the impedance matrices for the rod under longitudinal and torsional vibration, respectively; and* $\mathbf{Z_S}$ *and* $\mathbf{Z_B}$ *are the impedance matrices for the shear beam and Euler-Bernoulli beam, respectively.*

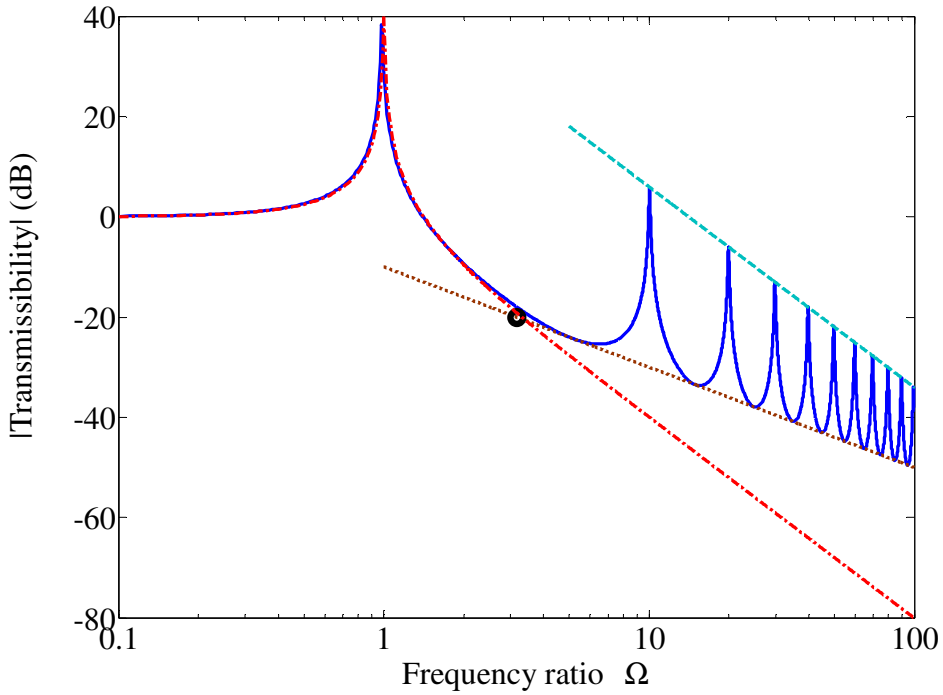

Figure 3.2 *Transmissibility of the passive vibration isolation systems with a non-dispersive isolator when the ratio of the mass of the isolator to the mass of the equipment* $\mu_i = 0.1$, *and the loss factor in the isolator* $\eta_i = 0.01$ *(solid line). The dashed line passes through the IR peaks. The dotted line passes through the troughs in the transmissibility. The dashed-dotted line is for the massless isolator. The point circled is the intersection of the transmissibilities for the system with a massless isolator and for the system with a non-dispersive isolator.*

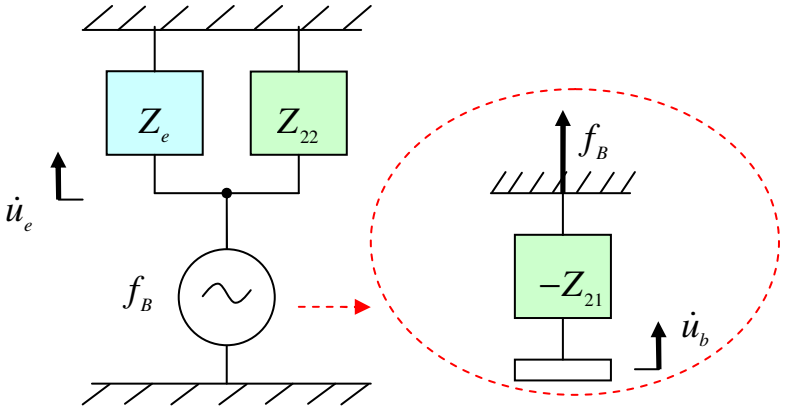

Figure 3.3 *Mechanical representation of the Thevenin equivalent system for the passive vibration isolation systems shown in Figure 3.1, where* Z_{21} *and* Z_{22} *are respectively the transfer and point impedances of the isolator and* f_B *is the blocked force.*

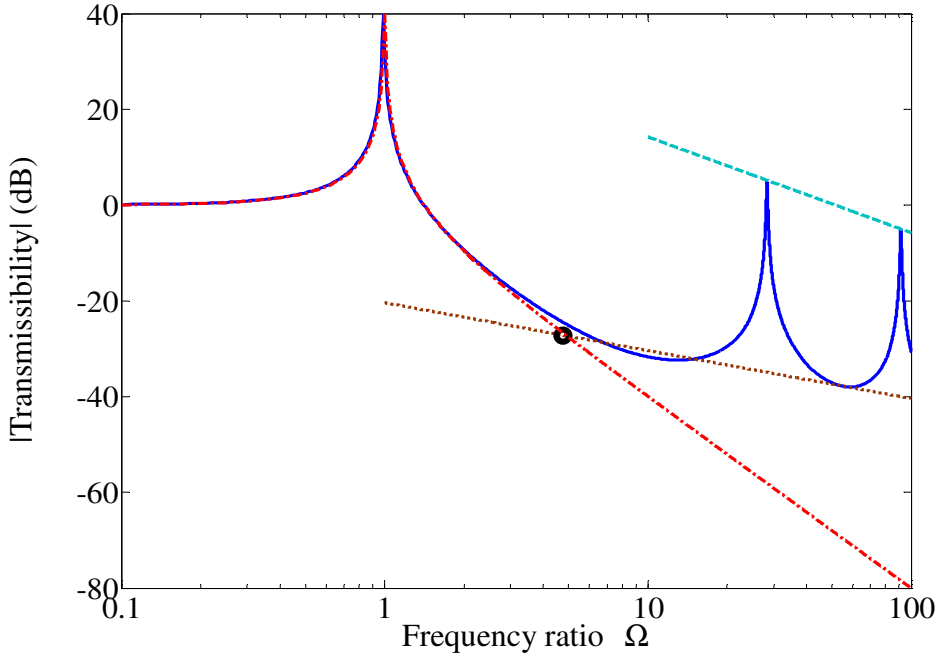

Figure 3.4 *Transmissibility of the passive vibration isolation system with a dispersive isolator when* $\mu_i = 0.1$ *and* $\eta_i = 0.01$ *(solid line). The dashed line passes through the IR peaks. The dotted line passes through the troughs in the transmissibility. The dashed-dotted line is for the massless isolator. The point circled is the intersection of the transmissibilities for the system with a massless isolator and for the system with a dispersive isolator.*

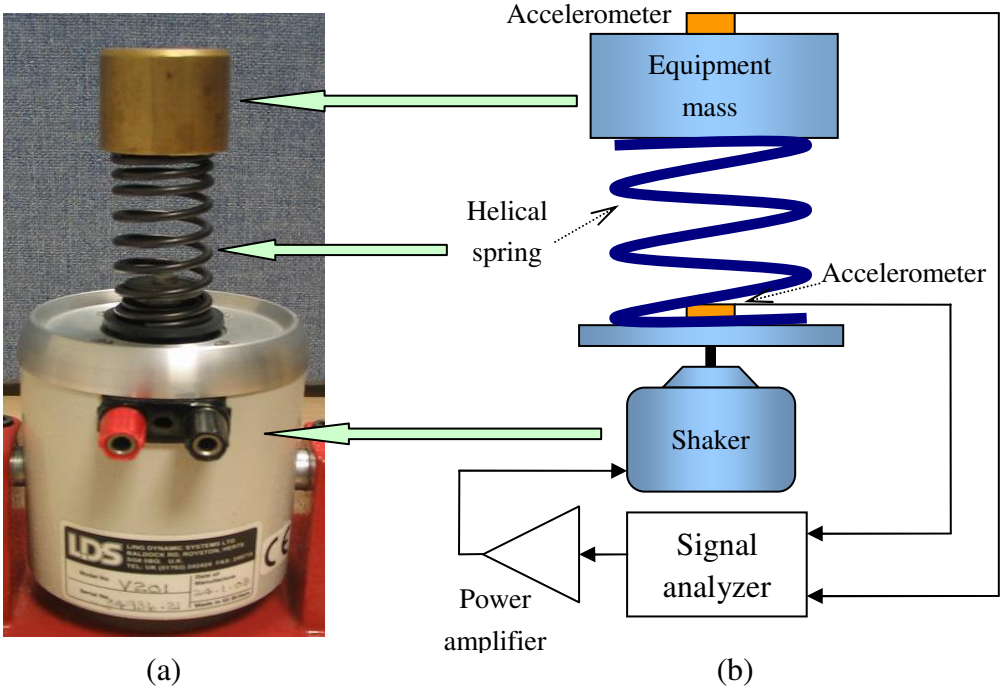

Figure 3.5 *(a) photograph and (b) schematic diagram of the experimental rig of a mass supported by a helical spring undergoing base motion.*

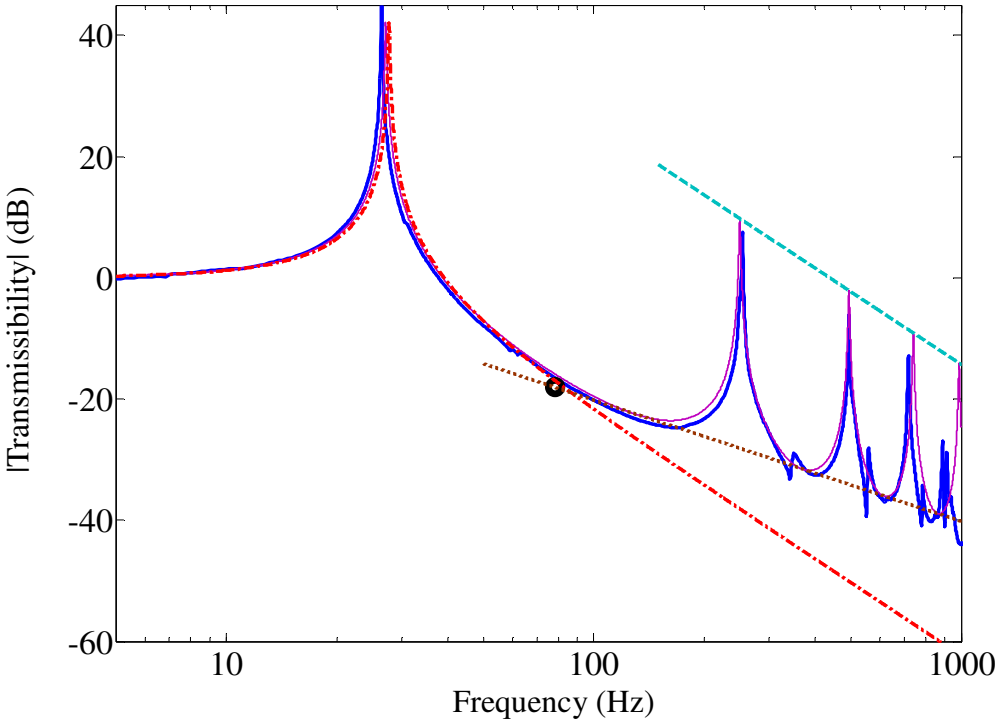

Figure 3.6 *Measured (solid bold) and predicted (solid faint) transmissibility of the experimental rig. The dashed line passes through the IR peaks. The dotted line passes through the troughs in the transmissibility. The dashed-dotted line is for the massless isolator. The point circled is the intersection of the transmissibilities for the system with a massless isolator and for the system with a distributed parameter isolator.*

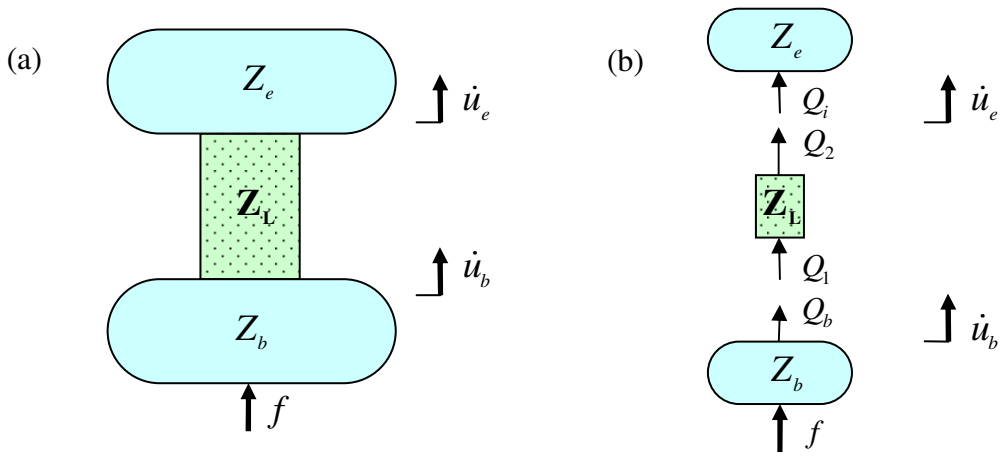

Figure 3.7 *(a) schematic diagram and (b) free body diagram of the passive vibration isolation system containing a distributed parameter isolator on a flexible base, where* f *is the primary force applied to the base,* Q_b *is an internal force and* Z_b *is the input impedance of the base.*

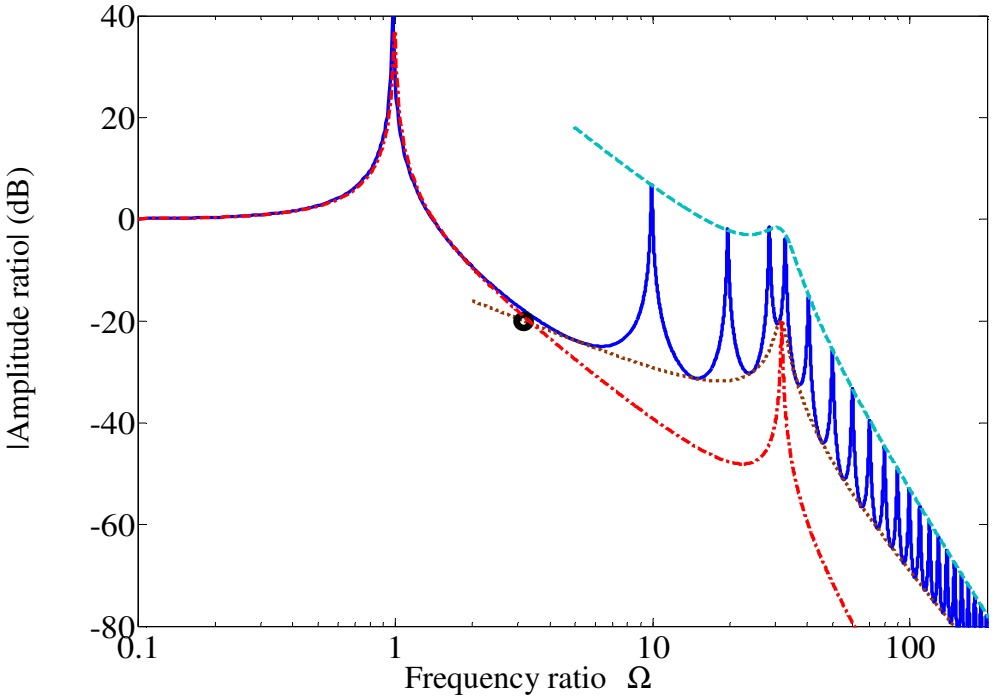

Figure 3.8 *Amplitude ratio of the passive vibration isolation system shown in Figure 3.7 when* $\mu_i = 0.1$, $\eta_i = 0.01$, *the ratio of the mass of the base to the mass of the equipment* $\mu_b = 0.1$, *the ratio of the static stiffness of the isolator to the stiffness of the base* $\mu_k = 0.01$ *and the loss factor in the base* $\eta_b = 0.01$ *(solid line). The dashed line passes through the IR peaks. The dotted line passes through the troughs in the amplitude ratio. The dashed-dotted line is for the massless isolator. The point circled is the intersection of the amplitude ratios for the system with a massless isolator and for the system with a distributed parameter isolator.*

Chapter 4

Active Vibration Isolation with a Distributed Parameter Isolator

4.1 Introduction

Passive vibration isolation systems containing a distributed parameter isolator have been discussed in Chapter 3. The significant detrimental effects of IRs in the isolator on the passive isolation performance and their characteristics have been investigated. With the development of computers fast enough to run control algorithms in real-time and more 'smart' materials, active devices have been widely used in vibration isolation to improve the isolation performance. However, stability and control performance are two crucial issues which may limit the application of active vibration isolation. Therefore, the effects of IRs in the isolator on the stability for commonly used control strategies in active vibration isolation need to be clarified. There is also a need to investigate the control performance around IRs in the isolator for these control strategies.

The aim of this chapter is to investigate theoretically the control performance and stability of active vibration isolation systems containing a distributed parameter isolator under various control strategies. First, active vibration isolation systems undergoing base motion is analyzed. Then the base structure is allowed to have its own resonances,

so that the effects of this on the control system can be investigated.

4.2 System undergoing base motion

In this section, active vibration isolation systems containing a distributed parameter isolator undergoing base motion are investigated. The control performance and stability of such systems are analyzed and compared for several control strategies.

4.2.1 Absolute Velocity Feedback (AVF) control

A base excited active vibration isolation system consisting of an isolated equipment represented by its impedance Z_e supported by a distributed parameter isolator under AVF control is shown in Figure 4.1. The isolator is modelled as a finite elastic rod. The control force f_a, which is in parallel with the isolator, acts between the equipment and the base. The control force is proportional to the velocity of the equipment, and fed back to the system through a feedback controller with a constant gain -*h*, which is given by equation (2.11).

4.2.1.1 Control performance

The dynamics of the system shown in Figure 4.1 can be described by equation (3.1b) and

$$Z_e \dot{u}_e = f_a + Q_e = f_a - Q_2 \tag{4.1}$$

The velocity of the equipment is thus given by

$$\dot{u}_e = \frac{1}{Z_e + Z_{22}} f_a + \frac{-Z_{21}}{Z_e + Z_{22}} \dot{u}_b \tag{4.2}$$

Substituting equation (2.11) into (4.2), the transmissibility of the system under AVF control is given by

$$T = \frac{\dot{u}_e}{\dot{u}_b} = \frac{-Z_{21}}{Z_e + Z_{22} + h} \tag{4.3}$$

If the equipment is modelled as a mass, i.e. $Z_e = j\omega m_e$, the transmissibility can be

written in non-dimensional form as

$$T = \frac{1}{\cos\left[\sqrt{\mu_i}\left(1 - j\frac{\eta_i}{2}\right)\Omega\right] - \frac{\Omega - j2\zeta_a}{\sqrt{\mu_i}}\left(1 - j\frac{\eta_i}{2}\right)\sin\left[\sqrt{\mu_i}\left(1 - j\frac{\eta_i}{2}\right)\Omega\right]} \tag{4.4}$$

where $\zeta_a = h/2\sqrt{K_L m_e}$ is the active damping ratio due to AVF control. It can be seen in equation (4.4) that AVF control adds a damping term to the denominator and leaves the numerator unchanged. Similar to the base excited system containing a massless isolator under AVF control discussed in Chapter 2, the action of absolute velocity feedback for base excited system containing a distributed parameter isolator is also the same as a skyhook damper. Figure 4.2 shows the mechanical representation of the AVF control system under base motion, where AVF control is equivalent to a viscous damper with damping coefficient *h* acting between the equipment and the inertial ground.

The transmissibility for this active vibration isolation system with different values of active damping ratio is plotted in Figure 4.3. It can be seen that the system fundamental resonance peak is attenuated when the active damping ratio is increased. However, little reduction at the IR peaks in the distributed parameter isolator is achieved by AVF control. The characteristic lines similar to those presented in Chapter 3 for the passive system are also plotted and identified in Figure 4.3. It should be noted that the AVF control system has almost the same maximum and minimum lines for IRs in the isolator as the passive system. These characteristic lines are determined as follows:

- Maximum line

Assuming light damping in the isolator, i.e. $\eta_i << 1$ in equation (4.4) and considering the response when $\sin\left(\sqrt{\mu_i}\Omega_e\right) = 0$, the maximum line of the transmissibility under AVF control is given by

$$\left|T\right|_{\max} \approx \frac{2}{\eta_i}\frac{1}{\left|\Omega\left(\Omega - j2\zeta_a\right)\right|} \tag{4.5}$$

At relatively high frequencies when $\Omega >> \zeta_a$, this equation can be reduced to equation (3.10), i.e. the system under AVF control and the passive system have equal amplitude resonance peaks at relatively high frequencies. This demonstrates that AVF control cannot suppress the IR peaks in the isolator at high frequencies.

The maximum line can also been derived from another point of view. The dynamics of the system described by equation (4.3) can be rearranged as

$$\left(Z_e + Z_{22} + h\right)\dot{u}_e = -Z_{21}\dot{u}_b = f_B \tag{4.6}$$

Based on this equation, the Thevenin equivalent system is depicted in Figure 4.4. It can be seen that, due to AVF control, the total impedance of the system which governs the equipment response is given by

$$Z_t = Z_e + Z_{22} + h \tag{4.7}$$

It is clear that the skyhook damper due to AVF control is effectively in parallel with the equipment. At relatively high frequencies, if the equipment has a mass-like impedance, i.e. $Z_e = j\omega m_e$ which increases with frequency, the equipment mass dominates the response, and the effect of AVF control is negligible. This explains why in Figure 4.3, little reduction is achieved at the IR peaks which occur at high frequencies. So at relatively high frequencies, equation (4.7) can be reduced to equation (3.16). Therefore, the transmissibility of the AVF control system can be simplified and given by equation (3.17) at relatively high frequencies. Similar to the descriptions in Chapter 3 for passive vibration isolation system, at IR frequencies for lightly damped isolators the blocked force f_B is given by equation (3.14), which is determined by the loss factor η_i and static stiffness K_L of the isolator. Therefore, the system under AVF control has the same maximum lines for IRs in the isolator as the passive system at relatively high frequencies.

- Minimum line

Assuming light damping in the isolator, i.e. $\eta_i << 1$, also considering $\sin\left(\sqrt{\mu_i}\Omega\right) = \pm 1$ in equation (4.4), the minimum line of the transmissibility under AVF control can be written as

$$\left|T\right|_{\min} \approx \sqrt{\mu_i}\,\frac{1}{\left|\Omega - j2\zeta_a\right|} \tag{4.8}$$

At relatively high frequencies when $\Omega >> \zeta_a$, this equation can be reduced to equation (3.20), i.e. the system under AVF control and the passive system have identical minimum lines at relatively high frequencies. So AVF control cannot reduce the minima of the transmissibility.

The minimum line can also be derived based on the Thevenin equivalent system shown in Figure 4.4. Similar to the description in Chapter 3, the minimum of the blocked force f_B for the AVF control system is also determined by equation (3.22). So the AVF control system has an identical minimum line to that of the passive system at relatively high frequencies.

4.2.1.2 Stability analysis

Because the feedback controller is a constant gain, the stability of the AVF control system can be analyzed by investigating the plant response of the system with unitary control gain (h=1). As shown in equation (4.2), for the base excited active vibration isolation system with a distributed parameter isolator under AVF control, the plant response from the active control force to the equipment velocity is given by

$$G = \left.\frac{\dot{u}_e}{f_a}\right|_{\dot{u}_b=0} = \frac{1}{Z_e + Z_{22}} \tag{4.9}$$

Because Z_e and Z_{22} are both point impedances, their phase is between -90º and 90º. Therefore the overall phase shift of the plant response G is between -90º and 90º, and is thus completely passive. Its Nyquist plot is entirely on the right-hand side of the complex plane and the feedback system has an infinite gain margin and a phase margin of at least 90º. Based on the Nyquist criterion, the AVF control system containing a distributed parameter isolator under base motion is unconditionally stable. From the point of view of collocation, because the base motion is prescribed which is not affected by the active control force, the actuator and the sensor are thus collocated, so that such a system under AVF control is unconditionally stable

4.2.2 Relative Velocity Feedback (RVF) control

A base excited system containing a distributed parameter isolator under RVF control is shown in Figure 4.5(a). A control force f_a in parallel with the isolator reacts between the equipment and the base. The control force is proportional to the difference between the velocity of the equipment and the velocity of the base, and fed back to the system through a feedback controller with a constant gain -h, which is given by equation (2.16).

4.2.2.1 Control performance

The velocity of the equipment is also given by equation (4.2). Substituting equation (2.16) into (4.2), the transmissibility of the system under RVF control is given by

$$T = \frac{\dot{u}_e}{\dot{u}_b} = \frac{-Z_{21} + h}{Z_e + Z_{22} + h} \tag{4.10}$$

If the equipment is modelled as a mass, the non-dimensional transmissibility under RVF control can be written as

$$T = \frac{1 + j2\zeta_a \frac{1}{\sqrt{\mu_i}}\left(1 - j\frac{\eta_i}{2}\right)\sin\left[\sqrt{\mu_i}\left(1 - j\frac{\eta_i}{2}\right)\Omega\right]}{\cos\left[\sqrt{\mu_i}\left(1 - j\frac{\eta_i}{2}\right)\Omega\right] - \frac{\Omega - j2\zeta_a}{\sqrt{\mu_i}}\left(1 - j\frac{\eta_i}{2}\right)\sin\left[\sqrt{\mu_i}\left(1 - j\frac{\eta_i}{2}\right)\Omega\right]} \tag{4.11}$$

It can be seen in equation (4.11) that a damping term is added to both the denominator and the numerator. Similar to the system containing a massless isolator under RVF control discussed in Chapter 2, the action of relative velocity feedback is the same as a viscous damper acting between the equipment and the base. Figure 4.5(b) shows the mechanical representation of the system under RVF control, which is equivalent to a viscous damper with damping coefficient *h* acting between the equipment and the base. Thus it is clear that the equivalent viscous damper due to RVF control is effectively in parallel with the distributed parameter isolator.

The transmissibility for the active vibration isolation system under RVF control is plotted in Figure 4.6, where the transmissibility of the corresponding passive system is also plotted for comparison. It can be seen that the system fundamental resonance peak and also some IR peaks in the isolator are attenuated with a high active damping ratio, which is a marginal advantage of RVF compared to AVF applied to the system containing a distributed parameter isolator. However, the transmissibility of the system is significantly amplified at high frequencies. This is because RVF control is equivalent to a viscous damper in parallel with the isolator, so that the compromise in the choice of damping inherent in passive vibration isolation occurs in this RVF control system. Characteristic lines for RVF control system are also plotted and identified in Figure 4.6. The two dashed-dotted lines namely maximum lines pass though the peaks at IR frequencies and the dotted line namely minimum line passes through the troughs

between IR peaks. These characteristic lines are determined as follows:

- Maximum line

Assuming light damping in the isolator, i.e. $\eta_i << 1$ in equation (4.11) and considering the response when $\sin\left(\sqrt{\mu_i}\Omega_e\right) = 0$, the maximum line of the transmissibility under RVF control is given by

$$\left|T\right|_{\max} \approx \frac{2}{\eta_i}\left|\frac{1 \pm \eta_i \zeta_a \Omega}{\Omega\left(\Omega - j2\zeta_a\right)}\right| \tag{4.12}$$

At relatively high frequencies when $\Omega >> \zeta_a$, this equation can be reduced to

$$\left|T\right|_{\max} \approx \left|1 \pm \eta_i \zeta_a \Omega\right| \frac{2}{\eta_i}\frac{1}{\Omega^2} \tag{4.13}$$

From this equation, it is clear that RVF control can either amplify or attenuate the IR peaks depending on the values of the active damping ratio ζ_a.

The maximum line can also be derived from another point of view. The dynamics of the system described in equation (4.10) can be rearranged as

$$\left(Z_e + Z_{22} + h\right)\dot{u}_e = \left(-Z_{21} + h\right)\dot{u}_b = f_B \tag{4.14}$$

Based on this equation, the Thevenin equivalent system is depicted in Figure 4.7. Due to RVF control, the total impedance of the system which governs the equipment response is also given by equation (4.7). At relatively high frequencies, if the equipment has a mass-like impedance, i.e. $Z_e = j\omega m_e$ which increases with frequency, the equipment mass dominates the response. Equation (4.7) can thus be reduced to equation (3.16). Therefore, at relatively high frequencies, the transmissibility of the system can be simplified and given by

$$T \approx \frac{-Z_{21} + h}{Z_e} \tag{4.15}$$

However, different from AVF control system, at IR frequencies for lightly damped isolators, the blocked force f_B for RVF control system is given by

$$f_B = \left(-Z_{21} + h\right)\dot{u}_b = \left(\pm\frac{2K_L}{\eta_i \omega} + h\right)\dot{u}_b \tag{4.16}$$

which is determined by not only the loss factor η_i and static stiffness K_L of the isolator, but also the feedback controller gain *h*. Therefore, RVF control may help to reduce the force transmitted to the equipment and the isolator at some IR frequencies so that the equipment response is attenuated, or it may increase the transmitted force at other IR frequencies so that the equipment response is amplified, especially at high frequencies. Combining equations (4.15) and (4.16), and noting that $Z_e = j\omega m_e$, the maximum line of the transmissibility under RVF control is given by

$$|T|_{\max} \approx \frac{\pm 2K_L + h\eta_i\omega}{\eta_i m_e \omega^2} = \left|1 \pm \eta_i \zeta_a \Omega\right| \frac{2}{\eta_i} \frac{1}{\Omega^2} \tag{4.17}$$

which is identical to the maximum line given by equation (4.13).

- Minimum line

Assuming light damping in the isolator, i.e. $\eta_i << 1$, also considering $\sin\left(\sqrt{\mu_i}\Omega\right) = \pm 1$ in equation (4.11), the minimum line of the transmissibility under RVF control can be written as

$$|T|_{\min} \approx \left| \frac{\sqrt{\mu_i} \pm j2\zeta_a}{\Omega - j2\zeta_a} \right| \tag{4.18}$$

At relatively high frequencies where $\Omega >> \zeta_a$, this equation can be reduced as

$$|T|_{\min} \approx \left|\sqrt{\mu_i} \pm j2\zeta_a\right| \frac{1}{\Omega} \tag{4.19}$$

Therefore, this minimum line for the transmissibility of the system under RVF control is greater than that for the passive system.

The minimum line can also be derived based on the Thevenin equivalent system shown in Figure 4.7. As discussed in Chapter 3, the minimum of the transfer impedance Z_{21} is given by equation (3.22). Substituting equation (3.22) into (4.15), the minimum line of the transmissibility under RVF control is given by

$$|T|_{\min} \approx \left| \frac{\pm j\sqrt{K_L m_i} + h}{j\omega m_e} \right| = \left|\sqrt{\mu_i} \pm j2\zeta_a\right| \frac{1}{\Omega} \tag{4.20}$$

which is identical to equation (4.19).

4.2.2.2 Stability analysis

For the active vibration isolation system under RVF control shown in Figure 4.5(a), the plant response from the active control force to the difference between the equipment velocity and the base velocity is also given by equation (4.9). Therefore, the RVF control system is also unconditionally stable and completely passive. The unconditional stability of the RVF control system undergoing base motion can also been concluded due to the collocation of the actuator and sensor.

4.2.3 Integral Force Feedback (IFF) control

A base excited active vibration isolation system containing a distributed parameter isolator under IFF control is shown in Figure 4.8. The control force f_a in parallel with the isolator reacts between the equipment and the base. The control force is generated by feeding the transmitted force to the equipment through a controller with frequency response $H_{\mathrm{IFF}}(j\omega)$ negatively, which is given by equation (2.19). Similar to the description for IFF control in Chapter 2, the transmitted force is given by equation (2.20) and the active control force is given by equation (2.21).

4.2.3.1 Control performance

The velocity of the equipment is also given by equation (4.2). Substituting equation (2.21) into (4.2), the transmissibility of the system under IFF control is given by

$$T = \frac{-Z_{21}}{Z_e + Z_{22} + \dfrac{h}{j\omega} Z_e} \tag{4.21}$$

If the equipment is modelled as a mass, i.e. $Z_e = j\omega m_e$, the transmissibility under IFF control can be written as

$$T = \frac{-Z_{21}}{Z_e + Z_{22} + h m_e} \tag{4.22}$$

Comparing equation (4.22) with (4.3) (the transmissibility of such a system under AVF

control), the action of IFF control applied to the system containing a mass-like equipment is also equivalent to a skyhook damper acting between the equipment and the inertial ground. However, this equivalent skyhook damper for IFF control has the damping coefficient of hm_e rather than h for AVF control. Therefore, this IFF control system has similar control performance as AVF control shown in Figure 4.3, depending on the feedback controller gain h and equipment mass m_e.

4.2.3.2 Stability analysis

Because the IFF controller is not a constant gain, to analyze the stability of the IFF control system, the open-loop frequency response of the system should be investigated. Combining equations (2.20) and (4.9), the plant response from the active control force to the transmitted force for the base excited system under IFF control is given by

$$G = \left.\frac{f_T}{f_a}\right|_{\dot{u}_b=0} = \frac{Z_e}{Z_e + Z_{22}} \tag{4.23}$$

So the open-loop frequency response of the system is described by

$$GH_{\text{IFF}} = \frac{h}{j\omega}\frac{Z_e}{Z_e + Z_{22}} \tag{4.24}$$

The stability of the IFF control system can be investigated by examining the reciprocal of the open-loop frequency response, which is given by

$$\left(GH_{\text{IFF}}\right)^{-1} = \left(hZ_e\right)^{-1} j\omega\left(Z_e + Z_{22}\right) = \frac{1}{h} j\omega\left(1 + Z_e^{-1}Z_{22}\right) \tag{4.25}$$

Z_e^{-1} is passive since Z_e is an input impedance, so that Z_e^{-1} has a phase shift between -90º and 90º. Because Z_{22} is a point impedance, its phase shift is also between -90º and 90º. The phase shift of $1 + Z_e^{-1}Z_{22}$ can thus potentially vary between -180º and 180º. Therefore the overall phase shift of $\left(GH_{\text{IFF}}\right)^{-1}$ is between -90º and 270º. The phase limitations on the open-loop frequency response are thus between -270º and 90º. Therefore, the base excited system containing a distributed parameter isolator under IFF system is only conditionally stable. The instability may occur when the equipment is stiffness controlled, i.e. the phase shift of Z_e^{-1} is 90º, so that the overall phase shift of the open-loop frequency response is between -270º and -90º. However, if the equipment

is rigid and has a mass-like impedance, i.e. $Z_e = j\omega m_e$, then the open-loop frequency response of the system in equation (4.24) can be reduced to $hm_e/(Z_e + Z_{22})$. The phase of the open-loop frequency response is thus restricted between -90º and 90º. The IFF control system is thus completely passive and unconditionally stable.

4.2.4 Positive Position Feedback (PPF) control

A base excited active vibration isolation system containing a distributed parameter isolator under PPF control is shown in Figure 4.9. The control force f_a in parallel with the isolator reacts between the equipment and the base. The control force is generated by feeding the displacement of the equipment through a controller with frequency response $H_{\mathrm{PPF}}(j\omega)$ in a positive sense. Similar to the description for PPF control in Chapter 2, the PPF control is implemented using an auxiliary dynamic system and the control force is given by equation (2.29).

4.2.4.1 Control performance

The velocity of the equipment is also given by equation (4.2). Substituting equation (2.29) into (4.2), the transmissibility of the system under PPF control is given by

$$T = \frac{-Z_{21}}{Z_e + Z_{22} - \dfrac{1}{j\omega}\dfrac{g\omega_f^2}{1-(\omega/\omega_f)^2 + j2\zeta_f\,\omega/\omega_f}} \tag{4.26}$$

If the equipment is modelled as a mass, i.e. $Z_e = j\omega m_e$, and the undamped natural frequency of the PPF controller ω_f is tuned to the system fundamental resonance frequency $\omega_e = \sqrt{K_L/m_e}$, the transmissibility of the system under PPF control can be written as

$$T = \frac{1}{\cos\left[\sqrt{\mu_i}\left(1 - j\frac{\eta_i}{2}\right)\Omega\right] - \dfrac{(1 - j\eta_i/2)}{\sqrt{\mu_i}}\left(\Omega + \dfrac{g}{m_e}\dfrac{1}{\Omega}\dfrac{1}{1-\Omega^2 + j2\zeta_f\Omega}\right)\sin\left[\sqrt{\mu_i}\left(1 - j\frac{\eta_i}{2}\right)\Omega\right]} \tag{4.27}$$

At frequencies much lower than the system fundamental resonance frequency, i.e.

$\Omega << 1$, assuming the damping in the isolator is small and using small angle approximations gives

$$\cos\left[\sqrt{\mu_i}\left(1-j\frac{\eta_i}{2}\right)\Omega\right]\approx 1$$
$$\sin\left[\sqrt{\mu_i}\left(1-j\frac{\eta_i}{2}\right)\Omega\right]\approx \sqrt{\mu_i}\Omega \qquad (4.28a,b)$$

Substituting equations (4.28a, b) into (4.27), and noting $\Omega << 1$ and $\eta_i << 1$, the transmissibility can be reduced to

$$T_{\Omega<<1}\approx\frac{1}{1-\frac{g}{m_e}} \qquad (4.29)$$

which is identical to equation (2.33) for PPF control applied to the system containing a massless isolator. Therefore, PPF control also adds a negative stiffness term $-g/m_e$ to the system containing a distributed parameter isolator, which may amplify the transmissibility of the system depending on the values of g and m_e. At the system fundamental resonance frequency, i.e. $\Omega = 1$, assuming the isolator is light compared to the equipment mass, i.e. $\mu_i << 1$, and the damping in the isolator is small, equations (4.28a, b) still hold true. Substituting equations (4.28a, b) into (4.27), and noting $\Omega = 1$ and $\eta_i << 1$, the transmissibility can be reduced to

$$T_{\Omega=1}\approx\frac{1}{j\frac{g}{m_e}\frac{1}{2\zeta_f}} \qquad (4.30)$$

As discussed in Chapter 2, the PPF controller has -90º phase shift at its cut-off frequency with high magnitude. PPF control is thus equivalent to a skyhook damper with damping ratio $g/\left(2\zeta_f m_e\right)$ around the system fundamental resonance frequency. Therefore, the system fundamental resonance peak can be effectively attenuated. At frequencies well above the system fundamental resonance frequency, i.e. $\Omega >> 1$, the frequency response of the PPF controller rolls off rapidly, and thus the effect of PPF control is negligible. Therefore, the IR peaks which occur at relatively high frequencies cannot be attenuated by PPF control when ω_f is tuned to ω_e.

Figure 4.10 shows the transmissibility for the active vibration isolation system containing a distributed parameter isolator under PPF control with various values for control gain g. It can be seen that the system fundamental resonance peak is attenuated by PPF control. However, the transmissibility is amplified at frequencies lower than the system fundamental resonance frequency due to the negative stiffness determined by the specific values of g and m_e. Also, the IR peaks in the distributed parameter isolator are not reduced by PPF control because the frequency response of the PPF controller rolls off rapidly at high frequencies.

4.2.4.2 Stability analysis

Due to the IRs in the isolator, the method used in Chapter 2 to analyze the stability of the PPF control system containing a massless isolator, which is a SDOF system, is not applicable for the PPF control system containing a distributed parameter isolator. Therefore, the Nyquist stability criterion is used to analyze the stability of such a system. From equation (4.9), the plant response from the active control force to the displacement of the equipment is given by

$$G = \left.\frac{u_e}{f_a}\right|_{\dot{u}_b=0} = \left.\frac{u_e / j\omega}{f_a}\right|_{\dot{u}_b=0} = \frac{1}{j\omega\left(Z_e + Z_{22}\right)} \tag{4.31}$$

Because the PPF controller is not a constant gain, the open-loop frequency response is used to analyze the stability, which is given by

$$GH_{\text{PPF}} = \frac{1}{j\omega\left(Z_e + Z_{22}\right)} \cdot \frac{g\omega_f^2}{1-\left(\omega/\omega_f\right)^2 + j2\zeta_f\,\omega/\omega_f} \tag{4.32}$$

The phase shift of $1/\left(Z_e + Z_{22}\right)$ is between -90º and 90º, so that the phase shift of the first term $1/j\omega\left(Z_e + Z_{22}\right)$ is between -180º and 0º. The phase shift of the PPF controller can potentially vary between -180º and 0º. Therefore the overall phase shift of the open-loop frequency response is between -360º and 0º. Based on the Nyquist stability criterion, such a PPF control system containing a distributed parameter isolator is only conditionally stable.

4.2.5 Acceleration-Position Feedback (APF) control

A base excited active vibration isolation system containing a distributed parameter isolator under APF control is shown in Figure 4.11. A control force f_a in parallel with the isolator reacts between the equipment and the base. The control force is generated by feeding the acceleration of the equipment through a second order low-pass filter with frequency response $H_{\mathrm{APF}}(j\omega)$ in a negative sense, which is given by equation (2.40).

4.2.5.1 Control performance

The velocity of the equipment is also given by equation (4.2). Substituting equation (2.40) into (4.2), the transmissibility of the system under APF control is given by

$$T = \frac{-Z_{21}}{Z_e + Z_{22} + h\dfrac{j2\zeta_f\,\omega/\omega_f}{1-(\omega/\omega_f)^2 + j2\zeta_f\,\omega/\omega_f}} \tag{4.33}$$

It can be seen that, around the natural frequency of the APF controller, i.e. $\omega = \omega_f$, the transmissibility can be reduced to equation (4.3), which is the transmissibility of such a system under AVF control. Therefore APF control is also equivalent to a skyhook damper around its natural frequency. However, at frequencies much lower or higher than its natural frequency, the effects of APF control are negligible because the active APF control force rolls off rapidly. So the APF controller has less spillover to both low and high frequency modes. As a consequence, the IR peaks which occur at relatively high frequencies cannot be attenuated by APF control.

If the equipment is modelled as a mass, i.e. $Z_e = j\omega m_e$, and the natural frequency of the APF controller ω_f is tuned to the system fundamental resonance frequency ω_e, the transmissibility of the system under APF control can be written as

$$T = \frac{1}{\cos\left[\sqrt{\mu_i}\left(1-j\frac{\eta_i}{2}\right)\Omega\right] - \dfrac{(1-j\eta_i/2)}{\sqrt{\mu_i}}\left(\Omega - j2\zeta_a\dfrac{j2\zeta_f\Omega}{1-\Omega^2+j2\zeta_f\Omega}\right)\sin\left[\sqrt{\mu_i}\left(1-j\frac{\eta_i}{2}\right)\Omega\right]} \tag{4.34}$$

Figure 4.12 shows the transmissibility for the active vibration isolation system

containing a distributed parameter isolator under APF control with various values for active damping ratio ζ_a. It can be seen that the transmissibility is attenuated around the system fundamental resonance frequency with an increase in the active damping ratio due to APF control. However, the transmissibility close to the system fundamental resonance frequency is amplified, since the PPF controller behaves as a dynamic vibration absorber. Also, the IR peaks which occur at relatively high frequencies are not reduced by APF control, because the active APF control force rolls off rapidly at high frequencies.

4.2.5.2 Stability analysis

From equation (4.9), the plant response from the active control force to the acceleration of the equipment is given by

$$G = \left.\frac{\ddot{u}_e}{f_a}\right|_{\dot{u}_b=0} = \left.\frac{j\omega\dot{u}_e}{f_a}\right|_{\dot{u}_b=0} = \frac{j\omega}{Z_e + Z_{22}} \tag{4.35}$$

Because the APF controller is not a constant gain, the open-loop frequency response is used to analyze the stability, which is given by

$$GH_{\text{APF}} = \frac{j\omega}{Z_e + Z_{22}} \cdot \left(h \frac{2\zeta_f / \omega_f}{1 - \left(\omega/\omega_f\right)^2 + j2\zeta_f \, \omega/\omega_f} \right) \tag{4.36}$$

The phase shift of $1/\left(Z_e + Z_{22}\right)$ is between -90º and 90º, so that the phase shift of the first term $j\omega/\left(Z_e + Z_{22}\right)$ is between 0º and 180º. Because the APF controller is a second order low-pass filter, its phase shift can thus potentially vary between -180º and 0º. Therefore the overall phase shift of the open-loop frequency response is between -180º and 180º. the APF control system containing a distributed parameter isolator undergoing base motion is thus unconditionally stable based on the Nyquist stability criterion. However, such an APF control system is not passive, and thus not robustly stable. It is sensitive to the unmodelled actuator dynamics and other uncertainties in the system which might destabilize the control system.

4.2.6 Comparison of the control performance

Similar to the discussion in Chapter 2 for the massless isolator, the comparison of the overall control performance for the active vibration isolation systems containing a distributed parameter isolator under above discussed control strategies can be realized by looking at their change in mean square response compared to the original passive system. Substituting the corresponding transmissibility into equation (2.46), the change in mean square velocity for the system under different control strategies compared to the passive system can be calculated. The equivalent active damping ratio for PPF control is also set to be $\zeta_a = g/\left(2\zeta_f m_e\right)$.

Figure 4.13 depicts the change in mean square velocity within the range $0.1 < \Omega < 1000$ when $\mu_i = 0.1$, $\eta_i = 0.01$, $m_e = 0.5$, $\zeta_f = 0.5$ and $\omega_f = \omega_e$. At high active damping ratios, AVF and IFF control provides increasing reduction in the mean square response. The performance of IFF control is determined by the mass of the equipment. In this case the mass of the equipment is 0.5, which is less than unity, the control performance of IFF control is therefore worse than AVF control. The RVF, PPF and APF control do not produce monotonically reducing mean square response for an increasing in active damping ratio. Furthermore, the instability of PPF control is seen to occur when the active damping ratio is increased.

4.2.7 Acceleration feedback control

A base excited active vibration isolation system containing a distributed parameter isolator under acceleration feedback control is shown in Figure 4.14(a). The control force f_a in parallel with the isolator reacts between the equipment and the base. The control force is proportional to the acceleration of the equipment, and fed back to the system through a feedback controller with a constant gain –*h*, which is given by equation (2.45).

4.2.7.1 Control performance

The velocity of the equipment is also given by equation (4.2). Substituting equation (2.45) into (4.2), the transmissibility of the system under acceleration feedback control is given by

$$T = \frac{-Z_{21}}{Z_e + Z_{22} + j\omega h} \tag{4.37}$$

If the equipment is modelled as a mass, the transmissibility can be written as

$$T = \frac{1}{\cos\left[\sqrt{\mu_i}\left(1 - j\frac{\eta_i}{2}\right)\Omega\right] - \frac{1}{\sqrt{\mu_i}}\left(1 + \frac{h}{m_e}\right)\Omega\left(1 - j\frac{\eta_i}{2}\right)\sin\left[\sqrt{\mu_i}\left(1 - j\frac{\eta_i}{2}\right)\Omega\right]} \tag{4.38}$$

Different from the aforementioned control strategies that all introduce active damping to the system, the action of acceleration feedback control for this base excited system is equivalent to adding a mass h on top of the equipment as shown in Figure 4.14(b).

Figure 4.15 shows the transmissibility for the active vibration isolation system containing a distributed parameter isolator under acceleration feedback control, where the transmissibility of such a system without control is also plotted for comparison. It can be seen that the system fundamental resonance peak moves to a lower frequency due to the acceleration feedback control, and thus the transmissibility at high frequencies including the IR peaks in the isolator is reduced. The effective attenuation of IR peaks in the isolator is the main advantage of acceleration feedback control over other control strategies.

4.2.7.2 Stability analysis

For acceleration feedback control, because the controller is a constant gain, the plant response of the system from the active control force to the acceleration of the equipment can be used for the stability analysis, which is given by equation (4.35). The overall phase shift of the plant response is between 0º and 180º, and thus the acceleration feedback control system containing a distributed parameter isolator undergoing base motion is unconditionally stable. However, such a control system is not completely passive, and thus not robustly stable.

4.2.8 Optimal control

Similar to the discussion in Chapter 2, to find out the best control strategy in attenuating the equipment response, the optimal control for active vibration isolation system containing a distributed parameter isolator undergoing base motion is investigated. Figure 4.16 shows a base excited system containing a distributed parameter isolator under optimal control. The equipment is modelled as a rigid mass. The distributed parameter isolator is modelled as a mass-spring-mass-spring-mass system in order to derive the state space representations for the optimal control system. Also the damping in the isolator is ignored for simplicity. The equations of motion for such a system are

$$\begin{aligned} &(m_e + m)\ddot{u}_e + k(u_e - u_l) = f_a \\ &m\ddot{u}_l + k(u_l - u_e) + k(u_l - u_b) = 0 \end{aligned} \tag{4.39a,b}$$

where u_l and $\ddot{u}_l$ are respectively the displacement and the acceleration of the middle mass, and

$$k = 2K_L, \qquad m = \frac{1}{3}m_i \tag{4.40a,b}$$

Equations (4.39a, b) can be rearranged to give

$$\begin{aligned} \ddot{u}_e &= -\frac{k}{m_e + m}u_e + \frac{k}{m_e + m}u_l + \frac{1}{m_e + m}f_a \\ \ddot{u}_l &= \frac{k}{m}u_e - \frac{2k}{m}u_l + \frac{k}{m}u_b \end{aligned} \tag{4.41a,b}$$

The state-space system equation is then given by:

$$\dot{\mathbf{x}} = \mathbf{A}\mathbf{x} + \mathbf{b}f_a + \mathbf{d}u_b \tag{4.42}$$

where

$$\mathbf{x} = \begin{bmatrix} u_e \\ \dot{u}_e \\ u_l \\ \dot{u}_l \end{bmatrix}, \ \mathbf{A} = \begin{bmatrix} 0 & 1 & 0 & 0 \\ \frac{-k}{m_e + m} & 0 & \frac{k}{m_e + m} & 0 \\ 0 & 0 & 0 & 1 \\ \frac{k}{m} & 0 & \frac{-2k}{m} & 0 \end{bmatrix}, \ \mathbf{b} = \begin{bmatrix} 0 \\ \frac{1}{m_e + m} \\ 0 \\ 0 \end{bmatrix}, \ \mathbf{d} = \begin{bmatrix} 0 \\ 0 \\ 0 \\ \frac{k}{m} \end{bmatrix} \tag{4.43a,b,c,d}$$

The general quadratic performance index required to be minimized is also given by

equation (2.52), in which the matrices $\mathbf{Q}$ and $\mathbf{R}$ are given by

$$\mathbf{Q}=\begin{bmatrix}0&0&0&0\\0&q&0&0\\0&0&0&0\\0&0&0&0\end{bmatrix}\ (q\geq 0),\ \mathbf{R}=[r]\ (r>0) \tag{4.44a,b}$$

The performance index has thus the same form as equation (2.54), where q is a weighting on the mean square velocity of the equipment mass and r is a weighting on the mean square control effort applied. The control force required to minimize the performance index is then given by equation (2.55), where

$$\mathbf{P}=\begin{bmatrix}p_{11}&p_{12}&p_{13}&p_{14}\\p_{12}&p_{22}&p_{23}&p_{24}\\p_{13}&p_{23}&p_{33}&p_{34}\\p_{14}&p_{24}&p_{34}&p_{44}\end{bmatrix} \tag{4.45}$$

is a positive-definite real symmetric matrix to ensure the control is stable, and satisfies the reduced-matrix Riccati equation given by equation (2.57). Substituting the appropriate matrices into equation (2.55), the optimal control force can be written as

$$f_a=-\frac{1}{r}\frac{1}{m_e+m}\left(p_{12}u_e+p_{22}\dot{u}_e+p_{23}u_l+p_{24}\dot{u}_l\right) \tag{4.46}$$

Therefore, only the four elements of the second row in **P** matrix are required to calculate the optimal control force. Substituting the appropriate matrices into the reduced-matrix Riccati equation, four equations in terms of p_{12}, p_{22}, p_{23} or p_{24} can be derived as

$$\begin{aligned}
&2p_{12}-\frac{1}{r\left(m_e+m\right)^2}p_{22}^2+q=0\\
&-\frac{2k}{m_e+m}p_{12}-\frac{1}{r\left(m_e+m\right)^2}p_{12}^2+\frac{2k}{rm\left(m_e+m\right)^2}p_{22}p_{24}-\frac{2k}{m}p_{23}=0\\
&\frac{2k}{m_e+m}p_{23}-\frac{1}{r\left(m_e+m\right)^2}p_{23}^2-\frac{2k}{rm\left(m_e+m\right)^2}p_{24}^2=0\\
&\frac{k}{m_e+m}p_{12}-\frac{1}{r\left(m_e+m\right)^2}p_{12}p_{23}+\frac{k}{2rm\left(m_e+m\right)^2}\left(p_{24}^2-4p_{22}p_{24}\right)+\frac{k\left(2m_e+m\right)}{m\left(m_e+m\right)}p_{23}=0
\end{aligned} \tag{4.47a,b,c,d}$$

From equations (4.47a-d), the only solution for the second row of the **P** matrix that ensures the **P** matrix is positive-definite and real is given by

$$\left[p_{12},\ p_{22},\ p_{23},\ p_{24}\right]=\left[0,\ \sqrt{rq}\left(m_e+m\right),\ 0,\ 0\right] \tag{4.48}$$

Substituting equation (4.48) into (4.46), the optimal control force can be written as

$$f_a = -\sqrt{\frac{q}{r}}\dot{u}_e \tag{4.49}$$

which is identical to equation (2.65) for the system containing a massless isolator. Therefore, the optimal control strategy to minimise the mean square velocity of the equipment mass supported by a distributed parameter isolator is also precisely the AVF control, which results in skyhook damping of the controlled system. The feedback control gain for optimal control is again given by $\sqrt{q/r}$, which is a simple function of the ratio of the relative penalty on minimising mean square equipment velocity response and mean square control effort. The smaller the control effort weighting *r*, the higher the feedback control gain, and thus the better the control performance.

4.2.9 Summary

The control performance and stability of the base excited system containing a distributed parameter isolator under different control strategies have been investigated and compared. Similar to the system containing a massless isolator, AVF control introduces skyhook damping to the system containing a distributed parameter isolator, which is effective in attenuating the system fundamental resonance peak. However, the IR peaks in the isolator cannot be attenuated by AVF control because the equipment mass dominates the response at high frequencies. AVF control has been shown to be robustly stable for the base excited system. RVF control is equivalent to a viscous damper between the equipment and the base. Thus the isolation performance at high frequency is degraded although some IR peaks can be attenuated. The RVF control system has been shown to be unconditionally stable. For the base excited system, if the equipment is a rigid mass, IFF control also introduces skyhook damping to the system and is unconditionally stable. However, the IFF control system may become unstable when the equipment is stiffness controlled. Both PPF and APF controllers are second order filters that introduce active damping at the system fundamental resonance frequency, and then roll off rapidly at high frequencies, so that they are not effective in

attenuating the IR peaks at high frequencies. Also PPF control may cause amplification at low frequencies due to the negative stiffness introduced, which may destabilize the PPF control system. The APF controller is not robustly stable and thus very sensitive to the unmodelled actuator dynamics and other uncertainties in the system which might destabilize the control system. Acceleration feedback control applied to the base excited system containing a distributed parameter isolator is equivalent to adding mass onto the equipment, so that the system fundamental resonance peak moves to a lower frequency, and thus the IR peaks in the isolator at high frequencies is reduced. The study for optimal control shows that, to minimise the mean square velocity of the equipment mass supported by a distributed parameter isolator, AVF control is the optimal solution.

4.3 System on a flexible base

In this section, active vibration isolation systems containing a distributed parameter isolator on a flexible base are investigated. The control performance and stability of such systems under several control strategies are analyzed and compared.

4.3.1 Absolute Velocity Feedback (AVF) control

An active vibration isolation system containing a distributed parameter isolator on a flexible base under AVF control is shown in Figure 4.17. The isolator is modelled as a finite elastic rod. The control force f_a, which is in parallel with the isolator, reacts between the equipment and the base. The control force is given by equation (2.11).

4.3.1.1 Control performance

The dynamics of the system shown in Figure 4.17 can be described by equations (3.1b), (4.1) and

$$Z_b \dot{u}_b = f - f_a + Q_b = f - f_a - Q_1 \tag{4.50}$$

The velocity of the equipment is thus given by

$$\dot{u}_e = \left(Y_{ee} - Y_{eb}\right) f_a + Y_{eb} f \tag{4.51}$$

where

$$Y_{ee} = \frac{Z_b + Z_{11}}{\left(Z_e + Z_{22}\right)\left(Z_b + Z_{11}\right) - Z_{12}Z_{21}} \tag{4.52}$$

is the input mobility of the equipment when coupled to the rest of the system. A detailed derivation is given in Appendix C. Substituting equation (2.11) into (4.51), the velocity of the equipment under AVF control can be written as

$$\frac{\dot{u}_e}{f} = \frac{Y_{eb}}{1 + h\left(Y_{ee} - Y_{eb}\right)} \tag{4.53}$$

If the equipment has a mass-like impedance, i.e. $Z_e = j\omega m_e$ and the base structure is modelled as a mass m_b on a complex spring, i.e. $K_b^* = K_b(1 + j\eta_b)$, the non-dimensional amplitude ratio of the system under AVF control is given by

$$\frac{u_e}{\delta_{st}} = \frac{1}{\left[\left(1 + j\eta_b\right) - \left(1 + \frac{1}{\mu_b}\right)\frac{\Omega^2}{\Gamma^2}\right]\cos\left[\sqrt{\mu_i}\left(1 - j\frac{\eta_i}{2}\right)\Omega\right]...}$$

$$...-\left[\left(1 + j\eta_b\right) + \mu_k\mu_i\left(1 + j\eta_i\right) - \frac{\Omega^2}{\Gamma^2}\right]\frac{\Omega}{\sqrt{\mu_i}}\left(1 - j\frac{\eta_i}{2}\right)\sin\left[\sqrt{\mu_i}\left(1 - j\frac{\eta_i}{2}\right)\Omega\right]...$$

$$...+ j2\zeta_a\left\{\begin{array}{l}\mu_k\Omega\left[\cos\left(\sqrt{\mu_i}\left(1 - j\frac{\eta_i}{2}\right)\Omega\right) - 1\right]... \\ ...+\frac{1}{\sqrt{\mu_i}}\left(1 - j\frac{\eta_i}{2}\right)\left(1 + j\eta_b - \frac{\Omega^2}{\Gamma^2}\right)\sin\left(\sqrt{\mu_i}\left(1 - j\frac{\eta_i}{2}\right)\Omega\right)\end{array}\right\} \tag{4.54}$$

It can be seen in equation (4.54) that the absolute velocity feedback adds a damping term to the denominator and leaves the numerator unchanged. Figure 4.18 shows the amplitude ratio for the system on a flexible base under AVF control with different values of the active damping ratio ζ_a. It can be seen that the equipment resonance peak is attenuated with an increase in the active damping ratio. The base resonance peak, which is the second peak in Figure 4.18, is also reduced for high active damping ratios. However, the IR peaks in the distributed parameter isolator are reduced much less, especially at relatively high frequencies. The reason is the same as that discussed for the base excited system under AVF control. The equipment mass rather than AVF control

dominates the response at high frequencies. Also it should be noted that some IR peaks in the distributed parameter isolator, such as the third peak in Figure 4.18, are amplified due to AVF control. This amplification may destabilize the control system at high control gains, and thus the control performance at system resonance frequencies is limited.

4.3.1.2 Stability analysis

From equation (4.51), the plant response from the active control force to the velocity of the equipment is given by

$$G = \left.\frac{\dot{u}_e}{f_a}\right|_{f=0} = Y_{ee} - Y_{eb} \tag{4.55}$$

From the point of view of the definitions of the input and transfer mobility, Y_{ee} is the response of the equipment per unit external force applied directly on the equipment, and Y_{eb} is the response of the equipment per unit external force applied to the base. Because Y_{ee} is an input mobility, it has a phase shift between -90º and 90º so that it is only in the right half in the complex plane. However, Y_{eb} is a transfer mobility, which could be in either left or right half in the complex plane. So it is a potential threat to the stability of the AVF control system. Moreover, if the AVF control system is only conditionally stable, there is at least one loop in the left half of the complex plane which crosses the negative real axis in the Nyquist plot of the plant response. For the system analyzed here, only at resonance frequencies can phase of the plant response generate such loops, and hence create an unstable system. Therefore, at some resonance frequencies, if the transfer mobility Y_{eb} is greater than the input mobility Y_{ee}, i.e. the equipment response due to the excitation at the base is greater than that due to the excitation at the equipment, and they are in phase, the AVF control system has the potential to become unstable at high control gains. A stability condition for such an AVF control system is derived as follows.

For a multi-degree-of freedom system, the mobility can be written as [19]

$$Y_{ts} = \frac{\dot{u}_t}{f_s} = \sum_{j=1}^{\infty} \frac{j\omega \cdot \phi_t^{(j)} \cdot \phi_s^{(j)}}{K_j \left(1 - \Omega_j^2 + j2\zeta_j \Omega_j\right)} \tag{4.56}$$

where $\phi_t^{(j)}$ and $\phi_s^{(j)}$ are respectively the j^{th} modal amplitudes evaluated at the response point *t* and excitation point *s*; K_j, M_j and ζ_j are respectively the modal stiffness, modal mass and modal damping ratio of the j^{th} mode with corresponding natural frequency $\omega_j = \sqrt{K_j / M_j}$; $\Omega_j = \omega / \omega_j$ is the non-dimensional frequency ratio.

Based on equation (4.56), at a resonance frequency with corresponding natural frequency $\omega_j = \sqrt{K_j / M_j}$, in a lightly damped system, when only one mode dominates the response, the input and transfer mobility for the system can be written as

$$Y_{ee} \approx \frac{\left[\phi_e^{(j)}\right]^2}{2\sqrt{K_j M_j}\zeta_j}, \qquad Y_{eb} \approx \frac{\left(\phi_b^{(j)} \phi_e^{(j)}\right)}{2\sqrt{K_j M_j}\zeta_j} \tag{4.57a,b}$$

where $\phi_e^{(j)}$ and $\phi_b^{(j)}$ are the j^{th} modal amplitudes evaluated at the equipment and base respectively. Substituting equations (4.57a, b) into (4.55), the plant response can be rearranged as

$$G = Y_{ee} - Y_{eb} \approx \frac{\left[\phi_e^{(j)}\right]^2 \left(1 - \dfrac{\phi_b^{(j)}}{\phi_e^{(j)}}\right)}{2\sqrt{K_j M_j}\zeta_j} \tag{4.58}$$

Based on the Nyquist criterion, for stability, one requires at a resonant frequency

$$\frac{\phi_b^{(j)}}{\phi_e^{(j)}} < 1 \tag{4.59}$$

for all *j*, i.e. $\left|\phi_e^{(j)}\right| > \left|\phi_b^{(j)}\right|$ if the modal amplitudes of the system evaluated at the equipment and base have the same phase. Therefore, equation (4.59) provides a simple method to determine the stability of the AVF control system in terms of the modal amplitudes of the system. According to the definition of modal amplitudes $\phi_e^{(j)}$ and $\phi_b^{(j)}$, this stability condition means that if the displacement of the base is greater than the displacement of the equipment and these two displacements are in phase at the j^{th} natural frequency, then the system may become unstable. This stability condition can direct the investigation into the approaches which can stabilize such a control system. This stability condition in terms of the modal amplitudes can also be applied to the

system containing a massless isolator on a flexible base, which has been investigated by Elliott et al. [41].

Figures 4.19 and 4.20 respectively depict the frequency response and Nyquist plot of the plant response for a potentially unstable AVF control system. It is clear in Figure 4.19 that the phase shift of the first IR peak in the isolator is less than -180º. This phase lag thus generates a loop on the left half of the complex plane in Figure 4.20 that crosses the negative real axis, which causes the system to be potentially unstable at high control gains. It can be shown that, at this first IR frequency, the displacement of the base is greater than the displacement of the equipment and they are in phase, so that instability may potentially occur.

At a resonance frequency where $\phi_b^{(j)} / \phi_e^{(j)} > 1$, i.e. the system has the potential to become unstable, with constant control gain h, the open-loop frequency response is given by

$$hG = h \frac{\left[\phi_e^{(j)}\right]^2 \left(1 - \dfrac{\phi_b^{(j)}}{\phi_e^{(j)}}\right)}{2\sqrt{K_j M_j}\,\zeta_j} \tag{4.60}$$

To guarantee stability, the quantity in equation (4.60) must be greater than -1, so that the maximum gain $h_{\max}$ that can be applied to the control system is thus given by

$$h_{\max} = \frac{2\sqrt{K_j M_j}\,\zeta_j}{\left[\phi_{\mathrm{e}}^{(j)}\right]^2 \left(\dfrac{\phi_{\mathrm{b}}^{(j)}}{\phi_{\mathrm{e}}^{(j)}} - 1\right)} \tag{4.61}$$

4.3.2 Relative Velocity Feedback (RVF) control

An active vibration isolation system containing a distributed parameter isolator on a flexible base under RVF control is shown in Figure 4.21. The control force f_a, which is in parallel with the isolator, reacts between the equipment and the base. The control force is given by equation (2.16).

4.3.2.1 Control performance

The velocity of the equipment under RVF control is also given by equation (4.51). Substituting equation (2.16) into (4.51), the velocity of the equipment under RVF control can be written as

$$\frac{\dot{u}_e}{f} = \frac{Y_{eb} + h(Y_{ee}Y_{bb} - Y_{eb}{}^2)}{1 + h(Y_{ee} + Y_{bb} - 2Y_{eb})} \tag{4.62}$$

where Y_{bb} is the input mobility of the base when coupled to the rest of the system, and is given by

$$Y_{bb} = \frac{Z_e + Z_{22}}{(Z_e + Z_{22})(Z_b + Z_{11}) - Z_{12}Z_{21}} \tag{4.63}$$

If the equipment has a mass-like impedance, i.e. $Z_e = j\omega m_e$ and the base structure is modelled as a mass m_b on a complex spring, i.e. $K_b^* = K_b(1 + j\eta_b)$, the non-dimensional amplitude ratio of the system under RVF control can be written as

$$\frac{u_e}{\delta_{st}} = \frac{1 + j2\zeta_a \frac{1}{\sqrt{\mu_i}}\left(1 - j\frac{\eta_i}{2}\right)\sin\left[\sqrt{\mu_i}\left(1 - j\frac{\eta_i}{2}\right)\Omega\right]}{\left[(1 + j\eta_b) - \left(1 + \frac{1}{\mu_b}\right)\frac{\Omega^2}{\Gamma^2}\right]\cos\left[\sqrt{\mu_i}\left(1 - j\frac{\eta_i}{2}\right)\Omega\right]...}$$

$$...-\left[(1 + j\eta_b) + \mu_k\mu_i(1 + j\eta_i) - \frac{\Omega^2}{\Gamma^2}\right]\frac{\Omega}{\sqrt{\mu_i}}\left(1 - j\frac{\eta_i}{2}\right)\sin\left[\sqrt{\mu_i}\left(1 - j\frac{\eta_i}{2}\right)\Omega\right]...$$

$$...+ j2\zeta_a\left\{\begin{array}{l} 2\mu_k\Omega\left[\cos\left(\sqrt{\mu_i}\left(1 - j\frac{\eta_i}{2}\right)\Omega\right) - 1\right]... \\ ...+ \frac{1}{\sqrt{\mu_i}}\left(1 - j\frac{\eta_i}{2}\right)\left[1 + j\eta_b - \left(1 + \frac{1}{\mu_b}\right)\frac{\Omega^2}{\Gamma^2}\right]\sin\left(\sqrt{\mu_i}\left(1 - j\frac{\eta_i}{2}\right)\Omega\right) \end{array}\right\} \tag{4.64}$$

It can be seen in equation (4.64) that the relative velocity feedback adds a damping term both to the denominator and the numerator. Figure 4.22 shows the amplitude ratio for the system under RVF control with different values of the active damping ratio. It can be seen that the system resonance peaks and some IR peaks in the distributed parameter isolator are attenuated with high active damping ratio. However, the amplitude ratio between resonance peaks and at relative high frequencies is amplified due to RVF control.

4.3.2.2 Stability analysis

The velocity of the base under RVF control is given by

$$\dot{u}_b = \left(Y_{eb} - Y_{bb}\right) f_a + Y_{bb} f \tag{4.65}$$

Combining equations (4.51) and (4.65), for the system under RVF control, the plant response from the active control force to the difference between velocity of the equipment and the velocity of the base is given by

$$G = \left.\frac{\dot{u}_e - \dot{u}_b}{f_a}\right|_{f=0} = Y_{ee} + Y_{bb} - 2Y_{eb} \tag{4.66}$$

At a resonance frequency, in a lightly damped system, when only one mode dominates the response, the input mobility of the base can be written as

$$Y_{bb} \approx \frac{\left[\phi_b^{(j)}\right]^2}{2\sqrt{K_j M_j}\zeta_j} \tag{4.67}$$

Substituting equations (4.57a, b) and (4.67) into (4.66), the plant response is given by

$$G = Y_{ee} + Y_{bb} - 2Y_{eb} \approx \frac{\left[\phi_e^{(j)} - \phi_b^{(j)}\right]^2}{2\sqrt{K_j M_j}\zeta_j} \tag{4.68}$$

which is always non-negative. Therefore, the Nyquist plot of the plant response of the RVF control system is always in the right half in the complex plane, and thus the RVF control system is unconditionally stable. This is the main advantage of RVF control.

From the point of view of the energy, the time averaged power generated by the active control force for the system under RVF control at any particular frequency can be written as [19]

$$P_{f_a} = \frac{1}{2}\mathrm{Re}\left\{f_a \cdot \dot{u}_e'\right\} + \frac{1}{2}\mathrm{Re}\left\{-f_a \cdot \dot{u}_b'\right\} \tag{4.69}$$

Substituting equation (2.16) into (4.69) gives

$$P_{f_a} = -\frac{1}{2} h \left|\dot{u}_e - \dot{u}_b\right|^2 \tag{4.70}$$

Therefore, the power generated by the control force is always negative. That means the RVF control law is designed such that energy can only be extracted from the mechanical structure. The RVF control system is thus unconditionally stable, and also said to be dissipative [89].

4.3.3 Integral Force Feedback (IFF) control

An active vibration isolation system containing a distributed parameter isolator on a flexible base under IFF control is shown in Figure 4.23. The control force f_a, which is in parallel with the isolator, reacts between the equipment and the base. The control force is given by equation (2.21).

4.3.3.1 Control performance

The velocity of the equipment under IFF control is given by equation (4.51). Substituting equation (2.21) into (4.51), the velocity of the equipment under IFF control can be written as

$$\frac{\dot{u}_e}{f} = \frac{Y_{eb}}{1 + \frac{h}{j\omega} Z_e \left(Y_{ee} - Y_{eb} \right)} \tag{4.71}$$

If the equipment has a mass-like mobility, i.e. $Z_e = j\omega m_e$, the velocity of the equipment under IFF control is given by

$$\frac{\dot{u}_e}{f} = \frac{Y_{eb}}{1 + h m_e \left(Y_{ee} - Y_{eb} \right)} \tag{4.72}$$

Comparing equations (4.72) with (4.53) (the velocity of the equipment of such a system under AVF control), it can be seen that the IFF control applied to the system containing a mass-like equipment is similar to AVF control. The only difference is that the control gain for IFF control is hm_e rather than h for AVF control. Therefore, this IFF control system has similar control performance as AVF control, depending on the feedback controller gain h and equipment mass m_e.

4.3.3.2 Stability analysis

Combining equations (2.20) and (4.55), the plant response from the active control force to the transmitted force for the system on a flexible base under IFF control is given by

$$G = \left. \frac{f_T}{f_a} \right|_{f=0} = Z_e \left(Y_{ee} - Y_{eb} \right) \tag{4.73}$$

So the open-loop frequency response of the IFF control system is described by

$$GH_{\text{IFF}} = \frac{h}{j\omega} Z_e \left(Y_{ee} - Y_{eb} \right) \tag{4.74}$$

Due to the effect of the transfer mobility Y_{eb}, the IFF control system containing a distributed parameter isolator on a flexible base is only conditionally stable. If the equipment has a mass-like mobility, the open-loop frequency response can be written as

$$GH_{\text{IFF}} = hm_e \left(Y_{ee} - Y_{eb} \right) \tag{4.75}$$

Because hm_e is a constant gain, similar to the AVF control system on a flexible base, the stability condition for such a IFF control system is also given by equation (4.59) in terms of modal amplitudes.

4.3.4 Positive Position Feedback (PPF) control

An active vibration isolation system containing a distributed parameter isolator on a flexible base under PPF control is shown in Figure 4.24. The control force f_a, which is in parallel with the isolator, reacts between the equipment and the base. The active control force is given by equation (2.29).

4.3.4.1 Control performance

The velocity of the equipment under PPF control is given by equation (4.51). Substituting equation (2.29) into (4.51), the velocity of the equipment under PPF control can be written as

$$\frac{\dot{u}_e}{f} = \frac{Y_{eb}}{1 - \dfrac{1}{j\omega} \dfrac{g\omega_f^2}{1 - \left(\omega / \omega_f \right)^2 + j2\zeta_f \, \omega / \omega_f} \left(Y_{ee} - Y_{eb} \right)} \tag{4.76}$$

If the equipment has a mass-like impedance, i.e. $Z_e = j\omega m_e$, the base structure is modelled as a mass m_b on a complex spring, i.e. $K_b^* = K_b(1 + j\eta_b)$, and the undamped natural frequency of the PPF controller ω_f is tuned to the system fundamental resonance frequency $\omega_e = \sqrt{K_L / m_e}$, the non-dimensional amplitude ratio of the system under PPF control is given by

$$\frac{u_e}{\delta_{st}} = \frac{1}{\left[\left(1+j\eta_b\right)-\left(1+\frac{1}{\mu_b}\right)\frac{\Omega^2}{\Gamma^2}\right]\cos\left[\sqrt{\mu_i}\left(1-j\frac{\eta_i}{2}\right)\Omega\right]...}$$

$$...-\left[\left(1+j\eta_b\right)+\mu_k\mu_i\left(1+j\eta_i\right)-\frac{\Omega^2}{\Gamma^2}\right]\frac{\Omega}{\sqrt{\mu_i}}\left(1-j\frac{\eta_i}{2}\right)\sin\left[\sqrt{\mu_i}\left(1-j\frac{\eta_i}{2}\right)\Omega\right]...$$

$$...-\frac{g}{m_e}\frac{1}{1-\Omega^2+j2\zeta_f\Omega}\left\{\begin{array}{l}\mu_k\left[\cos\left(\sqrt{\mu_i}\left(1-j\frac{\eta_i}{2}\right)\Omega\right)-1\right]... \\ ...+\frac{1}{\Omega}\frac{1}{\sqrt{\mu_i}}\left(1-j\frac{\eta_i}{2}\right)\left(1+j\eta_b-\frac{\Omega^2}{\Gamma^2}\right)\sin\left(\sqrt{\mu_i}\left(1-j\frac{\eta_i}{2}\right)\Omega\right)\end{array}\right\} \tag{4.77}$$

Assuming damping in the isolator and in the base is small, i.e. $\eta_i << 1$ and $\eta_b << 1$, and considering the base resonance frequency to be much greater than the system fundamental resonance frequency, i.e. $\Gamma >> 1$, equations (4.29) and (4.30) still hold valid respectively at low frequencies and around the system fundamental resonance frequency for the PPF control system on a flexible base. Figure 4.25 shows the amplitude ratio for the system under PPF control with various values for control gain *g*. It can be seen that the equipment resonance peak is attenuated by PPF control with an increase in the control gain *g*. However, the amplitude ratio is amplified at frequencies lower than the system fundamental resonance frequency due to the negative stiffness introduced by PPF control. Also, the base resonance peak and the IR peaks in the distributed parameter isolator are not reduced by PPF control because the frequency response of the PPF controller rolls off rapidly at high frequencies.

4.3.4.2 Stability analysis

From equation (4.55), the plant response from the active control force to the displacement of the equipment is given by

$$G = \left.\frac{u_e}{f_a}\right|_{f=0} = \left.\frac{\dot{u}_e / j\omega}{f_a}\right|_{f=0} = \frac{1}{j\omega}\left(Y_{ee} - Y_{eb}\right) \tag{4.78}$$

The open-loop frequency response of the PPF control system is thus given by

$$GH_{\text{PPF}} = \frac{1}{j\omega}\left(Y_{ee} - Y_{eb}\right)\frac{g\omega_f^2}{1-\left(\omega/\omega_f\right)^2 + j2\zeta_f\,\omega/\omega_f} \tag{4.79}$$

Due to the effect of the transfer mobility Y_{eb} and the PPF controller, the PPF control system containing a distributed parameter isolator on a flexible base is only conditionally stable.

4.3.5 Acceleration-Position Feedback (APF) control

An active vibration isolation system containing a distributed parameter isolator on a flexible base under APF control is shown in Figure 4.26. The control force f_a, which is in parallel with the isolator, reacts between the equipment and the base. The active control force is given by equation (2.40).

4.3.5.1 Control performance

The velocity of the equipment under APF control is given by equation (4.51). Substituting equation (2.40) into (4.51), the velocity of the equipment under APF control can be written as

$$\frac{\dot{u}_e}{f} = \frac{Y_{eb}}{1 + h\dfrac{j2\zeta_f\,\omega/\omega_f}{1-\left(\omega/\omega_f\right)^2 + j2\zeta_f\,\omega/\omega_f}\left(Y_{ee} - Y_{eb}\right)} \tag{4.80}$$

It can be seen that, around the natural frequency of the APF controller, i.e. $\omega = \omega_f$, equation (4.80) can be reduced to equation (4.53), which is the velocity of the equipment of such a system under AVF control. However, at frequencies much lower or higher than its natural frequency, the effects of APF control are negligible so that the IR peaks which occur at relatively high frequencies cannot be attenuated by APF control.

If the equipment has a mass-like impedance, i.e. $Z_e = j\omega m_e$, the base structure is modelled as a mass m_b on a complex spring, i.e. $K_b^* = K_b(1 + j\eta_b)$, and the natural frequency of the APF controller ω_f is tuned to the system fundamental resonance frequency ω_e, the amplitude ratio of the system under APF control can be written as

$$\frac{u_e}{\delta_{st}} = \frac{1}{\left[\left(1+j\eta_b\right)-\left(1+\frac{1}{\mu_b}\right)\frac{\Omega^2}{\Gamma^2}\right]\cos\left[\sqrt{\mu_i}\left(1-j\frac{\eta_i}{2}\right)\Omega\right]...}$$

$$...-\left[\left(1+j\eta_b\right)+\mu_k\mu_i\left(1+j\eta_i\right)-\frac{\Omega^2}{\Gamma^2}\right]\frac{\Omega}{\sqrt{\mu_i}}\left(1-j\frac{\eta_i}{2}\right)\sin\left[\sqrt{\mu_i}\left(1-j\frac{\eta_i}{2}\right)\Omega\right]...$$

$$...+j2\zeta_a\frac{j2\zeta_f\Omega}{1-\Omega^2+j2\zeta_f\Omega}\left\{\begin{array}{l}\mu_k\Omega\left[\cos\left(\sqrt{\mu_i}\left(1-j\frac{\eta_i}{2}\right)\Omega\right)-1\right]... \\ ...+\frac{1}{\sqrt{\mu_i}}\left(1-j\frac{\eta_i}{2}\right)\left(1+j\eta_b-\frac{\Omega^2}{\Gamma^2}\right)\sin\left(\sqrt{\mu_i}\left(1-j\frac{\eta_i}{2}\right)\Omega\right)\end{array}\right\} \tag{4.81}$$

Figure 4.27 shows the amplitude ratio for the system under APF control with various values for active damping ratio ζ_a. It can be seen that the amplitude ratio is attenuated around the equipment resonance frequency with an increase in the active damping ratio due to APF control. However, the amplitude ratio close to the system fundamental resonance frequency is amplified. Also, the base resonance peak and IR peaks in the distributed parameter isolator are not reduced by APF control, because the active APF control force rolls off rapidly at high frequencies.

4.3.5.2 Stability analysis

From equation (4.55), the plant response from the active control force to the acceleration of the equipment is given by

$$G = \left.\frac{\ddot{u}_e}{f_a}\right|_{f=0} = \left.\frac{j\omega\dot{u}_e}{f_a}\right|_{f=0} = j\omega\left(Y_{ee}-Y_{eb}\right) \tag{4.82}$$

The open-loop frequency response of the APF control system is thus given by

$$GH_{\text{APF}} = j\omega\left(Y_{ee}-Y_{eb}\right)\left(h\frac{2\zeta_f/\omega_f}{1-\left(\omega/\omega_f\right)^2+j2\zeta_f\,\omega/\omega_f}\right) \tag{4.83}$$

Due to the effect of the transfer mobility Y_{eb}, the APF control system containing a distributed parameter isolator on a flexible base is only conditionally stable.

4.3.6 Comparison of control performance

The comparison of the overall control performance for the active vibration isolation systems containing a distributed parameter isolator on a flexible base under above discussed control strategies can be realized by looking at their change in mean square response compared to the original passive system. The relationship between the power spectral densities of the primary disturbance applied on the base and equipment response can be written as [83]

$$S_e = \left|\frac{u_e}{\delta_{st}}\right|^2 S_b \tag{4.84}$$

The mean square displacement of the equipment is thus given by [83]

$$\overline{u_e^2} = \int_{-\infty}^{+\infty} S_e d\Omega = \int_{-\infty}^{+\infty} \left|\frac{u_e}{\delta_{st}}\right|^2 S_b d\Omega \tag{4.85}$$

Substituting the corresponding amplitude ratio into equation (4.85), the change in mean square displacement for the system under different control strategies compared to the passive system can be calculated. The equivalent active damping ratio for PPF control is also set to be $\zeta_a = g/\left(2\zeta_f m_e\right)$

Figure 4.28 depicts the change in mean square displacement within the range $0.1 < \Omega < 1000$ when $\mu_i = 0.1$, $\mu_b = 0.5$, $\mu_k = 0.01$, $\eta_i = \eta_b = 0.01$, $m_e = 0.5$, $\zeta_f = 0.5$ and $\omega_f = \omega_e$. At high active damping ratios, AVF and IFF control provides increasing reduction in the mean square response. The performance of IFF control is determined by the mass of the equipment. In this case the mass of the equipment is 0.5, which is less than unity, the control performance of IFF control is therefore worse than AVF control. The RVF, PPF and APF control do not produce monotonically reducing mean square response for an increasing in active damping ratio. For the parameters given in this case, AVF, IFF and APF control remains stable for the given range of the active damping ratio. However, the instability of PPF control is seen to occur when the active damping ratio is increased. Although the behaviour shown in Figure 4.28 is

similar to the case when the base is rigid, the additional mode due to the dynamics of the base has a negative contribution to the reduction of the mean square response.

4.3.7 Acceleration feedback control

An active vibration isolation system containing a distributed parameter isolator on a flexible base under acceleration feedback control is shown in Figure 4.29. The control force f_a, which is in parallel with the isolator, reacts between the equipment and the base. The active control force is given by equation (2.45).

4.3.7.1 Control performance

The velocity of the equipment under acceleration control is given by equation (4.51). Substituting equation (2.45) into (4.51), the velocity of the equipment under acceleration feedback control can be written as

$$\frac{\dot{u}_e}{f} = \frac{Y_{eb}}{1 + j\omega h\left(Y_{ee} - Y_{eb}\right)} \tag{4.86}$$

If the equipment has a mass-like impedance, i.e. $Z_e = j\omega m_e$ and the base structure is modelled as a mass m_b on a complex spring, i.e. $K_b^* = K_b(1 + j\eta_b)$, the amplitude ratio of the system under acceleration feedback control can be written as

$$\frac{u_e}{\delta_{st}} = \frac{1}{\left[\left(1 + j\eta_b\right) - \left(1 + \frac{1}{\mu_b}\right)\frac{\Omega^2}{\Gamma^2}\right]\cos\left[\sqrt{\mu_i}\left(1 - j\frac{\eta_i}{2}\right)\Omega\right]...}$$

$$...-\left[\left(1 + j\eta_b\right) + \mu_k\mu_i\left(1 + j\eta_i\right) - \frac{\Omega^2}{\Gamma^2}\right]\frac{\Omega}{\sqrt{\mu_i}}\left(1 - j\frac{\eta_i}{2}\right)\sin\left[\sqrt{\mu_i}\left(1 - j\frac{\eta_i}{2}\right)\Omega\right]...$$

$$...-\frac{h}{m_e}\Omega\left\{\begin{array}{l}\mu_k\Omega\left[\cos\left(\sqrt{\mu_i}\left(1 - j\frac{\eta_i}{2}\right)\Omega\right) - 1\right]... \\ ...+\frac{1}{\sqrt{\mu_i}}\left(1 - j\frac{\eta_i}{2}\right)\left(1 + j\eta_b - \frac{\Omega^2}{\Gamma^2}\right)\sin\left(\sqrt{\mu_i}\left(1 - j\frac{\eta_i}{2}\right)\Omega\right)\end{array}\right\} \tag{4.87}$$

Figure 4.30 shows the amplitude ratio for the system under acceleration feedback control, where the amplitude ratio of the system without control is also plotted for comparison. It can be seen that the equipment resonance peak moves to a lower

frequency due to the acceleration feedback control. As a consequence, the amplitude ratio at high frequencies including the base resonance peak and IR peaks in the isolator is reduced.

4.3.7.2 Stability analysis

For acceleration feedback control, the plant response from the active control force to the acceleration of the equipment is given by equation (4.82). Again, due to the effect of the transfer mobility Y_{eb}, the acceleration feedback control system containing a distributed parameter isolator on a flexible base is only conditionally stable.

4.3.8 Summary

The control performance and stability of the active vibration isolation system containing a distributed parameter isolator on a flexible base under different control strategies have been investigated and compared. The control strategies which can introduce active damping, such as AVF, RVF, IFF, PPF and APF, are effective in attenuating the equipment resonance peak. However, the IR peaks in the isolator cannot be attenuated by these control strategies because the equipment mass dominates the response at high frequencies. If the equipment is a rigid mass, IFF control is equivalent to AVF control. PPF control may cause amplification at low frequencies due to the negative stiffness introduced. Also APF control causes some amplification close to the system fundamental resonance frequency. Furthermore, for the system on a flexible base, AVF, IFF, PPF and APF control systems are only conditionally stable. A stability condition in terms of modal amplitudes has been proposed for AVF control. In contrast, the RVF control system on a flexible base remains unconditionally stable, although its control performance at high frequencies is degraded. Different from other control strategies, acceleration feedback control can reduce the IR peaks in the isolator at high frequencies. However, as a compromise, the equipment resonance peak moves to a lower frequency and cannot be reduced by acceleration feedback control.

4.4 Conclusions

Active vibration isolation systems containing a distributed parameter isolator, which is modelled as a finite elastic rod, under various control strategies have been investigated and compared in this chapter. The different control strategies have their own advantages and disadvantages in isolating a piece of equipment supported by a distributed parameter isolator. It has been shown that AVF control is again an optimal solution to minimise the mean square velocity of the equipment mass. A stability condition in terms of modal amplitudes has been proposed for AVF control system on a flexible base containing a distributed parameter isolator. The theoretical analysis for AVF control system discussed in this chapter is validated experimentally in the next chapter. Also, based on the proposed stability condition, approaches which can stabilize the AVF control system on a flexible base are investigated in the following chapter. The positive effect of acceleration feedback control at high frequencies gives a clue in attenuating the IR peaks in the distributed parameter isolator.

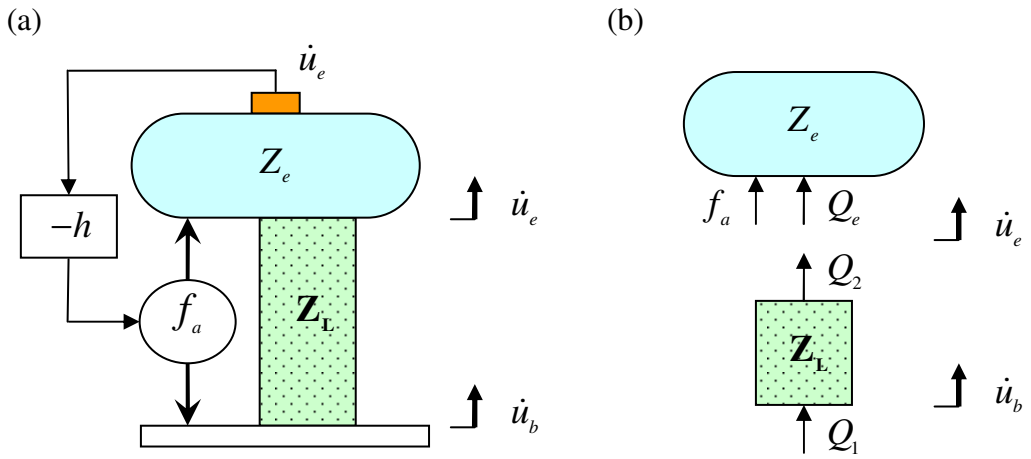

Figure 4.1 *(a) schematic diagram and (b) free body diagram of base excited active vibration isolation system containing a distributed parameter isolator under AVF control, where* $\dot{u}_e$ *and* $\dot{u}_b$ *are velocities of the equipment and the base respectively;* Z_e *is the input impedance of the unconnected equipment at the location of the isolator connection;* $\mathbf{Z}_\mathbf{L}$ *is the impedance matrix of the isolator; h is the constant feedback control gain;* f_a *is the active control force; and* Q_e, Q_1 *and* Q_2 *are internal forces.*

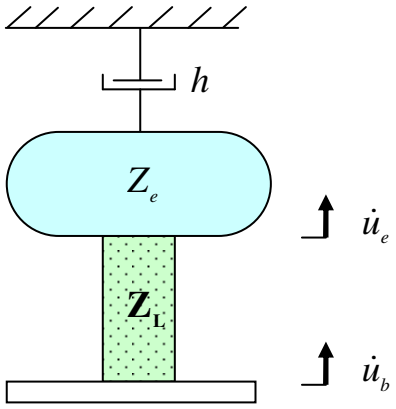

Figure 4.2 *Mechanical representation of the base excited active vibration isolation system containing a distributed parameter isolator under AVF control.*

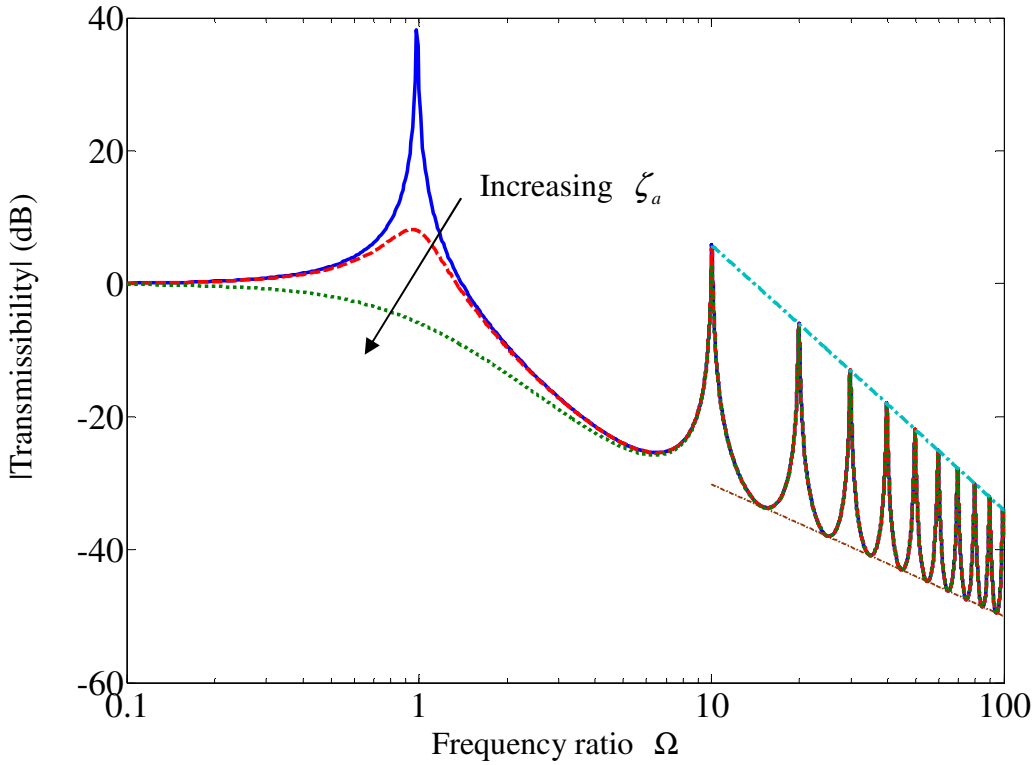

Figure 4.3 *Transmissibility of the active vibration isolation system under AVF control when the ratio of the mass of the isolator to the mass of the equipment* $\mu_i = 0.1$*, the loss factor in the isolator* $\eta_i = 0.01$*, and the active damping ratio* $\zeta_a = 0$ *(solid line),* $\zeta_a = 0.2$ *(dashed line) or* $\zeta_a = 1$ *(dotted line). The bold and faint dashed-dotted lines pass through the IR peaks and the troughs of the transmissibility respectively.*

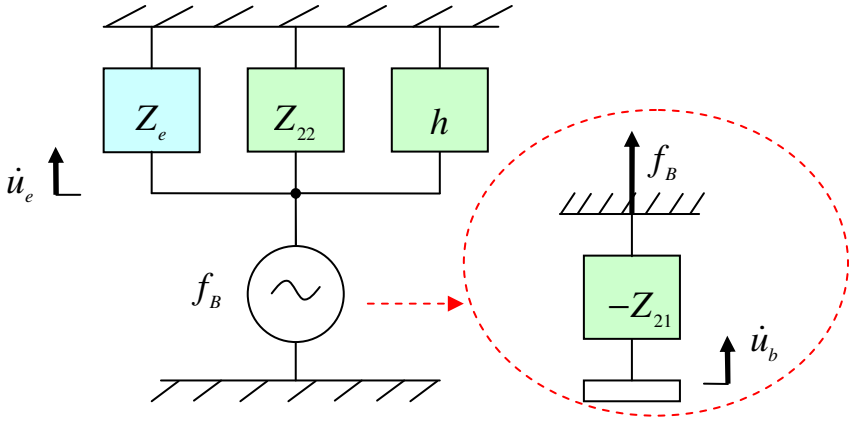

Figure 4.4 *Mechanical representation of the Thevenin equivalent system for the active vibration isolation system under AVF control shown in Figure 4.1, where* Z_{21} *and* Z_{22} *are respectively the transfer and point impedances of the isolator, and* f_B *is the blocked force.*

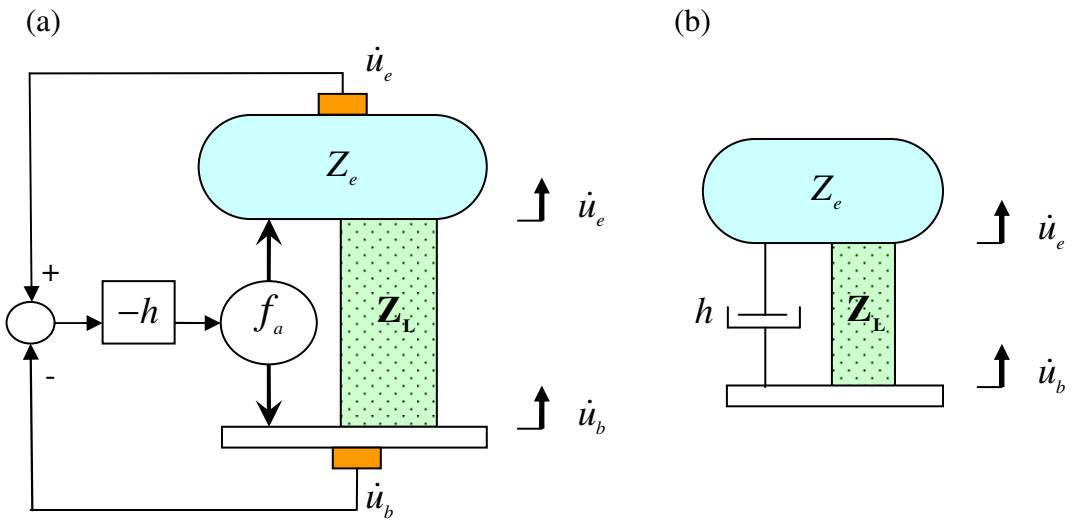

Figure 4.5 *(a) schematic diagram and (b) mechanical representation of base excited active vibration isolation system containing a distributed parameter isolator under RVF control.*

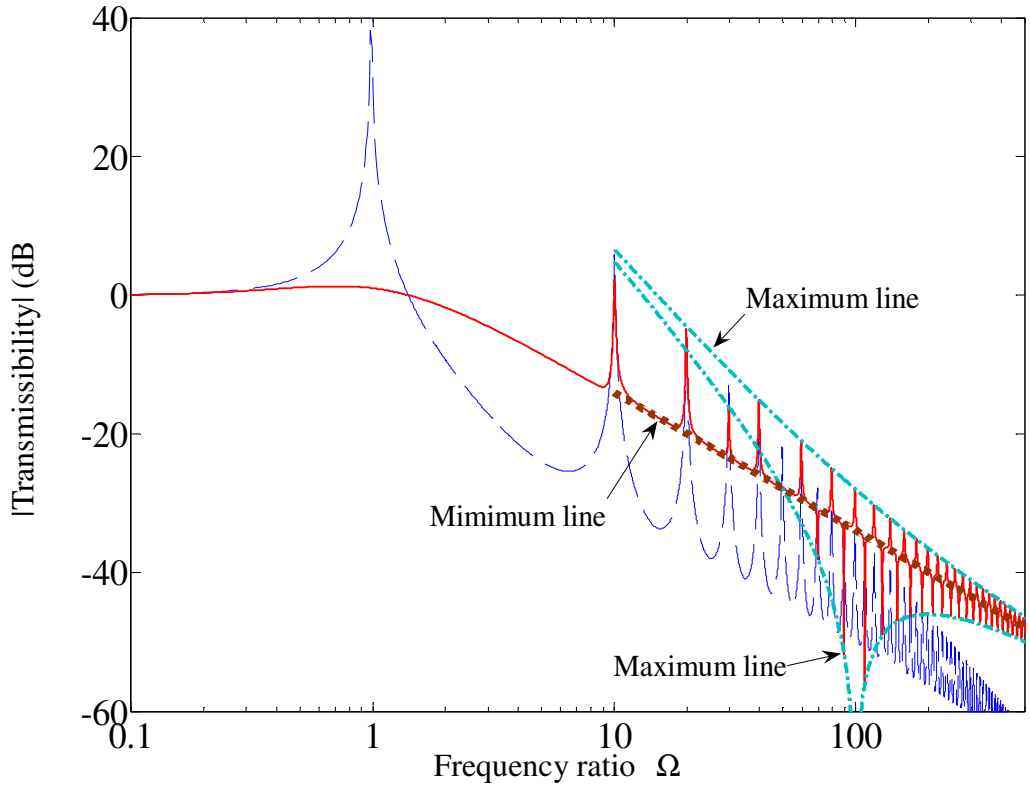

Figure 4.6 *Transmissibility of the active vibration isolation system under RVF control when* $\mu_i = 0.1$, $\eta_i = 0.01$, *and* $\zeta_a = 0$ *(dashed line) or* $\zeta_a = 1$ *(solid line). The two dashed-dotted lines pass through the IR peaks and the dotted line passes through the troughs of the transmissibility.*

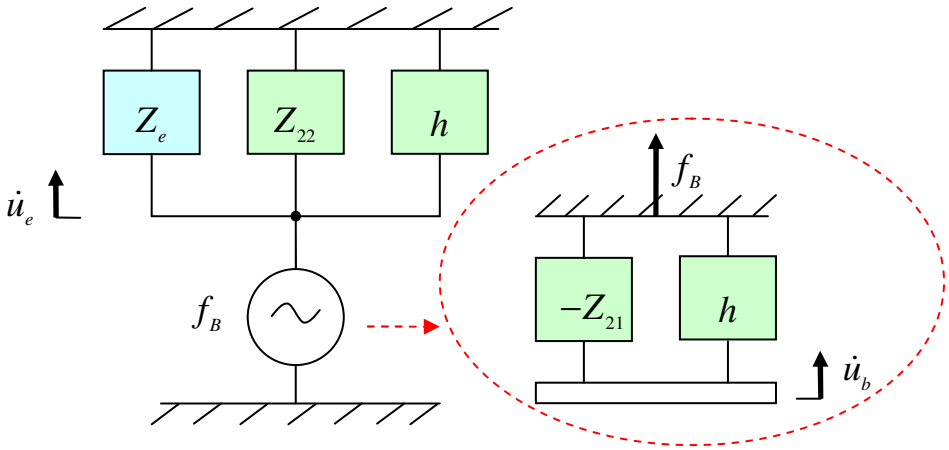

Figure 4.7 *Mechanical representation of the Thevenin equivalent system for the active vibration isolation system under AVF control shown in Figure 4.5.*

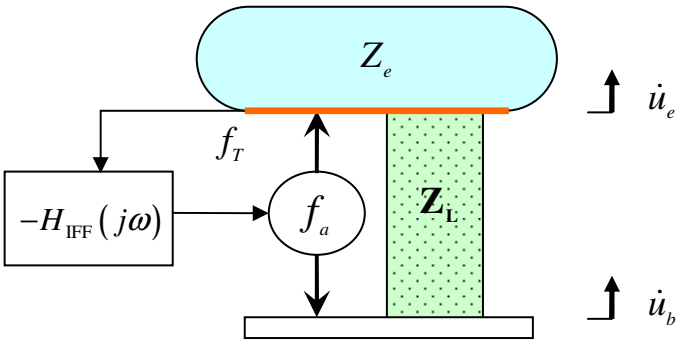

Figure 4.8 *Schematic diagram of base excited active vibration isolation system containing a distributed parameter isolator under IFF control, where* $H_{\mathrm{IFF}}(j\omega)$ *is the frequency response of the IFF controller and* f_T *is the transmitted force to the equipment.*

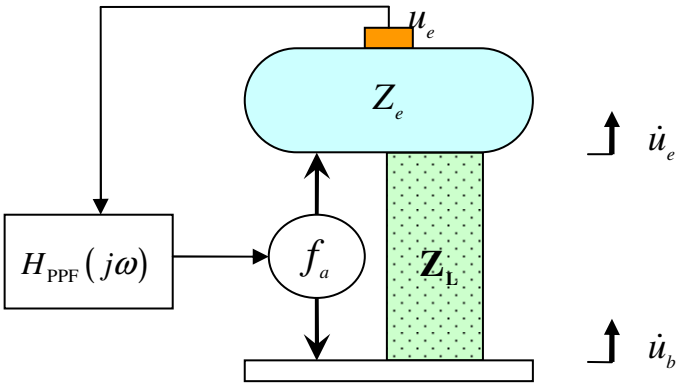

Figure 4.9 *Schematic diagram of base excited active vibration isolation system containing a distributed parameter isolator under PPF control, where* u_e *is the displacement of the equipment and* $H_{\mathrm{PPF}}(j\omega)$ *is the frequency response of the PPF controller.*

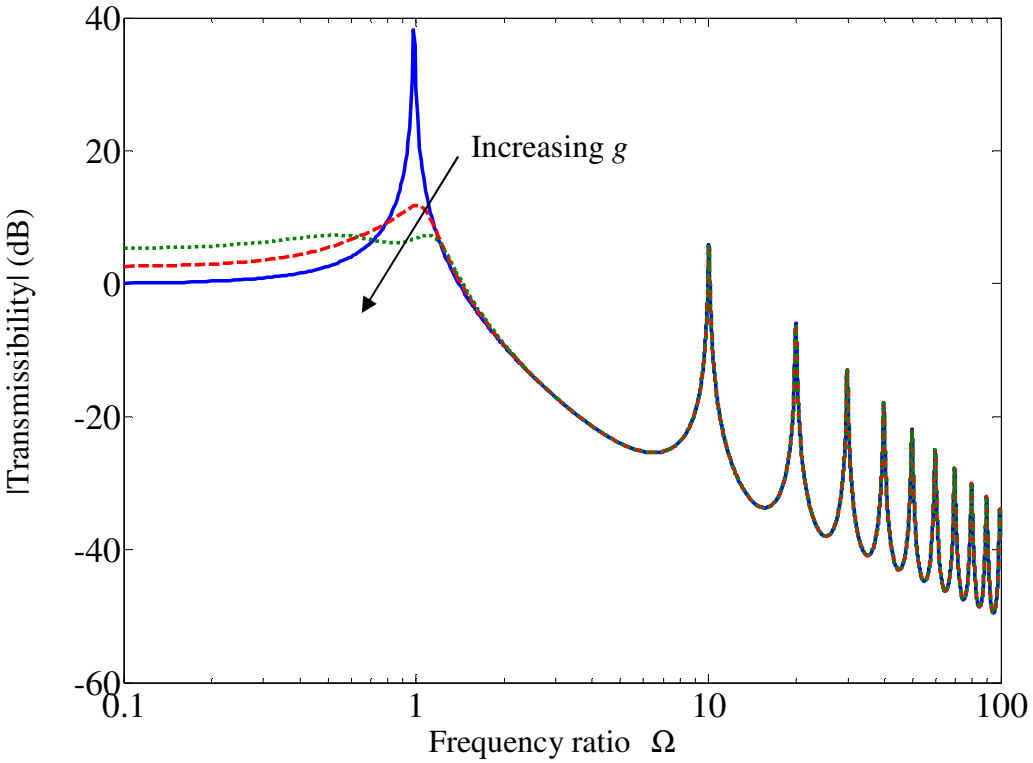

Figure 4.10 *Transmissibility of the active vibration isolation system under PPF control when* $\mu_i = 0.1$, $\eta_i = 0.01$, *the natural frequency of the filter* $\omega_f = \omega_e$, *the damping ratio of the filter* $\zeta_f = 0.5$, *the mass of the equipment* $m_e = 2$ *and the constant gain* $g = 0$ *(solid line),* $g = 0.5$ *(dashed line) or* $g = 0.9$ *(dotted line).*

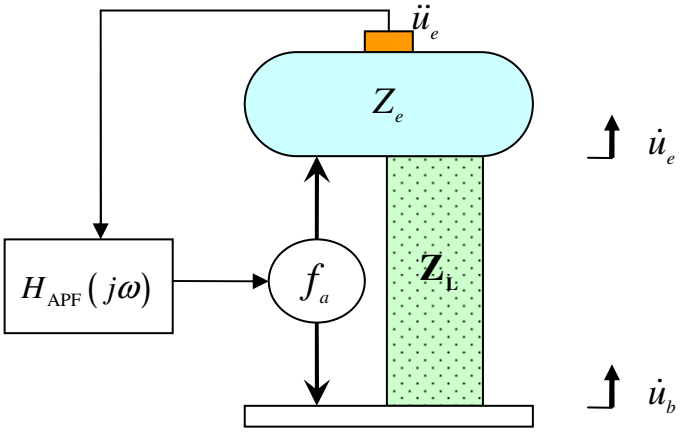

Figure 4.11 *Schematic diagram of base excited active vibration isolation system containing a distributed parameter isolator under APF control, where* $\ddot{u}_e$ *is the acceleration of the equipment and* $H_{\mathrm{APF}}(j\omega)$ *is the frequency response of the APF controller.*

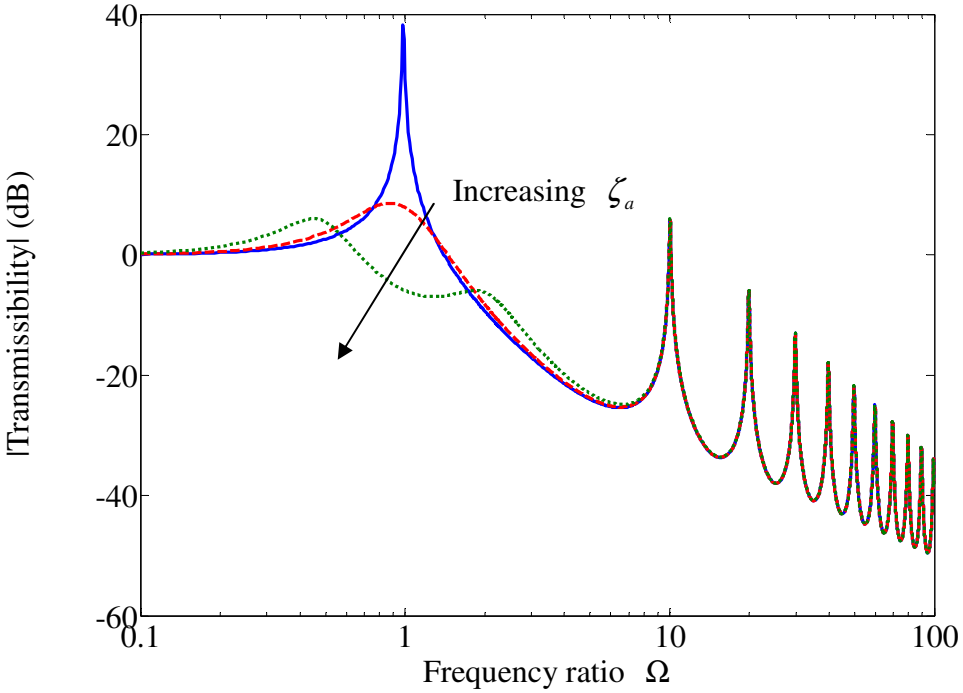

Figure 4.12 *Transmissibility of the active vibration isolation system under APF control when* $\mu_i = 0.1$, $\eta_i = 0.01$, $\omega_f = \omega_e$, $\zeta_f = 0.5$ *and* $\zeta_a = 0$ *(solid line),* $\zeta_a = 0.2$ *(dashed line) or* $\zeta_a = 1$ *(dotted line).*

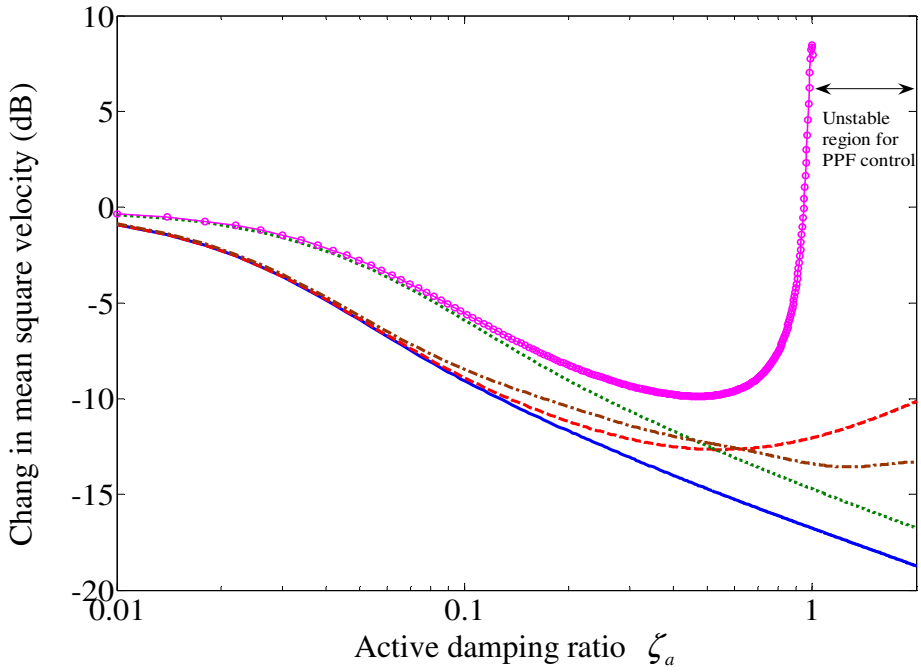

Figure 4.13 *Normalized change in mean square velocity for the base motion system under AVF (solid line), RVF (dashed line), IFF (dotted line), PPF (line with circle) and APF (dashed-dotted line) control compared to the passive system when* $\mu_i = 0.1$, $\eta_i = 0.01$, $m_e = 0.5$, $\omega_f = \omega_e$ *and* $\zeta_f = 0.5$.

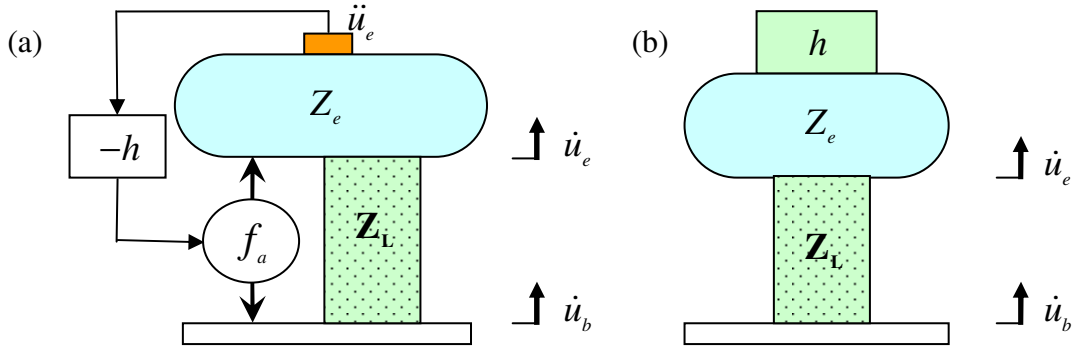

Figure 4.14 *(a) schematic diagram and (b) mechanical representation of a base excited system containing a distributed parameter isolator under acceleration feedback control.*

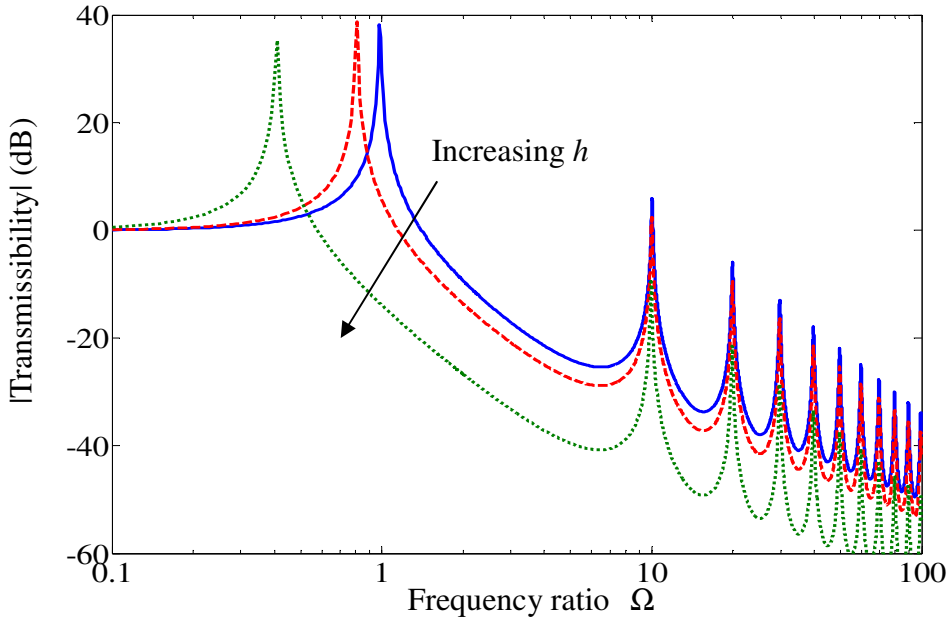

Figure 4.15 *Transmissibility of the active vibration isolation system under acceleration feedback control when* $\mu_i = 0.1$, $\eta_i = 0.01$ *and* $h = 0$ *(solid line),* $h/m_e = 0.5$ *(dashed line) or* $h/m_e = 5$ *(dotted line).*

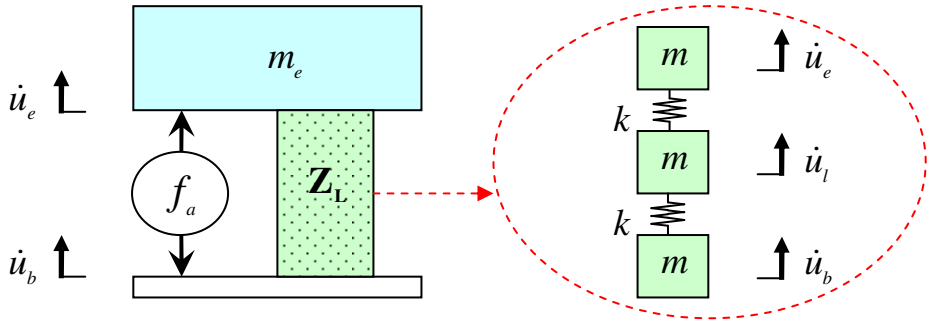

Figure 4.16 *Schematic diagram of a base excited system containing a distributed parameter isolator under optimal control, where* $\dot{u}_l$ *is the velocity of the middle mass.*

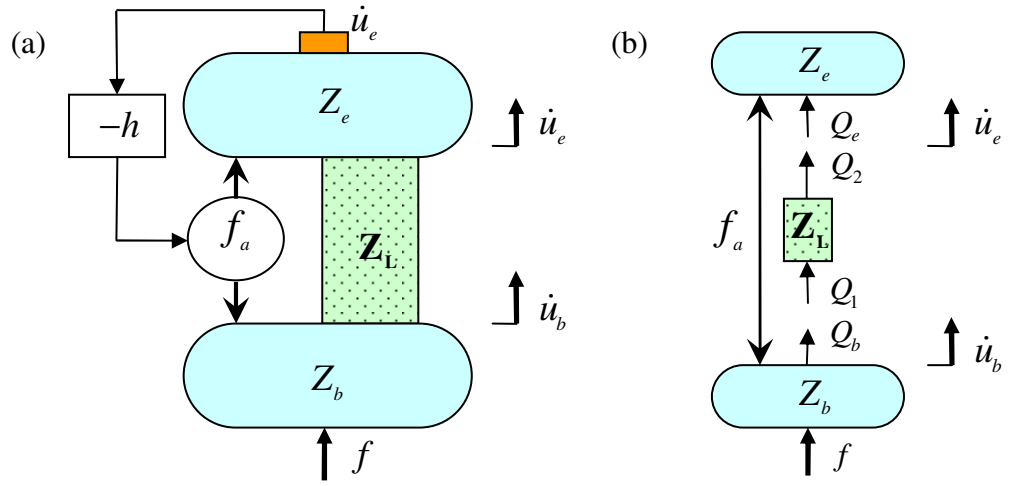

Figure 4.17 *(a) schematic diagram and (b) free body diagram of an active vibration isolation system containing a distributed parameter isolator on a flexible base under AVF control, where* Z_b *is the input impedance of the base,* f *is the primary force applied to the base and* Q_b *is an internal force.*

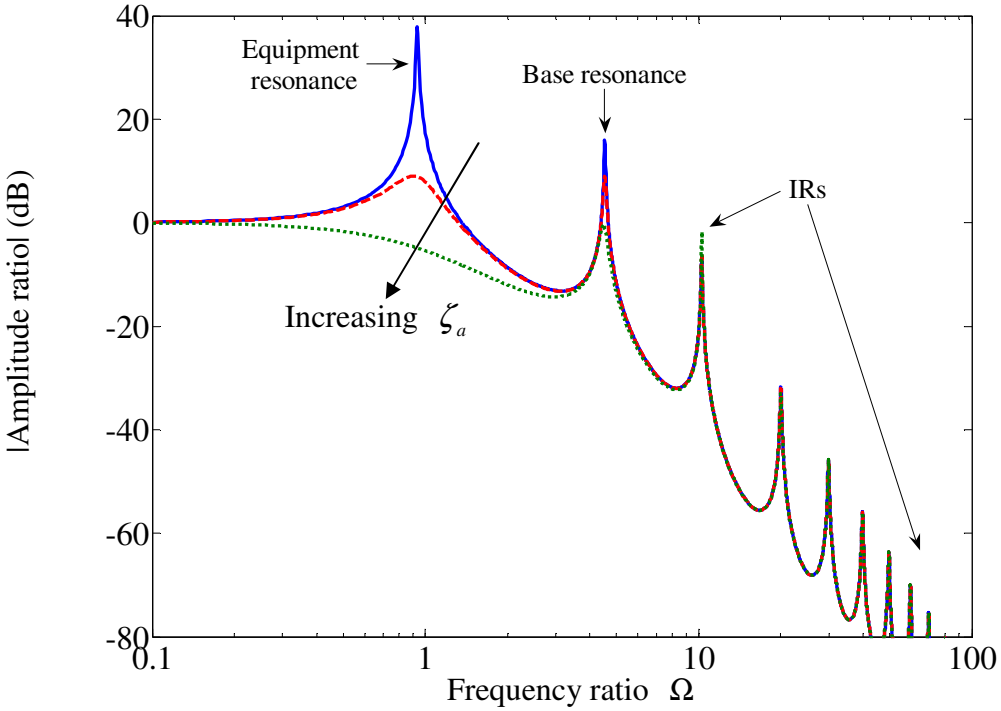

Figure 4.18 *Amplitude ratio of the active vibration isolation system on a flexible base under AVF control when* $\mu_i = 0.1$, $\eta_i = 0.01$, *the ratio of the mass of the base to the mass of the equipment* $\mu_b = 0.5$, *the ratio of the static stiffness of the isolator to the stiffness of the base* $\mu_k = 0.1$, *the loss factor in the base* $\eta_b = 0.01$ *and* $\zeta_a = 0$ *(solid line),* $\zeta_a = 0.2$ *(dashed line) or* $\zeta_a = 1$ *(dotted line).*

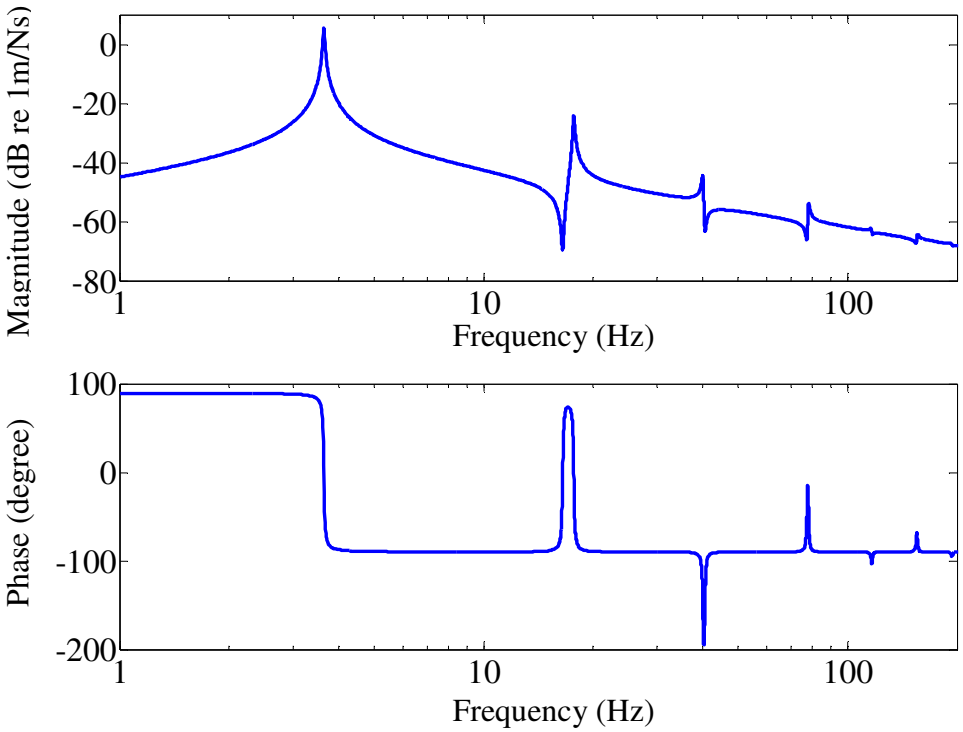

Figure 4.19 *Plant responses of the AVF control system containing a distributed parameter isolator on a flexible base when* $\mu_i = 0.1$, $\mu_b = 0.5$, $\mu_k = 0.1$, *and* $\eta_i = \eta_b = 0.01$.

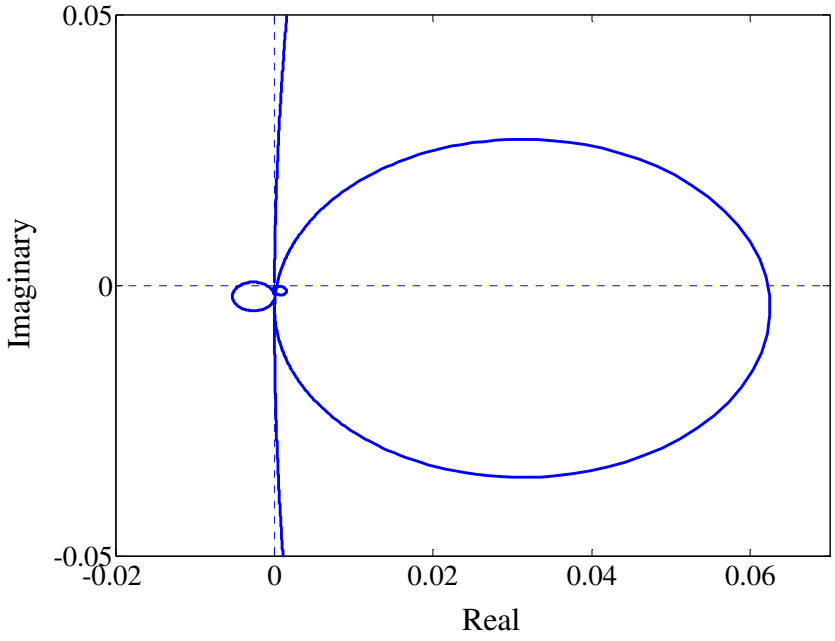

Figure 4.20 *Zoomed Nyquist plot of the plant responses of the AVF control system containing a distributed parameter isolator on a flexible base when* $\mu_i = 0.1$, $\mu_b = 0.5$, $\mu_k = 0.1$ *and* $\eta_i = \eta_b = 0.01$.

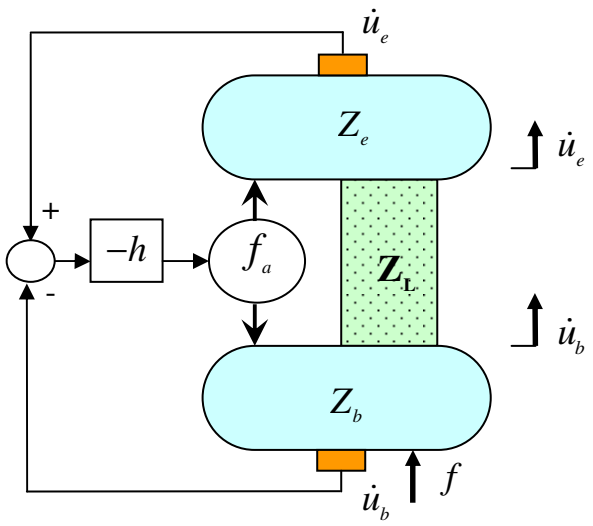

Figure 4.21 *Schematic diagram of an active vibration isolation system containing a distributed parameter isolator on a flexible base under RVF control.*

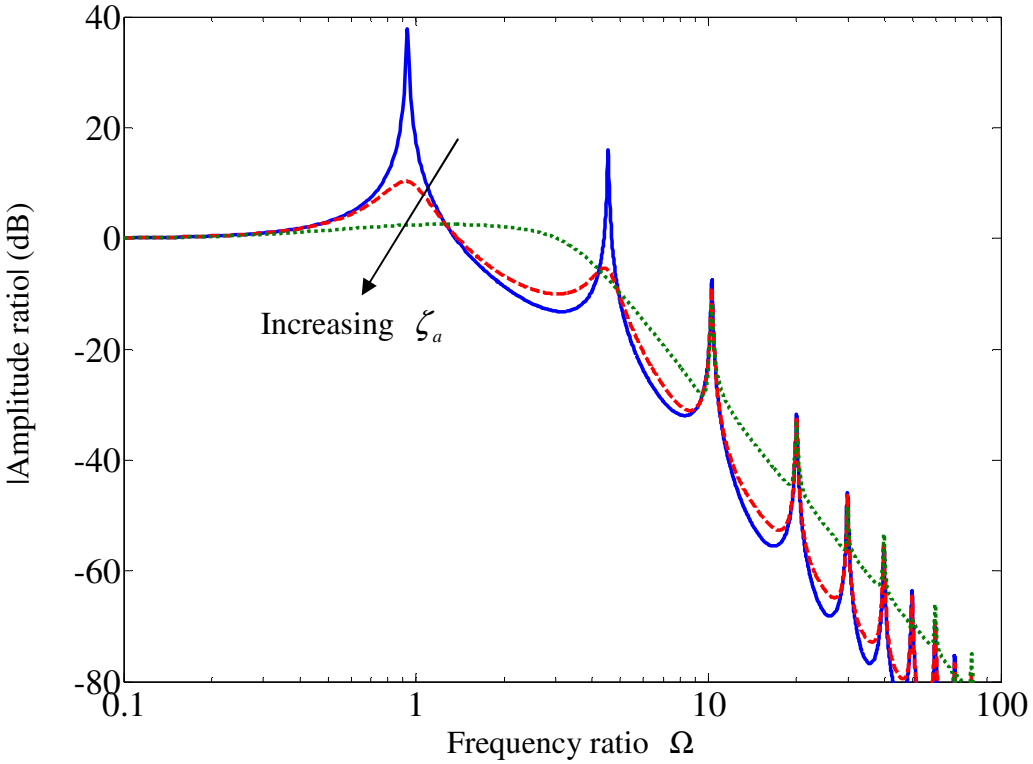

Figure 4.22 *Amplitude ratio of the active vibration isolation system on a flexible base under RVF control when* $\mu_i = 0.1$, $\mu_b = 0.5$, $\mu_k = 0.1$, $\eta_i = \eta_b = 0.01$ *and* $\zeta_a = 0$ *(solid line),* $\zeta_a = 0.2$ *(dashed line) or* $\zeta_a = 1$ *(dotted line).*

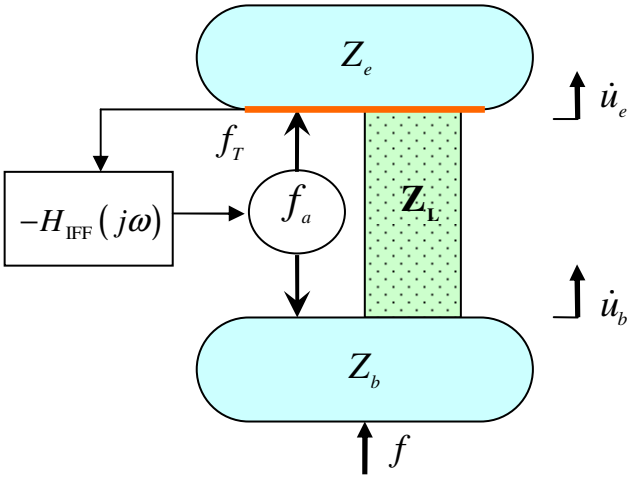

Figure 4.23 *Schematic diagram of an active vibration isolation system containing a distributed parameter isolator on a flexible base under IFF control.*

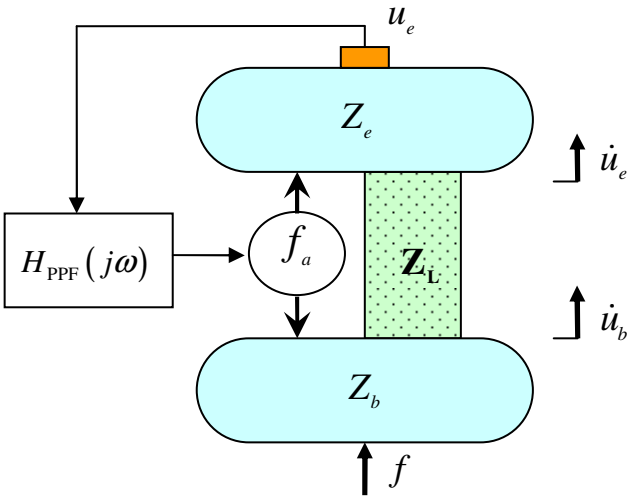

Figure 4.24 *Schematic diagram of an active vibration isolation system containing a distributed parameter isolator on a flexible base under PPF control.*

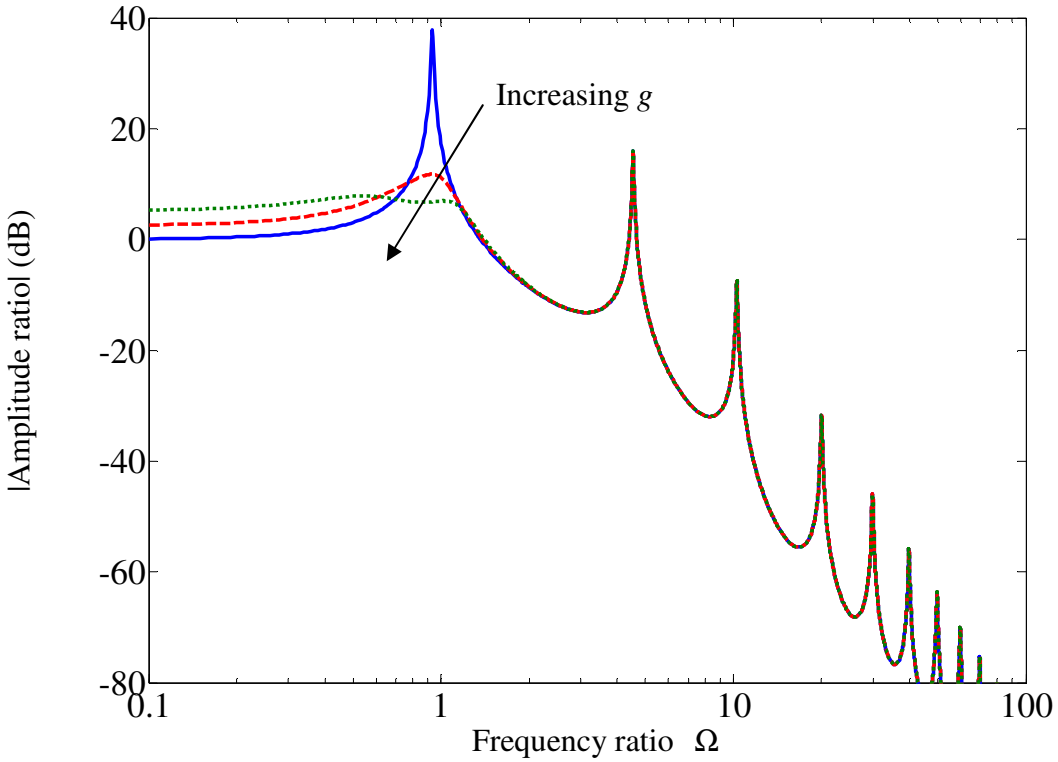

Figure 4.25 *Amplitude ratio of the active vibration isolation system on a flexible base under PPF control when* $\mu_i = 0.1$, $\mu_b = 0.5$, $\mu_k = 0.1$, $\eta_i = \eta_b = 0.01$, $\omega_f = \omega_e$, $\zeta_f = 0.5$, $m_e = 2$ *and* $g = 0$ *(solid line),* $g = 0.5$ *(dashed line) or* $g = 0.9$ *(dotted line).*

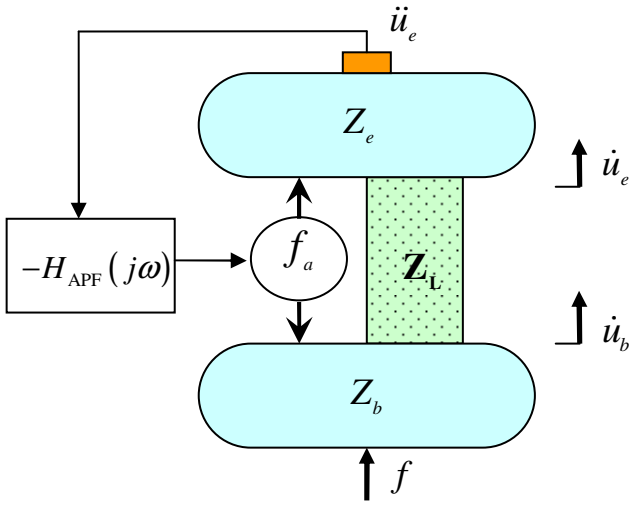

Figure 4.26 *Schematic diagram of an active vibration isolation system containing a distributed parameter isolator on a flexible base under APF control.*

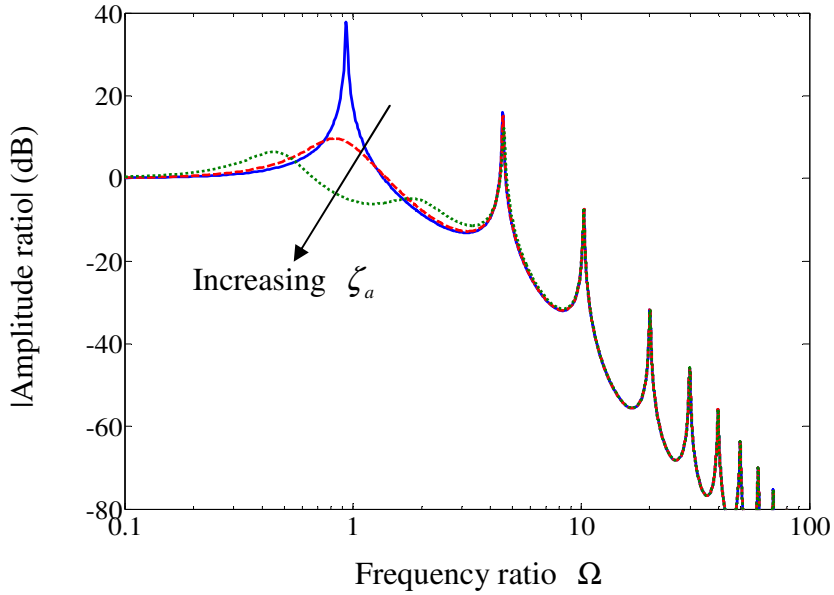

Figure 4.27 *Amplitude ratio of the active vibration isolation system on a flexible base under APF control when* $\mu_i = 0.1$, $\mu_b = 0.5$, $\mu_k = 0.1$, $\eta_i = \eta_b = 0.01$, $\omega_f = \omega_e$, $\zeta_f = 0.5$ *and* $\zeta_a = 0$ *(solid line),* $\zeta_a = 0.2$ *(dashed line) or* $\zeta_a = 1$ *(dotted line).*

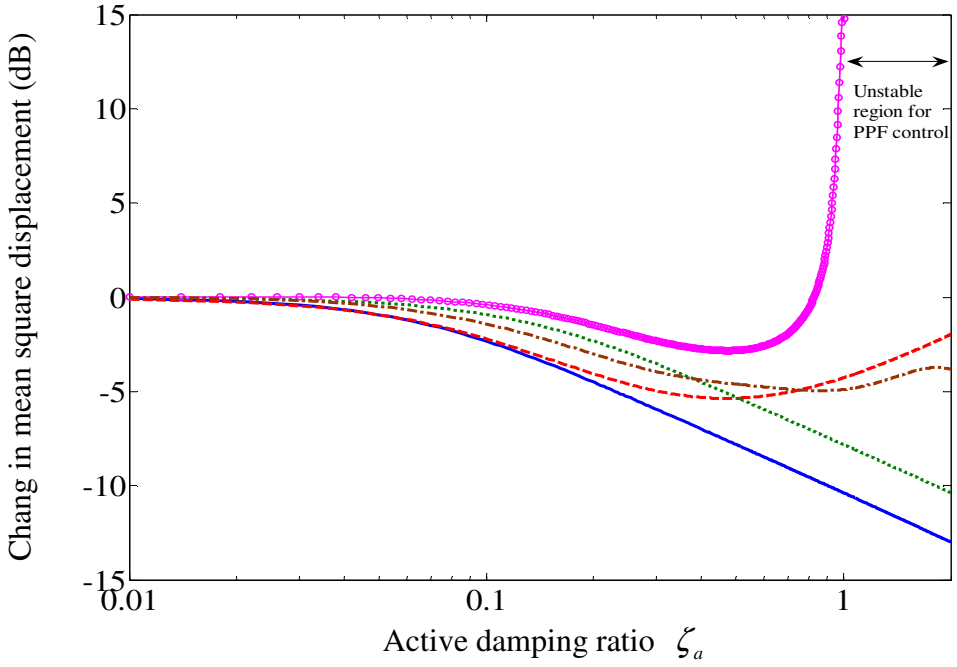

Figure 4.28 *Normalized change in mean square displacement for the system on a flexible base under AVF (solid line), RVF (dashed line), IFF (dotted line), PPF (line with circle) and APF (dashed-dotted line) control compared to the passive system when* $\mu_i = 0.1$, $\mu_b = 0.5$, $\mu_k = 0.1$, $\eta_i = \eta_b = 0.01$, $m_e = 0.5$, $\omega_f = \omega_e$ *and* $\zeta_f = 0.5$. *N.B. since AVF is only conditionally stable in this case, the solid line starts to increase if* $\zeta_a \approx 2.5$ *[73].*

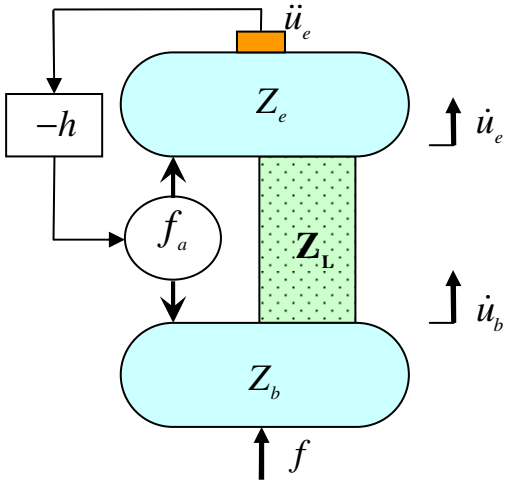

Figure 4.29 *Schematic diagram of an active vibration isolation system containing a distributed parameter isolator on a flexible base under acceleration feedback control.*

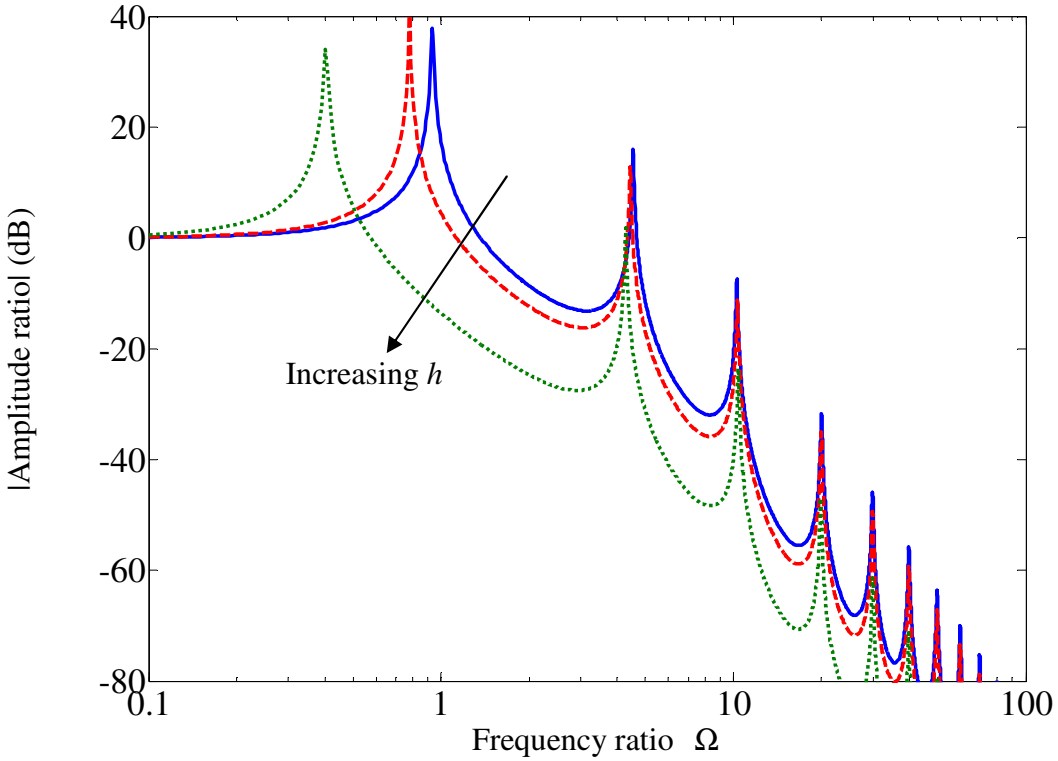

Figure 4.30 *Amplitude ratio of the active vibration isolation system on a flexible base under acceleration feedback control when* $\mu_i = 0.1$, $\mu_b = 0.5$, $\mu_k = 0.1$, $\eta_i = \eta_b = 0.01$ *and* $h = 0$ *(solid line),* $h/m_e = 0.5$ *(dashed line) or* $h/m_e = 5$ *(dotted line).*

Chapter 5

AVF Control on a System Containing a Distributed Parameter Isolator

5.1 Introduction

As discussed in Chapter 4, AVF control is an optimal solution to minimise the mean square velocity of the equipment mass in active vibration isolation with a distributed parameter isolator and a rigid base (section 4.2.8). The AVF control system, which could be considered as the simplest way to implement active damping, is effective in attenuating the resonance peaks at relatively low frequencies, whereas it is not effective in attenuating the isolator IRs. It was also shown that the AVF control system containing a distributed parameter isolator on a flexible base is only conditionally stable. Such a system may become unstable at high control gains, so that the AVF control performance is limited.

The aim of this chapter is to investigate the stability and performance of AVF control system containing a distributed parameter isolator and examine approaches to stabilize such a system both theoretically and experimentally. First, several approaches which can stabilize the AVF control system are presented theoretically. Then the stability and performance of the AVF control system containing a distributed parameter isolator are

investigated experimentally on a four-spring active vibration isolation system. The approaches to stabilize the AVF control system are also validated experimentally.

5.2 Approaches to stabilize the AVF control system

As presented in Chapter 4, the active vibration isolation system containing a distributed parameter isolator on a flexible base under AVF control is only conditionally stable. The stability condition proposed in Chapter 4 is given by $\phi_b^{(j)} / \phi_e^{(j)} < 1$ for all j in a lightly damped system, where $\phi_e^{(j)}$ and $\phi_b^{(j)}$ are respectively the modal amplitudes evaluated at the equipment and the base. This stability condition means that if the displacement of the base is greater than the displacement of the equipment and these two displacements are in phase at the j^{th} natural frequency, then the system may become unstable.

Therefore, to stabilize the AVF control system, the relative displacement between the equipment and the base at the troublesome natural frequency needs to be altered. In some situations, this can simply be achieved by adding more damping in the isolator as mentioned in [72, 90]. Additional mass could also be added to the base structure to change the modal amplitude in order to stabilize the AVF control system. Furthermore, some other mechanical approaches can also be applied to change the dynamics of the base structure. Alternatively, electronic means can be used to compensate for the phase lag at IRs in the isolator which causes instability. These approaches are discussed in the following sections.

5.2.1 Adding more damping in the isolator

Additional damping introduced in the isolator constrains the amplitude and phase shift of the open-loop frequency response at IRs, so that the instability due to the IRs can be eliminated. For the AVF control system on a flexible base shown in Figure 4.16, the simulation result of adding more damping in the isolator can be achieved if a larger

value for the loss factor in the isolator η_i is applied. Figure 5.1 shows the plant response of the active vibration isolation system on a flexible base under AVF control with high damping in the distributed parameter isolator. The plant response for such a system with low damping in the isolator is also plotted for comparison. It can be seen that with high damping in the isolator it helps limit the amplitude and phase shift of the plant response at IR frequencies, so that the phase at the first IR frequency (the third peak in Figure 5.1) where instability occurs becomes greater than -180°. It can also be noted that in the Nyquist plot of the plant response, shown in Figure 5.2, the loop on the left half of the complex plane caused by the first IR for the system with low damping in the isolator is shifted to the third quadrant. For large damping the loop never crosses the negative real axis. Thus the system becomes unconditionally stable. From the above analysis, it is demonstrated that the situation of having a lightly damped system, i.e. one mode dominating the response at resonance frequencies, is the worst case for stability.

This approach to stabilize the AVF control system is simple and straightforward. However, it is not always practical to introducing more damping in the isolator. Also, high damping materials may degrade the load capacity of the isolator and the performance of the system [67].

5.2.2 Adding more mass to the base

Adding more mass to the base structure can reduce the relative displacement between the base and the equipment at IRs, so that the proposed stability condition can be satisfied. The AVF control system can thus be stabilized. For the AVF control system on a flexible base shown in Figure 4.16, the simulation result of adding more mass to the base can be achieved if a larger value for the ratio of the mass of the base to the mass of the equipment μ_b is applied. Figure 5.3 shows the plant response of the AVF control system on a heavy flexible base. For comparison, the plant response of the system on a light flexible base is also plotted. It can be seen that the base resonance moves to a

lower frequency due to the extra mass on the base structure. It should also be noted that the phase shift due to the IRs in the isolator is limited by the addition of more mass to the base structure. Figure 5.4 shows the Nyquist plot of the plant response. The loop, which is on the left half of the complex plane caused by the first IR for the system on a light base, is shifted to the third quadrant rather than crossing the negative real axis, due to the effects of the additional base mass. Thus the system becomes unconditionally stable. However, this approach is also limited in practical use because it is again not always practical to add extra mass to the base.

5.2.3 Electronic means: introducing a lead compensator

Figure 5.5 shows a lead compensator that is introduced into the feedback loop to compensate for the phase lag due to the IRs in the distributed parameter isolator, which causes the instability. The open-loop frequency response of the modified control system is given by

$$G(j\omega)H(j\omega) = h \cdot G_{\text{lead}} \cdot G \tag{5.1}$$

where h is the constant feedback gain, $G = Y_{ee} - Y_{eb}$ is the plant response of the system, and G_{lead} is the frequency response function of the lead compensator, which is given by [74, 75, 91]

$$G_{\text{lead}} = \alpha \cdot \frac{1 + j\omega T_1}{1 + j\alpha\omega T_1} \quad (0 < \alpha < 1) \tag{5.2}$$

where α and T_1 are the coefficients of the lead compensator. The corresponding frequency where the maximum phase lead occurs is given by

$$\omega_c = \frac{1}{\sqrt{\alpha} T_1} \tag{5.3}$$

The corresponding maximum phase lead is given by

$$\varphi_{\max} = \arcsin\left(\frac{1-\alpha}{1+\alpha}\right) \tag{5.4}$$

Figure 5.6 shows the frequency response of a lead compensator. To compensate for the phase lag due to the IRs in the isolator, which causes the instability, the lead

compensator needs to be tuned. ω_c should be equal to the instability frequency, so that the maximum phase lead compensation can be achieved at the troublesome frequency. If a phase lead compensation of φ is required, the parameter α is given by

$$\alpha = \frac{1-\sin\varphi}{1+\sin\varphi} \tag{5.5}$$

so that the coefficient T_1 can be written as

$$T_1 = \frac{1}{\sqrt{\alpha}\omega_c} \tag{5.6}$$

Figure 5.7 illustrates the open-loop frequency response of the system with a lead compensator shown in Figure 5.5 when the feedback control gain is unity. For comparison, the open-loop frequency response of the original system without the lead compensator is also plotted. It can be seen that the phase shift at the first IR frequency where instability occurs is greater than -180° due to the phase compensation, so that the Nyquist plot of the open-loop frequency response does not cross the negative real axis as shown in Figure 5.8. Thus the system becomes unconditionally stable.

This approach to stabilize the AVF control system requires information on the IRs in the isolator before the lead compensator can be designed and implemented. Also higher control gains are required to achieve good control performance because the open-loop frequency response of the stabilized system is less due to the lead compensator. In practice, the higher order resonances in the equipment or base structures at high frequencies are likely to cause instabilities due to the higher control gain used.

5.2.4 Mechanical means

To stabilize the AVF control system, an additional SDOF mechanical system comprising a rigid mass m_a, an elastic spring with stiffness k_a and a viscous damper with damping coefficient c_a can be introduced to attach onto the base structure of the active vibration isolation system. Figure 5.9 shows the idealized situation. The hypothesis is

that the displacement of the base at the instability frequency can be altered. The active force due to AVF control acting on the equipment reacts against the additional mass, as shown in Figure 5.9, rather than acting directly onto the flexible base. The force transmitted to the base structure $f_a^{'}$ is thus given by

$$f_a^{'} = T_a f_a + Z_a \dot{u}_b \tag{5.7}$$

where

$$T_a = \frac{Z_{ia}}{Z_{ma} + Z_{ia}} \tag{5.8}$$

is the force transmissibility and

$$Z_a = \frac{Z_{ma} Z_{ia}}{Z_{ma} + Z_{ia}} \tag{5.9}$$

is the total impedance of the additional system, $Z_{ma} = j\omega m_a$ is the impedance of the additional mass, $Z_{ia} = k_a / j\omega + c_a$ is the impedance of the combined suspension of the additional system.

The velocity of the equipment for the stabilized system with the additional mechanical system on the base shown in Figure 5.9 is given by

$$\dot{u}_e = Y_{ee} f_a + Y_{eb} (f - f_a^{'}) \tag{5.10}$$

Substituting equations for Y_{ee}, Y_{eb} given in chapters 3 and 4 and equation (5.7) into (5.10), the velocity of the equipment can be rewritten as

$$\dot{u}_e = (Y_{ee}^{'} - T_a Y_{eb}^{'}) f_a + Y_{eb}^{'} f \tag{5.11}$$

where

$$Y_{ee}^{'} = \frac{Z_b + Z_{11} + Z_a}{(Z_e + Z_{22})(Z_b + Z_{11} + Z_a) - Z_{12} Z_{21}}$$
$$Y_{eb}^{'} = \frac{-Z_{21}}{(Z_e + Z_{22})(Z_b + Z_{11} + Z_a) - Z_{12} Z_{21}} \tag{5.12a,b}$$

where $Y_{ee}^{'}$ is the input mobility of the equipment when coupled to the rest of the stabilized system and $Y_{eb}^{'}$ is the transfer mobility from the force on the base to the

equipment velocity $\dot{u}_e$ when the stabilized system is coupled.

Therefore, the plant response from actuator force to absolute equipment velocity for the stabilized system is given by

$$G' = \left.\frac{\dot{u}_e}{f_a}\right|_{f=0} = Y'_{ee} - T_a Y'_{eb} \tag{5.13}$$

At resonance frequencies, in a lightly damped system, when only one mode dominates the response, the plant response can be written as

$$G' = Y'_{ee} - T_a Y'_{eb} \approx \frac{\left[\phi_e^{(j)}\right]^2 \left(1 - (T_a)_{\omega=\omega_j} \cdot \frac{\phi_b^{(j)}}{\phi_e^{(j)}}\right)}{2\sqrt{K_j M_j}\,\zeta_j} \tag{5.14}$$

The stability condition is thus given by

$$\mathrm{Re}(T_a)_{\omega=\omega_j} \cdot \frac{\phi_b^{(j)}}{\phi_e^{(j)}} < 1 \tag{5.15}$$

at a resonance frequency, where Re denotes the real part.

The force transmissibility in equation (5.15) can be written as

$$T_a = \frac{Z_{ia}}{Z_{ma} + Z_{ia}} = \frac{1 + j2\zeta_s \Omega_a}{1 - \Omega_a^2 + j2\zeta_s \Omega_a} \tag{5.16}$$

where non-dimensional frequency $\Omega_a = \omega / \omega_a$, $\omega_a = \sqrt{k_a / m_a}$ is the natural frequency of the additional system, and $\zeta_s = c_a / 2\sqrt{k_a m_a}$ is the viscous damping ratio of the additional system. According to the stability condition giving by equation (5.15), to stabilize the AVF control system, $\mathrm{Re}(T_a)$ should be as small as possible around potentially unstable frequencies. As shown in equation (5.16), it means that the natural frequency of the additional system ω_a should be much smaller than the potentially unstable frequencies. However, around the natural frequency of the additional system ω_a, if it is lightly damped, instability may occur due to the amplification of $\mathrm{Re}(T_a)$. In order to overcome this low frequency potential instability due to the natural frequency of the additional system, a relatively highly damped additional system should be used to attenuate $\mathrm{Re}(T_a)$ around its natural frequency.

The plant response of the active vibration isolation system with the additional mechanical system attached to the base shown in Figure 5.9 is plotted in Figure 5.10. The plant response of the original system is also plotted for comparison. It can be seen that the phase lag at the first IR in the isolator, which might cause instability, is eliminated due to the attachment of the mechanical system. But as a compromise, there is a new phase lead occurring at the natural frequency of the additional system. If the damping of the additional system is relatively high, this phase lead will not be a danger to stability for the AVF control. As shown in Figure 5.11 for the Nyquist plot of the plant responses, there is no loop which crosses the negative real axis for the stabilized system with the additional mechanical system attached to the base. The AVF control system is thus unconditionally stable.

The phase margin around the natural frequency of the additional system can be further increased by introducing a phase-lag compensator into the feedback control loop as shown in Figure 5.12. If a lag compensator is applied to the stabilized system, the open-loop frequency response becomes

$$G(j\omega)H(j\omega) = h \cdot G' \cdot G_{\text{lag}} \tag{5.17}$$

where the frequency response function of a lag compensator is given by [74]

$$G_{\text{lag}} = \frac{1 + j\omega T_2}{1 + j\beta\omega T_2} \quad (\beta > 1) \tag{5.18}$$

where β and T_2 are the coefficients of the lag compensator. The corresponding frequency where the maximum phase lag occurs is given by

$$\omega_c = \frac{1}{\sqrt{\beta}T_2} \tag{5.19}$$

The corresponding maximum phase lag is given by

$$\varphi_{\max} = \arcsin\left(\frac{1-\beta}{1+\beta}\right) \tag{5.20}$$

Figure 5.13 shows the frequency response of a lag compensator. To limit the phase shift around the natural frequency of the additional system, ω_c should be equal to ω_a, so

that the maximum phase lag compensation can be achieved. The appropriate parameters for the lag compensator need to be chosen based on this principle. If a phase lag compensation of φ is required, the parameter β is given by

$$\beta = \frac{1-\sin\varphi}{1+\sin\varphi} \tag{5.21}$$

so that the coefficient T_2 can be written as

$$T_2 = \frac{1}{\sqrt{\beta}\omega_c} = \frac{1}{\sqrt{\beta}\omega_a} \tag{5.22}$$

Figure 5.14 illustrates the open-loop frequency response and its Nyquist plot of the stabilized system with a lag compensator shown in Figure 5.12 when the feedback control gain is unity. For comparison, the open-loop frequency response of the system shown in Figure 5.9 is also plotted. It can be seen that the phase around the natural frequency of the additional system is further suppressed due to the lag compensator, so that a greater phase margin is achieved.

Compared to the aforementioned approach of adding more mass to the base to stabilize the AVF control, less mass is required in this mechanical configuration. As a compromise, it does increase the design complexity. The potential danger to stability at the natural frequency of the additional system should also be noted and considered.

5.3 Experimental validation for AVF control system

In the theoretical analysis described in this thesis, the distributed parameter isolator has been modelled as a 'long-rod', i.e. the lateral deformation of the isolator under the longitudinal excitation is ignored. As presented in Chapter 3, a helical spring is a typical lightly damped distributed parameter isolator. It can be modelled as a finite rod under longitudinal vibration for simplicity, because both objects are continuously distributed elements, in that their stiffness and mass are spread uniformly throughout their length. Therefore, a four-spring active vibration isolation system was designed and

implemented to show the validity of stability and control performance for vibration isolation system under AVF control. The purpose of using four springs that are in parallel in the experimental rig is to eliminate the effect of any rotation. It is also less likely to result in lateral isolator deformation. Different aforementioned approaches which can stabilize the AVF control system are also implemented experimentally. Part of the experimental results has been reported in [92].

5.3.1 Experimental setup

A four-spring active vibration isolation system was built as shown in Figure 5.15. It consisted of an equipment plate together with four actuators mounted on a base plate through four springs under excitation of a primary vibrator. A symmetrical aluminium plate representing the equipment was installed on top of another symmetrical aluminium plate representing the base via four identical helical springs. A large electromagnetic vibrator (Derritron type VP4) underneath the base plate acted as the primary force actuator, and the four small electromagnetic actuators (LDS V101) fixed on the equipment plate were the control actuators at each mount position. The equipment to be isolated was thus a combined structure of the aluminium equipment plate and four actuators. Each helical spring was bolted to the equipment plate through an aluminium washer underneath each actuator. A stinger was connected through the inside of the spring between each actuator and the corresponding washer at the foot of each spring. The base plate, to which the washers were attached by wax, was bolted to the primary vibrator with four bolts. The detailed physical and geometrical parameters of the experimental setup are listed in Table 5.1.

Figure 5.16 shows a schematic diagram of the experimental setup and signal path with details of one actuator and the corresponding spring underneath. The primary vibrator was driven with white noise from a dynamic signal analyzer (Data Physics-Signalcalc Mobilyzer II) through a power amplifier (Ariston AX-910). The base response was measured using an accelerometer (B&K type 4375) at the centre of the base plate. The

equipment response was monitored by five accelerometers (B&K type 4375) located along two central lines of the equipment plate, so that the average vertical equipment response and the dynamic behaviour of the equipment plate could be analyzed, and the effect of any rigid body equipment plate rotation reduced. The acceleration signals from the equipment plate and the base plate were then passed through charge amplifiers (B&K type 2635). These include an integrator and high and low-pass filter modules, so that the velocity response of the equipment and base can be obtained. The high-pass filter cut-off frequency was set to 1 Hz to avoid DC signal overflow, and the low-pass filter cut-off frequency was set to 10 kHz. The velocity response at the centre of the equipment plate was fed back to the actuators via a power amplifier (Cambridge audio AI V2.0) with gain control to generate the active control force.

5.3.2 Passive response

The base dynamics were firstly measured when it was uncoupled from the springs and equipment structure, i.e. the equipment plate, actuators and springs were removed from the base plate. The base plate was driven by the large vibrator using broadband white noise from the signal analyzer through a power amplifier. The vibrator input voltage to the power amplifier was used as the reference signal instead of the input force because the input voltage is approximately proportional to the force input within the frequency range of interest in this study [93]. The acceleration response at the centre of the base plate was measured and passed through a charge amplifier to obtain the velocity response. The base dynamics is then the measured transfer function from the input of the power amplifier to the output of the charge amplifier. Different masses were used to change the weight of the base structure.

Figure 5.17 shows the base dynamics with different additional weight added to the base structure. It can be seen that the base structure behaves as SDOF system which is a mass supported by a spring upto about 600 Hz at least. The solid line is for a 0.8 kg mass attached to the base plate with a resonance frequency of about 23.3 Hz. The dashed line

is for a 1.8 kg mass attached to the base plate, so that the resonance frequency of the system is reduced to about 19 Hz. These resonance frequencies are the effective mass of the base structure resonant on the internal support stiffness of the vibrator. Therefore, the effective mass of 1.18 kg and effective stiffness of 4.25×10^4 N/m can be estimated from these two resonance frequencies, assuming light damping. Based on the above results, the base structure can be modelled as a SDOF system, i.e. a flexible base with an effective mass supported by a spring. Therefore, the active vibration isolation system used in the experiment can be simulated using the theoretical model described in the earlier chapters, which is an equipment mass mounted on a flexible base structure through a distributed parameter isolator.

To measure the performance of the system without control, the equipment structure and springs were reassembled onto to the base plate. The transmissibility and velocity response of the active vibration isolation system without control were measured when the large vibrator was driven with white noise and the actuators on the equipment plate were inactive. The vibrator input voltage was again used as the reference signal. The acceleration responses were passed through charge amplifiers to obtain the velocity responses. The measured data was then averaged to obtain the transmissibility and the velocity response of the equipment plate per unit voltage to the power amplifier as shown in Figures 5.18 and 5.19. The predicted results are obtained using the parameters listed in Table 5.1.

There is a reasonable agreement between the measured and predicted results. The responses below 3 Hz are very noisy due to low sensitivity of the actuators and the mechanical plant, so that they are not presented. For the transmissibility shown in Figure 5.18, the base dynamics is excluded by definition of the transmissibility. The first peak at 18.4 Hz is the fundamental resonance peak of the system when the equipment structure is resonant on the stiffness of the four parallel springs. In the velocity response of the equipment plate shown in Figure 5.19, the base dynamics is included. The

resonance peaks at approximately 11.8 Hz and 50 Hz are the natural frequencies of the coupled system. In both figures the first internal resonance in the helical springs occurs around 404 Hz, which is well predicted by the theoretical model at 400 Hz. The second internal resonance in the springs, which is predicted to occur at 800 Hz, is strongly coupled with high-order modes in the equipment plate, which can no longer be assumed to be rigid at these relatively high frequencies. The resonance around 289 Hz is a rotational mode with a diagonal nodal line on the equipment plate and the resonance around 327 Hz is a flexural mode in the equipment plate, which were detected by analyzing the phase differences between the responses at different locations on the equipment plate. Therefore discrepancies at high frequencies are mainly due to the effect of the modal behaviour of the equipment plate, which are not considered in the theoretical study. The discrepancies at low frequencies in Figure 5.19 are due to high-pass filters incorporated in the power amplifier and charge amplifiers, which are also not accounted for in the theoretical model.

5.3.3 Stability analysis

To measure the open-loop frequency response, the four actuators fixed on top of the equipment plate were driven with the same white noise from the dynamic signal analyser through a power amplifier, while the primary vibrator was connected but inactive. The open-loop frequency response of the system was measured and averaged using the input to the power amplifier and the integrated output from the charge amplifiers.

The predicted and measured open-loop frequency responses of the four-spring active vibration isolation system are shown in Figure 5.20. Apart from some differences in the resonant amplitudes, the theoretical results agree fairly well with the experimental measurements, except for the unmodelled rotational modes around 32 Hz and 289 Hz, the unmodelled flexural modal behaviour around 327 Hz and in the frequency range above 500 Hz. The data below 3 Hz had low coherence due to the low instrumentation

sensitivity, so again they are not presented. The first IR in the helical springs around 404 Hz can be clearly identified and compares well with predictions. The second IR is again strongly coupled with some flexural modes in the equipment plate. The phase shift at low frequencies, which is greater than 90º, is due to the phase advances in the power amplifier and charge amplifiers. The phase shift at high frequencies, where the phase tends to decrease below -90º, is due to the phase lag in the low-pass filters incorporated inside the charge amplifiers.

The measured potential instability occurs at the first IR of the helical springs as predicted. This supports the stability analysis in the former theoretical study that the IRs might destabilize the AVF control system when the mass of the isolators becomes significant. The flexural mode in the equipment plate at 327 Hz also has the potential to destabilize the system, which is not considered in the theoretical study here but was identified and reported by Kim et al [52]. The cause of the instability in the experiment also includes the phase advances in the power amplifier and charge amplifiers. The power amplifier has a phase advance of up to about 90º at very low frequencies (under 5 Hz). Furthermore, an additional phase advance occurs in the charge amplifier. A phase advance of greater than 90º at very low frequencies can cause the Nyquist plot of the plant response to cross the negative real axis, thus making the system unstable to high gain [15, 43]. The experimental plant can also be potentially unstable at very high frequencies due to the high-order modes in the experimental structure as well as electrical causes. The low-pass filter incorporated inside the charge amplifier produces an effective time delay in the control loop, which can make the system unstable at high frequencies. Furthermore, the phase shift in the electromagnetic actuators can also be modelled as an additional time delay [52]. In this experiment, it has been found that the AVF control system first becomes unstable at very low frequencies, due to the phase advances in the charge amplifier and power amplifier with increased feedback control gain.

Figure 5.21 depicts the Nyquist plot of the open-loop frequency response of the active

vibration isolation system corresponding to the results and frequency range shown in Figure 5.20. Two loops in the left half of the complex plane crossing the negative real axis are caused by the first IR in the helical springs at 404 Hz (smaller loop on left half) and the flexural mode in the equipment plate at 327 Hz (larger loop on left half) respectively. The Nyquist plot of the plant response also crosses the negative real axis at very low frequencies due to the phase advances in the power amplifier and charge amplifiers, which is not shown in Figure 5.21 since this is only plotted for frequencies from 3 Hz to 1 kHz. In these experiments, it was this phase shift that caused instability at very low frequencies before the potential instabilities above became important.

5.3.4 Control performance

A single-channel AVF control on the active vibration isolation system was implemented on each of the four springs when the equipment structure was mounted on the base structure. The primary vibrator was again driven with white noise. The velocity responses of the equipment and base were also obtained using accelerometers through charge amplifiers and then passed to the signal analyzer. The velocity response at the centre of the equipment plate was fed back into four actuators through a power amplifier to generate the control forces, which were identical for each actuator. Each feedback channel had thus an equal, constant feedback gain.

Figure 5.22 shows the predicted and measured transmissibility of the active vibration isolation system with various control gains, where the original transmissibility without control is also shown for comparison. Figure 5.23 shows the velocity response of the equipment plate per unit voltage to the power amplifier, which drove the primary vibrator, without control and with various control gains. Responses less than 3 Hz are again excluded from the plots. There is good agreement between the predicted and measured results for low and high gains used. The system resonance peaks at low frequencies are well attenuated with an increased control gain as predicted. However, the resonance peaks at high frequencies including the first IR peak in the springs are not

reduced because the mass of the equipment structure dominates the response at this frequency range as discussed in the theoretical study. Zooming into the amplitude at the first IR in the helical springs at 404 Hz shows that there is a small amplification caused by the phase shift at this frequency. The similar amplification in the amplitude occurs around 327 Hz also due to the corresponding phase shift. The gain margin for the higher feedback gain used in Figures 5.22 and 5.23 was 1.8 dB, determined by the very low frequency instability.

Therefore, as predicted theoretically, good control performance is achieved around the system resonance peaks at low frequencies, while the isolation performance is not improved at high frequencies where the equipment mass dominates the response. Furthermore, there are small amplifications at some frequencies due to the potential instability caused by IRs in the spring and flexural modal behaviour of the equipment plate.

5.3.5 Approaches to stabilize the AVF control system

In this experiment, because the base structure is much lighter and more flexible than the equipment structure, the system is then much more likely to be unstable at some IR frequencies in the isolator. Two approaches discussed in section 5.2 were implemented experimentally and presented in following sections.

5.3.5.1 Adding more mass to the base

As presented theoretically, adding mass to the base structure is a simple way to change the base response. A mass of 1.8 kg was attached to the base plate to investigate its stabilizing effect on the experimental plant. The measured open-loop frequency responses of the potential stabilized system are shown in Figure 5.24, where the original open-loop frequency responses are also shown for comparison. It can be seen that the base resonance is reduced to a lower frequency due to the attachment of the mass, as predicted in the theoretical study. The amplitude and phase of the first IR are also restricted. As shown in Figure 5.25 for the zoomed open-loop frequency response, it can

be seen that the phase at the first IR is reduced from -235º to -175º, which means the potential instability is eliminated by adding mass to the base. However, the flexural mode in the equipment plate at 327 Hz is not affected, because the change of the base dynamics does not affect the flexural modal behaviour in the equipment plate. Figure 5.26 depicts the Nyquist plot of the open-loop frequency response for the original and stabilized system. The detailed Nyquist plot between 350 and 450 Hz where only the first IR occurs is shown in Figure 5.27. It can be seen that, for the stabilized system with more mass on the base, the loop on the left half of the complex plane due to the first IR in the spring is shifted to the third quadrant rather than crossing the negative real axis, so that the AVF control system becomes stable at this frequency. However, due to the phase advances in the charge amplifier and power amplifier, the instability of the control system with additional mass on the base again still first occurred at very low frequencies. The control performance of the system with more mass on the base is shown in Figure 5.28. It can be seen that the resonance peaks at low frequencies are attenuated without the compromise of an increase at the first IR in the helical springs.

5.3.5.2 Electronic means: introducing a lead compensator

A schematic diagram of an electrical circuit for a lead compensator is shown in Figure 5.29(a), which consists of two resistors (R_1, R_2) and one capacitor (C). The transfer function between the output e_o and input e_i is given by [74]

$$\frac{e_o}{e_i} = \frac{R_2}{R_1 + R_2} \frac{1 + R_1 C s}{1 + \dfrac{R_2}{R_1 + R_2} R_1 C s} \tag{5.23}$$

Letting $\alpha = R_2 / (R_1 + R_2)$ and $T_1 = R_1 C$, the transfer function can be written as

$$\frac{e_o}{e_i} = \alpha \frac{1 + j\omega T_1}{1 + j\alpha\omega T_1} \quad (\alpha < 1) \tag{5.24}$$

which is identical to equation (5.2). In the experiment, the phase of the open-loop frequency response of the AVF control system at the first IR is -235º. To stabilize the control system at this frequency, a phase lead compensator of at least 55º is required. The coefficient α can thus be determined by equation (5.5) to give

$$\alpha = \frac{R_2}{R_1 + R_2} < 0.1 \tag{5.25}$$

If $\alpha = 0.03$ is chosen, in order to achieve the maximum phase lead compensation at 404 Hz, where the first IR occurs, the coefficient T_1 can be determined by equation (5.6) to give

$$T_1 \approx 0.0023 \tag{5.26}$$

By choosing the appropriate values for the resistances and the capacitance, the required lead compensator can be realized as shown in Figure 5.29(b). The measured and predicted frequency responses of the lead compensator agree well, see Figure 5.30.

The four-spring active vibration isolation system with a lead compensator and its signal path are shown in Figure 5.31. The lead compensator was introduced between the charge amplifier and the power amplifier. The velocity response at the centre of the equipment plate was obtained using an accelerometer connected to the charge amplifier, integrated and then passed to the signal analyzer. The velocity response was also fed back into the four actuators through the power amplifier to generate the control forces.

The measured open-loop frequency responses of the potential stabilized system are shown in Figure 5.32, where the original open-loop frequency responses are also shown for comparison. It can be noted that the phase is constrained to be less than -180º both at the first IR frequency of 404 Hz and at the flexural mode in the equipment plate of 327 Hz, which means that these potential instabilities are eliminated by introducing the particular lead compensator. Figure 5.33 shows the Nyquist plot of the open-loop frequency response for the stabilized system with the lead compensator. It can be seen that there is no loop on the left half of the complex plane crossing the negative real axis, so that the AVF control system becomes unconditionally stable within this frequency range. However, it should also be noted that the magnitude of the open-loop frequency response is reduced due to the lead compensator. As a consequence, the instability in such a control system does not first occur at low frequencies. As shown in Figure 5.34, which depicts the open-loop frequency response of the system with the lead compensator up to 5 kHz, the control system first became unstable at a natural

frequency of the system at about 1160 Hz, corresponding to the Nyquist plot crossing the negative real axis shown in Figure 5.35.

The decrease in the magnitude of the open-loop frequency response also means that greater feedback control gain is required for the stabilized system with the lead compensator to achieve the same control performance as that of the original system. The control performance of the stabilized system with the lead compensator is shown in Figure 5.36. It can be seen that the resonance peaks at low frequencies are attenuated without the compromise of the increase at both the first IR in the helical springs and the flexural mode in the equipment plate of 327 Hz. But the control performance is limited due to the instability occurring at a natural frequency of the system at approximately 1160 Hz. Figure 5.37 shows the control performance of the system upto 5 kHz. It can be clearly seen that the velocity response of the equipment is amplified around 1160 Hz, which will cause instability with increased control gain.

5.4 Conclusions

Active vibration isolation system containing a distributed parameter isolator under AVF control has been investigated experimentally on a four-spring active vibration isolation system. The effects of IRs on the stability and control performance of AVF control system have been examined experimentally. It has been shown that the first IR in the helical spring is a potential danger to the stability of the AVF control system. It has also been shown that the AVF control is only effective in attenuating the resonance peaks at relatively low frequencies, while it cannot suppress the IRs at higher frequencies where the equipment mass dominates the response. Different approaches to stabilize the AVF control system have also been investigated theoretically and experimentally based on the proposed stability condition. It has been confirmed experimentally that adding more mass to the base and introducing a lead compensator are effective solutions to eliminate the potential instability at IRs in the isolator. However, in the experiment instabilities still occur both at low frequencies due to the phase advances in the charge amplifier and power amplifier, and at high frequencies due to the unmodelled high-order modes in the

equipment and base plate, which have not been considered theoretically. The control performance of AVF control system is thus limited by these instabilities which are not internal isolator resonances.

In this experimental work, the base plate was attached to the washers underneath the helical springs by wax. For stronger bondage between the base plate and the isolators, glue can be used in further experimental validation instead of wax.

Equipment structure	Material of the equipment plate	Aluminum
	Dimension of the equipment plate	(160×160×10mm)
	Mass of each actuator	0.91 kg
	Mass of the equipment structure	5 kg
Spring	Mass of each spring	27.1 g
	Stiffness of each spring	1.73×10^4 N/m
Base structure	Material of the base plate	Aluminum
	Dimension of the base plate	(160×160×10mm)
	Effective mass	1.18 kg
	Effective stiffness	4.25×10^4 N/m

Table 5.1 *Physical properties and geometrical data of the four-spring active vibration isolation system.*

Natural Frequency (Hz) $f_{ij}=\frac{\lambda_{ij}^2}{2\pi a^2}\left(\frac{Eh^2}{12\rho\left(1-\nu^2\right)}\right)^{\frac{1}{2}}$; $i=1,2,3...$; $\mathrm{j}=1,2,3...$

Mode Sequence	1	2	3	4	5	6
$\lambda_{ij}^2\ (i,j)$	13.49 (22)	19.79 (13)	24.43 (31)	35.02 (32)	35.02 (23)	61.53 (41)
f_{ij}	1297	1902	2348	3366	3366	5914

Table 5.2 *Natural frequencies of a free-free-free-free plate, when the length and width of the plate a=b=*0.16 m*, the thickness h=*0.01 m*, Young's modulus E=*69 Gpa*, density* $\rho=2700$ kg/m^3 *and Poisson's ratio* $\nu=0.33$*. i is the number of half-waves in mode shape along horizontal axis and j is the number of half-waves in mode shape along vertical axis [94].*

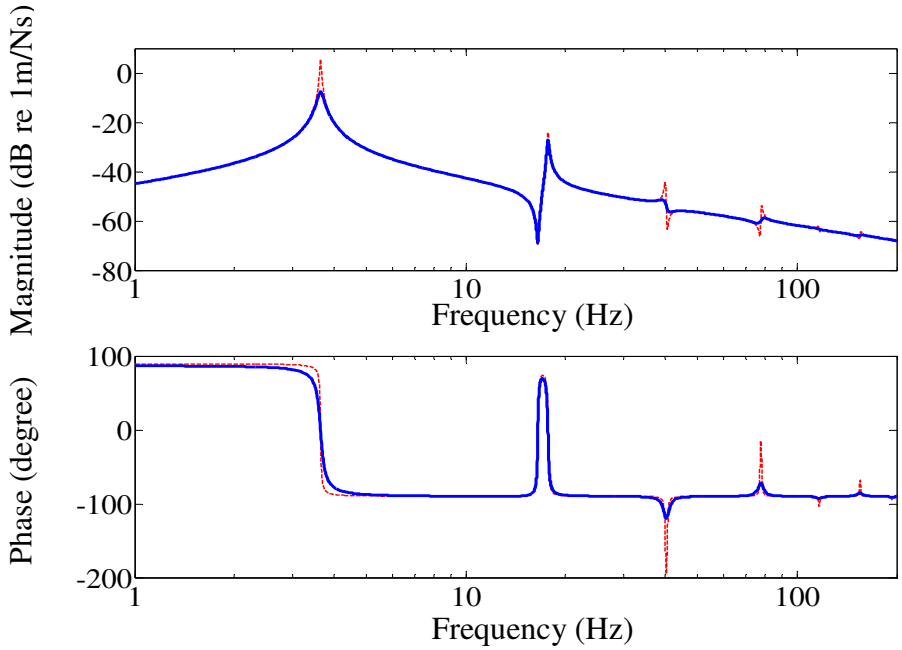

Figure 5.1 *Plant responses of the AVF control system on a flexible base containing a highly damped (solid line, loss factor in the isolator* $\eta_i = 0.05$*) or lightly damped (dashed line,* $\eta_i = 0.01$*) distributed parameter isolator, when the ratio of the mass of the isolator to the mass of the equipment* $\mu_i = 0.1$*, the ratio of the mass of the base to the mass of the equipment* $\mu_b = 0.5$*, the ratio of the static stiffness of the isolator to the base stiffness* $\mu_k = 0.1$*, and loss factor in the base* $\eta_b = 0.01$*.*

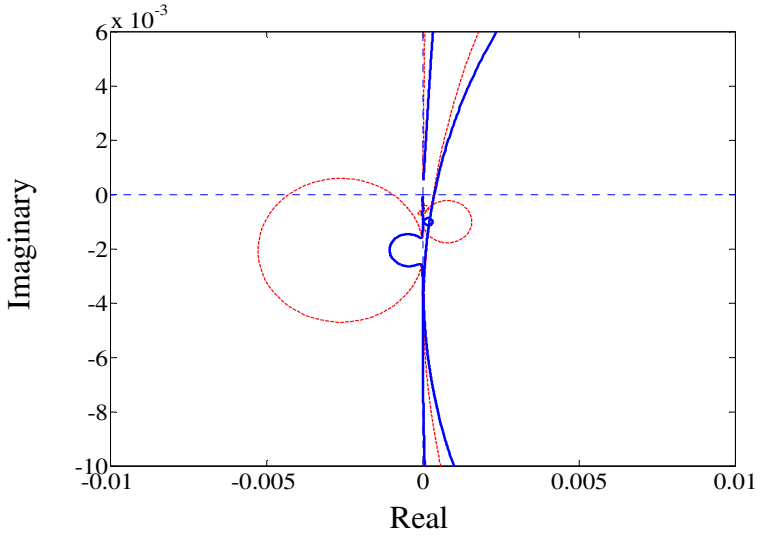

Figure 5.2 *Zoomed Nyquist plot of the plant responses of the AVF control system on a flexible base containing a highly damped (solid line,* $\eta_i = 0.05$*) or lightly damped (dashed line,* $\eta_i = 0.01$*) distributed parameter isolator when* $\mu_i = 0.1$*,* $\mu_b = 0.5$*,* $\mu_k = 0.1$ *and* $\eta_b = 0.01$*.*

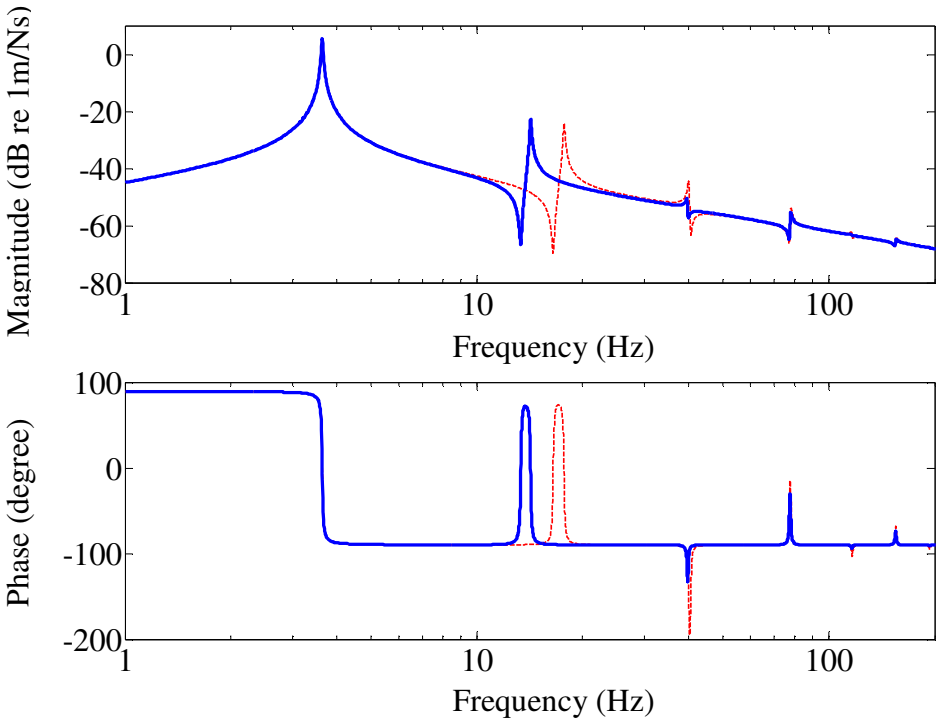

Figure 5.3 *Plant responses of the AVF control system containing a distributed parameter isolator on a heavy (solid line, $\mu_b = 0.8$) or light (dashed line, $\mu_b = 0.5$) flexible base when $\mu_i = 0.1$, $\mu_k = 0.1$ and $\eta_i = \eta_b = 0.01$.*

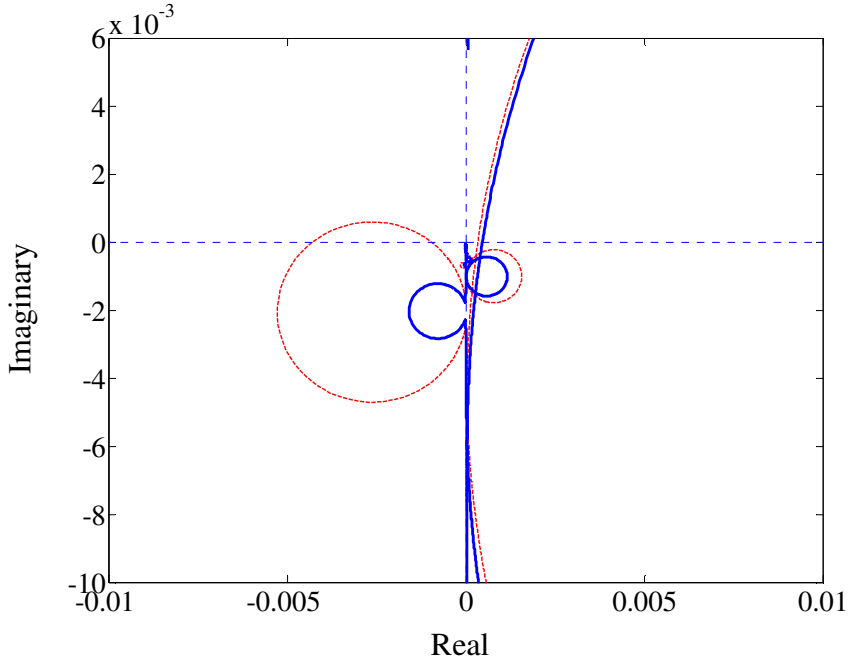

Figure 5.4 *Zoomed Nyquist plot of the plant responses of the AVF control system containing a distributed parameter isolator on a heavy (solid line, $\mu_b = 0.8$) or light (dashed line, $\mu_b = 0.5$) flexible base when $\mu_i = 0.1$, $\mu_k = 0.1$ and $\eta_i = \eta_b = 0.01$.*

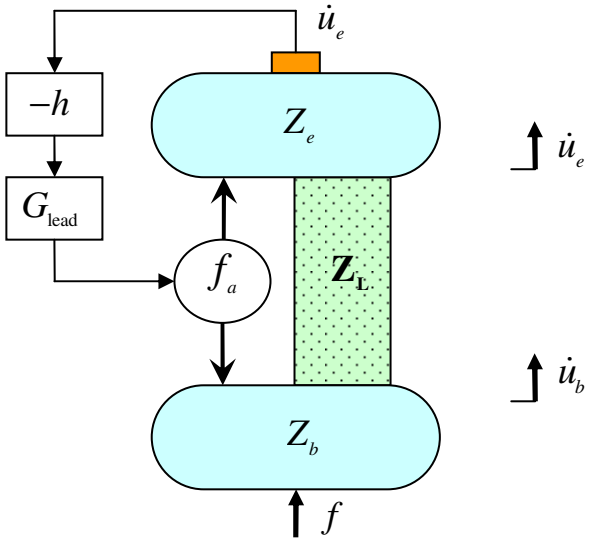

Figure 5.5 *Schematic diagram of the active vibration isolation system containing a distributed parameter isolator on a flexible base under AVF control with a lead compensator, where* $\dot{u}_e$ *and* $\dot{u}_b$ *are velocity of the equipment and the base respectively;* Z_e *and* Z_b *are the input impedances of the equipment and the base, respectively;* $\mathbf{Z}_\mathbf{L}$ *is the impedance matrix of the isolator; h is the constant feedback control gain; f is the primary force;* f_a *is the active control force and* G_{lead} *is the frequency response of the lead compensator.*

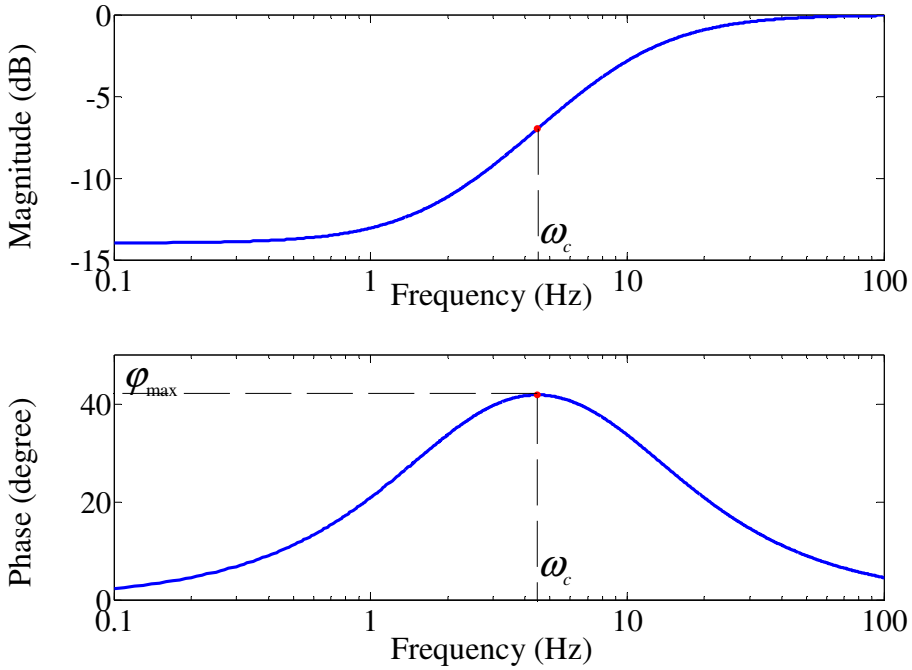

Figure 5.6 *Frequency response of a lead compensator when the coefficients* $\alpha = 0.2$ *and* $T_1 = 0.5$.

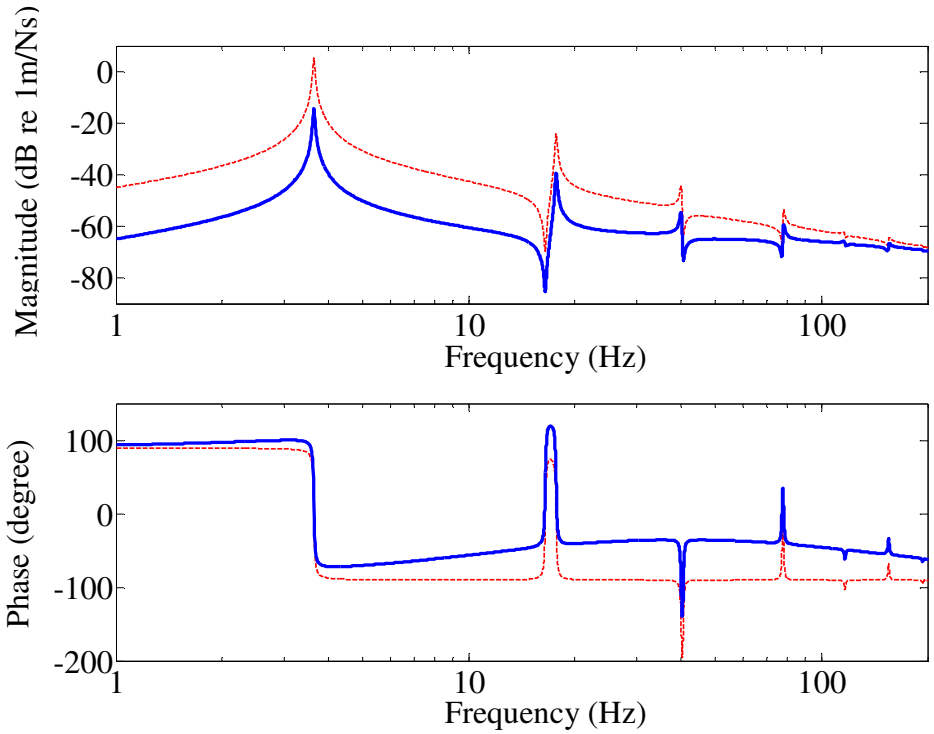

Figure 5.7 *Open-loop frequency responses of the AVF control system on a flexible base with (solid line) or without (dashed line) a lead compensator when* $\mu_i = 0.1$, $\mu_b = 0.5$, $\mu_k = 0.1$, $\eta_i = \eta_b = 0.01$, $\alpha = 0.1$ *and* $T_1 = 0.0125$.

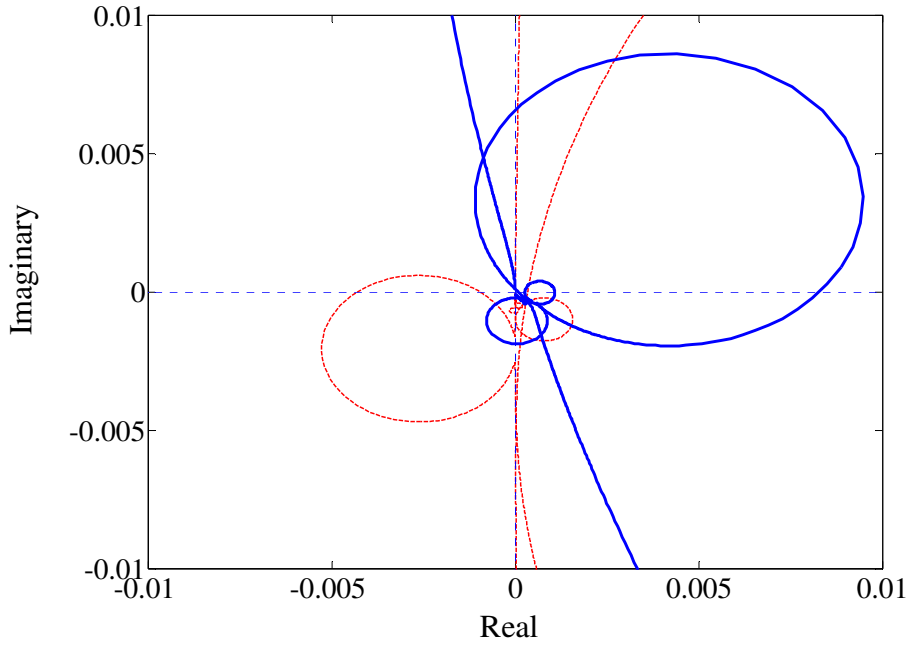

Figure 5.8 *Zoomed Nyquist plot of the open-loop frequency responses of the AVF control system on a flexible base with (solid) or without (dashed) a lead compensator when* $\mu_i = 0.1$, $\mu_b = 0.5$, $\mu_k = 0.1$, $\eta_i = \eta_b = 0.01$, $\alpha = 0.1$ *and* $T_1 = 0.0125$.

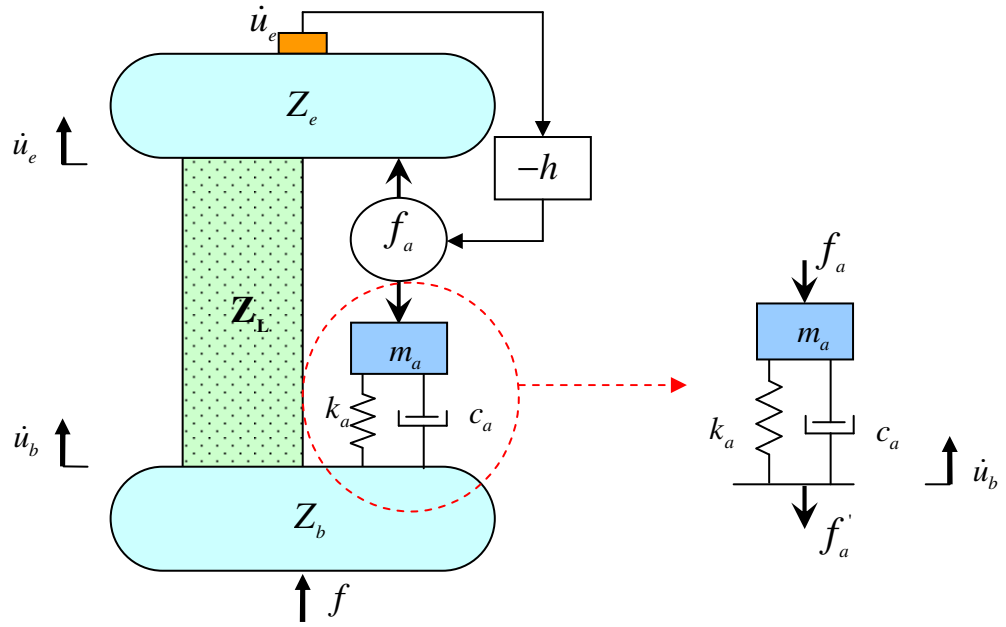

Figure 5.9 *Schematic diagram of the active vibration isolation system containing a distributed parameter isolator on a flexible base under AVF control with an additional system attached on the base, where* m_a, k_a *and* c_a *are the mass, stiffness and damping coefficient of the additional system, respectively, and* f_a' *is the active control force transmitted to the base through the additional system.*

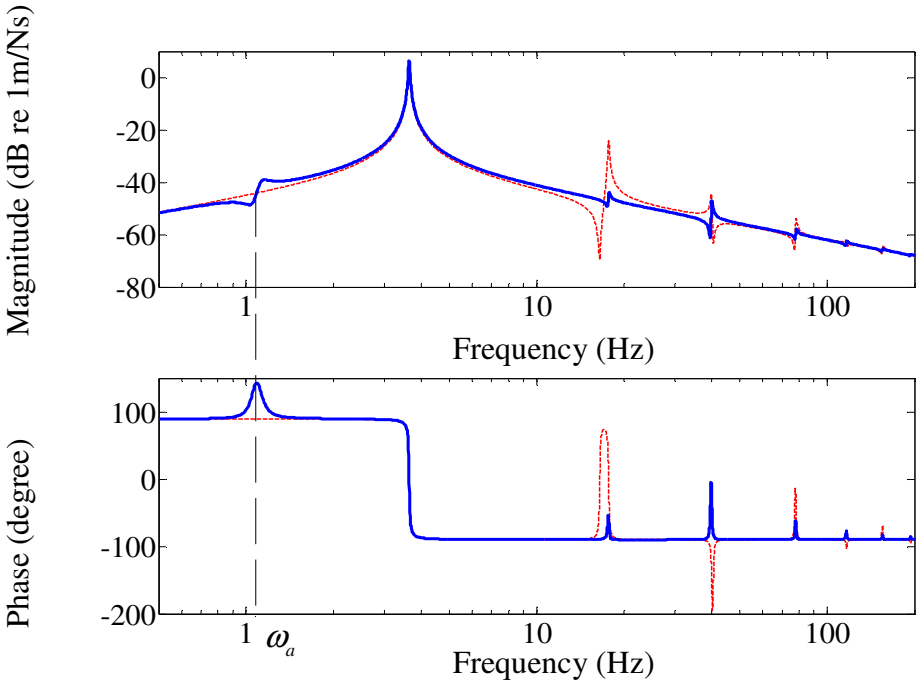

Figure 5.10 *Plant responses of the AVF control system on a flexible base with (solid) or without (dashed) an additional system attached on the base when* $\mu_i = 0.1$, $\mu_b = 0.5$, $\mu_k = 0.1$, $\eta_i = \eta_b = 0.01$, *the natural frequency and damping ratio of the additional system respectively* $\omega_a \approx 0.29\omega_e$ *and* $\zeta_s = 0.05$.

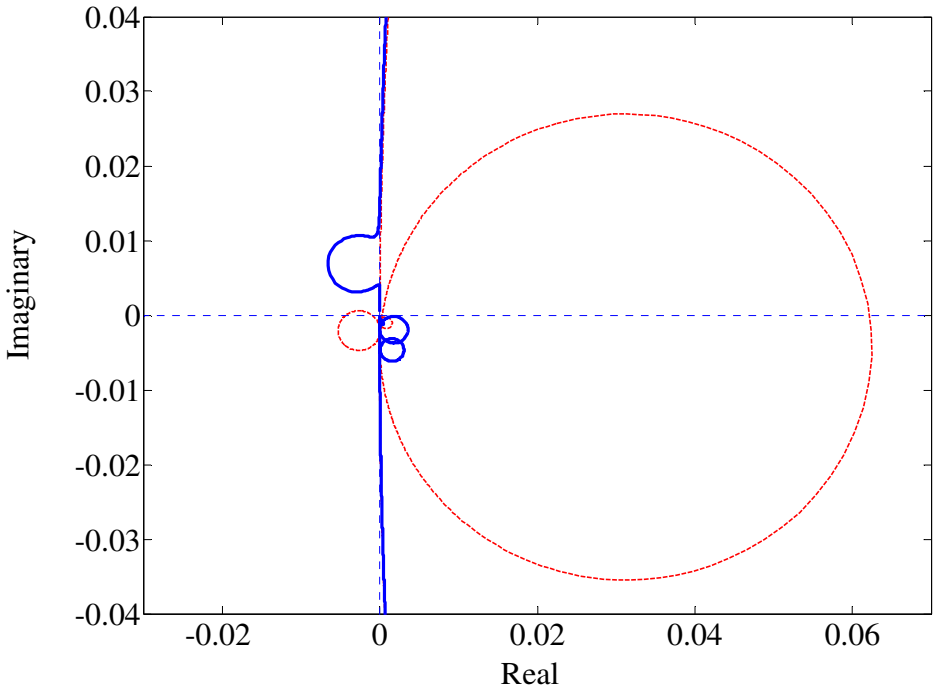

Figure 5.11 *Zoomed Nyquist plot of the plant responses of the AVF control system on a flexible base with (solid) or without (dashed) an additional system attached on the base when* $\mu_i = 0.1$, $\mu_b = 0.5$, $\mu_k = 0.1$, $\eta_i = \eta_b = 0.01$, $\omega_a \approx 0.29\omega_e$ *and* $\zeta_s = 0.05$.

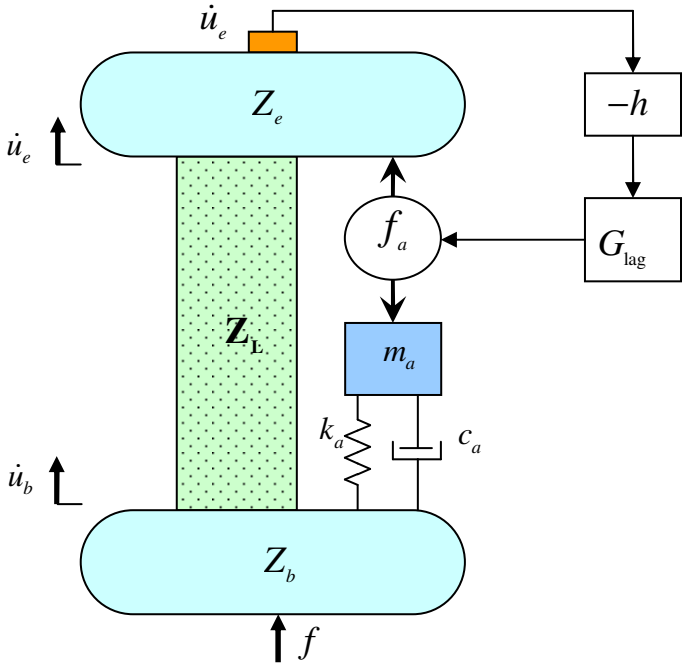

Figure 5.12 *Schematic diagram of the active vibration isolation system containing a distributed parameter isolator on a flexible base under AVF control with an additional system attached on the base and a lag compensator with frequency response* G_{lag} *in the feedback loop.*

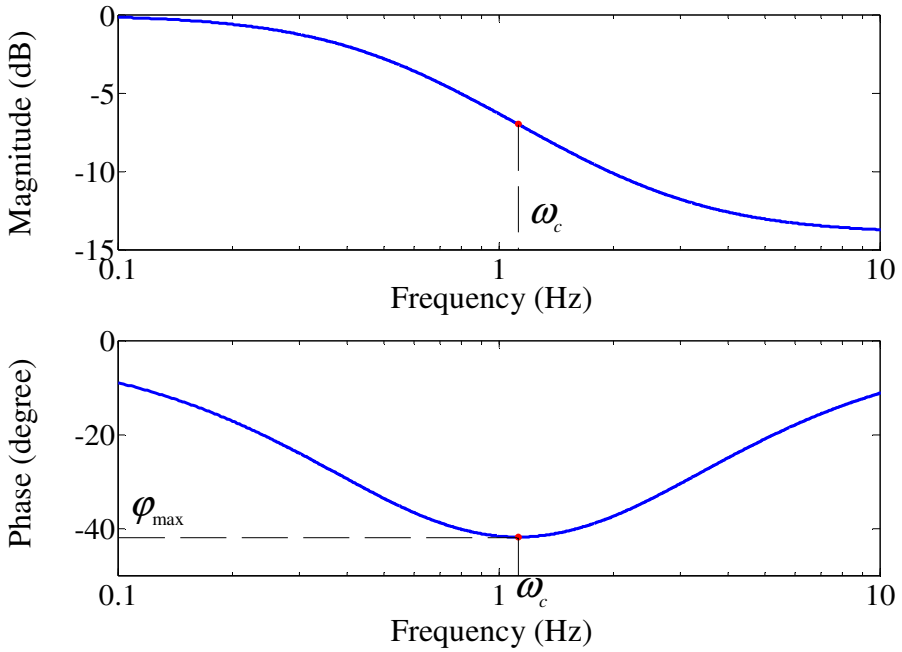

Figure 5.13 *Frequency response of a lag compensator when the coefficient* $\beta = 5$ *and the frequency where the maximum phase lag occurs* $\omega_c = \omega_a$.

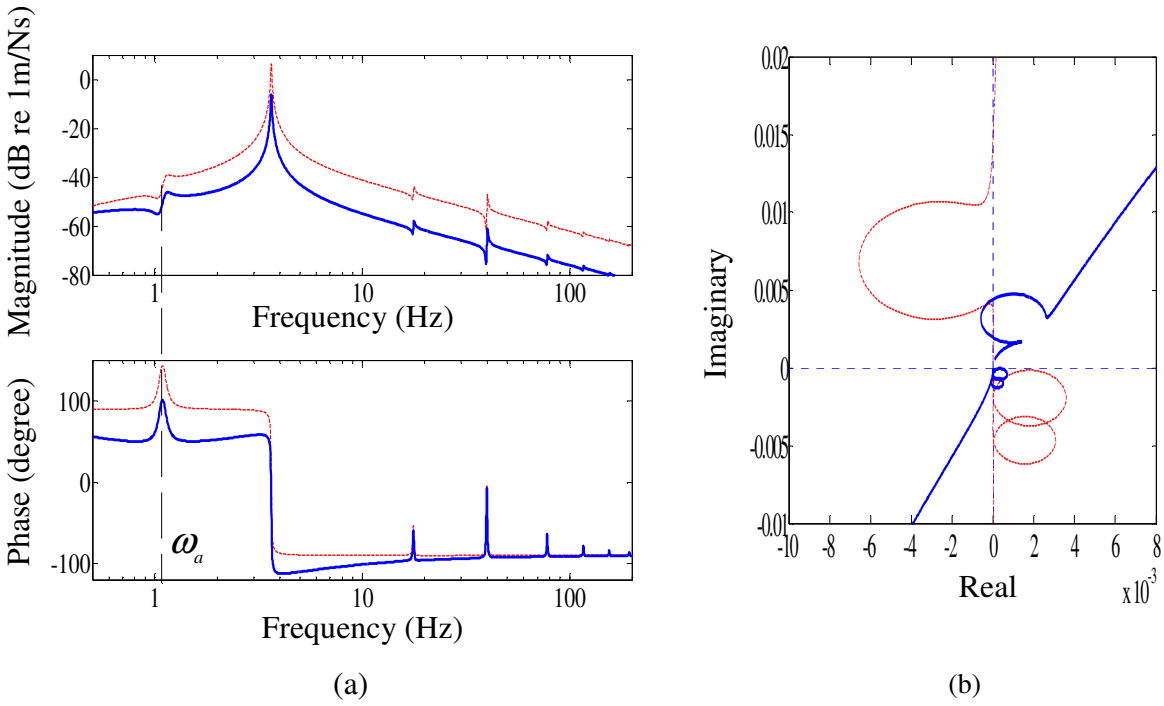

Figure 5.14 *(a) open-loop frequency response and (b) its Nyquist plot of the stabilized AVF control system with an additional system on the base and with (solid) or without (dashed) a lag compensator in the feedback loop when* $\mu_i = 0.1$, $\mu_b = 0.5$, $\mu_k = 0.1$, $\eta_i = \eta_b = 0.01$, $\omega_a \approx 0.29\omega_e$, $\zeta_s = 0.05$, $\beta = 5$ *and* $\omega_c = \omega_a$.

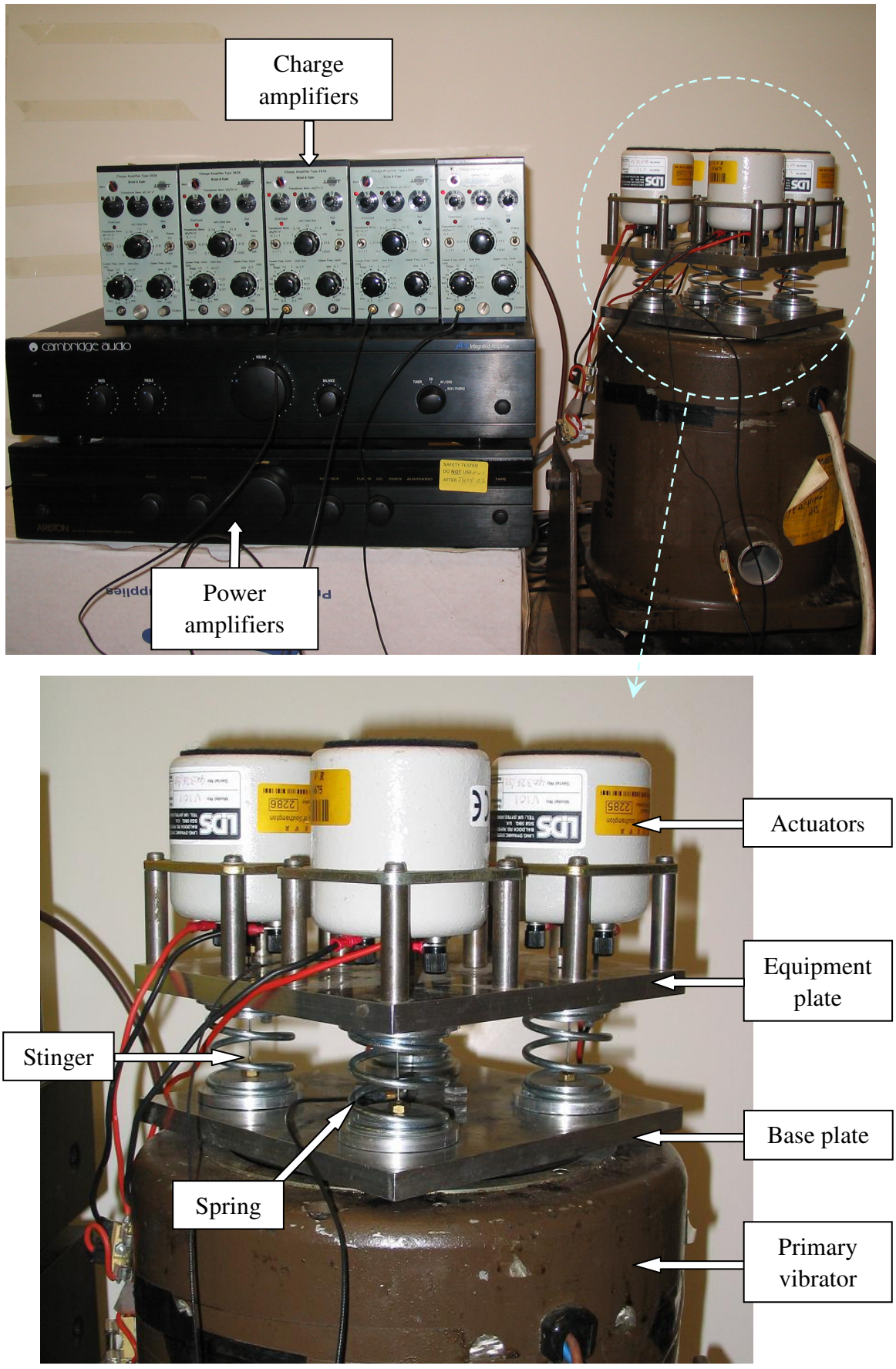

Figure 5.15 *Photographs of the four-spring active vibration isolation system.*

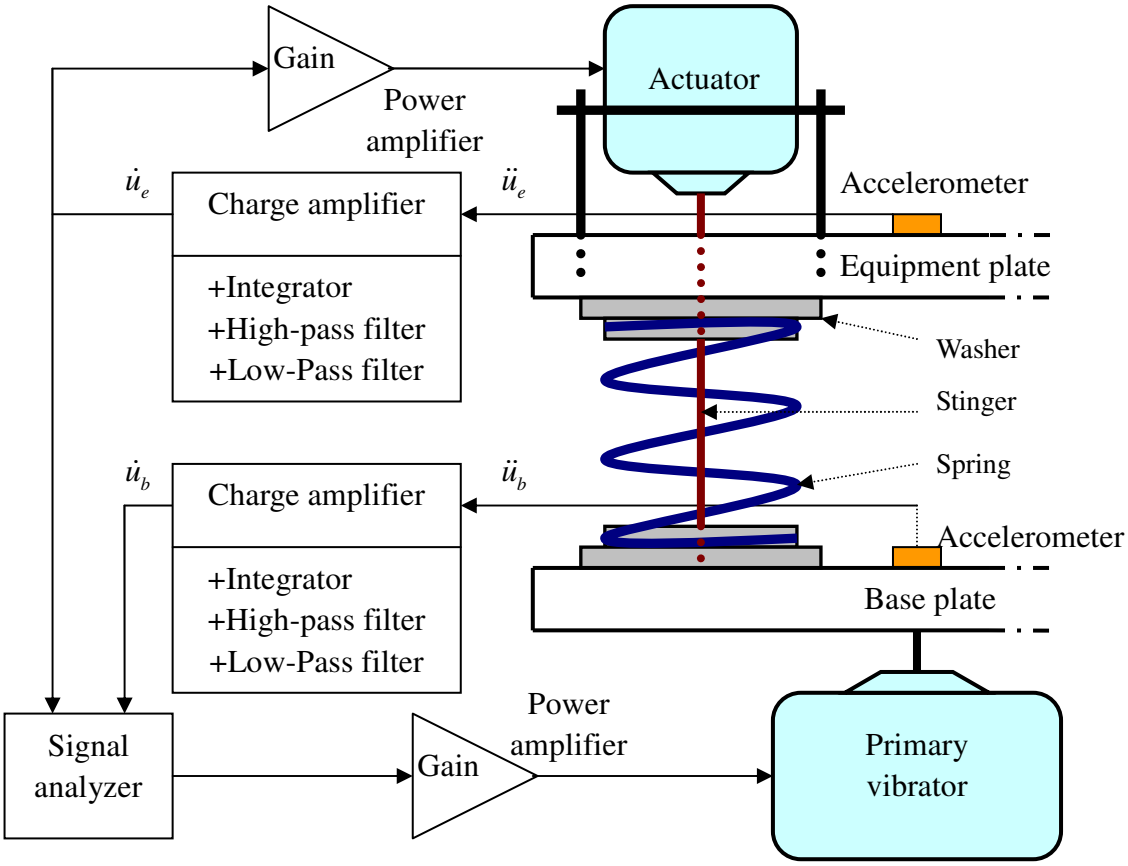

Figure 5.16 *Schematic diagram of one corner of the four-spring active vibration isolation system, where* $\ddot{u}_e$ *and* $\ddot{u}_b$ *are acceleration of the equipment and the base respectively.*

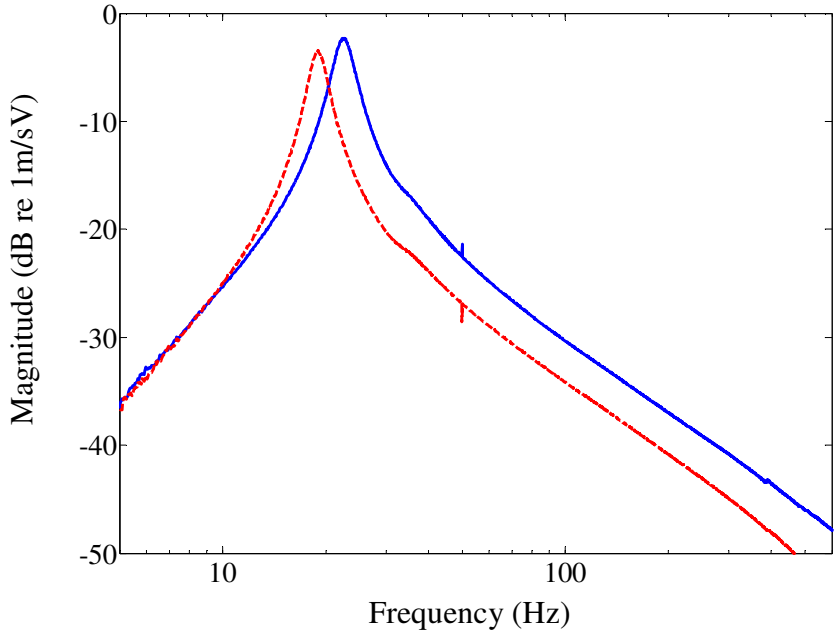

Figure 5.17 *Measured velocity response of the base plate per unit voltage to the power amplifier with different weight on the base structure: base plate with 0.8 kg mass attached (solid line) and base plate with 1.8 kg mass attached (dashed line).*

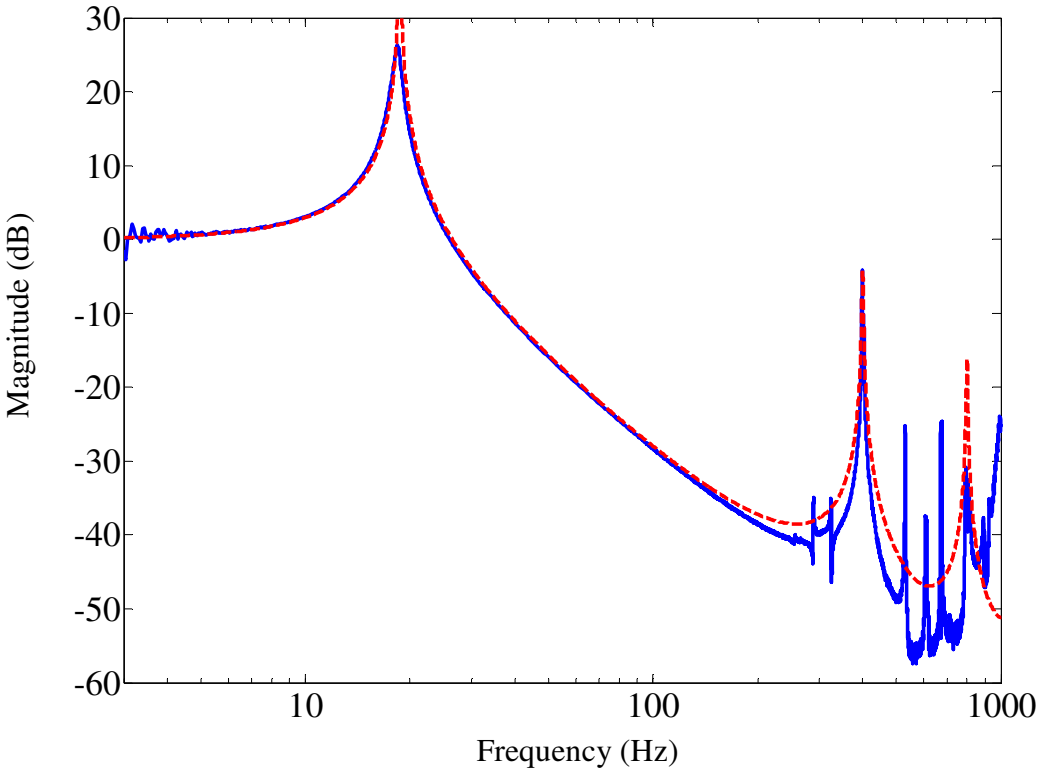

Figure 5.18 *Measured (solid line) and predicted (dashed line) transmissibility of the active vibration isolation system without control.*

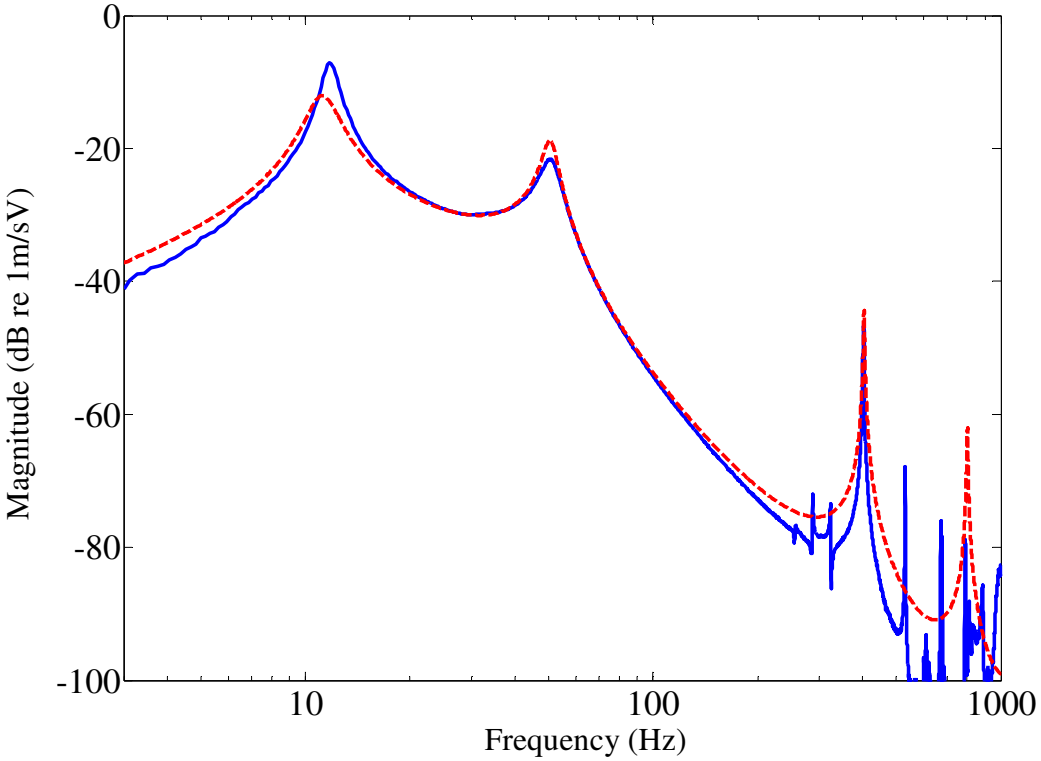

Figure 5.19 *Measured (solid line) and predicted (dashed line) velocity response of the equipment plate per unit voltage to the power amplifier without control.*

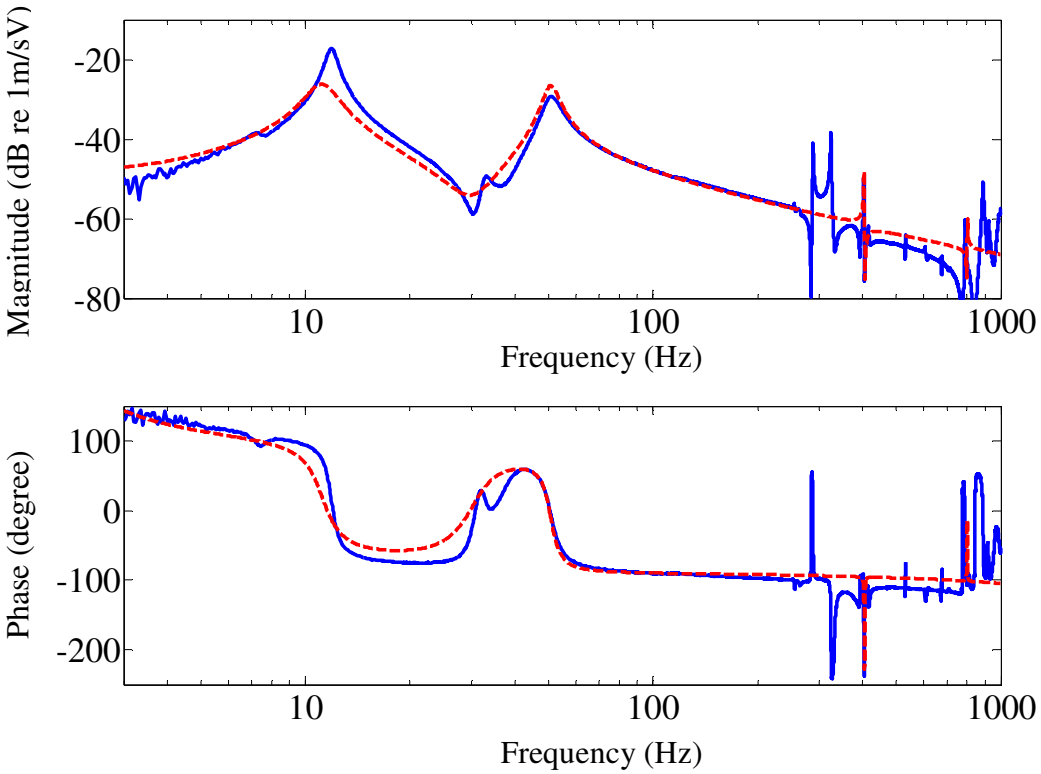

Figure 5.20 *Measured (solid line) and predicted (dashed line) open-loop frequency response of the active vibration isolation system.*

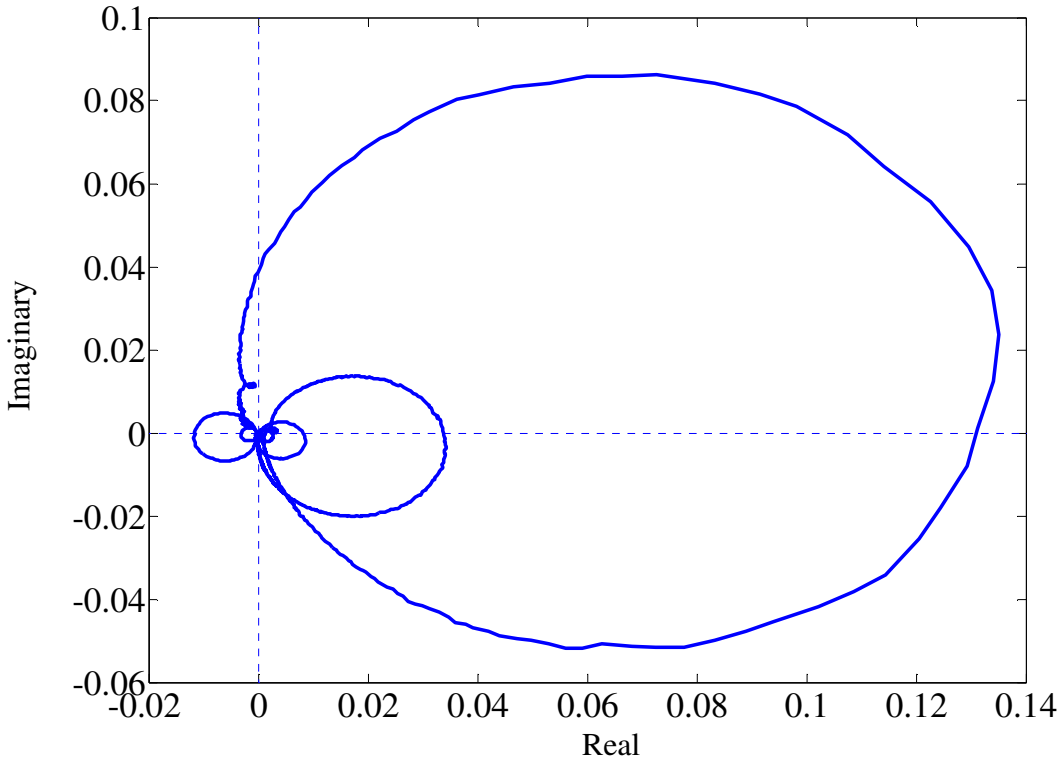

Figure 5.21 *Measured Nyquist plot of the open-loop frequency response of the active vibration isolation system.*

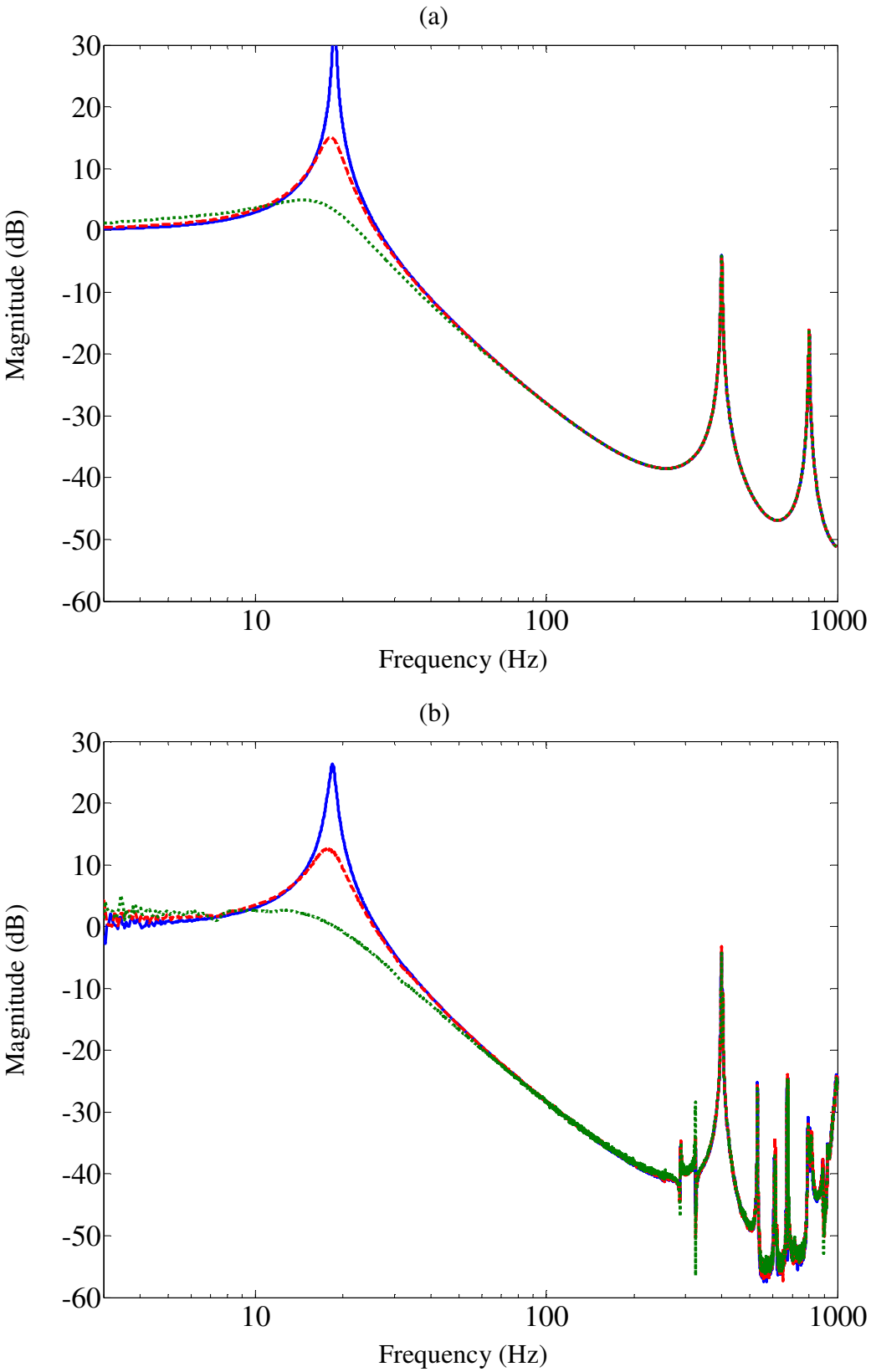

Figure 5.22 *(a) predicted and (b) measured transmissibility of the active vibration isolation system with various feedback gains: without control (solid line), low control gain (dashed line) and high control gain (dotted line).*

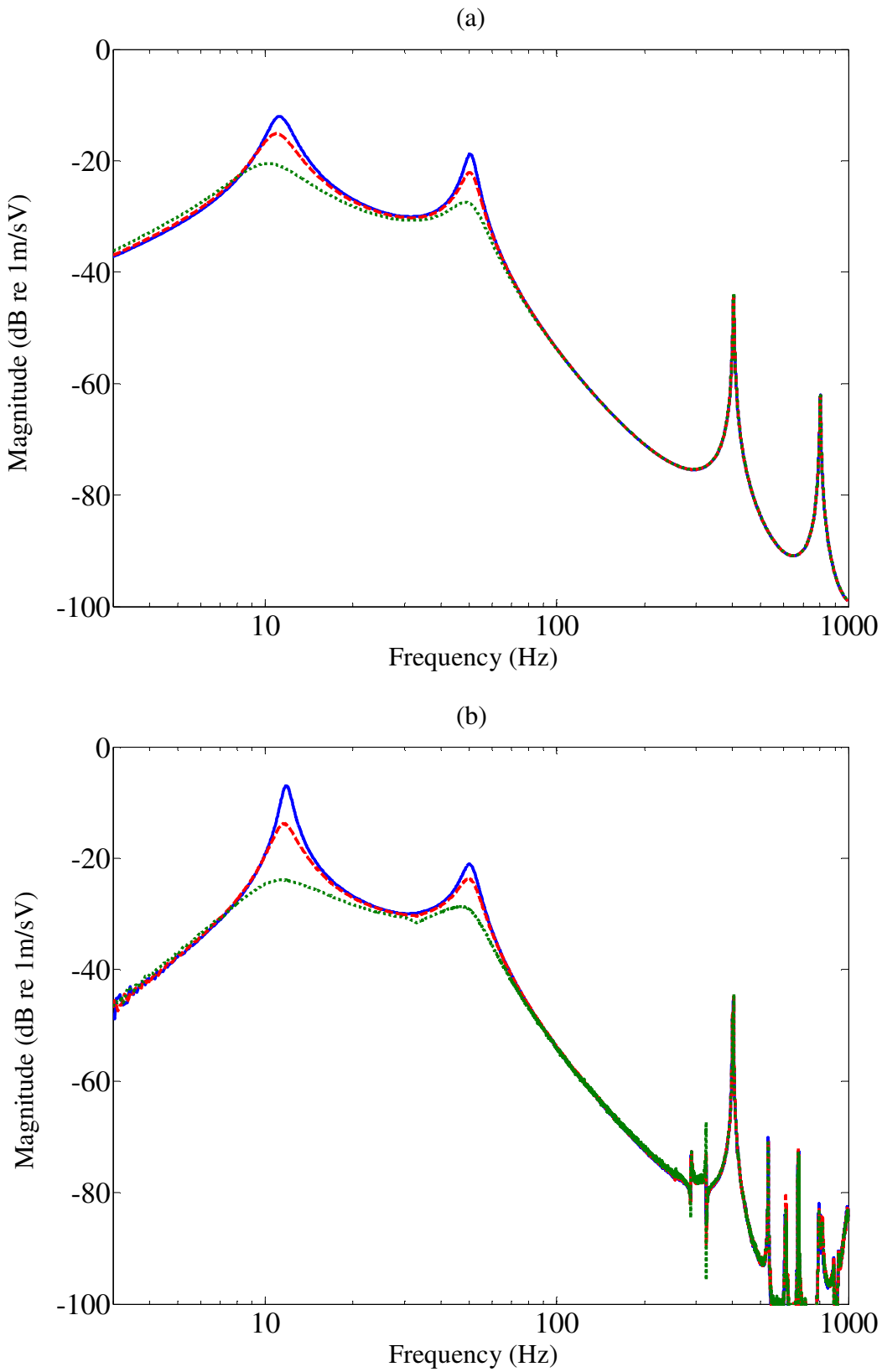

Figure 5.23 *(a) predicted and (b) measured velocity response of the equipment plate per unit voltage to the power amplifier of the active vibration isolation system with various feedback gains: without control (solid line), low control gain (dashed line) and high control gain (dotted line).*

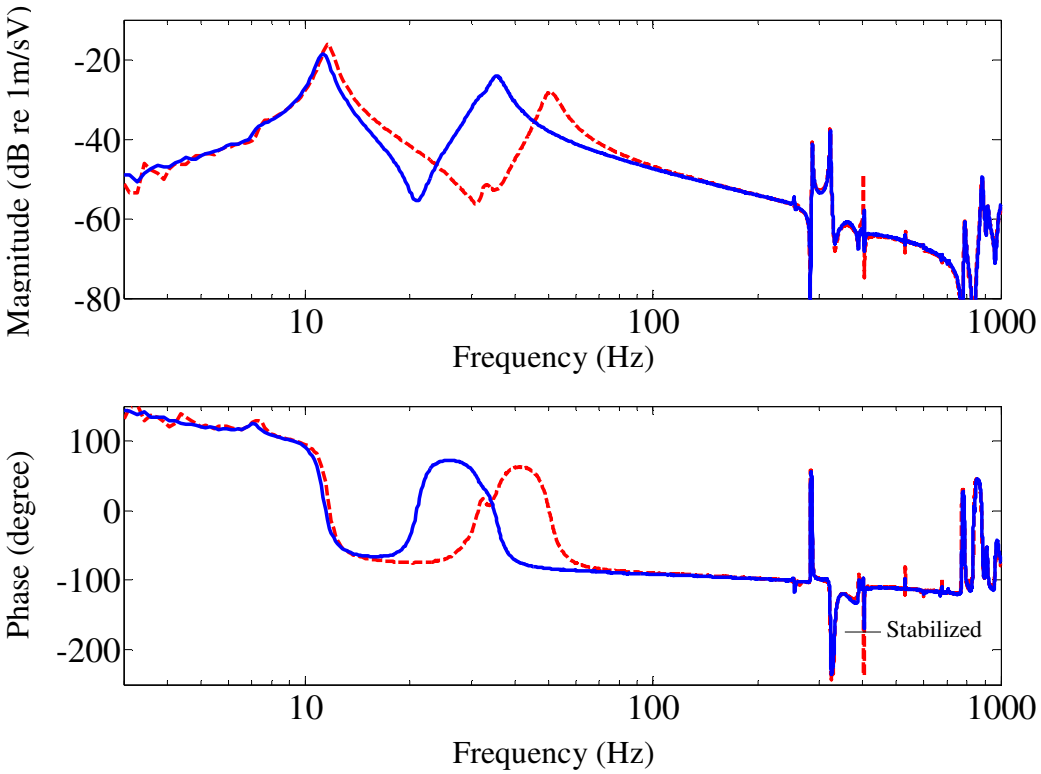

Figure 5.24 *Measured open-loop frequency response of the active vibration isolation system: stabilized system (solid line) and original system (dashed line).*

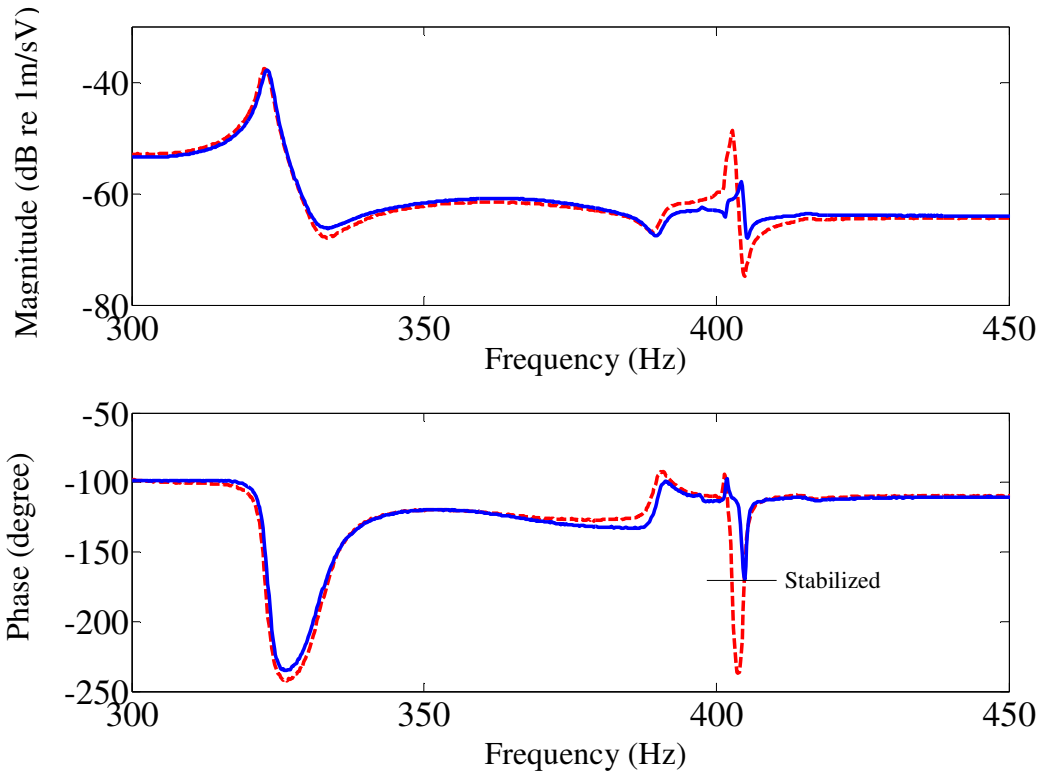

Figure 5.25 *Zoomed experimental open-loop frequency response of the active vibration isolation system: stabilized system (solid line) and original system (dashed line).*

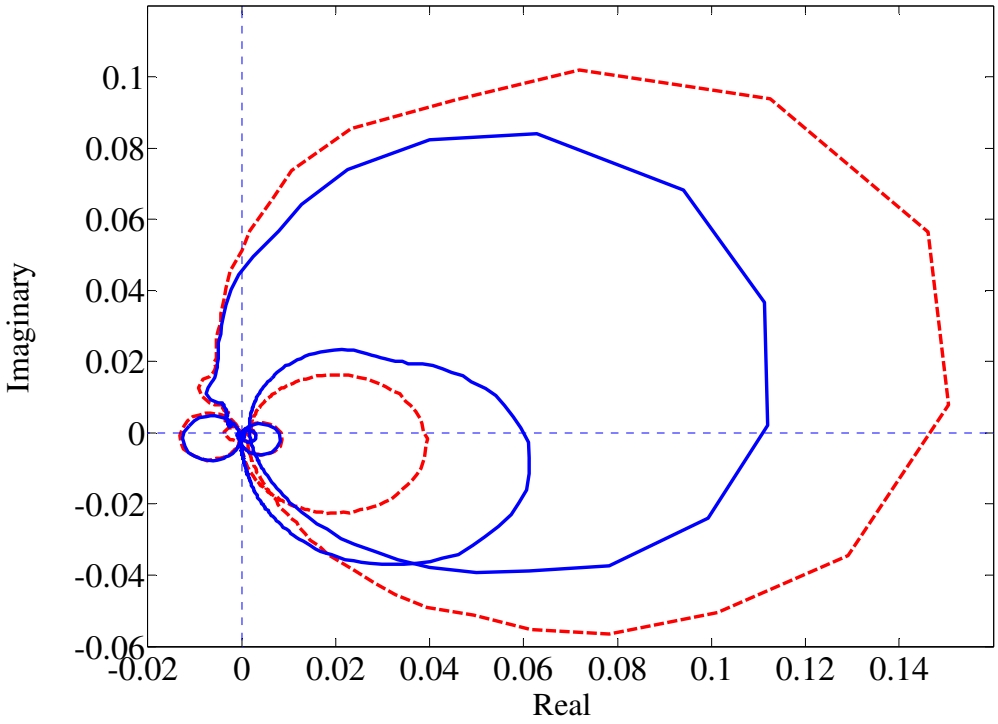

Figure 5.26 *Measured Nyquist plot of the open-loop frequency response of the active vibration isolation system: stabilized system (solid line) and original system (dashed line).*

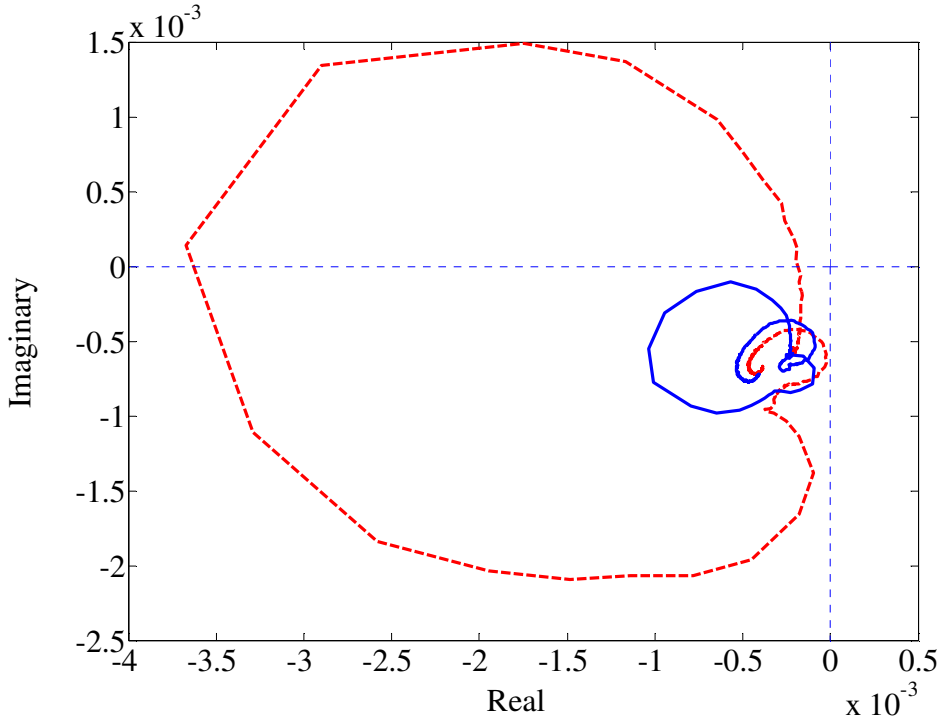

Figure 5.27 *Measured Nyquist plot of the open-loop frequency response of the active vibration isolation system between 350 Hz and 450 Hz: stabilized system (solid line) and original system (dashed line).*

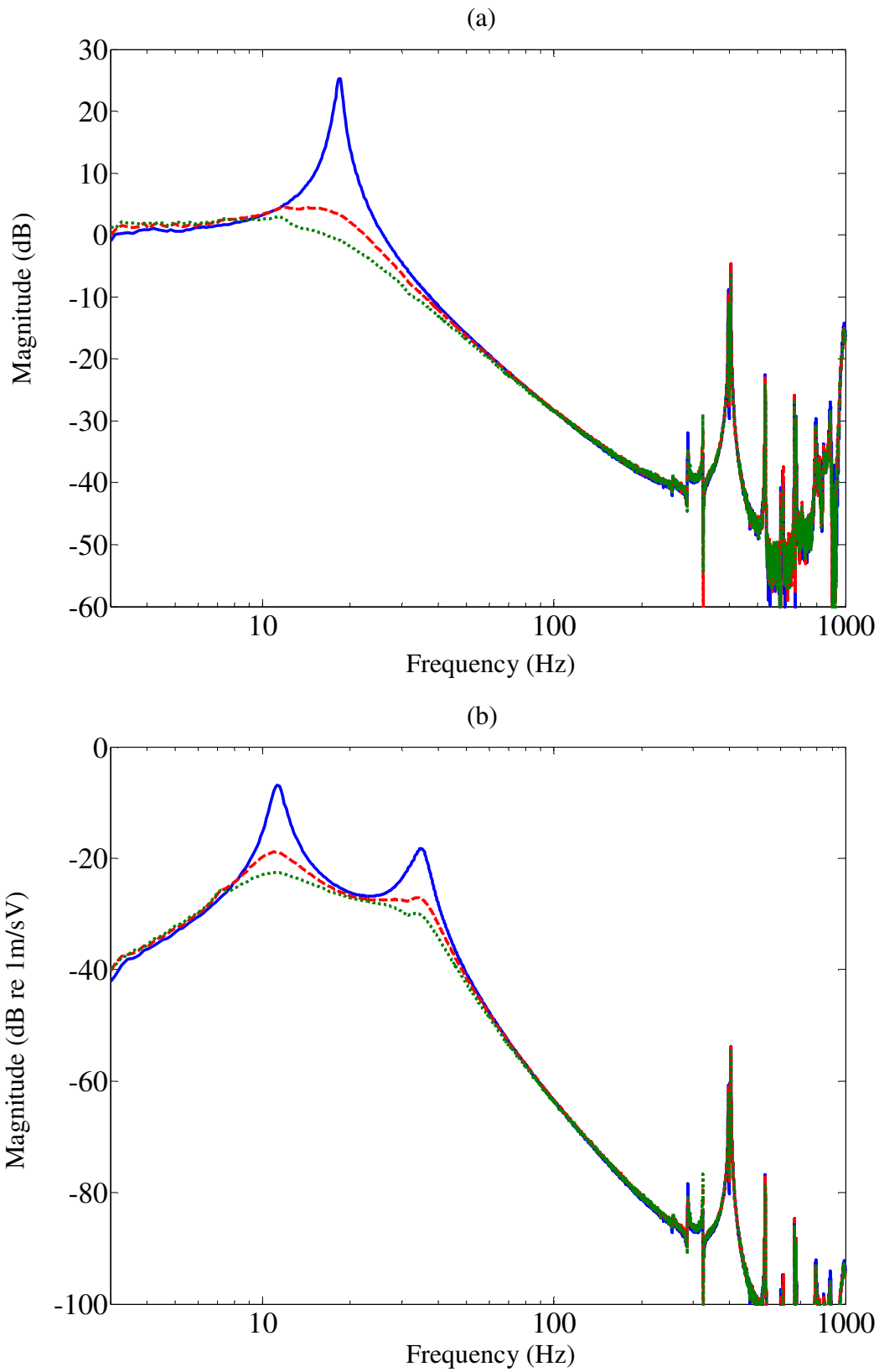

Figure 5.28 *Measured (a) transmissibility and (b) velocity response of the equipment plate per unit voltage to the power amplifier of the stabilized active vibration isolation system with more mass on the base under various feedback gains: without control (solid line), low control gain (dashed line) and high control gain (dotted line).*

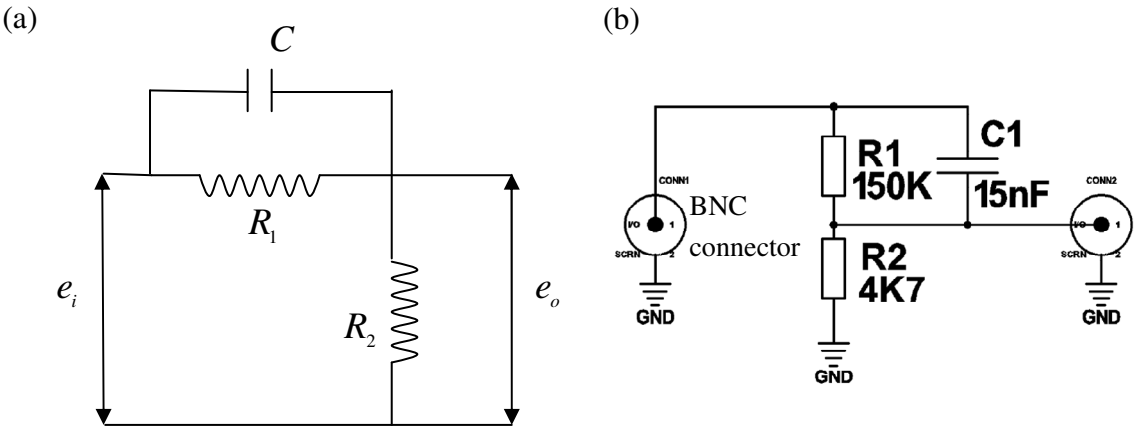

Figure 5.29 *(a) schematic diagram and (b) physical configuration of an electrical circuit of lead compensator, where* e_i *and* e_o *are the input and output, respectively;* R_1 *and* R_2 *are resistors and C is capacitor.*

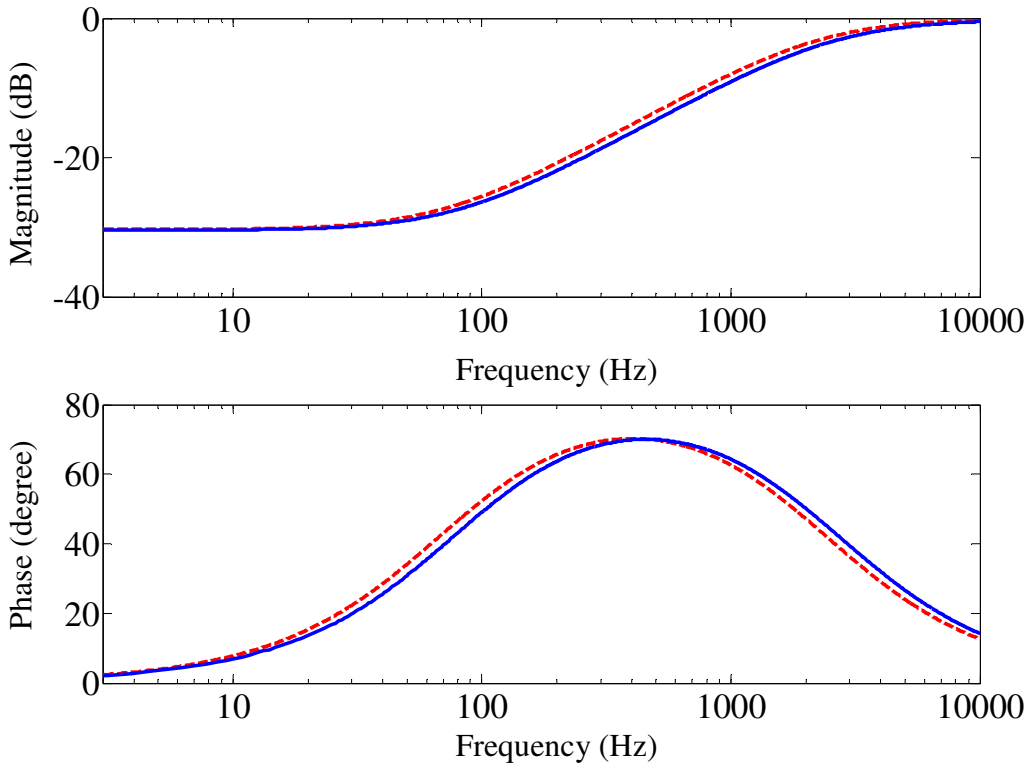

Figure 5.30 *Measured (solid line) and predicted (dashed line) frequency response of the lead compensator shown in Figure 5.29(b).*

(a)

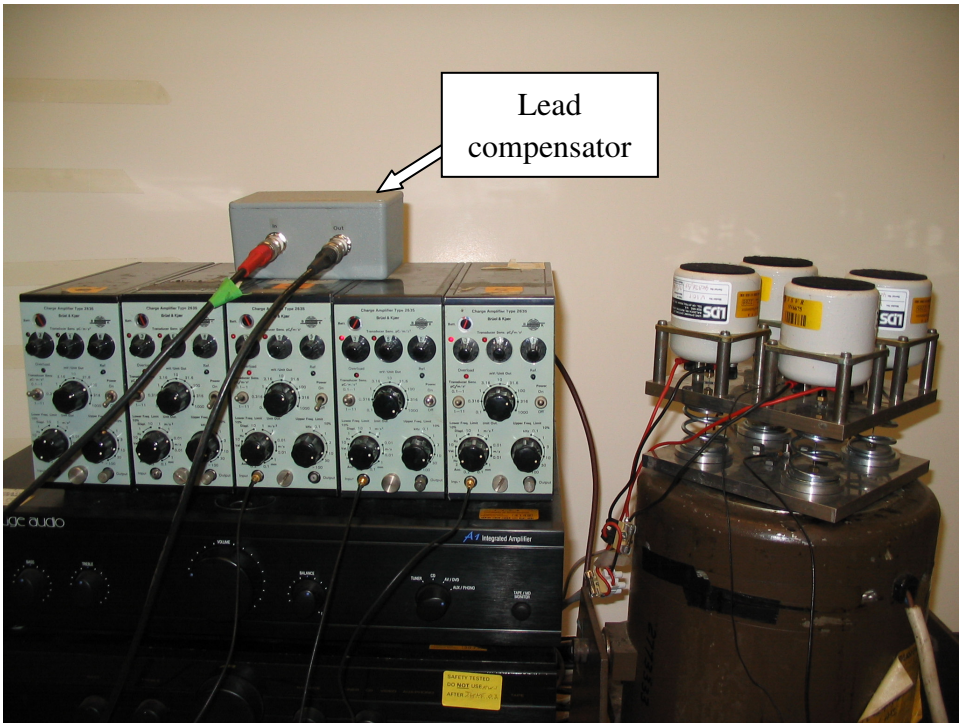

(b)

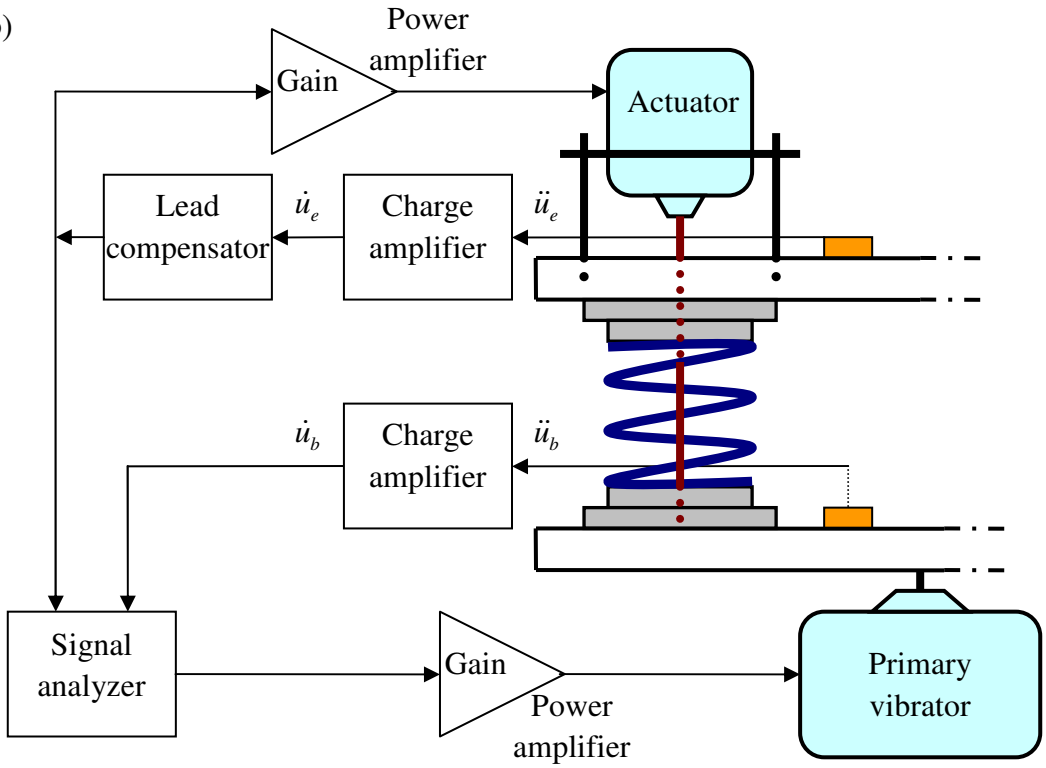

Figure 5.31 *(a) photograph and (b) schematic diagram of one corner of the four-spring active vibration isolation system with a lead compensator.*

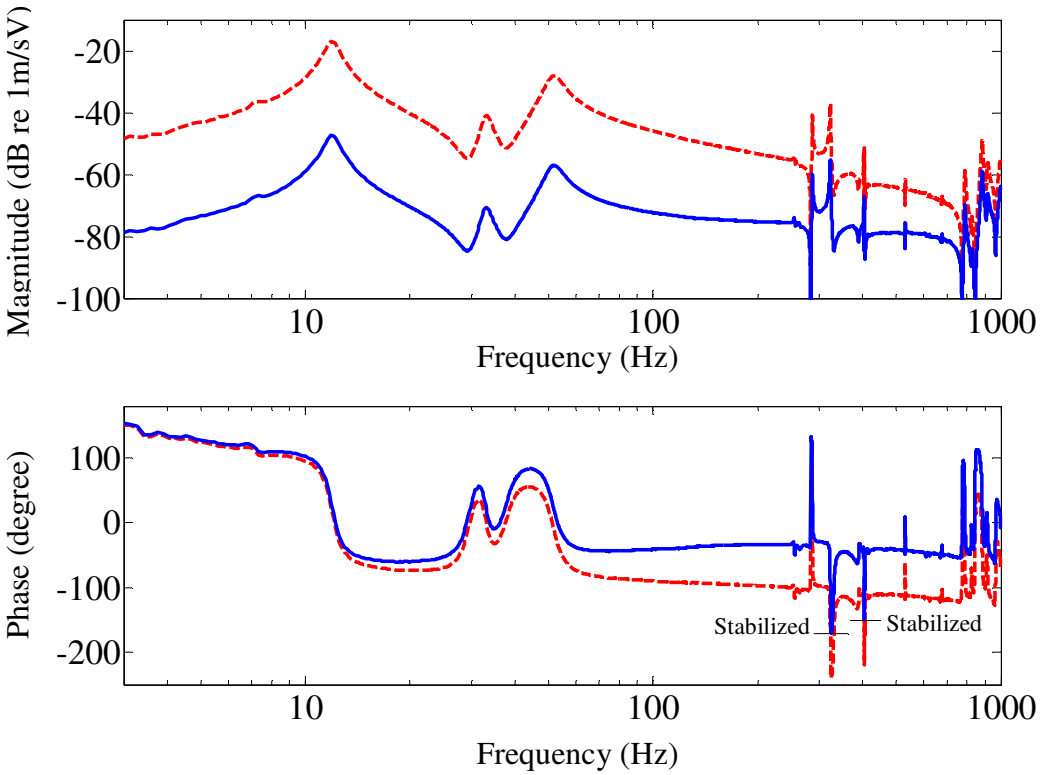

Figure 5.32 *Measured open-loop frequency response of the active vibration isolation system: stabilized system (solid line) and original system (dashed line).*

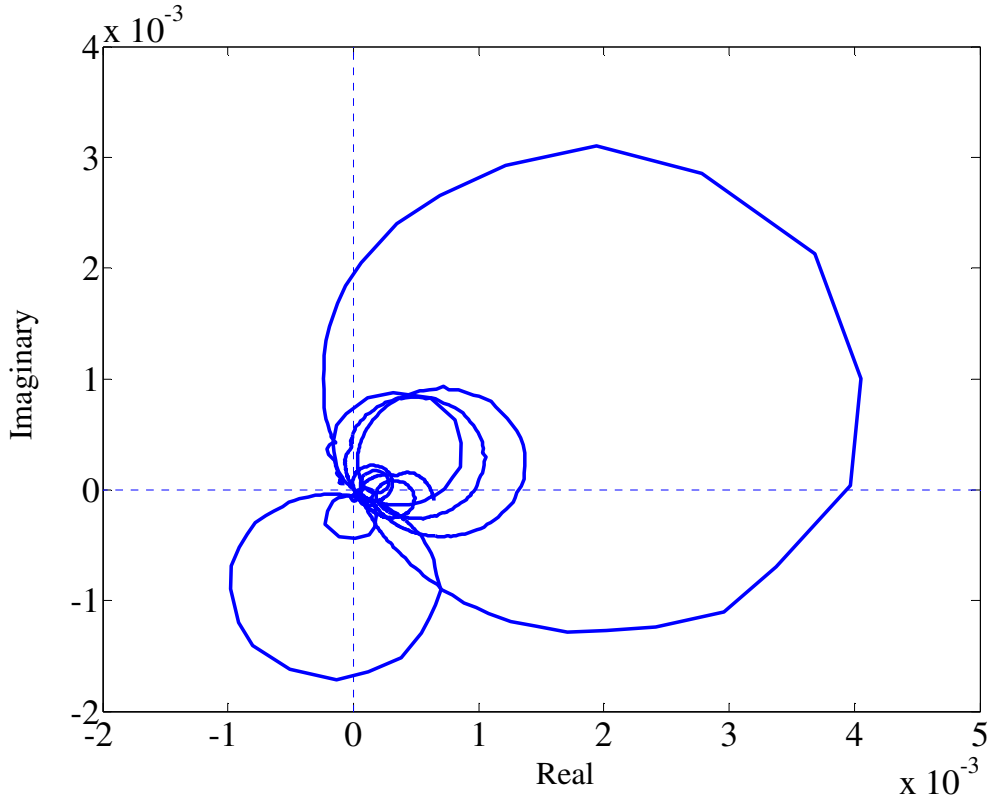

Figure 5.33 *Measured Nyquist plot of the open-loop frequency response of the active vibration isolation system with a lead compensator.*

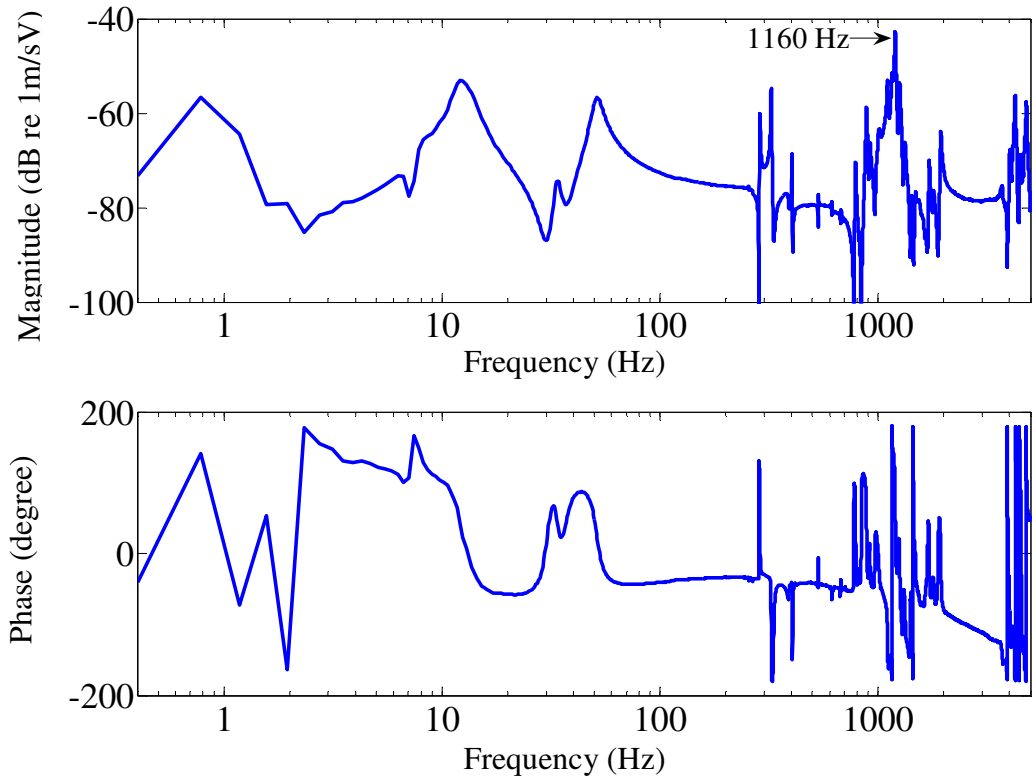

Figure 5.34 *Measured open-loop frequency response of the active vibration isolation system with a lead compensator up to 5 kHz.*

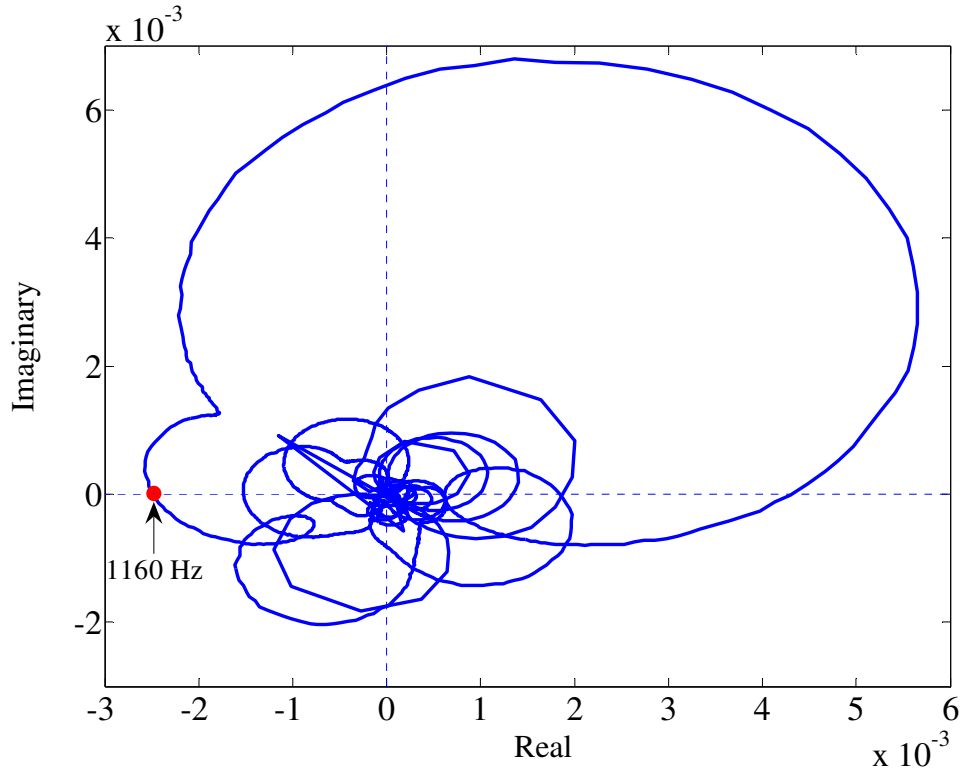

Figure 5.35 *Measured Nyquist plot of the open-loop frequency response of the active vibration isolation system with a lead compensator up to 5 kHz.*

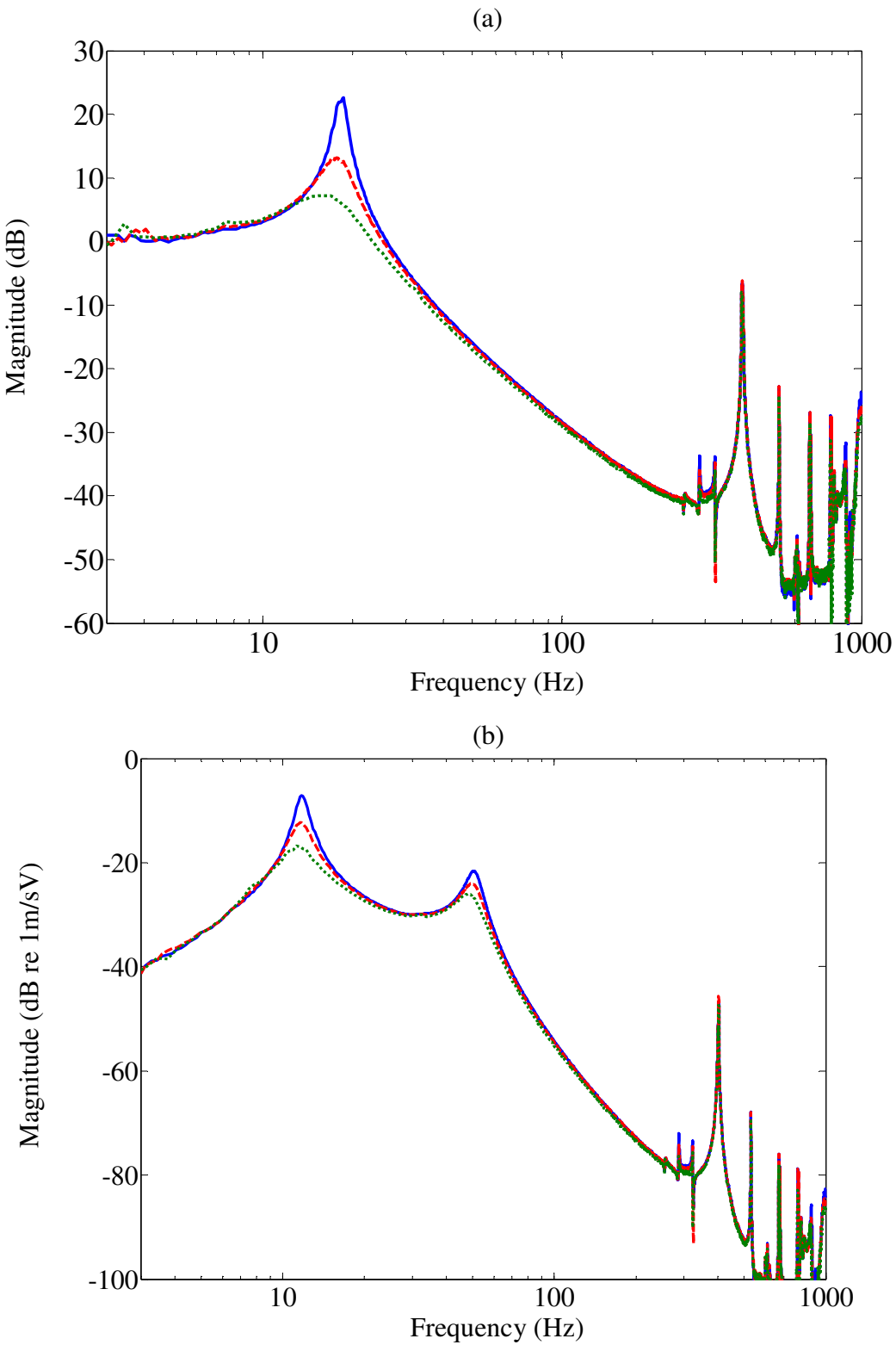

Figure 5.36 *Measured (a) transmissibility and (b) velocity response of the equipment plate per unit voltage to the power amplifier of the stabilized active vibration isolation system with a lead compensator under various feedback gains: without control (solid line), low control gain (dashed line) and high control gain (dotted line).*

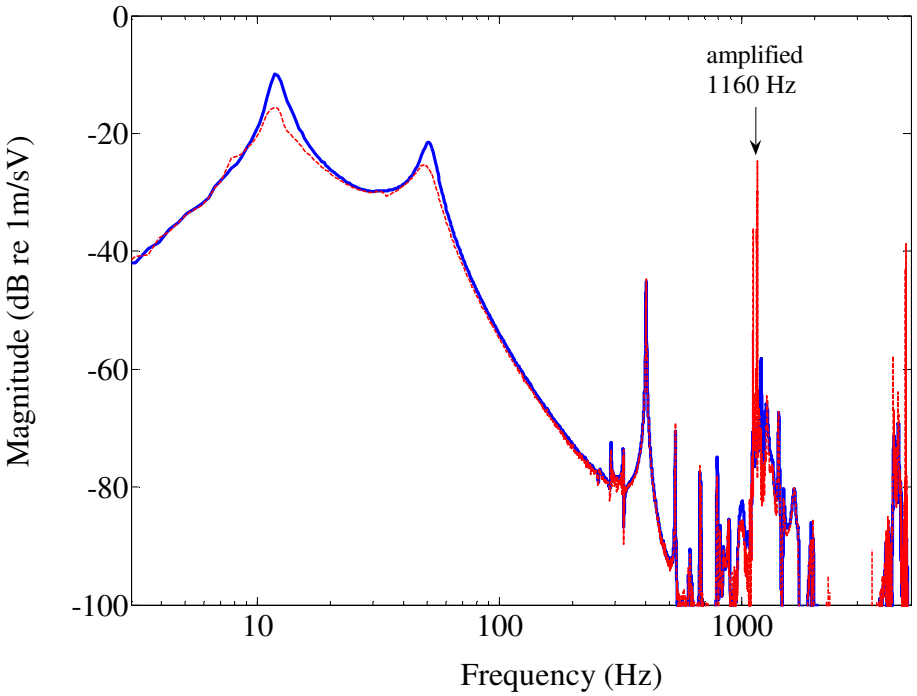

Figure 5.37 *Measured velocity response of the equipment plate per unit voltage to the power amplifier of the stabilized active vibration isolation system with a lead compensator upto 5 kHz without control (solid line) and with control (dashed line).*

Chapter 6

Control of Internal Resonances

6.1 Introduction

In Chapter 4, the commonly used control strategies in active vibration isolation, which can introduce active damping, have been shown to be effective in attenuating the system resonance peaks at relatively low frequencies. However, none of them can suppress the IR peaks in the distributed parameter isolator, because the IR peaks occur at relatively high frequencies where the equipment mass dominates the response. Due to the significant effects of IRs in lightly damped isolators, effort has been expended by previous researchers to attenuate the IRs, which has been discussed in Chapter 1. However, all of the solutions have their inherent limitations either on the performance, or the practical complexity in design and implementation. Therefore, novel approaches to suppress IRs in the distributed parameter isolator are required, based on the understanding of the characteristics of IRs in the distributed parameter isolator.

The aim of this chapter is to investigate theoretically strategies to attenuate IRs in the isolator in order to improve the isolation performance of a distributed parameter isolator over a broad range of frequencies. First, based on the earlier discussion on the maximum response of the equipment at the IRs, an isolator with greater damping under AVF control is investigated. Then, based on the knowledge that the equipment mass

dominates the isolation performance at relatively high frequencies and the characteristics of acceleration feedback control, a combined control strategy of absolute velocity plus acceleration feedback control is presented. This is followed by the analysis of AVF control on a fraction of the isolator length.

6.2 AVF control with more damping in the isolator

As discussed in Chapter 3, the response at the IRs is determined by the damping in the isolator. It can be seen from equation (3.10) that the higher the damping in the isolator, the lower the response at the IR frequencies. To achieve high damping in the isolator, one can choose isolators made of highly damped material to increase the inherent damping in the isolator [66], or use a polymeric material, which has a high loss factor, in parallel with the original isolator [63]. For metal isolators, e.g. helical springs, which have low damping, the latter approach offers a practical solution. In contrast with previous work on applying polymeric damping materials in attenuating the IR peaks in the isolator, in this thesis AVF control is applied together with an increase in the isolator damping to further suppress the system fundamental resonance peaks. As discussed in Chapter 5, high damping in the isolator is also beneficial to the stability of the AVF control system.

Figures 6.1 and 6.2 depict respectively the transmissibility of the base excited system (shown in Figure 4.1) and the amplitude ratio of the system on a flexible base (shown in Figure 4.15), both of which contain a relatively highly damped isolator $\eta_i = 0.05$ under AVF control. The transmissibility and amplitude ratio of the corresponding passive systems with low damping and high damping in the isolator are also plotted for comparison. It can be seen that the system resonance peaks in Figures 6.1 and 6.2 are attenuated, which are mainly due to AVF control. The IR peaks in the distributed parameter isolator are also effectively suppressed by the additional damping introduced in the isolator.

However, the above discussion only shows the idealized situation for introducing more damping in the isolator. In practice, the high damping materials applied in parallel with the original isolator increase not only the overall damping in the isolator, but also the overall static stiffness of the isolator [14]. As a consequence, although the IR peaks can be suppressed, the system resonances in Figures 6.1 and 6.2 will move to higher frequencies. Therefore, the velocity response of the equipment above the system resonances will be amplified compared to that for the original systems. Furthermore, as discussed in Chapter 1, there are other limitations in the use of high damping materials to suppress the IRs, since typically these materials exhibit poor returnability and great creep, which degrade the load capacity of isolators and the performance of the system [57, 67].

6.3 Absolute velocity plus acceleration feedback control

It was concluded in Chapter 4 that the commonly used control strategies in active vibration isolation cannot attenuate the IR peaks in the distributed parameter isolator, because the mass dominates the equipment response at relatively high frequencies. Therefore, it is possible that acceleration feedback control may suppress the IR peaks at high frequencies, since it is equivalent to adding a mass to the system as discussed in Chapter 4. However, the system resonance peaks at low frequencies cannot be attenuated by acceleration feedback control. On the contrary, AVF control was shown to be effective in attenuating the equipment response at the system resonances at low frequencies, while it is not effective in suppressing the IR peaks. Therefore, in this section these two control strategies are combined together to form a new control method, namely absolute velocity plus acceleration feedback control. An investigation is conducted into whether this improves the isolation performance of systems containing a distributed parameter isolator over a broad range of frequencies

6.3.1 System undergoing base motion

Figure 6.3 shows a base excited vibration isolation system containing a distributed parameter isolator under absolute velocity plus acceleration feedback control. In practice the acceleration response of the equipment is measured, and then the velocity response of the equipment is obtained by the integration of the acceleration. The control force f_a is proportional to the sum of the velocity and the acceleration of the equipment and is then fed back to the system through a controller with a constant gain $-h$, so that

$$f_a = -h\left(\dot{u}_e + \lambda \ddot{u}_e\right) \tag{6.1}$$

where $\ddot{u}_e = j\omega\dot{u}_e$ is the acceleration of the equipment and λ is a real coefficient, so that

$$f_a = -h\left(1 + j\omega\lambda\right)\dot{u}_e \tag{6.2}$$

As shown in equation (6.2), if the velocity of the equipment is assumed to be constant with frequency, the control force increases with frequency. In practice, the control force has to be constrained at high frequencies. Therefore, a first order low-pass filter is introduced into the system shown in Figure 6.3 to limit the control signal. The frequency response function for a first order low-pass filter can be written as [74]

$$H_{\mathrm{LPF}} = \frac{1}{1 + j\,\omega/\omega_f} \tag{6.3}$$

where ω_f is the corner frequency of the filter. The control force is thus given by

$$f_a = -h\left(1 + j\omega\lambda\right) H_{\mathrm{LPF}}\dot{u}_e = -h\frac{1 + j\omega\lambda}{1 + j\,\omega/\omega_f}\dot{u}_e \tag{6.4}$$

6.3.1.1 Control performance

The dynamic behaviour of the active vibration isolation system containing a distributed parameter isolator undergoing base motion has been presented in Chapter 4. The velocity of the equipment is given by equation (4.2). Substituting equation (6.4) into (4.2), the transmissibility of the system under absolute velocity plus acceleration feedback control is given by

$$T = \frac{-Z_{21}}{Z_e + Z_{22} + h\dfrac{1+ j\omega\lambda}{1+ j\,\omega/\omega_f}} \tag{6.5}$$

If the equipment is modelled as a mass, i.e. $Z_e = j\omega m_e$, the transmissibility can be written in non-dimensional form as

$$T = \frac{1}{\cos\left[\sqrt{\mu_i}\left(1- j\frac{\eta_i}{2}\right)\Omega\right] - \frac{1}{\sqrt{\mu_i}}\left(\Omega - j2\zeta_a\frac{1+ j\lambda'\Omega}{1+ j\,\Omega/\Gamma_f}\right)\left(1- j\frac{\eta_i}{2}\right)\sin\left[\sqrt{\mu_i}\left(1- j\frac{\eta_i}{2}\right)\Omega\right]} \tag{6.6}$$

where $\lambda' = \lambda\omega_e$ is a real coefficient and $\Gamma_f = \omega_f/\omega_e$ is a ratio of the corner frequency of the low-pass filter to the system fundamental resonance frequency.

The transmissibility for the base excited system containing a distributed parameter isolator under absolute velocity plus acceleration feedback control is plotted in Figure 6.4, where the transmissibility of the passive system is also plotted for comparison. It can be seen that both the system fundamental resonance peak and the IR peaks in the distributed parameter isolator are reduced due to the control. The troughs in the transmissibility are also reduced. Characteristic lines are plotted and identified for the transmissibility under control. These characteristic lines are presented as follows:

- Maximum line

Similar to the derivation for the maximum line for the passive vibration isolation system containing a distributed parameter isolator discussed in Chapter 3, assuming light damping in the isolator, i.e. $\eta_i << 1$ and considering the response when $\sin\left(\sqrt{\mu_i}\Omega\right) = 0$, the maximum line of the transmissibility under absolute velocity plus acceleration feedback control is given by

$$\left|T\right|_{\max} \approx \frac{2}{\left|\eta_i\Omega\left(\Omega - j2\zeta_a\dfrac{1+ j\lambda'\Omega}{1+ j\,\Omega/\Gamma_f}\right)\right|} \tag{6.7}$$

Within the frequency range $1/\lambda' << \Omega << \Gamma_f$, the maximum line can be reduced to

$$\left|T\right|_{\max} \approx \frac{2}{\eta_i\Omega^2\left(1+2\lambda'\zeta_a\right)} \tag{6.8}$$

This equation is a function of not only the loss factor η_i and frequency ratio Ω, but also the active damping ratio ζ_a and coefficient λ'. It is clear that the absolute velocity plus acceleration feedback control is effective in suppressing the IR peaks depending on its parameters. The greater the values of active damping ratio ζ_a and coefficient λ', the better the control performance.

- Minimum line

Similar to the derivation for the minimum line for the passive vibration isolation system containing a distributed parameter isolator discussed in Chapter 3, assuming light damping in the isolator, i.e. $\eta_i << 1$, also considering $\sin\left(\sqrt{\mu_i}\Omega_e\right) = \pm 1$, the minimum line of the transmissibility under absolute velocity plus acceleration feedback control can be approximated by

$$|T|_{\min} \approx \frac{\sqrt{\mu_i}}{\left|\Omega - j2\zeta_a \dfrac{1 + j\lambda'\Omega}{1 + j\,\Omega/\Gamma_f}\right|} \tag{6.9}$$

Within frequency range $1/\lambda' << \Omega << \Gamma_f$, the minimum line can be reduced to

$$|T|_{\min} \approx \frac{\sqrt{\mu_i}}{\Omega\left(1 + 2\lambda'\zeta_a\right)} \tag{6.10}$$

It can be seen that the minima of the transmissibility can also be reduced by the absolute velocity plus acceleration feedback control. The greater the values of active damping ratio ζ_a and coefficient λ', the better the control performance.

6.3.1.2 Stability analysis

The plant response from the active control force to the equipment velocity for the base excited system under absolute velocity plus acceleration feedback control shown in Figure 6.3 is given by equation (4.9). The open-loop frequency response of such a control system is thus given by

$$G(j\omega)H(j\omega) = \frac{1}{Z_e + Z_{22}} \cdot h \frac{1 + j\omega\lambda}{1 + j\,\omega/\omega_f} \tag{6.11}$$

The phase shift of the plant response $1/(Z_e + Z_{22})$ is between -90º and 90º. The phase shift of the controller is 0º at very low frequencies, increasing to 90º when $1/\lambda << \omega << \omega_f$, and reducing to 0º again at frequencies much higher than the corner frequency of the low-pass filter ω_f. Therefore, the overall phase shift of the open-loop frequency response is between -90º and 180º. The absolute velocity plus acceleration feedback control system containing a distributed parameter isolator undergoing base motion is thus unconditionally stable based on the Nyquist stability criterion. However, such a control system is not completely passive, and thus not robustly stable as an AVF control system containing a distributed parameter isolator undergoing base motion.

6.3.2 System on a flexible base

Figure 6.5 shows an absolute velocity plus acceleration feedback control system consisting of an isolated equipment mounted on a base structure that possesses its own dynamics under excitation of the primary force f.

6.3.2.1 Control performance

The dynamics of the active vibration isolation system containing a distributed parameter isolator on a flexible base has been presented in Chapter 4. The velocity of the equipment is given by equation (4.52). Substituting equation (6.4) into (4.52), the velocity of the equipment under absolute velocity plus acceleration feedback control is given by

$$\dot{u}_e = \frac{Y_{eb}}{1 + h\dfrac{1 + j\omega\lambda}{1 + j\,\omega/\omega_f}\left(Y_{ee} - Y_{eb}\right)} f \tag{6.12}$$

If the equipment is modelled as a mass, i.e. $Z_e = j\omega m_e$, and the base structure is modelled as a mass on a complex spring, i.e. $Z_b = j\omega m_b + K_b^*/j\omega$, the amplitude ratio of the system under absolute velocity plus acceleration feedback control is given by

$$\frac{u_e}{\delta_{st}} = \frac{1}{\left[(1+j\eta_b)-\left(1+\frac{1}{\mu_b}\right)\frac{\Omega^2}{\Gamma^2}\right]\cos\left[\sqrt{\mu_i}\left(1-j\frac{\eta_i}{2}\right)\Omega\right]...}$$
$$...-\left[(1+j\eta_b)+\mu_k\mu_i(1+j\eta_i)-\frac{\Omega^2}{\Gamma^2}\right]\frac{\Omega}{\sqrt{\mu_i}}\left(1-j\frac{\eta_i}{2}\right)\sin\left[\sqrt{\mu_i}\left(1-j\frac{\eta_i}{2}\right)\Omega\right]...$$
$$...+j2\zeta_a\frac{1+j\lambda'\Omega}{1+j\Omega/\Gamma_f}\left\{\begin{array}{l}\mu_k\Omega\left[\cos\left(\sqrt{\mu_i}\left(1-j\frac{\eta_i}{2}\right)\Omega\right)-1\right]... \\ ...+\frac{1}{\sqrt{\mu_i}}\left(1-j\frac{\eta_i}{2}\right)\left(1+j\eta_b-\frac{\Omega^2}{\Gamma^2}\right)\sin\left(\sqrt{\mu_i}\left(1-j\frac{\eta_i}{2}\right)\Omega\right)\end{array}\right\} \tag{6.13}$$

The amplitude ratio for this system is plotted in Figure 6.6, where the amplitude ratio of the corresponding passive system is also plotted for comparison. It can be seen that the system resonance peaks and the IR peaks in the distributed parameter isolator are all reduced due to absolute velocity plus acceleration feedback control. The troughs in the amplitude ratio are also reduced.

6.3.2.2 Stability analysis

The plant response from the active control force to the equipment velocity for the system on a flexible base under absolute velocity plus acceleration feedback control shown in Figure 6.5 is given by equation (4.56). The open-loop frequency response of such a control system is thus given by

$$G(j\omega)H(j\omega) = h\frac{1+j\omega\lambda}{1+j\omega/\omega_f}(Y_{ee}-Y_{eb}) \tag{6.14}$$

The frequency response of the absolute velocity plus acceleration feedback controller is shown in Figure 6.7. The phase shift of the frequency response of the controller is 0º at both low frequencies and high frequencies, while it has a phase lead upto 90º when $1/\lambda < \omega < \omega_f$. It can be seen that the feedback controller is similar to a lead compensator that is used in Chapter 5 to stabilize the AVF control system. But the difference between this feedback controller and the lead compensator is that the magnitude of the frequency response of the controller is greater than unity and increases with frequency. This is why the absolute velocity plus acceleration feedback control can

attenuate the IRs in the distributed parameter isolator at high frequencies. Based on the analysis for the lead compensator in Chapter 5, the parameters of the absolute velocity plus acceleration feedback controller can be tuned so that it can both attenuate the IR peaks in the isolator and stabilize the control system.

As discussed in the last section, the greater the values of the coefficient λ, the better the control performance. However, due to the stability issues for the system on a flexible base, the coefficient λ should be carefully chosen to provide sufficient phase lead compensation at the unstable frequency, but not to be a danger to stability at other frequencies. Also, the first order low-pass filter needs to be carefully designed so that the controller can both constrain the control signal and provide sufficient phase lead compensation at the unstable frequency. The general rules to determine these parameters are discussed below.

The phase of the controller has two contributions: the phase lead due to the frequency response function $1+j\omega\lambda$ and the phase lag due to the first order low-pass filter. As shown in Figure 6.7, $f_1 = 1/2\pi\lambda$ (in Hz) is the corner frequency of the frequency response function $1+j\omega\lambda$, and $f_2 = \omega_f/2\pi$ (in Hz) is the corner frequency of the first order low-pass filter. To stabilize the control system, the unstable frequency should lie between f_1 and f_2 so that the compensation for the phase lag which causes the instability can take place. For the transfer function $1+j\omega\lambda$, if a least phase lead θ_1 is required at the unstable frequency ω_L, i.e. $\arctan(\lambda\omega_L) > \theta_1$, the coefficient λ is determined by

$$\lambda > \frac{\tan\theta_1}{\omega_L} \tag{6.15}$$

For the first order low-pass filter, if a maximum phase lag θ_2 $(\theta_2 < 0)$ is required at ω_L, i.e. $\arctan(-\omega_L/\omega_f) > \theta_2$, the corner frequency of the low-pass filter ω_f can be

determined by

$$\omega_f > \frac{\omega_L}{-\tan\theta_2} \tag{6.16}$$

The required overall phase lead compensation of the controller at the unstable frequency can thus be obtained by choosing appropriate phase lead θ_1 and phase lag θ_2. As a result, the controller parameters λ and ω_f can be determined from equations (6.15) and (6.16).

There is another limitation on the selection of the coefficient λ. Because the phase shift of the plant response G is approximately 90º at frequencies lower than the equipment resonance and around the base resonance, the phase lead due to the controller should be minimized at those frequencies, so that the open-loop frequency response of the control system can maintain its phase margin. As a consequence, the frequency f_1 cannot be too small, i.e. λ cannot be too large. If at a low frequency ω_{low} the phase shift due to the controller is required to be less than θ_{low}, i.e. $\arctan(\lambda\omega_{\text{low}}) < \theta_{\text{low}}$, the coefficient λ is given by

$$\lambda < \frac{\tan\theta_{\text{low}}}{\omega_{\text{low}}} \tag{6.17}$$

Figure 6.8 shows the open-loop frequency response of the vibration isolation system on a flexible base under absolute velocity plus acceleration feedback control. The plant response of the system is also plotted to show the stability of such a system under AVF control. It can be seen that the instability that occurs under AVF control at the first IR in the isolator is stabilized by the phase lead due to the controller. The phase shift of the open-loop frequency response is thus limited between -180º and 180º, so that the system on a flexible base under absolute velocity plus acceleration feedback control is unconditionally stable. However, the phase shifts around the system resonance frequencies are also increased due to the control, which are now greater than 90º.

Therefore, the controller should be carefully designed to allow the phase lead compensation to occur around the instability frequency, but it should minimize the phase shifts at low frequencies.

6.3.3 Limitations in practice

For both a base excited system and a system on a flexible base under absolute velocity plus acceleration feedback control, to achieve good control performance, the frequency response of the controller cannot be constrained too much by the low-pass filter. So the magnitude of the open-loop frequency response of the control system does not roll off rapidly and remains large over a broad range of frequencies. This is not a problem for the simplified models used in the above stability analysis, in which the resonance behaviour in the equipment and the base is neglected since the equipment is modelled as a rigid mass, and the base is simplified as a rigid mass on a complex spring. Also only the longitudinal vibration of the system is considered. Any rotational or lateral modes are ignored. However, in practice unmodelled dynamics of the system that are not considered in this analysis may be a danger to the stability of the control system, and thus result in the problem of spillover.

6.4 AVF control on a fraction of the isolator length

As discussed in Chapter 4, AVF control applied to a base excited vibration isolation system containing a distributed parameter isolator is equivalent to a skyhook damper with a constant damping coefficient, which is effectively in parallel with the equipment mass. The equipment response is thus determined by the total impedance of the equipment mass, isolator and the skyhook damper, and the transmitted force from the base excitation to the equipment and the isolator. Since the impedance of the equipment mass increases with frequency, it dominates the response at high frequencies. Also, the transmitted force to the equipment and the isolator is solely determined by the transfer impedance of the isolator. Therefore, AVF control cannot attenuate the IR peaks in the

isolator which occur at relatively high frequencies. To overcome the disadvantages of AVF control applied in parallel to the entire isolator, AVF control can be applied in parallel with the lower part of the isolator to change the dynamics of the active vibration isolator system. As a consequence, the equivalent skyhook damper due to AVF control is no longer in parallel with the equipment mass. Also the transmitted force from the base excitation to the equipment will be altered.

In the following sections, the active vibration isolation system containing a distributed parameter isolator under AVF control on a fraction of the isolator length is investigated.

6.4.1 System undergoing base motion

Figure 6.9 shows a base excited vibration isolation system containing a distributed parameter isolator under AVF control on a fraction of the isolator length. The isolator is modelled as a finite elastic rod. Different from AVF control discussed in the previous chapters, the active control force f_a, which is in parallel with the lower part of the isolator, acts between the base and a point along the isolator. The length of the upper and the lower part of the isolator are respectively denoted as x and y, and thus $x + y = L$, which is the total length of the isolator. The control force is generated by feeding back the velocity $\dot{u}_r$ of the point along the isolator where the active control force applied (defined as point *r* in the following discussion), through a controller with a constant feedback gain –*h*. The control force is thus given by

$$f_a = -h\dot{u}_r \tag{6.18}$$

6.4.1.1 Control performance

The dynamics of the active vibration isolation system shown in Figure 6.9 can be described by

$$
\begin{aligned}
&Q_e = -Q_{x2} = Z_e \dot{u}_e \\
&\begin{bmatrix} Q_{x1} + f_a \\ Q_{x2} \end{bmatrix} = \mathbf{Z_x} \begin{bmatrix} \dot{u}_r \\ \dot{u}_e \end{bmatrix} = \begin{bmatrix} Z_{x11} & Z_{x12} \\ Z_{x21} & Z_{x22} \end{bmatrix} \begin{bmatrix} \dot{u}_r \\ \dot{u}_e \end{bmatrix} \\
&Q_{x1} = -Q_{y2} \\
&\begin{bmatrix} Q_{y1} \\ Q_{y2} \end{bmatrix} = \mathbf{Z_y} \begin{bmatrix} \dot{u}_b \\ \dot{u}_r \end{bmatrix} = \begin{bmatrix} Z_{y11} & Z_{y12} \\ Z_{y21} & Z_{y22} \end{bmatrix} \begin{bmatrix} \dot{u}_b \\ \dot{u}_r \end{bmatrix}
\end{aligned}
\qquad \text{(6.19a,b,c,d)}
$$

where Q_e, Q_{x1}, Q_{x2}, Q_{y1} and Q_{y2} are internal forces; $\dot{u}_e$ and $\dot{u}_b$ are respectively the velocities of the equipment and the base; $\mathbf{Z_x}$ and $\mathbf{Z_y}$ are respectively the impedance matrices for the upper and lower part of the isolator, and are given by:

$$
\begin{aligned}
\mathbf{Z_x} &= \begin{bmatrix} Z_{x11} & Z_{x12} \\ Z_{x21} & Z_{x22} \end{bmatrix} = \frac{S\sqrt{E^* \rho}}{j \sin\left(k_l^* x\right)} \begin{bmatrix} \cos\left(k_l^* x\right) & -1 \\ -1 & \cos\left(k_l^* x\right) \end{bmatrix} \\
\mathbf{Z_y} &= \begin{bmatrix} Z_{y11} & Z_{y12} \\ Z_{y21} & Z_{y22} \end{bmatrix} = \frac{S\sqrt{E^* \rho}}{j \sin\left(k_l^* y\right)} \begin{bmatrix} \cos\left(k_l^* y\right) & -1 \\ -1 & \cos\left(k_l^* y\right) \end{bmatrix}
\end{aligned}
\qquad \text{(6.20a,b)}
$$

Combining equations (6.18) and (6.19a-d) gives

$$
\begin{aligned}
\left(Z_e + Z_{x22}\right) \dot{u}_e &= -Z_{x21} \dot{u}_r \\
\left(Z_{x11} + Z_{y22} + h\right) \dot{u}_r &= -Z_{x12} \dot{u}_e - Z_{y21} \dot{u}_b
\end{aligned}
\qquad \text{(6.21a,b)}
$$

From equations (6.21a, b), the transmissibility of the system under AVF control on a fraction of the isolator length can be written as

$$
T = \frac{\dot{u}_e}{\dot{u}_b} = \frac{Z_{x21} Z_{y21}}{\left(Z_e + Z_{x22}\right)\left(Z_{x11} + Z_{y22} + h\right) - Z_{x12} Z_{x21}} \qquad \text{(6.22)}
$$

It should be noted that, if the control gain h=0, i.e. without control, this equation is equivalent to the transmissibility of the passive system given by equation (3.6).

If the equipment is modelled as a mass, i.e. $Z_e = j\omega m_e$, the transmissibility can be written in non-dimensional form as

$$T = \frac{1}{\cos\left[\sqrt{\mu_i}\left(1-j\frac{\eta_i}{2}\right)\Omega\right] - \frac{\Omega}{\sqrt{\mu_i}}\left(1-j\frac{\eta_i}{2}\right)\sin\left[\sqrt{\mu_i}\left(1-j\frac{\eta_i}{2}\right)\Omega\right]... \\ ...+ j\frac{2\zeta_a}{\sqrt{\mu_i}}\left(1-j\frac{\eta_i}{2}\right)\sin\left[\frac{y}{L}\sqrt{\mu_i}\left(1-j\frac{\eta_i}{2}\right)\Omega\right]\left\{\begin{matrix}\cos\left[\frac{x}{L}\sqrt{\mu_i}\left(1-j\frac{\eta_i}{2}\right)\Omega\right]... \\ ...-\frac{\Omega}{\sqrt{\mu_i}}\left(1-j\frac{\eta_i}{2}\right)\sin\left[\frac{x}{L}\sqrt{\mu_i}\left(1-j\frac{\eta_i}{2}\right)\Omega\right]\end{matrix}\right\}} \quad (6.23)$$

It can be seen that the first two parts in the denominator are the same as that in the non-dimensional transmissibility for the passive system given in equation (3.7). AVF control on a fraction of the isolator length adds an active damping term in the denominator, but leaves the numerator unchanged. Therefore, this feedback control is equivalent to a skyhook damper.

Figure 6.10 shows the transmissibility of the active vibration isolation system under AVF control on a fraction of the isolator length when $\mu_i = 0.1$, $\eta_i = 0.01$. For comparison, the transmissibility for such a system without control and under AVF control on the entire isolator length is also plotted. It can be seen that AVF control on a fraction of the isolator length can attenuate not only the system fundamental resonance peak, but also the IR peaks in the distributed parameter isolator. However, for the same control gain applied, its control performance around the system fundamental resonance frequency is worse than that under AVF control on the entire isolator length. Furthermore, it should be noted that its control performance around the system fundamental resonance frequency is worse when $y = 2L/\pi$ than that when $y = 3L/4$. Also when $y = 2L/\pi$, some IR peaks (e.g. the third and sixth IR peaks) shown in Figure 6.10 are reduced much less than the other IR peaks, although some reduction are achieved. However, when $y = 3L/4$, some IR peaks (e.g. the fourth and eighth IR peaks) shown in Figure 6.10 are almost not reduced at all.

The mechanical analogue of the base excited system under AVF control on a fraction of

the isolator length is shown in Figure 6.11. It should be noted that, different from a skyhook damper acting between the inertial ground and the equipment for AVF control discussed in Chapter 4, AVF control on a fraction of the isolator length is equivalent to a skyhook damper acting between the inertial ground and the point *r* along the isolator where the active control force is applied. Thus this equivalent skyhook damper damps the response at the point *r*, but not directly the equipment response. It thus explains why the control performance of AVF control on a fraction of the isolator length around the system fundamental resonance frequency is worse than that for AVF control on the entire isolator length shown in Figure 6.10. Also in the mechanical analogue, it can be seen that the closer the point *r* to the equipment, i.e. the closer the attachment point of the equivalent skyhook damper to the equipment, the more the equipment response can be attenuated around the system fundamental resonance frequency. It can thus be concluded that the longer the fraction of the isolator length controlled by AVF control, i.e. the longer the length *y*, the better the control performance around the system fundamental resonance frequency.

The above discussion gives the design guideline for modifying the system response around the fundamental resonance frequency. In the following discussion, the control performance of the system at IRs and at high frequencies is investigated. Equations (6.21a, b) can be rearranged as

$$\begin{aligned} \left(Z_e + Z_{x22}\right)\dot{u}_e &= -Z_{x21}\dot{u}_r = f_{B1} \\ \left(Z_{x11} + Z_{y22} + h\right)\dot{u}_r &= -Z_{x12}\dot{u}_e - Z_{y21}\dot{u}_b = f_{B2} \end{aligned} \qquad (6.24a,b)$$

where the blocked force f_{B1} is the force transmitted from the excitation at point *r* to an infinitely rigid fixed point by the attachment point between the equipment and the isolator, and the blocked force f_{B2} is the force transmitted from the equipment and base excitation to an infinitely rigid fixed point by the point *r*. Based on equations (6.24a, b), the Thevenin equivalent systems for the active vibration isolation system under AVF control on a fraction of the isolator length is shown in Figure 6.12. It can be seen that the equivalent skyhook damper due to the control is in parallel with the point

impedances Z_{x11} and Z_{y22} to determine the velocity $\dot{u}_r$.

Similar to the description in Chapter 3, when $\sin(k_l x)=0$, i.e. $\omega=\omega_x=(L/x)\omega_l$ where ω_l is the IR frequencies for the entire isolator given in Appendix B, the maxima of the point and transfer impedances of the upper part of the isolator are given by

$$Z_{x11}=Z_{x22}=\frac{L}{x}\frac{2K_L}{\eta_i\omega}=\frac{L}{x}Z_{11},\ Z_{x12}=Z_{x21}=\pm\frac{L}{x}\frac{2K_L}{\eta_i\omega}=\frac{L}{x}Z_{21} \qquad (6.25a,b)$$

Similarly when $\sin(k_l y)=0$, i.e. $\omega=\omega_y=(L/y)\omega_l$, the maxima of the point and transfer impedances of the lower part of the isolator are given by

$$Z_{y11}=Z_{y22}=\frac{L}{y}\frac{2K_L}{\eta_i\omega}=\frac{L}{y}Z_{11},\ Z_{y12}=Z_{y21}=\pm\frac{L}{y}\frac{2K_L}{\eta_i\omega}=\frac{L}{y}Z_{21} \qquad (6.26a,b)$$

It can be seen that these impedances decrease with frequency. So at relatively high frequencies and at frequencies where $\omega\neq\omega_x$ and $\omega\neq\omega_y$, one has $h>\left|Z_{x11}+Z_{y22}\right|$, so that the velocity $\dot{u}_r$ is reduced due to AVF control on a fraction of the isolator length. Thus the equipment response is attenuated. While at frequencies where $\left|Z_{x11}\right|$ or $\left|Z_{y22}\right|$ is much greater than *h*, there are a few different situations that affect the control performance, and this is discussed below.

When $\omega=\omega_x\neq\omega_y$, although $\left|Z_{x11}+Z_{y22}\right|\approx\left|Z_{x11}\right|>>h$ and thus the control effort is negligible, the transfer impedance Z_{y21} is small so that the transmitted force from the base excitation is small. As a consequence, the velocity $\dot{u}_r$ and thus the equipment response are small. Similarly, when $\omega=\omega_y\neq\omega_x$, although $\left|Z_{x11}+Z_{y22}\right|\approx\left|Z_{y22}\right|>>h$ and thus the control effort is negligible, the transfer impedance Z_{x21} is small so that the transmitted force to the equipment and the isolator f_{C1} is small. So the equipment response is small.

However, when $\omega = \omega_x = \omega_y$, one has $\left|Z_{x11} + Z_{y22}\right| >> h$ so that the control effort is negligible. Also the transfer impedances $\left|Z_{x21}\right|$ and $\left|Z_{y21}\right|$ are large. The transmissibility of the system can thus be reduced to that of the passive system given by equation (3.6). So if at a frequency where $\omega = \omega_x = \omega_y = \omega_l$, the IR peaks in the isolator at these frequencies will not be attenuated by AVF control on a fraction of the isolator length. To avoid this situation, the ratios L/x and L/y should be irrational numbers. So both ω_x and ω_y will not equal ω_l, although they may approach it. From another point of view, if the ratios L/x and L/y are rational numbers, the point *r* where the active force is applied will be a nodal point at some frequencies depending on the values of L/x and L/y. Because there is no movement at a nodal point, no signal will be fed back through the controller to generate the control force. Therefore, to avoid the nodal points along the rod, an irrational number for the ratios L/x and L/y is required.

The above discussion explains the reduction at IRs in Figure 6.10. When L/y is a rational number $4/3$, the condition $\omega = \omega_x = \omega_y = \omega_l$ occurs at the fourth IR peak and every other fourth IR peaks at higher frequencies, i.e. the control point *r* is a nodal point of the fourth mode and every other subsequent fourth modes in the isolator, so that these peaks are almost not reduced at all. When L/y is an irrational number $\pi/2$, because $\pi \approx 3$, the condition $\omega = \omega_x = \omega_y = \omega_l$ approximately occurs at the third and the sixth IR peaks, i.e. the control point *r* is close to the nodal point in the third and sixth mode in the isolator, so that these peaks are reduced much less than the other IR peaks.

From the above discussion, the control performance at both the fundamental resonance frequency and at IRs is related to the length *y* under AVF control. To evaluate the overall control performance of the system under AVF control on a fraction of the isolator length, its mean square response can be compared to that for AVF control on

the entire isolator length. The mean square velocity of the equipment is given by equation (2.46). Substituting the corresponding transmissibility into equation (2.46), the change in the mean square velocity for the system under AVF control on a fraction of the isolator length compared to that under AVF control on the entire isolator length can be calculated. Figure 6.13 depicts such a change in mean square velocity within the range $0.1<\Omega<1000$ when $\mu_i = 0.1$, $\eta_i = 0.01$, with respect to the length ratio y/L and active damping ratio ζ_a. It can be seen that when the length *y* under AVF control is very short, the control performance of AVF control on a fraction of the isolator length is much worse than that under AVF control on the entire isolator length at high active damping ratios. With an increase in the controlled length *y*, AVF control on a fraction of the isolator length provides increasing reduction in the mean square velocity. Furthermore, for the given parameters, the change in the mean square velocity is slightly less than 0 dB at high length ratios y/L, i.e. the overall control performance under AVF control on a fraction of the isolator length is better than that under AVF control on the entire isolator length.

To further improve the control performance around the system fundamental resonance frequency, AVF control on a fraction of the isolator length can be combined with AVF on the entire isolator length, as shown in Figure 6.14(a). The dynamics for the control system are given by

$$\begin{aligned}\left(Z_e + Z_{x22}\right)\dot{u}_e &= f_{a1} - Z_{x21}\dot{u}_r \\ \left(Z_{x11} + Z_{y22}\right)\dot{u}_r &= f_{a2} - Z_{x12}\dot{u}_e - Z_{y21}\dot{u}_b\end{aligned} \qquad (6.27a,b)$$

where the active control forces are given by

$$f_{a1} = -h_1\dot{u}_e, \quad f_{a2} = -h_2\dot{u}_r \qquad (6.28a,b)$$

Substituting equations (6.28a, b) into (6.27a, b), the transmissibility of the system is given by

$$T = \frac{Z_{x21}Z_{y21}}{\left(Z_e + Z_{x22} + h_1\right)\left(Z_{x11} + Z_{y22} + h_2\right) - Z_{x12}Z_{x21}} \qquad (6.29)$$

It can be seen in the mechanical analogue shown in Figure 6.14(b) that AVF control on the entire isolator length is equivalent to a skyhook damper acting between the inertial ground and the equipment, and AVF control on a fraction of the isolator length is

equivalent to a skyhook damper acting between the inertial ground and the point *r*. So the isolation performance can be improved at both the system fundamental resonance frequency and IR frequencies. The transmissibility of the system is shown in Figure 6.15 when $\mu_i = 0.1$, $\eta_i = 0.01$, $y = 2L/\pi$ and $\zeta_{a1} = \zeta_{a2} = 0.3$, where the active damping ratios are defined as $\zeta_{a1} = h_1 / 2\sqrt{K_L m_e}$ and $\zeta_{a2} = h_2 / 2\sqrt{K_L m_e}$. For comparison, such a system without control, under AVF control on a fraction of the isolator length alone and under AVF control on the entire isolator length alone are also plotted. It can be seen that the control performance at IR frequencies of the system under AVF control on both the entire and a fraction of the isolator length is as good as that under AVF control on a fraction of the isolator length. Also its control performance around the system fundamental resonance frequency is even better than that for AVF control on the entire isolator length.

6.4.1.2 Stability analysis

For the base excited system under AVF control on a fraction of the isolator length, because the base motion is prescribed which is not affected by the active control force, the actuator and the sensor are thus collocated, so that such a control system is unconditionally stable.

6.4.2 System on a flexible base

Figure 6.16 shows a vibration isolation system containing a distributed parameter isolator on a flexible base under AVF control on a fraction of the isolator length. The isolator is modelled as a finite elastic rod. The active control force f_a, which is in parallel with the lower part of the isolator, reacts between the base and a point along the isolator. The control force is also given by equation (6.18).

6.4.2.1 Control performance

The dynamics of the active vibration isolation system shown in Figure 6.16 can be

described by equations (6.19a-d) and

$$Z_b \dot{u}_b = f + Q_b = f - Q_{y1} \tag{6.30}$$

From these equations, the velocity of the equipment can be written as

$$\dot{u}_e = Y_{er} f_a + Y_{eb}\left(f - f_a\right) = \left(Y_{er} - Y_{eb}\right) f_a + Y_{eb} f \tag{6.31}$$

where the transfer mobility Y_{eb} was defined in Chapter 3 and Y_{er} is the transfer mobility from the force applied to the point *r* to the equipment velocity, $\dot{u}_e$ when the system is coupled. The velocity at the point *r* where the active control force is applied can be written as

$$\dot{u}_r = Y_{rr} f_a + Y_{rb}\left(f - f_a\right) = \left(Y_{rr} - Y_{rb}\right) f_a + Y_{rb} f \tag{6.32}$$

where Y_{rr} is the point mobility from the force applied to the point *r* to the velocity, $\dot{u}_r$ when the system is coupled, and Y_{rb} is the transfer mobility from the force applied to the base to the velocity, $\dot{u}_r$ when the system is coupled. These mobilities are given by

$$\begin{aligned} Y_{er} &= \frac{-Z_{x21}\left(Z_b + Z_{y11}\right)\left(Z_{x11} + Z_{y22}\right)}{Z_e Z_b Z_{te} Z_{tb} - Z_{x12} Z_{x21} Z_{y12} Z_{y21}} \\ Y_{rb} &= \frac{-Z_{y12}\left(Z_e + Z_{x22}\right)\left(Z_{x11} + Z_{y22}\right)}{Z_e Z_b Z_{te} Z_{tb} - Z_{x12} Z_{x21} Z_{y12} Z_{y21}} \\ Y_{rr} &= \frac{1 - Z_{x12} Y_{er} - Z_{y21} Y_{rb}}{Z_{x11} + Z_{y22}} \end{aligned} \tag{6.33a,b,c}$$

where

$$\begin{aligned} Z_{te} &= \frac{\left(Z_e + Z_{x22}\right)\left(Z_{x11} + Z_{y22}\right) - Z_{x12} Z_{y21}}{Z_e} \\ Z_{tb} &= \frac{\left(Z_b + Z_{y11}\right)\left(Z_{x11} + Z_{y22}\right) - Z_{y12} Z_{y21}}{Z_b} \end{aligned} \tag{6.34a,b}$$

A detailed derivation can be found in Appendix C.

Substituting equation (6.18) into (6.32) gives

$$\dot{u}_r = \frac{1}{1 + h\left(Y_{rr} - Y_{rb}\right)} f \tag{6.35}$$

Substituting equations (6.18) and (6.35) into (6.31), the velocity of the equipment is

given by

$$\dot{u}_e = \frac{Y_{eb} + h\left(Y_{eb}Y_{rr} - Y_{er}Y_{rb}\right)}{1 + h\left(Y_{rr} - Y_{rb}\right)} f \tag{6.36}$$

If the base is modelled as a mass m_b on a complex spring, i.e. $K_b^* = K_b(1 + j\eta_b)$, the amplitude ratio of the system is given by

$$\frac{u_e}{\delta_{st}} = \frac{K_b}{j\omega}\frac{\dot{u}_e}{f} = \frac{K_b}{j\omega}\frac{Y_{eb} + h\left(Y_{eb}Y_{rr} - Y_{er}Y_{rb}\right)}{1 + h\left(Y_{rr} - Y_{rb}\right)} \tag{6.37}$$

Figure 6.17 shows the amplitude ratio of system on a flexible base under AVF control on a fraction of the isolator length when $\mu_i = 0.1,\ \mu_b = 0.5\ \ \mu_k = 0.1,\ \eta_i = \eta_b = 0.01$ and $y = 2L/\pi$. For comparison, the amplitude ratio for such a system without control and under AVF control on the entire isolator length is also plotted. It can be seen that AVF control on a fraction of the isolator length can effectively attenuate the system resonance peaks and the IR peaks in the distributed parameter isolator. However, for the same control gain applied, its control performance around the equipment resonance frequency is worse than that under AVF control on the entire isolator. The reason is the same as that for the base excited system discussed in the last section. Because the ratio L/y is also set to be $\pi/2$, the third and sixth IR peaks (corresponding to the fifth and eighth peak shown in Figure 6.15) are again reduced much less than other IR peaks.

To further improve the control performance of the system on a flexible base around the equipment resonance frequency, AVF control on a fraction of the isolator length can also be combined with AVF on the entire isolator length, as shown in Figure 6.18. The velocity of the equipment can be written as

$$\dot{u}_e = Y_{ee}f_{a1} + Y_{er}f_{a2} + Y_{eb}\left(f - f_{a1} - f_{a2}\right) = \left(Y_{ee} - Y_{eb}\right)f_{a1} + \left(Y_{er} - Y_{eb}\right)f_{a2} + Y_{eb}f \tag{6.38}$$

where the input mobility Y_{ee} was defined in Chapter 4. The velocity at the point *r* can be written as

$$\dot{u}_r = Y_{er}f_{a1} + Y_{rr}f_{a2} + Y_{rb}\left(f - f_{a1} - f_{a2}\right) = \left(Y_{er} - Y_{rb}\right)f_{a1} + \left(Y_{rr} - Y_{rb}\right)f_{a2} + Y_{rb}f \tag{6.39}$$

Combining equations (6.28), (6.38) and (6.39), the velocity of the equipment is given by

$$\dot{u}_e = \frac{Y_{eb} + h_2\left(Y_{eb}Y_{rr} - Y_{er}Y_{rb}\right)}{1 + h_1\left(Y_{ee} - Y_{eb}\right) + h_2\left(Y_{rr} - Y_{rb}\right)} f \tag{6.40}$$

If the base is modelled as a mass m_b on a complex spring, i.e. $K_b^* = K_b(1 + j\eta_b)$, the amplitude ratio of the system is given by

$$\frac{u_e}{\delta_{st}} = \frac{K_b}{j\omega}\frac{\dot{u}_e}{f} = \frac{K_b}{j\omega}\frac{Y_{eb} + h_2\left(Y_{eb}Y_{rr} - Y_{er}Y_{rb}\right)}{1 + h_1\left(Y_{ee} - Y_{eb}\right) + h_2\left(Y_{rr} - Y_{rb}\right)} \tag{6.41}$$

The amplitude ratio of the system is shown in Figure 6.19 when $\mu_i = 0.1$, $\mu_b = 0.5$ $\mu_k = 0.1$, $\eta_i = \eta_b = 0.01$, $y = 2L/\pi$ and $\zeta_{a1} = \zeta_{a2} = 0.3$. For comparison, such a system without control, under AVF control on a fraction of the isolator length alone and under AVF control on the entire isolator length alone are also plotted. It can be seen that the system under AVF control on both the entire and a fraction of the isolator length has the best performance at the equipment resonance frequencies compared to other control methods. Also its control performance at IR frequencies is as good as that under AVF control on a fraction of the isolator length.

6.4.2.2 Stability analysis

Because the feedback controller is a constant gain, the plant response of the control system can be used to analyze the stability. From equation (6.32), the plant response from the active control force to the velocity of the control point *r* can be written as

$$G = \left.\frac{\dot{u}_r}{f_a}\right|_{f=0} = Y_{rr} - Y_{rb} \tag{6.42}$$

Although the input mobility Y_{rr} has a phase shift between -90º and 90º and is thus only in the right half in the complex plane, the transfer mobility Y_{rb} could be in either left or right half in the complex plane. So it is a potential threat to stability of the control system. Therefore, the system containing a distributed parameter isolator on a flexible base under AVF control on a fraction of the isolator length is only conditionally stable. Similar to the discussion for AVF control in Chapter 4, at a resonance frequency, in a lightly damped system, when only one mode dominates the response, the plant response given by equation (6.42) can be written as

$$G = Y_{rr} - Y_{rb} \approx \frac{\left[\phi_r^{(j)}\right]^2 \left(1 - \frac{\phi_b^{(j)}}{\phi_r^{(j)}}\right)}{2\zeta_j \sqrt{K_j M_j}} \tag{6.43}$$

where $\phi_r^{(j)}$ and $\phi_b^{(j)}$ are the j^{th} modal amplitudes evaluated at the control point *r* and base respectively. Based on the Nyquist criterion, for stability, one requires at a resonant frequency

$$\frac{\phi_b^{(j)}}{\phi_r^{(j)}} < 1 \tag{6.44}$$

for all *j*, i.e. $\left|\phi_b^{(j)}\right| < \left|\phi_r^{(j)}\right|$ if the modal amplitudes of the system evaluated at the control point *r* and base have the same phase. According to the definition of modal amplitudes $\phi_r^{(j)}$ and $\phi_b^{(j)}$, this stability condition means that if the displacement of the base is greater than the displacement of the control point *r* and these two displacements are in phase at the j^{th} natural frequency, then the system may become unstable.

Figures 6.20 shows the Nyquist plot of the plant response for a potentially unstable system on a flexible base under AVF control on a fraction of the isolator length. It can be seen that there is a loop on the left half of the complex plane crossing the negative real axis, which causes the system to be potentially unstable at high control gains. This potential instability occurs at the base resonance, at which the phase shift results in the small amplification in the magnitude of the base resonance peak shown in Figure 6.17.

At a resonance frequency where $\phi_b^{(j)} / \phi_r^{(j)} > 1$, i.e. the system has a potential to become unstable, with constant controller gain *h*, the open-loop response of the control system is given by

$$G(j\omega)H(j\omega) = hG = h\frac{\left[\phi_r^{(j)}\right]^2 \left(1 - \frac{\phi_b^{(j)}}{\phi_r^{(j)}}\right)}{2\zeta_j \sqrt{K_j M_j}} \tag{6.45}$$

To guarantee stability, the quantity in equation (6.45) must be greater than -1, so that the maximum gain $h_{\max}$ that can be applied to the control system is thus given by

$$h_{\max} = \frac{2\zeta_j \sqrt{K_j M_j}}{\left[\phi_r^{(j)}\right]^2 \left(\frac{\phi_b^{(j)}}{\phi_r^{(j)}} - 1\right)} \tag{6.46}$$

It should be noted that the stability condition proposed in equation (6.44) has the same form and physical meaning as that for AVF control on the entire isolator length concluded in Chapter 4. Therefore, such a system under AVF control on a fraction of the isolator length can also be stabilized by the approaches proposed in Chapter 5, e.g. adding more damping in the isolator, adding more mass to the base, etc.

6.4.3 Limitations in practice

Although AVF control on a fraction of the isolator length performs well in attenuating the IR peaks in the isolator for both base excited system and system on a flexible base, there are difficulties in implementing it in practice. As discussed in Chapter 5 in the experimental work, to realize AVF control on the entire isolator length, the actuators can be installed on top of the equipment reacting between the equipment and the base through corresponding stingers to generate active control forces, which are in parallel with the entire isolator. If such arrangements applied on a fraction of the isolator, i.e. actuators are attached on top of the control point *r* reacting between the control point and the base through stingers to generate active control forces, the mass of the actuators will change the dynamics at the control point *r*. The masses of actuators which perform as intermediate masses as discussed in Chapter 1 will dominate the response at the control point. Although better performance is achieved at high frequencies, the penalty is that the isolation performance at low frequencies is degraded [59]. The advantages of using AVF control on a fraction of the isolator length are thus lost. Therefore, how to generate an active control force in parallel with a fraction of the isolator without changing the dynamics at the control point is crucial in implementing AVF control on a fraction of the isolator length.

6.5 Conclusions

Three approaches which can attenuate the IRs in the distributed parameter isolator have been investigated theoretically in this chapter. These control methods demonstrate their own advantages and disadvantages in attenuating the IR peaks and improving the isolation performance over a broad range of frequencies.

Based on the equation for the maximum line of the IR peaks derived in Chapter 3, AVF control with more damping in the isolator has been investigated and shown to be a simple and straightforward method to attenuate the IR peaks. However, in practice due to the increase in the static stiffness of the isolator caused by the high damping materials applied in parallel with the isolator, the isolation performance at frequencies greater than the original system fundamental resonance frequency or the equipment resonance frequency will be degraded.

Based on the knowledge that the mass dominates the response of the equipment at high frequencies, acceleration feedback control, which electronically introduces extra mass into the system, has been investigated in combination with AVF control. It has been shown that the absolute velocity plus acceleration feedback control is effective in suppressing the IR peaks. Furthermore, for the system on a flexible base, the controller can also be carefully designed to make the control system unconditionally stable. However, to achieve good control performance at IRs, the magnitude of the open-loop frequency response of the control system remains large over a broad range of frequencies. Thus, the unmodelled dynamics of the system might be a danger to stability in practice.

Finally, AVF control on a fraction of the isolator length has been analyzed. It has been shown that the IR peaks can be effectively attenuated by AVF control on the lower part of the isolator. It is concluded that the longer the fraction of the isolator length controlled by AVF control, the better the control performance around the system

fundamental resonance frequency or the equipment resonance frequency. Also the ratio of the controlled length to the entire length of the isolator should be an irrational number in order to suppress all the IR peaks. However, the difficulty in implementing this control method in practice is how to generate an active control force in parallel with a fraction of the isolator without changing the dynamics at the control point.

To validate the theoretical analysis discussed in this chapter for the strategies which can attenuate the IRs in the distributed parameter isolator, the experiments are designed and conducted in the next chapter.

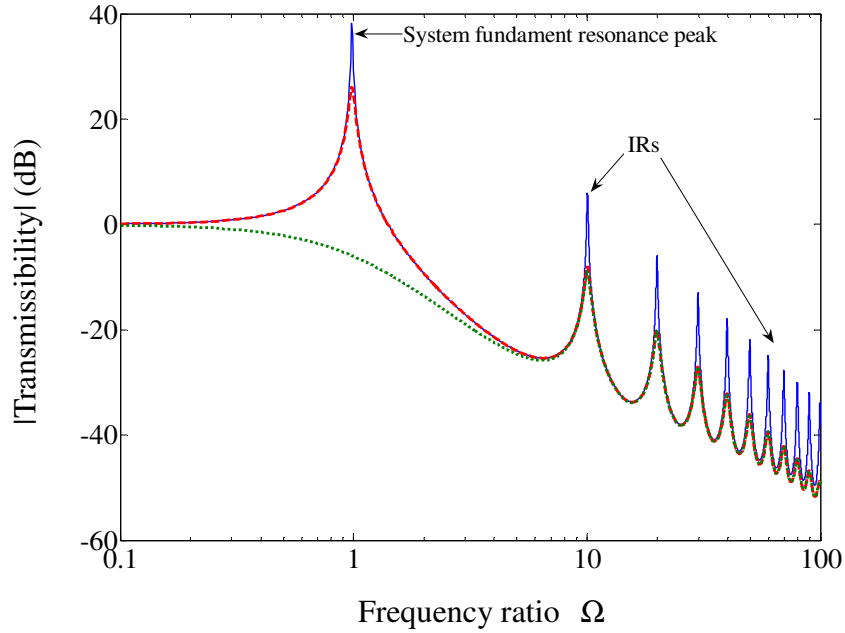

Figure 6.1 *Transmissibility of the base excited system under AVF control when the ratio of the mass of the isolator to the mass of the equipment* $\mu_i = 0.1$. *The solid line is for* $\eta_i = 0.01$ *(loss factor in the isolator),* $\zeta_a = 0$ *(active damping ratio), the dashed line is for* $\eta_i = 0.05$, $\zeta_a = 0$ *and the dotted line is for* $\eta_i = 0.05$, $\zeta_a = 1$.

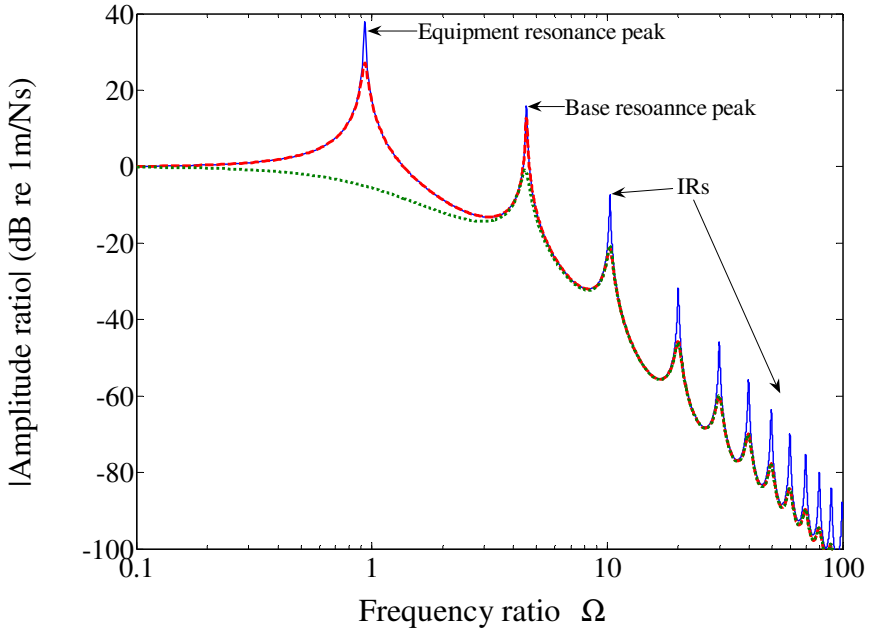

Figure 6.2 *Amplitude ratio of the system on a flexible base under AVF control when* $\mu_i = 0.1$, *the ratio of the mass of the base to the mass of the equipment* $\mu_b = 0.5$, *the ratio of the static stiffness of the isolator to the stiffness of the base* $\mu_k = 0.1$ *and the loss factor in the base* $\eta_b = 0.01$. *The solid line is for* $\eta_i = 0.01$, $\zeta_a = 0$, *the dashed line is for* $\eta_i = 0.05$, $\zeta_a = 0$ *and the dotted line is for* $\eta_i = 0.05$, $\zeta_a = 1$.

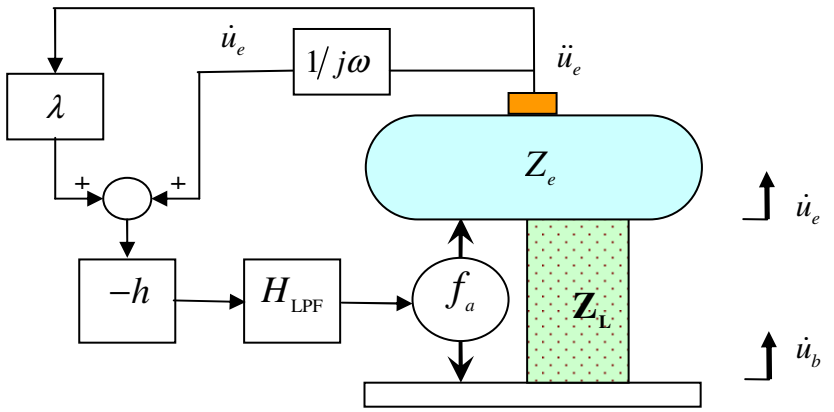

Figure 6.3 *Schematic diagram of a base excited system containing a distributed parameter isolator under absolute velocity plus acceleration feedback control, where* $\dot{u}_e$, $\ddot{u}_e$ *and* $\dot{u}_b$ *are velocity and acceleration of the equipment and velocity of the base respectively,* Z_e *is the input impedance of the equipment,* $\mathbf{Z}_{\mathbf{L}}$ *is the impedance matrix of the isolator, h is the constant feedback gain,* f_a *is the active control force,* λ *is a real coefficient, and* H_{LPF} *is the frequency response function of the low-pass filter.*

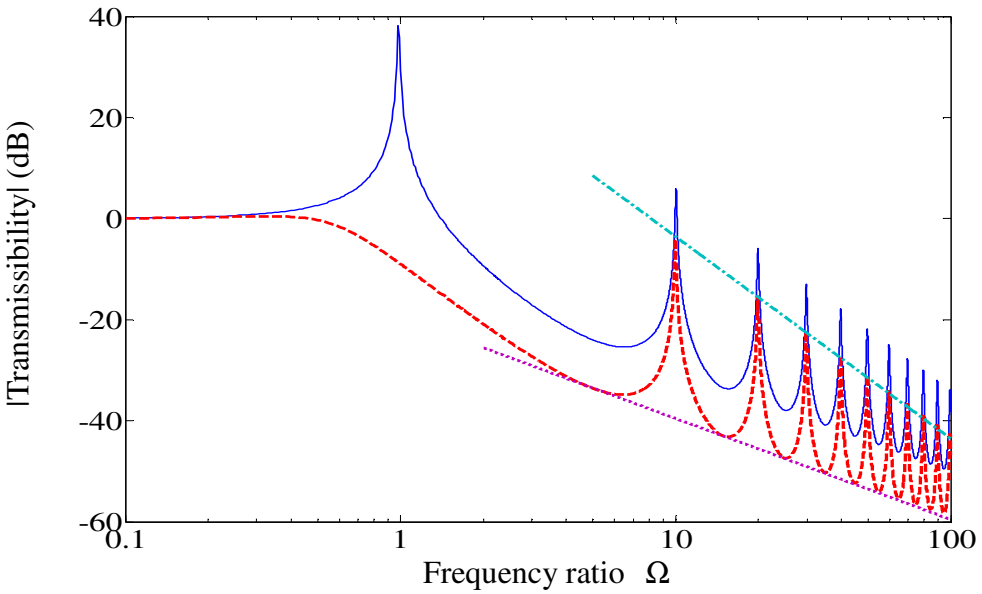

Figure 6.4 *Transmissibility of a base excited system under absolute velocity plus acceleration feedback control when* $\mu_i = 0.1$, $\eta_i = 0.01$, $\zeta_a = 1$, *the ratio of the corner frequency of the low-pass filter to the system fundamental resonance frequency* $\Gamma_f = 200$ *and the coefficient* $\lambda' = 1$ *(dashed line). The solid line is for the transmissibility of the corresponding passive system. The dashed-dotted line and the dotted line respectively pass through the IR peaks (equation (6.8)) and the troughs (equation (6.10)) in the transmissibility under control.*

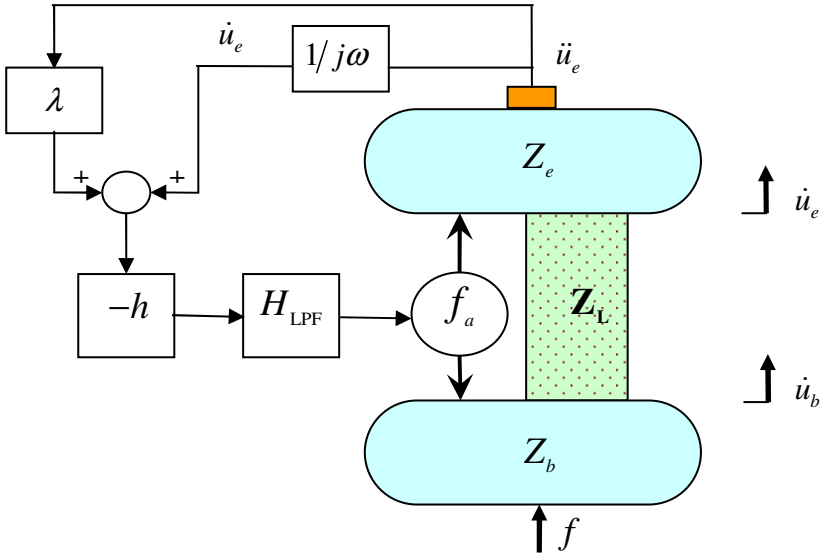

Figure 6.5 *Schematic diagram of an active vibration isolation system containing a distributed parameter isolator on a flexible base under absolute velocity plus acceleration feedback control, where* Z_b *is the input impedance of the base and f is the primary force.*

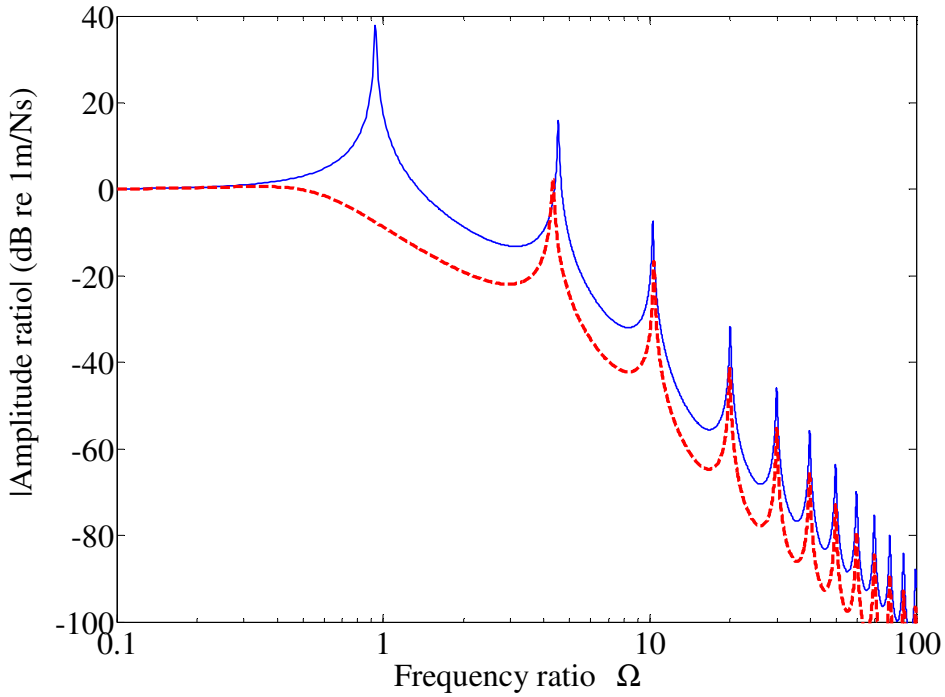

Figure 6.6 *Amplitude ratio of the systems on a flexible base under absolute velocity plus acceleration feedback control when* $\mu_i = 0.1$, $\mu_b = 0.5$, $\mu_k = 0.1$, $\eta_i = \eta_b = 0.01$, $\zeta_a = 1$, $\Gamma_f = 200$ *and* $\lambda' = 1$ *(dashed line). The solid line is for the amplitude ratio of the corresponding passive system.*

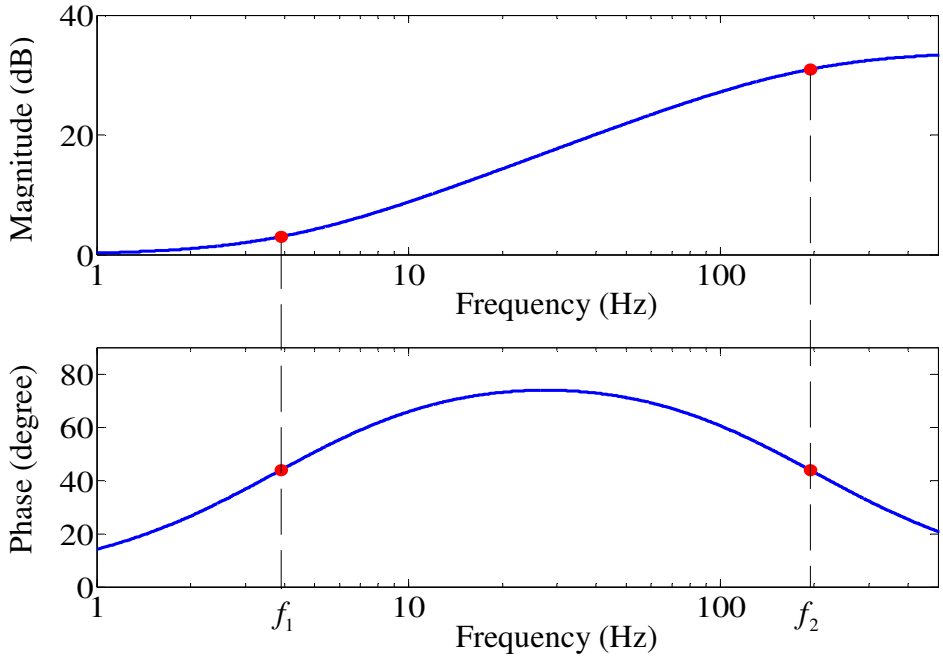

Figure 6.7 *Frequency response of the absolute velocity plus acceleration feedback controller when* $\Gamma_f = 50$, $\lambda' = 1$ *and h=1, where* $f_1 = 1/2\pi\lambda$, *and* $f_2 = \omega_f / 2\pi$ *is the corner frequency of the first order low-pass filter.*

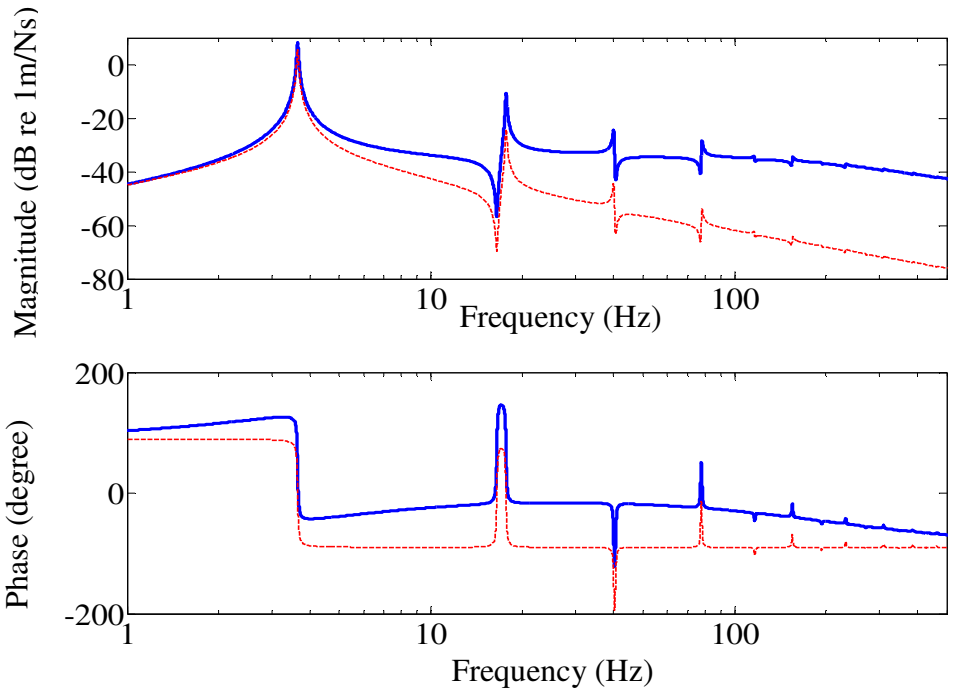

Figure 6.8 *Open-loop frequency responses (solid line) and plant response (dashed line) of the absolute velocity plus acceleration feedback control system on a flexible base when* $\mu_i = 0.1$, $\mu_b = 0.5$, $\mu_k = 0.1$, $\eta_i = \eta_b = 0.01$, $\Gamma_f = 50$, $\lambda' = 1$ *and h=1.*

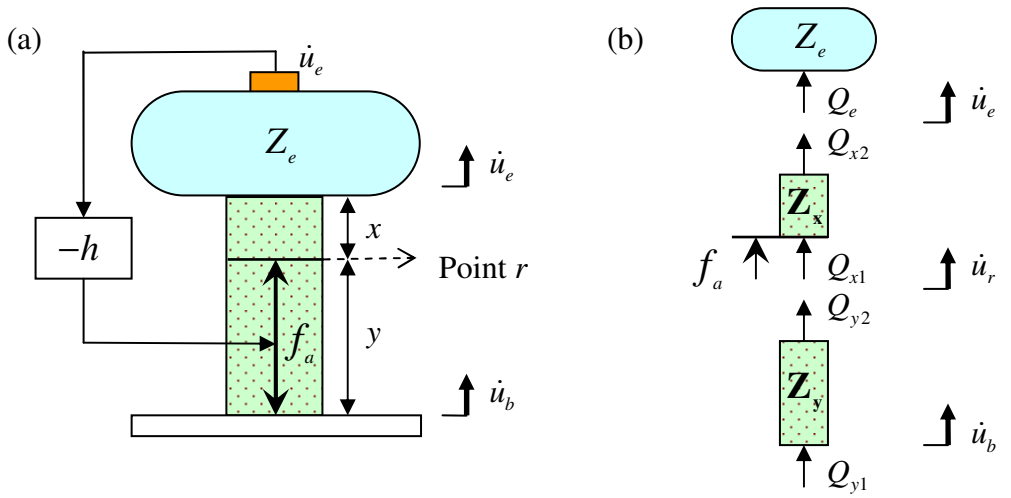

Figure 6.9 *(a) schematic diagram and (b) free body diagram of a base excited system containing a distributed parameter isolator under AVF control on a fraction of the isolator length, where* $\dot{u}_r$ *is the velocity at the control point r;* Q_e, Q_{x1}, Q_{x2}, Q_{y1} *and* Q_{y2} *are internal forces; x and y are respectively the length of the upper and lower part of the isolator; and* $\mathbf{Z}_x$ *and* $\mathbf{Z}_y$ *are respectively the impedance matrices for the upper and lower part of the isolator.*

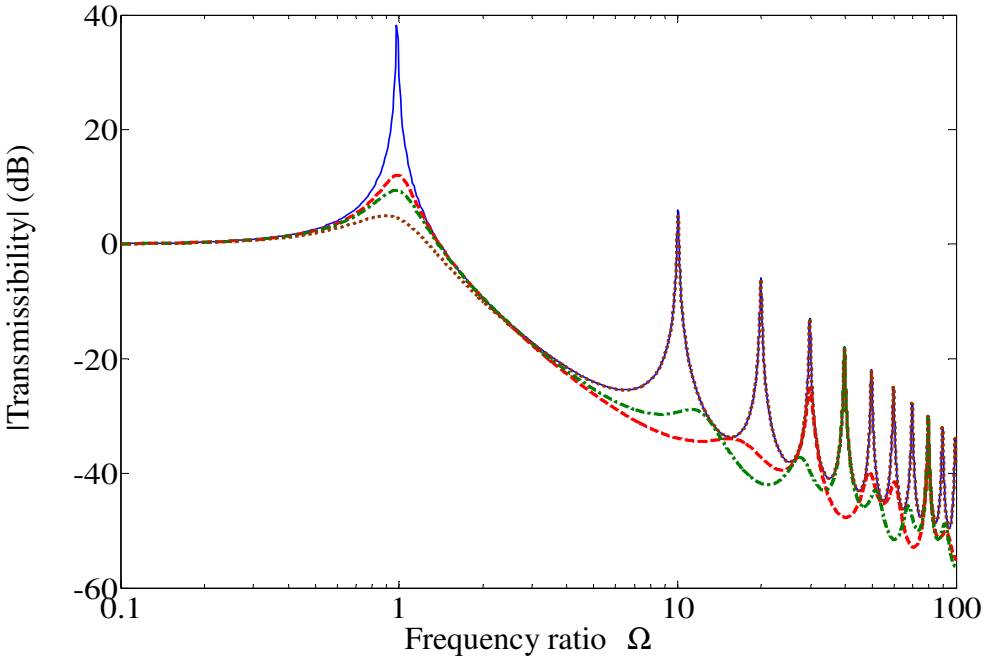

Figure 6.10 *Transmissibility of the base excited system containing a distributed parameter isolator under AVF control on a fraction of the isolator length when* $\mu_i = 0.1$, $\eta_i = 0.01$, $\zeta_a = 0.3$ *and* $y = 2L/\pi$ *(dashed line) or* $y = 3L/4$ *(dashed-dotted line). The solid line and the dotted line are respectively for such a system without control and under AVF control on the entire isolator length when* $\zeta_a = 0.3$.

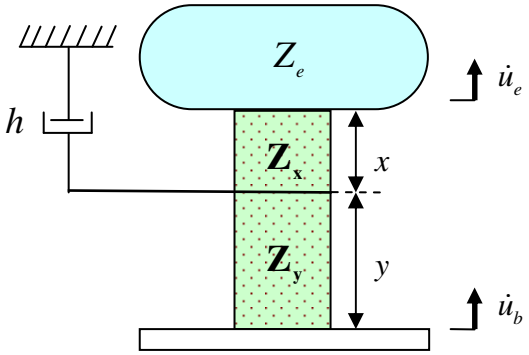

Figure 6.11 *Mechanical analogue of the active vibration isolation system under AVF control on a fraction of the isolator length shown in Figure 6.9.*

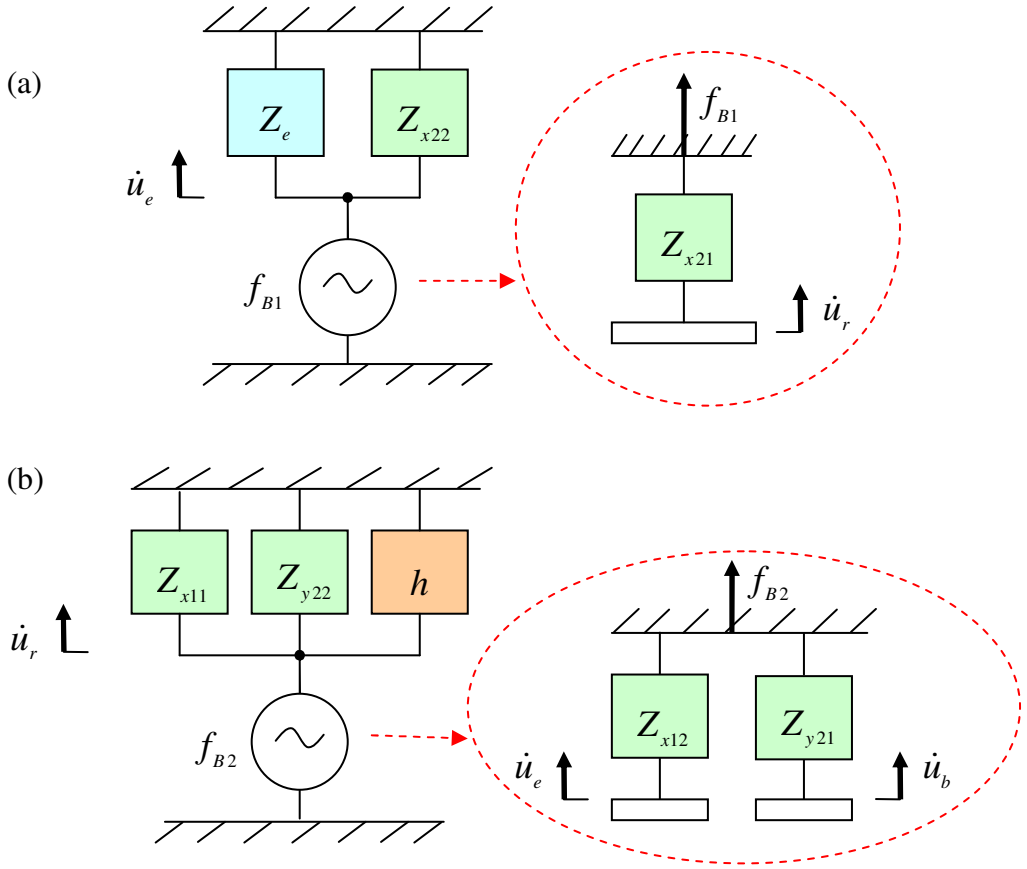

Figure 6.12 *Mechanical representations of the Thevenin equivalent systems for the system under AVF control on a fraction of the isolator length shown in Figure 6.9, (a) at the attachment point between the equipment and the isolator, and (b) at the control point r, where* Z_{x21} *and* Z_{x22} *are respectively the point and transfer impedances of the upper part of the isolator;* Z_{y21} *and* Z_{y22} *are respectively the point and transfer impedances of the lower part of the isolator; and* f_{B1} *and* f_{B2} *are the blocked forces.*

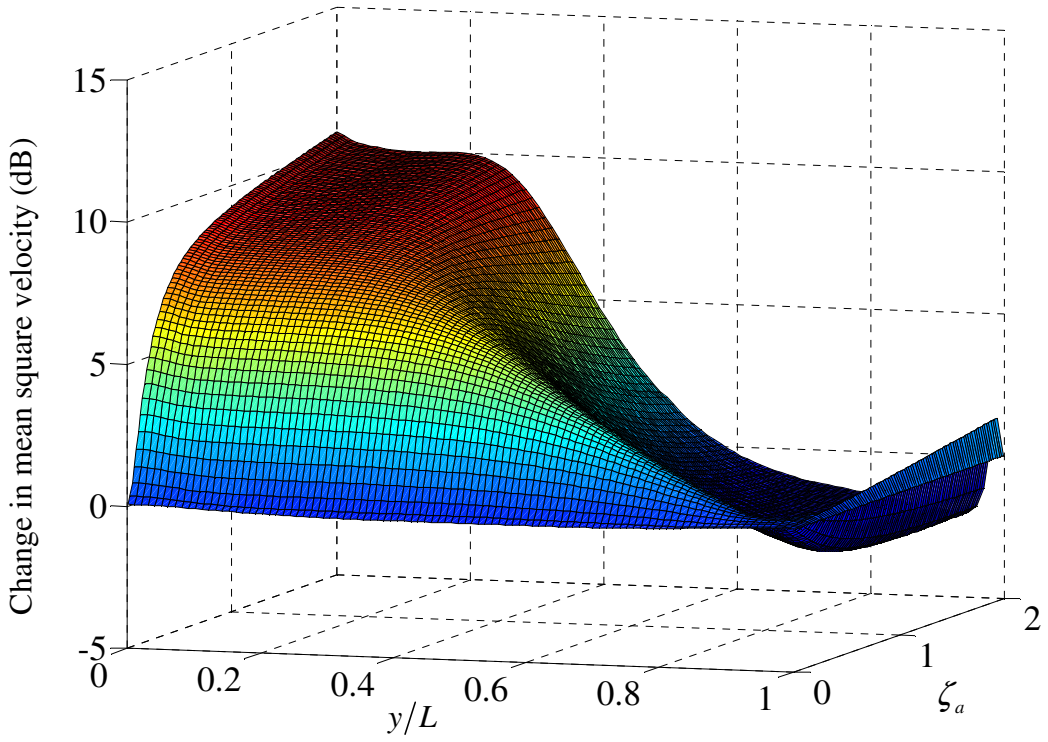

Figure 6.13 *Normalized change in mean square velocity for the system under AVF control on a fraction of the isolator length compared to that under AVF control on the entire isolator length within* $0.1<\Omega<1000$ *when* $\mu_i = 0.1$ *and* $\eta_i = 0.01$.

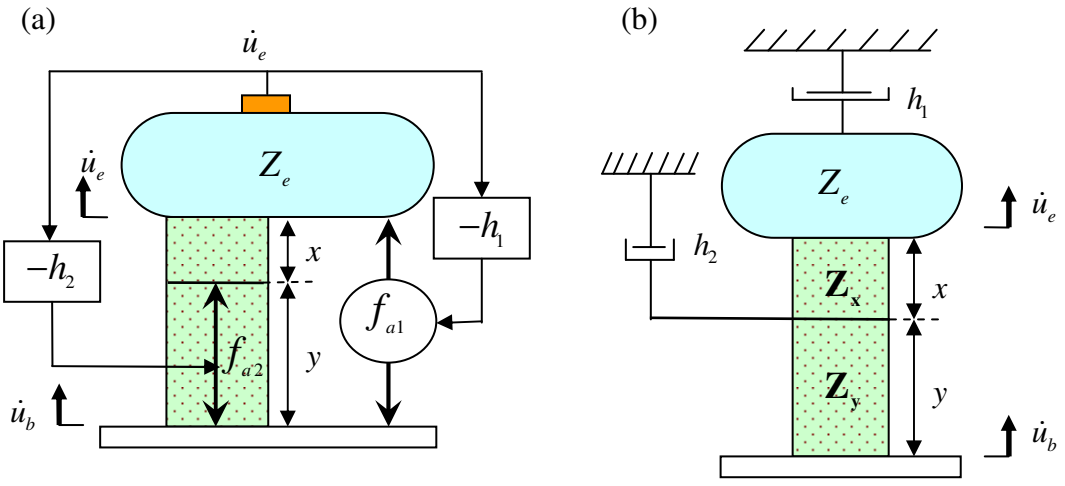

Figure 6.14 *(a) schematic diagram and (b) its mechanical analogue of a base excited system containing a distributed parameter isolator under both AVF control on a fraction of the isolator length and AVF control on the entire isolator length, where* h_1 *and* h_2 *are constant feedback control gains, and* f_{a1} *and* f_{a2} *are control forces.*

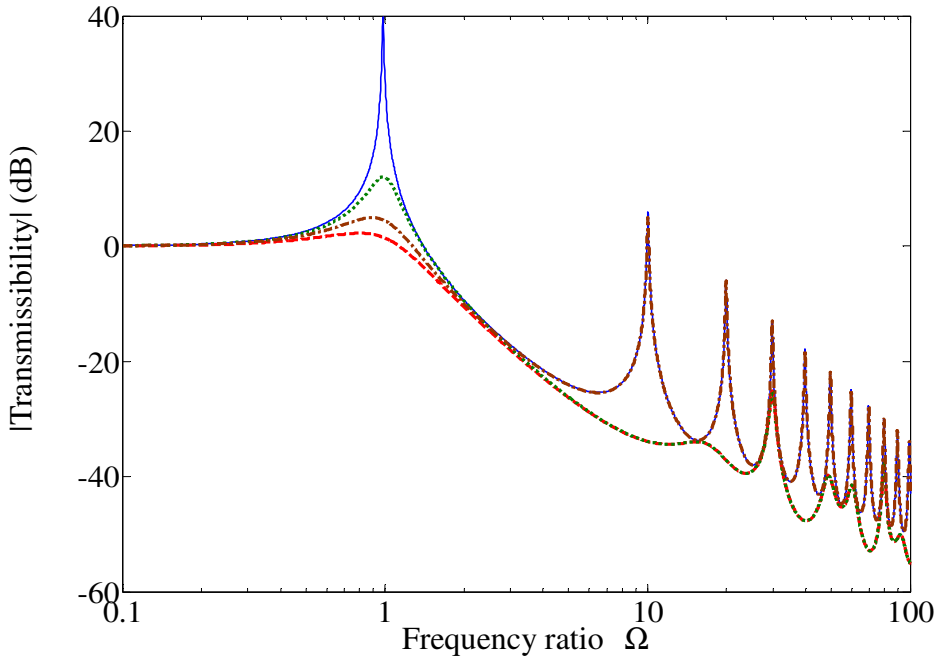

Figure 6.15 *Transmissibility of the base excited system containing a distributed parameter isolator under both AVF control on a fraction of the isolator length and AVF on the entire isolator length when* $\mu_i = 0.1$, $\eta_i = 0.01$, $y = 2L/\pi$ *and active damping ratios* $\zeta_{a1} = \zeta_{a2} = 0.3$ *(dashed line). The solid line, dotted line and dashed-dotted line are respectively for such a system without control, under AVF control on a fraction of the isolator length, and under AVF control on the entire isolator length when* $\zeta_a = 0.3$.

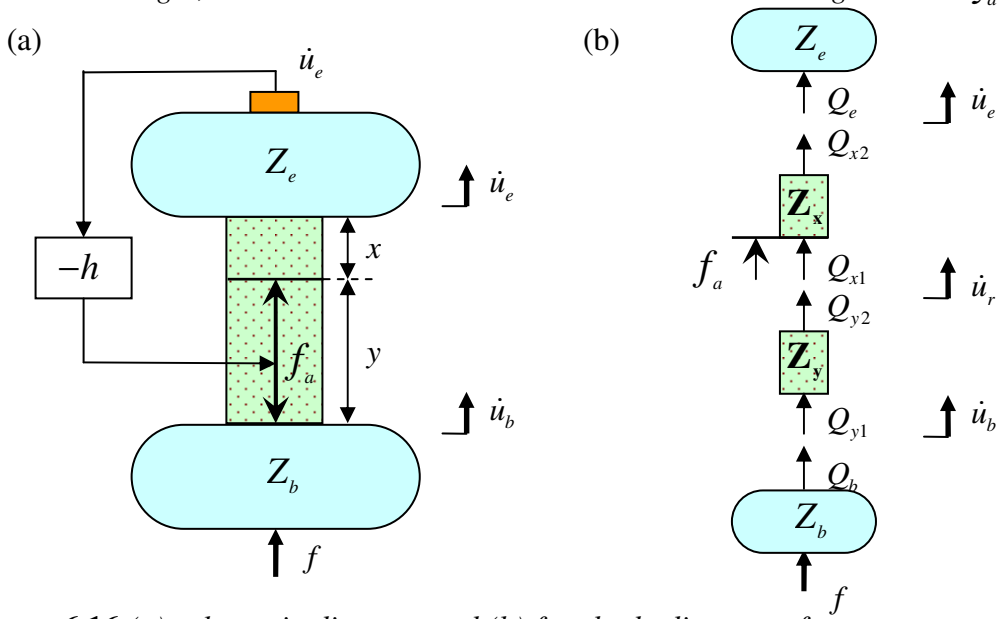

Figure 6.16 *(a) schematic diagram and (b) free body diagram of a system containing a distributed parameter isolator on a flexible base under AVF control on a fraction of the isolator length, where* Q_b *is an internal force.*

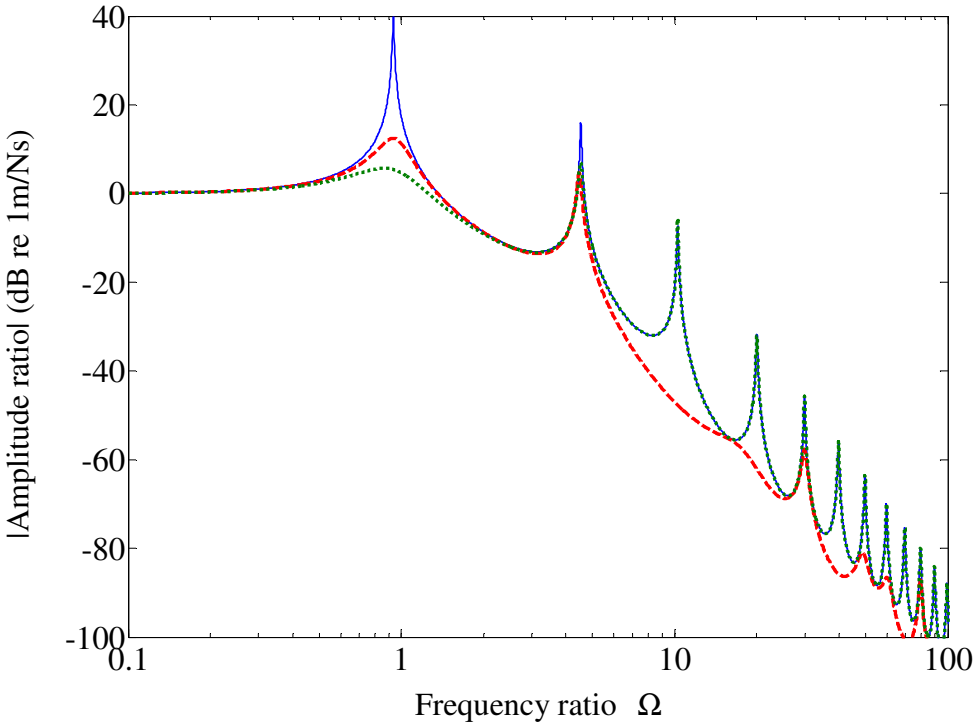

Figure 6.17 *Amplitude ratio of the system containing a distributed parameter isolator on a flexible base under AVF control on a fraction of the isolator length when* $\mu_i = 0.1$, $\mu_b = 0.5$ $\mu_k = 0.1$, $\eta_i = \eta_b = 0.01$, $y = 2L/\pi$ *and* $\zeta_a = 0$ *(solid line) or* $\zeta_a = 0.3$ *(dashed line). The dotted line is for such a system under AVF control on the entire isolator when* $\zeta_a = 0.3$.

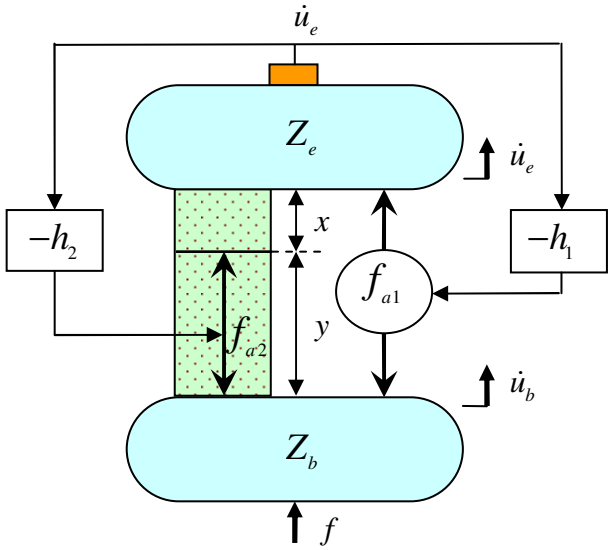

Figure 6.18 *Schematic diagram of a system containing a distributed parameter isolator on a flexible base under both AVF control on a fraction of the isolator length and AVF control on the entire isolator length.*

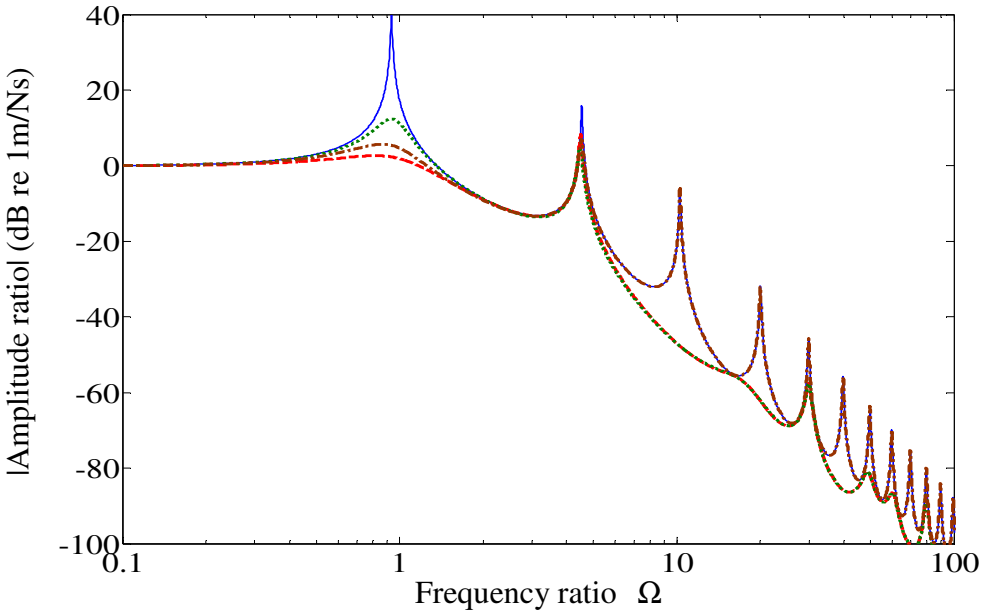

Figure 6.19 *Amplitude ratio of the system containing a distributed parameter isolator on a flexible base under both AVF control on a fraction of the isolator length and AVF on the entire isolator length when* $\mu_i = 0.1$, $\mu_b = 0.5$ $\mu_k = 0.1$, $\eta_i = \eta_b = 0.01$, $y = 2L/\pi$ *and* $\zeta_{a1} = \zeta_{a2} = 0.3$ *(dashed line). The solid line, dotted line and dashed-dotted line are respectively for such a system without control, under AVF control on a fraction of the isolator length and under AVF control on the entire isolator length when* $\zeta_a = 0.3$.

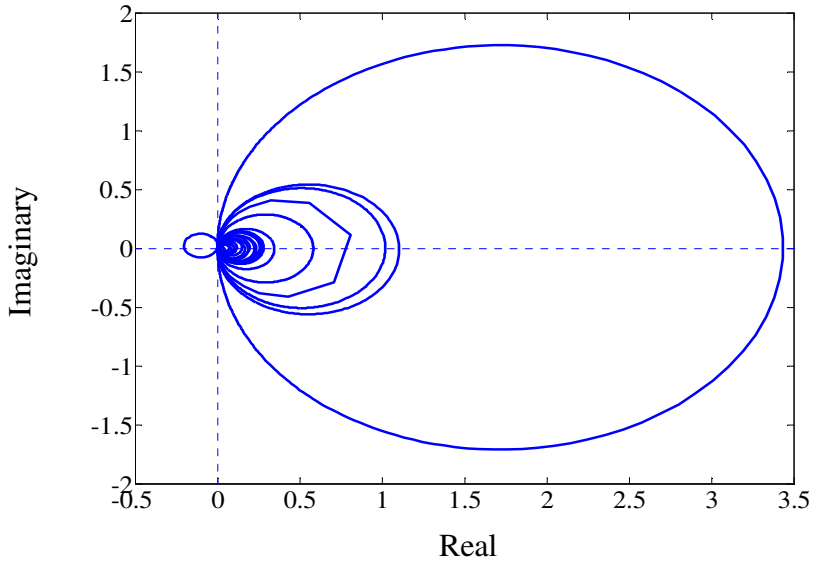

Figure 6.20 *Nyquist plot of the plant response of the system on a flexible base under AVF control on a fraction of the isolator length when* $\mu_i = 0.1$, $\mu_b = 0.5$ $\mu_k = 0.1$, $\eta_i = \eta_b = 0.01$ *and* $y = 2L/\pi$.

Chapter 7

Control of Internal Resonances: Experimental Validation

7.1 Introduction

In Chapter 6, a few strategies which can attenuate the IR peaks in the distributed parameter isolator have been investigated theoretically. The equation derived for the maximum response of the equipment at the IRs shows that the damping in the isolator governs the IR peaks. Therefore, AVF control with more damping in the isolator was investigated and shown to be a simple and straightforward method to attenuate the IR peaks. Also, it was concluded in Chapter 5 that more damping in the isolator helps stabilize the AVF control system. Based on the knowledge that the mass dominates the equipment response at high frequencies, acceleration feedback control, which electronically introduces extra mass into the system, has been investigated in combination with AVF control. It has been shown that absolute velocity plus acceleration feedback control is effective in suppressing both system resonance peaks at low frequencies and IR peaks at high frequencies. Furthermore, for the system on a flexible base, an absolute velocity plus acceleration feedback controller can be carefully designed to stabilize the control system at IR frequencies.

The aim of this chapter is to validate experimentally the strategies which can attenuate the IRs in the distributed parameter isolator. First, AVF control with more damping in the isolator is investigated experimentally. A highly damped non-elastomeric material, steel wool, is introduced in parallel with the original isolator under AVF control. It is followed by the experimental validation of the absolute velocity plus acceleration feedback control.

7.2 Experimental validation for AVF control with additional damping in the isolator

As discussed in Chapter 6, to achieve high damping in the isolator, one can either choose isolators made of highly damped material to increase the inherent damping in the isolator, or use highly damped material in parallel with the original isolator. For metal isolators, e.g. helical springs that have inherently low damping, a highly damped material is required to offer a practical solution. In this section, fine steel wool (Oakey) that has a high loss factor due to internal friction is used to perform as a highly damped material in parallel with the isolator to increase the overall damping.

To realize AVF control with more damping in the isolator, the four-spring active vibration isolation system used in Chapter 5 to validate AVF control was modified. As shown in Figure 7.1, the difference between the modified system and the original one is that the fine steel wool was inserted inside each helical spring surrounding the corresponding stinger. Therefore, the steel wool is effectively in parallel with each spring, and thus the overall damping in the isolator is increased.

7.2.1 Stability analysis

To measure the open-loop frequency response of the AVF control system with additional damping in the isolator, the four actuators fixed on top of the equipment plate were

driven with white noise from the dynamic signal analyser through a power amplifier, while the primary vibrator was connected but inactive. The equipment response was monitored by five accelerometers located along two central lines of the equipment plate, so that the average vertical equipment response could be analyzed, and the effect of any rigid body equipment plate rotation reduced. The acceleration signals from the equipment plate were then passed through charge amplifiers. These include an integrator and high and low-pass filter modules, so that the velocity response of the equipment can be obtained. The high-pass filter cut-off frequency was set to 1 Hz to avoid DC signal overflow, and the low-pass filter cut-off frequency was set to 10 kHz. The open-loop frequency response of the AVF control system with additional damping in the isolator on the modified system was then measured and averaged using the input to the power amplifier and the integrated output from the charge amplifiers.

The measured open-loop frequency response of the modified four-spring active vibration isolation system with steel wool in the springs is shown in Figure 7.2. The open-loop frequency response of the original system without steel wool is also plotted for comparison. The data below 3 Hz had low coherence due to the low instrumentation sensitivity, so they are not presented. It can be seen that the system resonance peaks are attenuated due to the extra damping introduced by the steel wool. Also, the fist IR peak in the helical springs around 404 Hz is suppressed and has almost disappeared due the increased damping in the isolator. Furthermore, the phase lag at the first IR was constrained to be in the range of -238º to -100º, so that the potential instability at the first IR is eliminated by the extra damping introduced into the isolator. This result validates the conclusion in Chapter 5 that adding more damping in the isolator can stabilize the AVF control system. The system resonances of the open-loop frequency response with additional damping in the isolator also move to higher frequencies compared to those for the original system. This phenomenon has been predicted in the theoretical analysis in Chapter 6. The reason is that the steel wool applied in parallel with the helical springs increases not only the damping, but also the static stiffness of the isolator, so that the system resonance frequencies are increased. Also it should be

noted that the rotational mode around 289 Hz, the flexural mode in the equipment plate around 327 Hz, and those modes above 500 Hz are affected much less by the change of the damping and static stiffness of the isolator. Therefore, the phase lag due to the flexural mode in the equipment plate around 327 Hz still occurs, which may destabilize the control system at high control gains. Furthermore, in this experiment, it has been found that the AVF control system with additional damping in the isolator first becomes unstable at very low frequencies, due to the phase advances in the charge amplifiers and power amplifiers with increased feedback control gain.

Figure 7.3 depicts the Nyquist plot of the open-loop frequency response of the AVF control system with additional damping in the isolator corresponding to the results and frequency range shown in Figure 7.2. The only loop in the left half of the complex plane crossing the negative real axis is caused by the flexural mode in the equipment plate at 327 Hz. The potential instability for the original system at the first IR in the helical springs at 404 Hz has been eliminated by the extra damping introduced into the isolator.

7.2.2 Control performance

A single-channel AVF control on the modified active vibration isolation system with additional damping in the isolator was implemented on each of the four springs. The primary vibrator was driven with white noise. The velocity responses of the equipment and base were obtained using accelerometers through charge amplifiers and then passed to the signal analyzer. The velocity response at the centre of the equipment plate was fed back to four actuators through a power amplifier to generate the control forces, which were identical for each actuator. Each feedback channel had thus an equal, constant feedback gain.

Figure 7.4 shows the transmissibility for the modified active vibration isolation system with additional damping in the isolator with various control gains, where the transmissibility for the original active vibration isolation system without control is also

plotted for comparison. Figure 7.5 shows the velocity response of the equipment plate per unit voltage to the power amplifier, which drove the primary vibrator, for the modified active vibration isolation system with additional damping in the isolator under various control gains. For comparison, the velocity response of the equipment plate per unit voltage to the power amplifier for the original active vibration isolation system without control is also plotted. Responses less than 3 Hz are again excluded from the plots. It can be seen that, for the modified system without control, the system resonance peaks in Figures 7.4 and 7.5 are attenuated due to the extra damping introduced by the steel wool compared to those in the original system. Furthermore, the fist IR peak in the helical springs around 404 Hz is well suppressed and has almost disappeared due the increased damping in the isolator. With an increase in the AVF control gain, the system resonance peaks in Figures 7.4 and 7.5 are further reduced, while the first IR peak is affected much less. These results validate the conclusion in Chapter 6 that AVF control with more damping in the isolator is effective in attenuating both the system resonance peaks at low frequencies and the IR peaks in the isolator at high frequencies. However, it should be noted that the system resonances in Figures 7.4 and 7.5 for the modified system move to higher frequencies compared to those for the original system, because the static stiffness of the isolator is increased due to the steel wool introduced. It should also be noted that there is amplification at the flexural mode in the equipment plate around 327 Hz with an increase in the control gain.

7.2.3 Summary

The theoretical analysis on AVF control with more damping in the isolator has been validated by the experiment on the modified four-spring active vibration isolation system with the steel wool in parallel with helical springs. It has been shown that, as predicted in the theoretical analysis, AVF control with more damping in the isolator is effective in attenuating both the system resonance peaks at low frequencies and the IR peaks in the isolator at high frequencies. Also, the high damping introduced into the isolator can stabilize the AVF control system at the IR frequencies. However, the

increase of the static stiffness of the isolator due to the high damping material introduced pushes the system resonances to higher frequencies. Also, the instability occurred at the flexural mode in the equipment plate, which is not considered in the theoretical analysis, cannot be eliminated by the high damping introduced.

7.3 Experimental validation for absolute velocity plus acceleration feedback control

Based on the conclusion in Chapter 4 that the mass dominates the equipment response at relatively high frequencies, acceleration feedback control is used to suppress the IR peaks at high frequencies, since it is equivalent to adding a mass to the system. On the other hand, AVF control was shown to be effective in attenuating the equipment response at the system resonances at low frequencies. Therefore, absolute velocity plus acceleration feedback control was investigated in Chapter 6 to improve the isolation performance of systems containing a distributed parameter isolator over a broad range of frequencies. In this section, absolute velocity plus acceleration feedback control is investigated experimentally on the four-spring active vibration isolation rig.

7.3.1 Experimental setup

To realize the absolute velocity plus acceleration feedback, the acceleration response at the centre of the equipment plate for the four-spring active vibration isolation system was measured by accelerometers. Then the corresponding velocity response was obtained through a charge amplifier. By setting the gain in the charge amplifier, the ratio between the acceleration and the velocity (i.e. λ defined in equation (6.1)) can be adjusted. A summing amplifier was designed to sum up the obtained absolute velocity and acceleration signal. Its physical configuration is shown in Figure 7.6. A first order low-pass filter was also included in this summing amplifier to constrain the control signal at high frequencies. The corner frequency of the low-pass filter is adjustable

between 1 kHz and 5 kHz. The summing amplifier is powered by a stabilised power supply (Farnell instruments LTD LT30-1).

Figure 7.7 shows a photograph of the experimental setup and the schematic diagram of the signal path with details of one actuator and the corresponding spring underneath. The primary vibrator was driven with white noise from a dynamic signal analyzer through a power amplifier. The base response was measured using an accelerometer at the centre of the base plate and then passed through a charge amplifier to obtain the velocity response. The equipment response was monitored by two accelerometers at the centre of the equipment plate. One acceleration signal from the equipment plate was passed through a charge amplifier to obtain the velocity response. The other one was also passed through a charge amplifier to introduce a gain. Then the velocity and acceleration responses were input into the summing amplifier. Its output was then fed back to the actuators via a power amplifier with gain control to generate the active control force.

7.3.2 Stability analysis

To measure the open-loop frequency response, the four actuators fixed on top of the equipment plate were driven with the same white noise from the dynamic signal analyzer through a power amplifier, while the primary vibrator was connected but inactive. The open-loop frequency response for the absolute velocity plus acceleration feedback control system was measured using the input to the power amplifier and the output from the summing amplifier.

The measured open-loop frequency response of the absolute velocity plus acceleration feedback control system is shown in Figure 7.8. For comparison, the open-loop frequency response of the AVF control system is also plotted. The data below 3 Hz had low coherence due to the low instrumentation sensitivity, so again they are not presented. It can be seen that the phase lag that occurs at the first IR in the helical springs around

404 Hz and the flexural mode in the equipment plate around 327 Hz was compensated by the phase lead due to the absolute velocity plus acceleration feedback controller. The phase shifts at these two frequencies are now greater than -180º, so that the phase shift of the open-loop frequency response in the frequency range shown in Figure 7.8 is between -180º and 180º. Therefore, the experimental result validates the conclusion in Chapter 6 that a carefully designed absolute velocity plus acceleration feedback controller can help stabilize the control system at IR frequencies without compromising the stability at other frequencies.

Figure 7.9 depicts the Nyquist plot of the open-loop frequency response of the absolute velocity plus acceleration feedback control system corresponding to the results and frequency range shown in Figure 7.8. It can be seen that, due to the phase lead of the controller, the Nyquist plot of the open-loop frequency response of the absolute velocity plus acceleration feedback control system is shifted clockwise compared to that of AVF control system. Therefore, there is no loop in the left half of complex plane which crosses the negative real axis shown in Figure 7.9.

However, it should be noted in Figure 7.8 that, above the equipment resonance frequency, the magnitude of open-loop frequency response of the absolute velocity plus acceleration feedback control system is increased with frequency due to the acceleration feedback incorporated. This amplification may cause stability problems at high frequencies before the open-loop frequency response can be effectively limited by the first order low-pass filter in the summing amplifier. Figure 7.10 depicts the open-loop frequency of the absolute velocity plus acceleration feedback control system up to 5 kHz. It can be seen that, in this experiment, the instability does not first occur at low frequencies due to the phase advances in the charge amplifiers and power amplifiers. Instead, the control system first became unstable at a natural frequency of the system at about 1160 Hz, corresponding to the Nyquist plot of the open-loop frequency response crossing the negative real axis as shown in Figure 7.11. Furthermore, the magnitude of the open-loop frequency response at 1160 Hz is very large, so that its Nyquist plot is

close to the unstable point (-1, 0j). Thus the absolute velocity plus acceleration feedback control system became unstable at very low control gains. As a consequence, very poor control performance at system resonance peaks and IR peaks in the isolator can be achieved in this experiment. Therefore, as discussed in Chapter 6, the unmodelled dynamics in the system that are not considered in the theoretical analysis may be a danger to stability of the control system, and thus limit the control performance.

7.4 Conclusions

AVF control with more damping in the isolator and absolute velocity plus acceleration feedback control have been investigated experimentally in this chapter. Some theoretical results given in Chapter 5 and Chapter 6 have been validated experimentally.

The AVF controller with additional damping in the isolator has been shown experimentally to be a simple approach to attenuate the IR peaks in the isolator. Also, the additional damping in the isolator is beneficial to the stability of the AVF control system at IR frequencies. However, the system resonances move to higher frequencies because the static stiffness of the isolator is increased due to the high damping material introduced. Furthermore, the instability occurred in other modes, such as the flexural mode in the equipment plate, which was not considered in the theoretical analysis, cannot be eliminated by the high damping introduced in the isolator.

The absolute velocity plus acceleration feedback control was shown to be effective in stabilizing the control system at the first IR frequency, as well as the flexural mode in the equipment plate, due to the phase lead introduced by the controller. However, the increase in the magnitude of the open-loop frequency response of the control system due to the acceleration feedback incorporated causes stability problem at high frequencies. In the experiment, the absolute velocity plus acceleration feedback control system first became unstable at a natural frequency of the system at high frequencies,

and very small control gains can be applied. Therefore the control performance is limited. It shows that, although absolute velocity plus acceleration feedback control is theoretically effective in attenuating both system resonance peaks at low frequencies and IR peaks at high frequencies, in practice the unmodelled dynamics at high frequencies may destabilize the control system and thus limit the control performance.

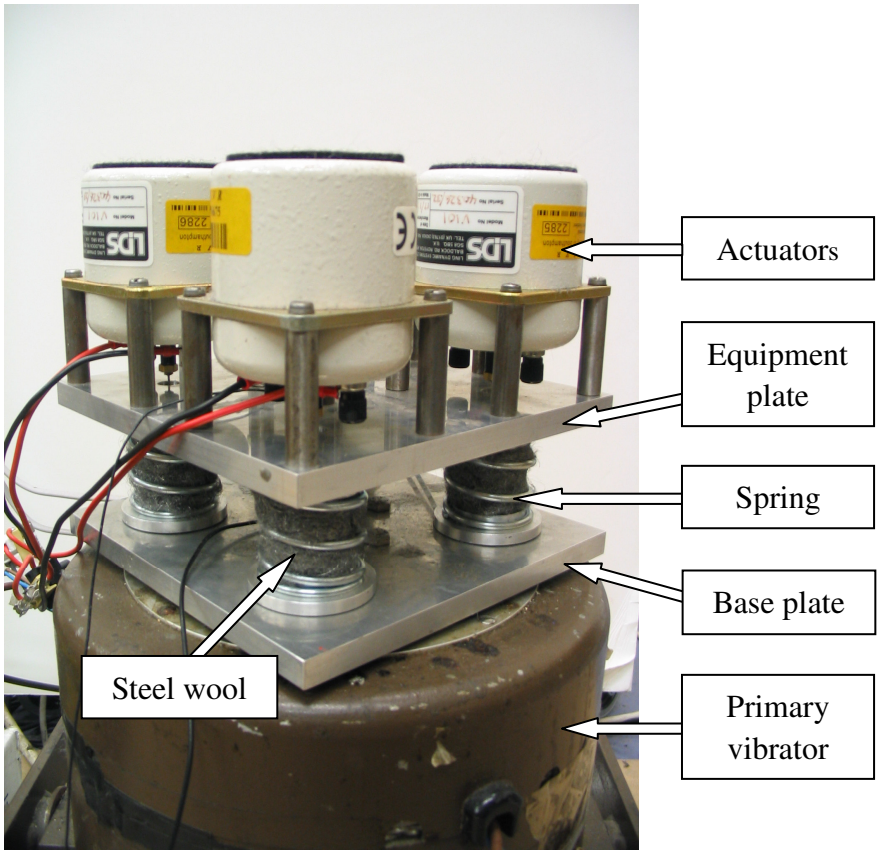

Figure 7.1 *Photograph of the modified four-spring active vibration isolation system with steel wool inside the helical springs.*

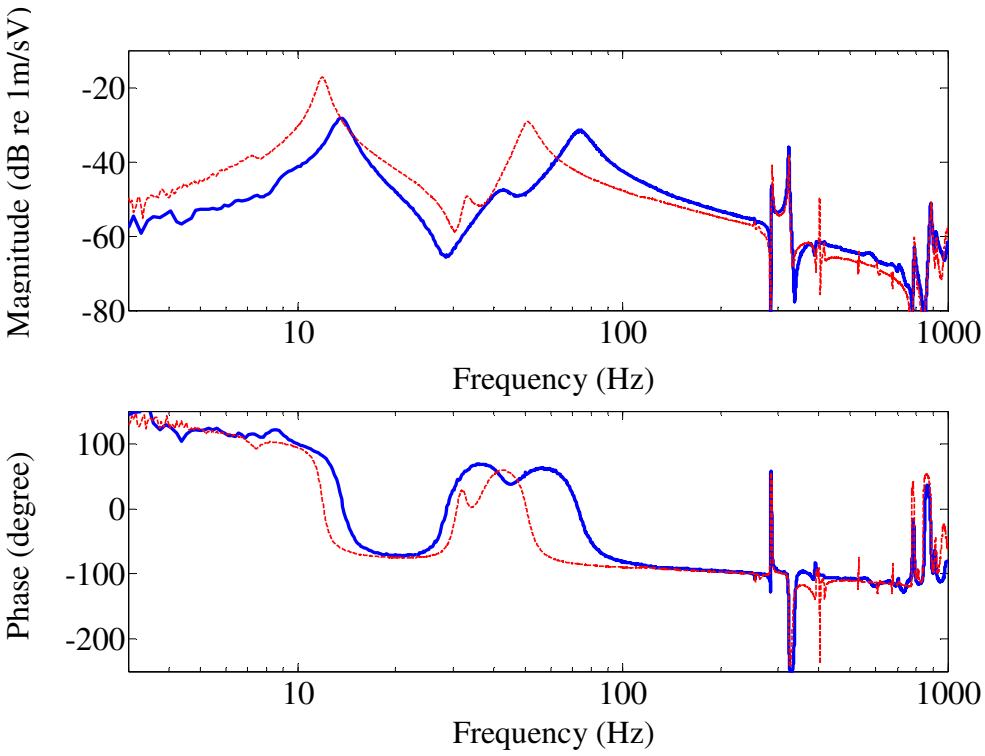

Figure 7.2 *Measured open-loop frequency response of the AVF control system with (solid line) or without (dashed line) additional damping in the isolator.*

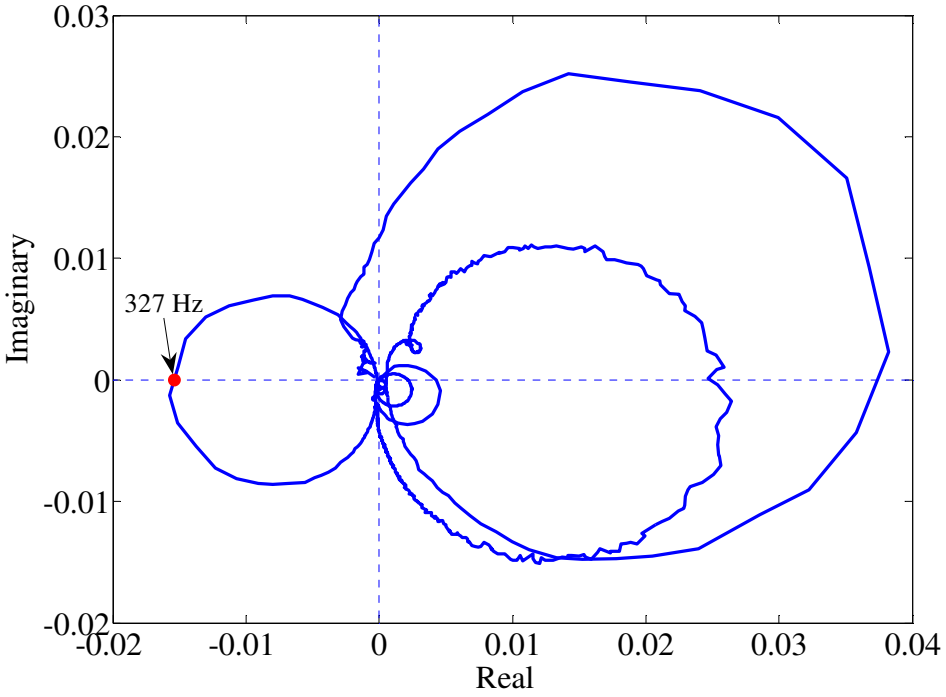

Figure 7.3 *Measured Nyquist plot of the open-loop frequency response of the AVF control system with additional damping in the isolator.*

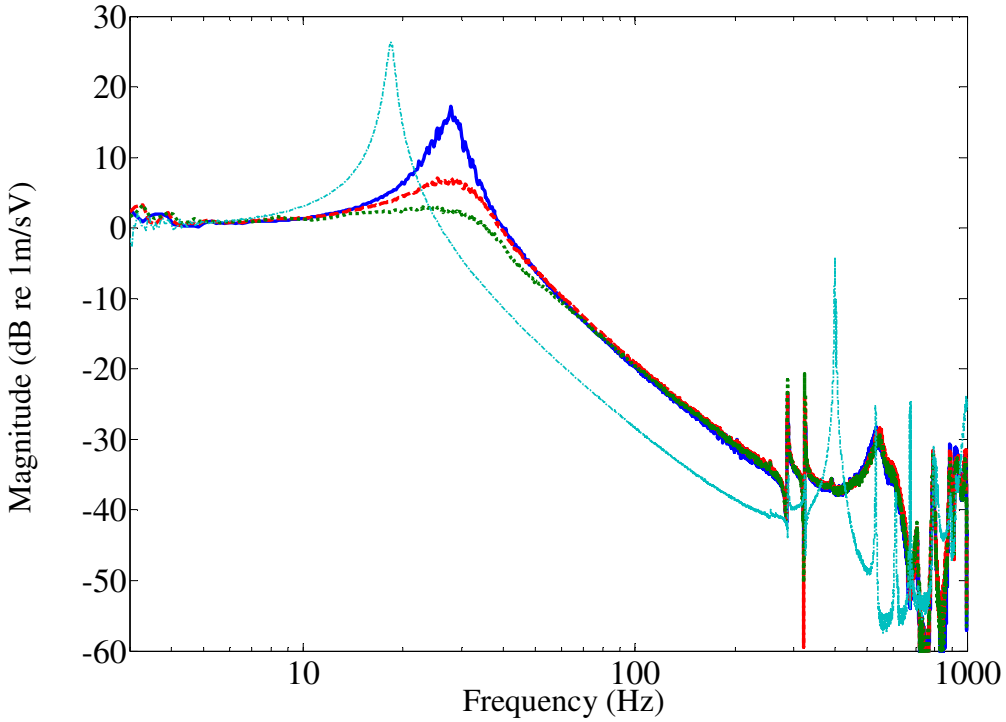

Figure 7.4 *Measured transmissibility of the original active vibration isolation system without control (dashed-dotted line), and the modified active vibration isolation system with additional damping in the isolator under various feedback gains: without control (solid line), low control gain (dashed line) and high control gain (dotted line).*

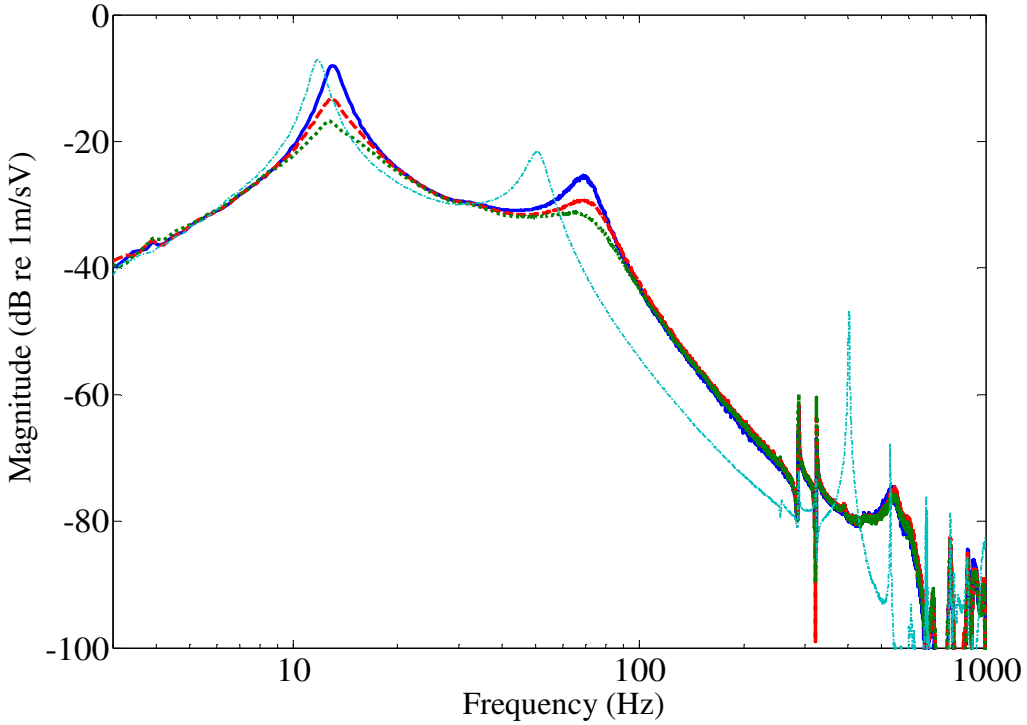

Figure 7.5 *Measured velocity response of the equipment plate per unit voltage to the power amplifier of the original active vibration isolation system without control (dashed-dotted line), and the modified active vibration isolation system with additional damping in the isolator under various feedback gains: without control (solid line), low control gain (dashed line) and high control gain (dotted line).*

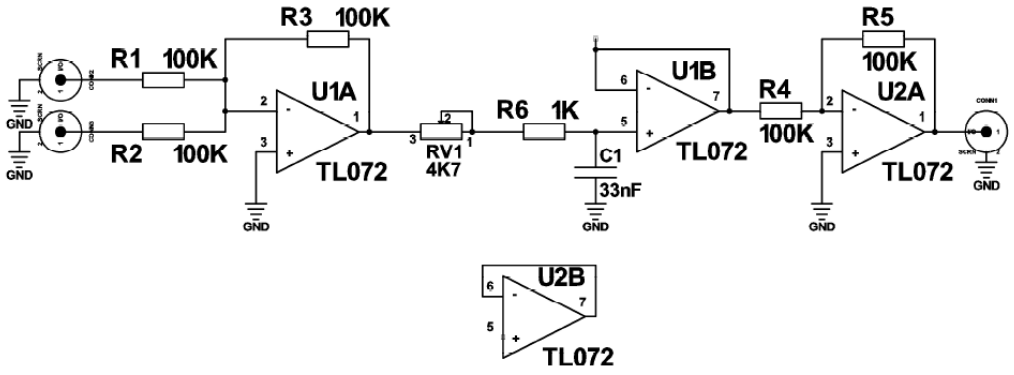

Figure 7.6 *Physical configuration of a summing amplifier with a first order low-pass filter included.*

(a)

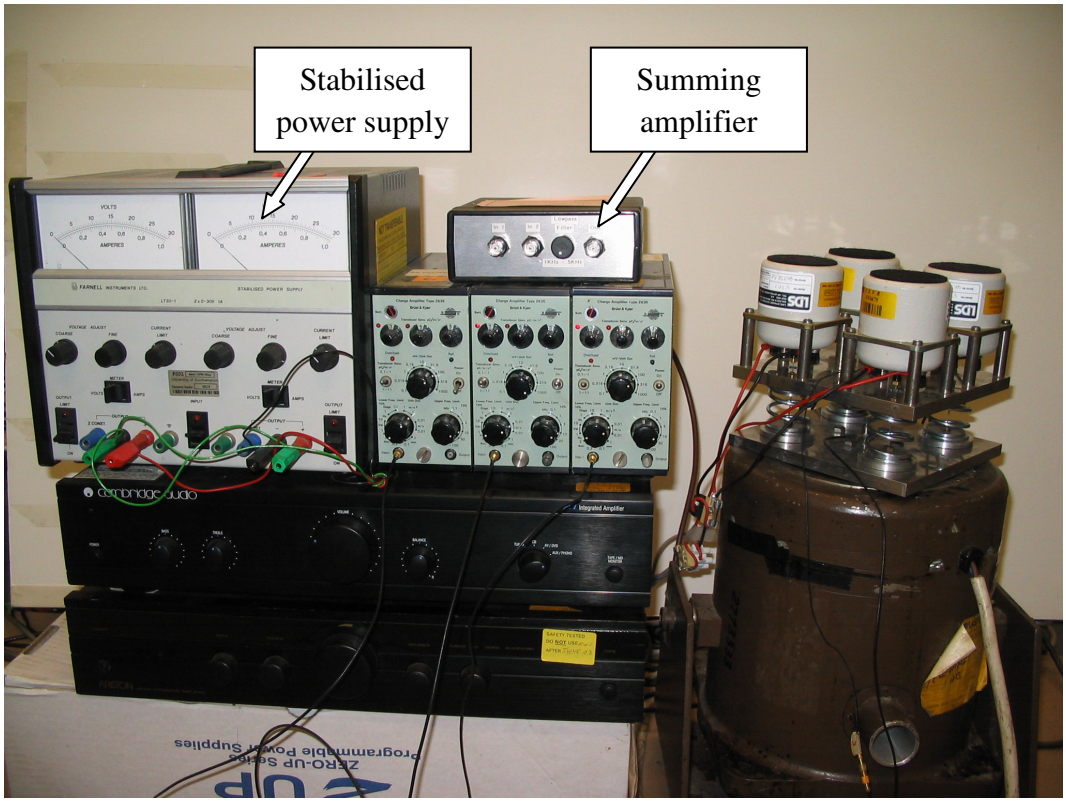

(b)

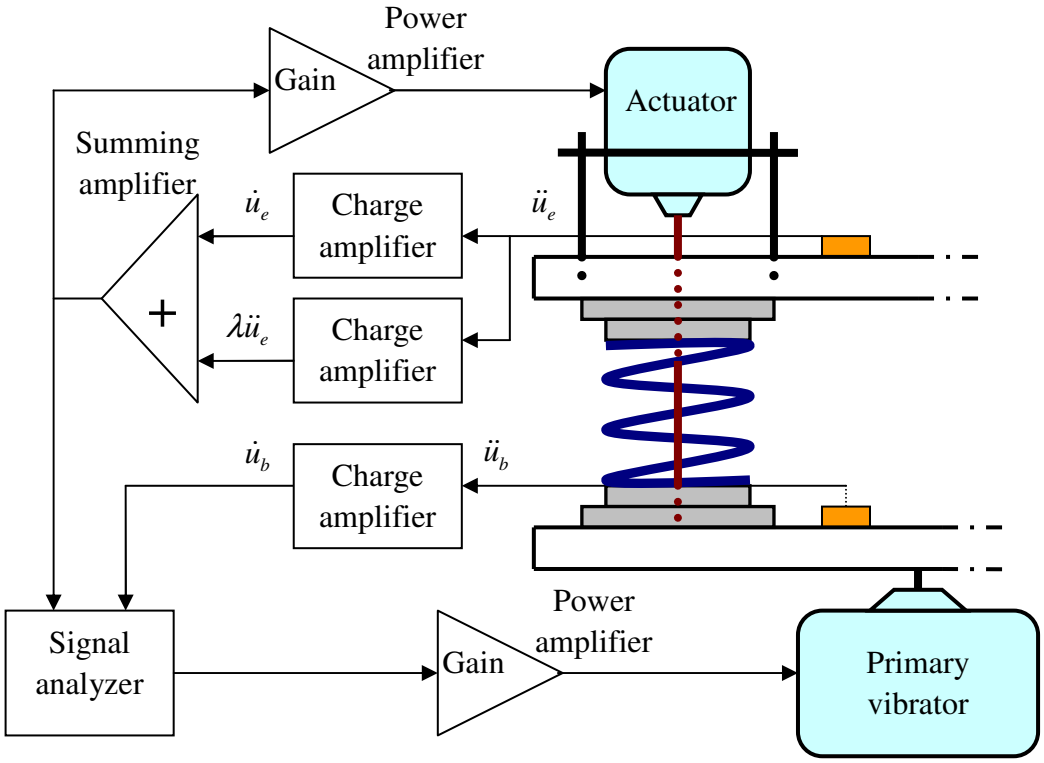

Figure 7.7 *(a) photograph and (b) schematic diagram of one corner of the four-spring active vibration isolation system for absolute velocity plus acceleration feedback control, where* $\dot{u}_e$, $\dot{u}_b$, $\ddot{u}_e$ *and* $\ddot{u}_b$ *are velocities and accelerations of the equipment and the base respectively, and* λ *is the real coefficient.*

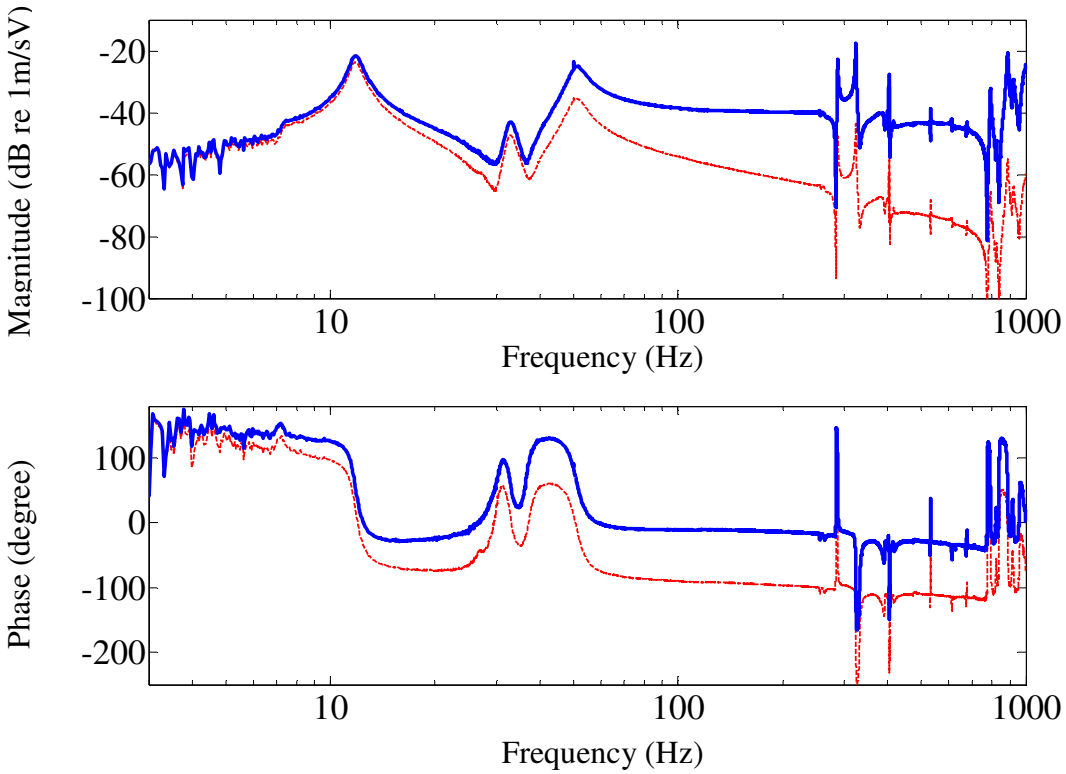

Figure 7.8 *Measured open-loop frequency response of the absolute velocity plus acceleration feedback control system when* $\lambda = 0.01$ *and the corner frequency of the first order low-pass filter is 5 kHz (solid line), and AVF control system (dashed line).*

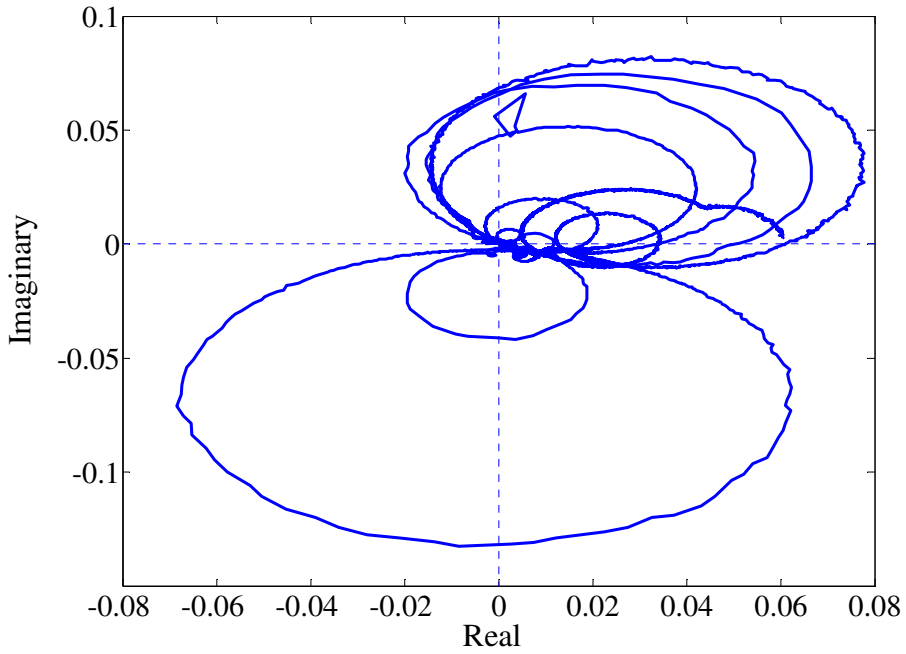

Figure 7.9 *Measured Nyquist plot of the open-loop frequency response of the absolute velocity plus acceleration feedback control system when* $\lambda = 0.01$ *and the corner frequency of the first order low-pass filter is 5 kHz.*

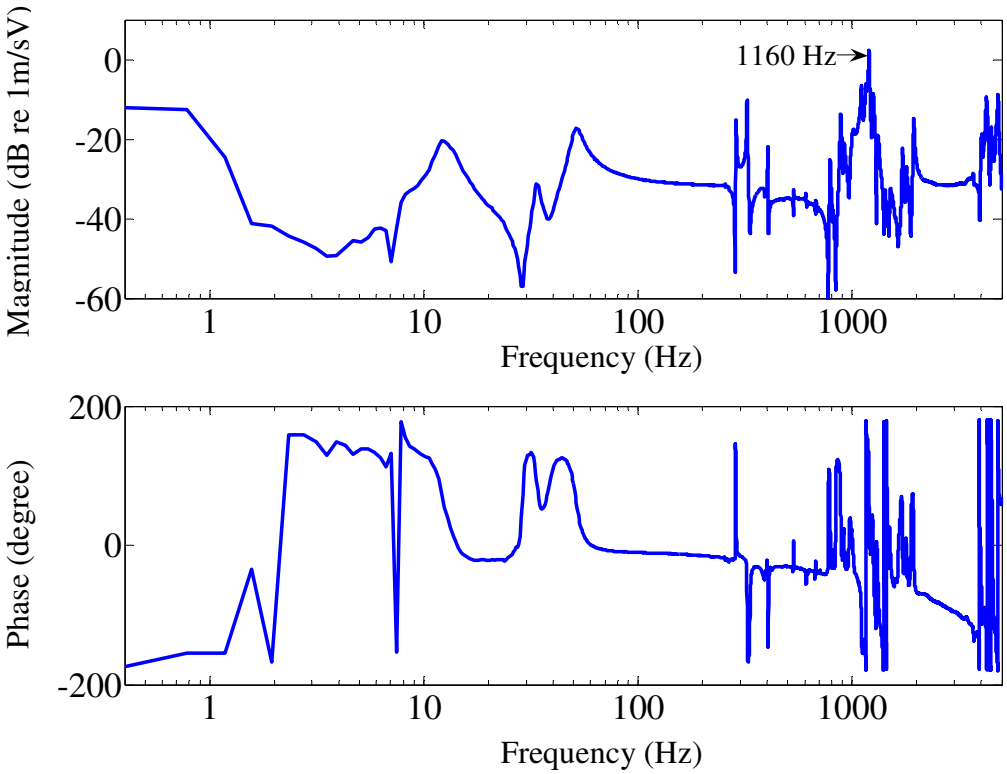

Figure 7.10 *Measured open-loop frequency response of the absolute velocity plus acceleration feedback control system up to 5 kHz when* $\lambda = 0.01$ *and the corner frequency of the first order low-pass filter is 5 kHz (solid line).*

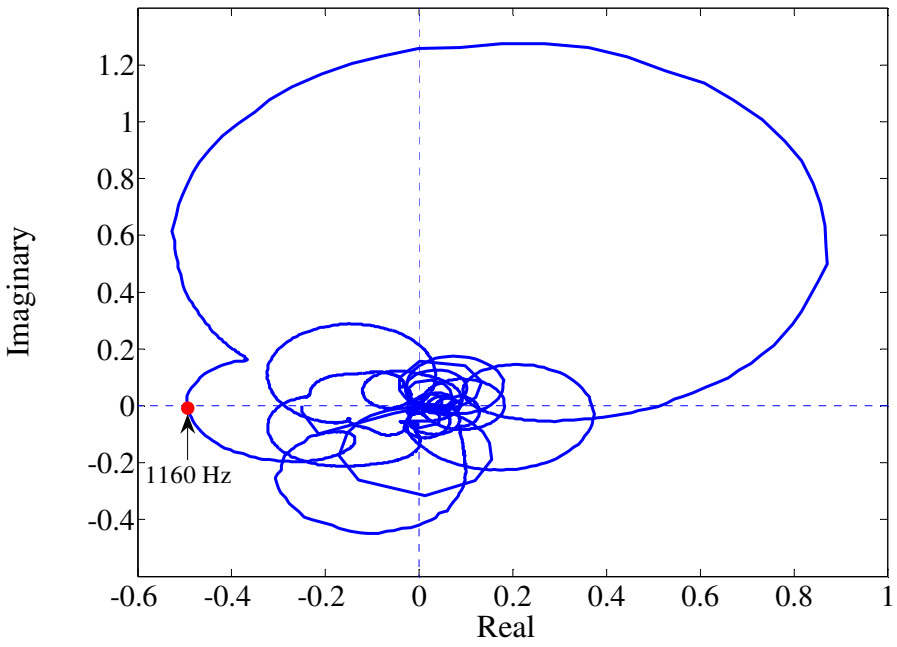

Figure 7.11 *Measured Nyquist plot of the open-loop frequency response of the absolute velocity plus acceleration feedback control system up to 5 kHz when* $\lambda = 0.01$ *and the corner frequency of the first order low-pass filter is 5 kHz (solid line).*

Chapter 8

Conclusions and Future Work

In this thesis, the active vibration isolation of a piece of delicate equipment mounted on a distributed parameter isolator has been investigated. This chapter summarizes the overall conclusions of the thesis and the recommendations for future work.

8.1 Conclusions

In traditional vibration isolation theory, vibration isolators are usually considered as simple lumped parameter elements, e.g. elastic springs and viscous dampers, which are assumed to be massless for the purpose of modelling. However, this simplification is only valid at frequencies low enough that the wavelength in the isolator is long compared to its dimension. At higher frequencies, realistic isolators, which have distributed mass, stiffness and damping, do not behave like the idealized massless models. The dynamics introduced by these distributed parameter elements inherent in the isolator are associated with the internal resonance behaviour of the isolator. The presence and significance of IRs in realistic isolators has been identified by many researchers. The degradation in performance due to the IRs in vibration isolation is especially important for lightly damped metallic isolators.

For a better description of the dynamic behaviour of vibration isolators, different

idealised distributed parameter models under various types of deformation have been investigated. These distributed parameter models for realistic isolator have been categorized into two types for the purpose of dynamic analysis, namely a non-dispersive isolator and a dispersive isolator. It has been shown that the isolation performance is significantly affected by the IRs in both isolator types. Simple expressions which describe the behaviour for distributed parameter isolators have been derived. The parameters which control the isolator performance at various frequencies have been clarified. The damping in the isolator, the ratio of the isolator mass (or polar moment of inertia) to the equipment mass (or polar moment of inertia) and the system fundamental resonance frequency are all crucial to the isolation performance. This offers basic guidelines for the isolation design of a distributed parameter isolator, which directs effective ways to improve the isolator performance. Also, it is concluded that, in general for the examples considered, the IR effects in the non-dispersive isolator on the isolation performance are more significant than that for the dispersive isolator. The experiment on a helical spring has supported and validated the theoretical analysis and predictions.

Stability and control performance are two crucial issues in active vibration isolation systems, since they may limit the application of active vibration isolation in practice. The effects of IRs in the distributed parameter isolator on the stability and control performance for commonly used control strategies in active vibration isolation have been investigated. The AVF control system containing a distributed parameter isolator is only conditionally stable if the base of the system has its own resonance behaviour. A stability condition in terms of the modal amplitudes evaluated at the equipment and base for such an AVF control system has been proposed. This stability condition means that if the displacement of the base is greater than the displacement of the equipment and these two displacements are in phase at a resonance frequency, the AVF control system may become unstable. The RVF control system containing a distributed parameter isolator is always unconditionally stable, which is its main advantage, although its control performance is much worse than AVF control. The IFF control system containing a distributed parameter isolator may become unstable even if the base is rigid while the

equipment is stiffness controlled. However, if the equipment is a rigid mass, IFF control is equivalent to AVF control. The PPF and APF control systems containing a distributed parameter isolator on a flexible base are also only conditionally stable. All these control strategies can introduce active damping into the system, and are thus effective in attenuating the system fundamental resonance peak. However, the IR peaks in the distributed parameter isolator cannot be attenuated by these control strategies because the equipment mass dominates the response at high frequencies. Based on this knowledge, acceleration feedback control has been applied to suppress the IR peaks, because it is equivalent to adding a mass electronically onto the equipment. However, as a compromise, the system fundamental resonance peak moves to a lower frequency and cannot be reduced by acceleration feedback control. The study for optimal control has shown that, to minimise the mean square velocity of the equipment mass, AVF control is the optimal solution. The theoretical results for the effects of IRs on the stability and control performance of AVF control system have been validated experimentally on a four-spring active vibration isolation system.

Different approaches to stabilize the AVF control system have been investigated theoretically and experimentally based on the proposed stability condition. It has been validated experimentally that adding more damping into the isolator, adding more mass to the base, and introducing a lead compensator are all effective in stabilizing the AVF control system. An additional SDOF mechanical mass-spring-damper system has also been introduced to attach onto the base structure to effectively stabilize the AVF control system.

Because the commonly used control strategies in active vibration isolation cannot suppress the IRs in the distributed parameter isolator due to the dominant effect of the equipment mass at high frequencies, various approaches have been investigated based on the understanding of the characteristics of IRs in the distributed parameter isolator. AVF control with more damping in the isolator has been investigated theoretically and experimentally. It was shown to be a simple and straightforward method to attenuate the

IR peaks. However, in practice due to the increase in the static stiffness of the isolator caused by the high damping materials applied in parallel with the isolator, the isolation performance at frequencies greater than the system fundamental resonance frequency is degraded. Based on the knowledge that the mass dominates the response of the equipment at high frequencies, absolute velocity plus acceleration feedback control has been investigated, which was shown to be effective in suppressing the IR peaks. Furthermore, for the system on a flexible base, the absolute velocity plus acceleration feedback controller can be carefully designed to make the control system unconditionally stable. However, such a controller is sensitive to the unmodelled dynamics of the system at high frequencies, which may destabilize the control system and has been validated experimentally. AVF control on a fraction of the isolator length has also been investigated theoretically. It was shown that the IR peaks can be effectively attenuated by AVF control on the lower part of the isolator. It has been concluded that the longer the fraction of the isolator length controlled by AVF control, the better the control performance around the system fundamental resonance frequency. Also the ratio of the controlled length to the entire length of the isolator should be an irrational number in order to suppress all of the IR peaks. Otherwise, at some frequencies the control point in the isolator corresponds to a node in a particular mode. However, the practical limitation in implementing this control method is to generate an active control force in parallel with a fraction of the isolator without changing the dynamics at the control point.

Overall, this thesis has presented an investigation on the active vibration isolation of a piece of delicate equipment mounted on a distributed parameter isolator. The characteristics of a distributed parameter isolator have been clarified. The effects of IRs in the distributed parameter isolator on the control performance and stability of several control strategies have been determined. Different novel strategies to attenuate IRs and improve the isolation performance of the distributed parameter isolator over a broad range of frequencies have been proposed.

8.2 Recommendations for further work

The research presented in this thesis has improved the understanding of the characteristics and effects of a distributed parameter isolator in isolating a piece of delicate equipment. This study has also highlighted several issues discussed below which are thought to be worth of further study:

i. In this thesis, only one distributed parameter isolator is applied to isolate the delicate equipment from the base disturbance in the longitudinal direction. Any rotational effects are neglected. However, in practice, more isolators may be used in active vibration isolation. Therefore, the active vibration isolation systems containing two or more distributed parameter isolators should be investigated in future work.
ii. Although the equipment and base dynamics have been considered in the stability analysis for active vibration isolation systems containing a distributed parameter isolator, the equipment and base have been respectively simplified as a rigid mass or a rigid mass on a complex spring in the analysis of control performance. In future research, more complex combinations of the equipment and base dynamics should be considered.
iii. In the experimental results, the unmodelled modes in the equipment and the base have been demonstrated to be potential dangers to stability of the control system other than the IRs in the isolator. Although several approaches proposed in the thesis can eliminate these instabilities, further research could be carried out on this issue.
iv. In attenuating the IRs in the isolator, although absolute velocity plus acceleration feedback control and AVF control on a fraction of the isolator length are effective theoretically, there are limitations in implementing these control strategies in practice. Further efforts should be expended on this issue.

References

1. Harris, C.M., 2002, Introduction to the handbook, Chapter 1 in *Shock and Vibration Handbook*, ed. Harris, C.M. and Piersol, A.G., 5th Edition, McGraw Hill, New York.
2. Mead, D.J., 1999, *Passive Vibration Control*, John Wiley & Sons, Chichester.
3. Franchek, M.A., Ryan, M.W. and Bernhard, R.J., 1994, Adaptive passive vibration control, *Journal of Sound and Vibration*, **189**(5), 565-585.
4. Inman, D.J., 1994, *Engineering Vibration*, Prentice-Hall, Englewood Cliffs, New Jersey.
5. Jalili, N., 2002, A Comparative Study and Analysis of Semi-Active Vibration-Control Systems, *Transactions of the American Society of Mechanical Engineers, Journal of Vibration and Acoustics*, **124**(4), 593-605.
6. Fuller, C.R., Elliott, S.J. and Nelson, P.A., 1996, *Active Control of Vibration*, Academic Press, New York.
7. Liu, Y., Waters, T.P. and Brennan, M.J., 2003, A comparison of semi-active damping control strategies for vibration isolation of harmonic disturbances, *Journal of Sound and Vibration*, **280**, 21-39.
8. Preumont, A., 2002, *Vibration Control of Active Structures*, 2nd Edition, Kluwer Academic Publishers, Dordrecht.
9. Karnopp, D.C., Crosby, M.J. and Harwood, R.A., 1974, Vibration control using semi-active force generators, *Transactions of the American Society of Mechanical Engineers, Journal of Engineering for Industry*, **96**(2), 619–626.
10. Benassi, L., 2004, *Feedback control of vibration with inertial actuators*, PhD Thesis, ISVR, University of Southampton.
11. Karnopp, D.C., 1995, Active and semi-active vibration isolation, *Transactions of the American Society of Mechanical Engineers, Journal of Mechanical Design*, **177**, 177-185.
12. Brennan, M.J. and Ferguson, N.S., 2004, Vibration control, Chapter 12 in

Advanced Applications in Acoustics, Noise and Vibration, ed. Fahy, F.J. and Walker, J.G., E&FN SPON, London.

13. Ungar, E.E. and Dietrich, C.W., 1966, High-frequency vibration isolation, *Journal of Sound and Vibration*, **4**, 224-241.
14. Crede, C.E. and Ruzicka, J.E., 2002, Theory of vibration isolation, Chapter 30 in *Shock and Vibration Handbook*, ed. Harris, C.M. and Piersol, A.G., 5th Edition, McGraw Hill, New York. .
15. Ananthaganeshan, K.A., 2002, *Stability and performance of active vibration isolation systems*, PhD thesis, ISVR, University of Southampton.
16. Thomson, W.T., 1993, *Theory of Vibration with Applications*, Prentice Hall.
17. Beranek, L.L., 1971, *Noise and Vibration Control*, McGraw-Hill, New York.
18. Bies, D.A. and Hansen, C.H., 1988, *Engineering Noise Control: Theory and Practice*, Unwin Hyman, London.
19. Rao, S.S., 1984, *Mechanical Vibrations*, Addison-Wesley, Reading, Massachusetts.
20. Harrison, M., Sykes, A.O. and Martin, M., 1952, Wave effects in isolation mounts, *Journal of the Acoustical Society of America*, **24**, 62-71.
21. Snowdon, J.C., 1979, Vibration isolation: use and characterization, *Journal of the Acoustical Society of America*, **66**, 1245-1274.
22. Lalor, N., 1998, Fundamentals of vibration, Chapter 2 in *Fundamentals of Noise and Vibration*, ed. Fahy, F.J. and Walker, J.G., E&FN SPON, London.
23. Spanos, J.T., Rahman, Z.H. and Von Flotow, A.H., 1993, Active vibration isolation on an experimental flexible structure, *Proceedings of SPIE, Smart Structures and Materials 1993: Smart Structures and Intelligent Systems*, Albuquerque, USA, 674-680
24. Vaillon, L., Petitjean, B., Frapard, B. and Lebihan, D., 1999, Active isolation in space truss structures: from concept to implementation, *Smart Materials and Structures*, **8**, 781-790.
25. Kaplow, C.F. and Velman, J.R., 1980, Application of an Active local vibration isolation concept to a flexible space telescope, *Journal of Guidance and Control*,

3(3), 227-233.

26. Schulz, G., 1979, Active multivariable vibration isolation for a helicopter, *Automatica*, **15**(4), 461-466.
27. Pearson, J.T., Gooddall, R.M. and Lyndon, I., 1994, Active control of helicopter vibration, *Computing and Control Engineering Journal*, **5**(6), 277-284.
28. Sutton, T.J., Elliott, S.J., M. J. Brennan, Heron, K.H. and Jessop, D.A.C., 1997, Active isolation of multiple structural waves on a helicopter gearbox support strut, *Journal of Sound and Vibration*, **205**(1), 81-101.
29. Elbeheiry, E.M. and Karnopp, D.C., 1996, Optimal control of vehicle random vibration with constrained suspension deflection, *Journal of Sound and Vibration*, **189**(5), 547-564.
30. Yoshimura, T., Nakaminami, K., Kurimoto, M. and Hino, J., 1999, Active suspension of passenger cars using linear and fuzzy-logic controls, *Control Engineering Practice*, **7**, 41-47.
31. Yu, Y., Naganathan, N.G. and Dukkipati, R.V., 2001, A literature review of automotive vehicle engine mounting systems, *Mechanism and Machine Theory*, **36**, 123-142.
32. Olsson, C., 2006, Active automotive engine vibration isolation using feedback control, *Journal of Sound and Vibration*, **294**, 162-176.
33. Hillis, A.J., Harrison, A.J.L. and Stoten, D.P., 2005, A comparison of two adaptive algorithms for the control of active engine mounts, *Journal of Sound and Vibration*, **286**, 37-54.
34. Karnopp, D.C., 1983, Active damping in road vehicle suspension systems, *Vehicle System Dynamics*, **12**, 291-316.
35. Winberg, M., Crolla, D.A. and Plummer, A.R., 1999, Active vibration isolation in ships: An ASAC (active structure acoustic control) approach, *Proceedings of Active 99: The International Symposium on Active Control of Sound and Vibration*, Fort Lauderdale, USA
36. Daley, S., Johnson, F.A., Pearson, J.B. and Dixon, R., 2004, Active vibration control for marine applications, *Control Engineering Practice*, **12**, 465-474.

37. Jalihal, P. and Utku, S., 1998, Active control in passively base isolated buildings subjected to low power excitations, *Computers & Structures*, **66**(2-3), 211-224.

38. Loh, C.H. and Ma, M.J., 1996, Control of seismically excited building structures using variable damper systems, *Engineering Structures*, **18**(4), 279-287.

39. Loh, C.H. and Chao, C.H., 1996, Effectiveness of active tuned mass damper and seismic isolation on vibration control of multi-storey building, *Journal of Sound and Vibration*, **193**(4), 773-792.

40. Balas, M.J., 1979, Direct velocity feedback control of large space structures, *Journal of Guidance and Control*, **2**(3), 252-253.

41. Elliott, S.J., Benassi, L., Brennan, M.J., Gardonio, P. and Huang, X., 2004, Mobility analysis of active isolation systems, *Journal of Sound and Vibration*, **271**, 297-321.

42. Elliott, S.J., Serrand, M. and Gardonio, P., 2001, Feedback stability limits for active isolation systems with reactive and inertial actuators, *Transactions of the American Society of Mechanical Engineers, Journal of Vibration and Acoustics*, **123**, 250-261.

43. Brennan, M.J., Ananthaganeshan, K.A. and Elliott, S.J., 2007, Instabilities due to instrumentation phase-lead and phase-lag in the feedback control of a simple vibrating system, *Journal of Sound and Vibration*, **304**, 466-478.

44. Hansen, C.H. and Snyder, S.C., 1997, *Active Control of Noise and Vibration*, 2nd Edition, E&FN SPON, London.

45. Brennan, M.J. and Kim, S.M., 2001, Feedforward and feedback control of sound and vibration-A Wiener filter approach, *Journal of Sound and Vibration*, **246**(2), 281-296.

46. Serrand, M. and Elliott, S.J., 2000, Multichannel feedback control for the isolation of base-excited vibration, *Journal of Sound and Vibration*, **234**(4), 681-704.

47. Serrand, M., 2000, *Direct velocity feedback control of equipment vibration*, MPhil Thesis, ISVR, University of Southampton.

48. Meirovitch, L., 1990, *Dynamics and Control of Structures*, Wiley, New York.

49. Benassi, L. and Elliott, S.J., 2004, Active vibration isolation using an inertial actuator with local displacement feedback control, *Journal of Sound and Vibration*, **278**(4-5), 705-724.

50. Benassi, L., Elliott, S.J. and Gardonio, P., 2004, Active vibration isolation using an inertial actuator with local force feedback control, *Journal of Sound and Vibration*, **276**(1-2), 157-179.

51. Preumont, A., Francois, A., Bossens, F. and Abu-Hanieh, A., 2002, Force feedback versus acceleration feedback in active vibration isolation, *Journal of Sound and Vibration*, **257**(4), 605-613.

52. Kim, S.M., Elliott, S.J. and Brennan, M.J., 2001, Decentralized control for multichannel active vibration isolation, *IEEE Transactions on control systems technology*, **9**(1), 93-100.

53. Huang, X., Elliott, S.J. and Brennan, M.J., 2003, Active isolation of a flexible structure from base vibration, *Journal of Sound and Vibration*, **263**, 357-376.

54. Joshi, S.M., 1986, Robustness properties of collocated controllers for flexible spacecraft, *Journal of Guidance and Control*, **9**, 85-91.

55. Sciulli, D. and Inman, D.J., 1998, Isolation design for a flexible system, *Journal of Sound and Vibration*, **216**(2), 251-267.

56. Ungar, E.E., 1963, Wave effects in viscoelastic leaf and compression spring mounts, *Transactions of the American Society of Mechanical Engineers, Journal of Engineering for Industry*, **85**, 243-246.

57. Sykes, A.O., 1960, Isolation of vibration when machine and foundation are resilient and when wave effects occur in the mount, *Noise Control*, **6**(3), 115-130.

58. Love, A.E.H., 1944, *A Treatise on the Mathematical Theory of Elasticity*, Dover, New York.

59. Snowdon, J.C., 1968, *Vibration and Shock in Damped Mechanical Systems*, Wiley, New York.

60. Sorensen, A., 1960, A discussion of the vibration characteristics of a simple mechanical connection, *Transactions of the American Society of Mechanical*

Engineers, Journal of Engineering for Industry, **82**, 415-422.

61. Snowdon, J.C., 1965, Rubberlike materials, their internal damping and role in vibration isolation, *Journal of Sound and Vibration*, **2**, 175-193.
62. Du, Y., Burdisso, R.A., Nikolaidis, E. and Tiwari, D., 2003, Effects of isolators internal resonances on force transmissibility and radiated noise, *Journal of Sound and Vibration*, **268**, 751-778.
63. Tomlinson, G.R., 1982, Vibration isolation in the low and high frequency range, *Proceedings of Dynamic Vibration and Absorption Conference*, Southampton, UK, Mechanical Engineering Publication LTD, Edmunds, 21-29.
64. Lee, J. and Thomson, D.J., 2001, Dynamic stiffness formulation, free vibration and wave motion of helical springs, *Journal of Sound and Vibration*, **239**, 297-320.
65. Warring, R.H., 1972, *Handbook of Noise and Vibration Control*, 2nd Edition, Trade and Technical Press LTD, Morden, Surrey, England.
66. Snowdon, J.C., 1962, Isolation from vibration with a mounting utilizing low- and high-damping rubberlike materials, *Journal of the Acoustical Society of America*, **34**(1), 54-61.
67. Du, Y., Burdisso, R.A., Nikolaidis, E. and Tiwari, D., 2005, Control of internal resonances in vibration isolators using passive and hybrid dynamic vibration absorbers, *Journal of Sound and Vibration*, **286**, 697-727.
68. Snowdon, J.C., 1975, Compound mounting systems that incorporate dynamic vibration absorbers, *Transactions of the American Society of Mechanical Engineers, Journal of Engineering for Industry*, November, 1204-1211.
69. Lalanne, M., Berthier, P. and Hagopian, J.D., 1983, *Mechanical Vibrations for Engineers*, John Wiley & Sons, Chichester.
70. Santen, G.W.V., 1958, *Mechanical Vibration*, Cleaver-Hume Press, London.
71. Collins, S.A. and von Flotow, A.H., 1991, Active isolation for spacecraft, *Proceedings of the 42nd Congress of the International Astronautical Federation*, Montreal, Canada
72. Yan, B., Brennan, M.J., Elliott, S.J. and Ferguson, N.S., 2006, *Velocity feedback*

control of vibration isolation systems, Technical Memorandum No. 962, ISVR, University of Southampton

73. Yan, B., Brennan, M.J., Elliott, S.J. and Ferguson, N.S., 2006, Velocity feedback control of vibration isolation systems containing a distributed parameter isolator, *Proceedings of the 9th International Conference on Recent Advances in Structural Dynamics*, Southampton, UK, Paper 68, CD-ROM.
74. Ogata, K., 1990, *Modern Control Engineering*, Prentice Hall, Englewood Cliffs, New Jersey.
75. Dutton, K., Thompson, S. and Barraclough, B., 1997, *The Art of Control Engineering*, Addison-Wesley, Harlow, Essex.
76. Franklin, G.F., Powell, J.D. and Emami-Naeini, A., 1994, *Feedback Control of Dynamic Systems*, 3rd Edition, Addison Wesley, Reading, Massachusetts.
77. Friswell, M.I. and Inman, D.J., 1999, The relationship between positive position feedback and output feedback controllers, *Smart Materials and Structures*, **8**, 285-291.
78. Goh, C.J. and Caughey, T.K., 1985, On the stability problem caused by finite actuator dynamics in the control of large space structures, *International Journal of Control*, **41**(3), 787-802.
79. Poh, A. and Baz, A., 1990, Active control of a flexible structure using a modal positive position feedback controller, *Journal of Intelligent Material Systems and Structures*, **1**, 273-288.
80. Fanson, J.L. and Caughey, T.K., 1990, Positive position feedback for large space structures, *American Institute of Aeronautics and Astronautics Journal*, **28**(4), 717-724.
81. Kwak, M.K. and Heo, S., 2007, Active vibration control of smart grid structure by multiinput and multioutput positive position feedback controller, *Journal of Sound and Vibration*, **304**, 230-245.
82. Kim, S.M., Pietrzko, S. and Brennan, M.J., 2007 Active vibration isolation using an electrical damper or an electrical dynamic absorber, *IEEE Transactions on Control Systems Technology*, In Press.

83. DeJong, R.G., 2002, Statistical methods for analyzing vibration systems, Chapter 11 in *Shock and Vibration Handbook*, ed. Harris, C.M. and Piersol, A.G., 5th Edition, McGraw Hill, New York. .

84. Gardonio, P. and Brennan, M.J., 2004, Mobility and impedance methods in structural dynamics, Chapter 9 in *Advanced Applications in Acoustics, Noise and vibration*, ed. Fahy, F.J. and Walker, J.G., E&FN SPON, London.

85. Bishop, R.E.D. and Johnson, D.C., 1960, *The Mechanics of Vibration*, Cambridge University Press.

86. Rafezy, B. and Howson, W.P., 2006, Exact natural frequencies of a three-dimensional shear-torsion beam with doubly asymmetric cross-section using a two-dimensional approach*, Journal of Sound and Vibration*, **295**, 1044-1059.

87. Hixson, E.L., 2002, Mechanical impedance, Chapter 10 in *Shock and Vibration Handbook*, ed. Harris, C.M. and Piersol, A.G., 5th Edition, McGraw Hill, New York. .

88. Stokey, W.F., 2002, Vibration of systems having distributed mass and elasticity, Chapter 7 in *Shock and Vibration Handbook*, ed. Harris, C.M. and Piersol, A.G., 5th Edition, McGraw Hill, New York.

89. Holterman, J. and de Vries, T.J.A., 2005, Active damping based on decoupled collocated control*, IEEE Transactions on mechatronics*, **10**(2), 135-145.

90. von Flotow, A.H. and Vos, D.W., 1990, The need for passive damping in feedback controlled flexible structures, *Proceedings of the 61st Shock and Vibration Symposium*, Pasadena, CA, 593-603.

91. Loh, A.P., Cai, X. and Tan, W.W., 2004, Auto-tuning of phase lead/lag compensators*, Automatica*, **40**, 423-429.

92. Yan, B., Brennan, M.J., Elliott, S.J. and Ferguson, N.S., 2007, The effects of internal resonances in vibration isolators under absolute velocity feedback control, *Proceedings of the 19th International Congress on Acoustics*, Madrid, Spain, Paper SAV-03-009, CD-ROM.

93. Ren, M.Z., Seto, K. and Doi, F., 1997, Feedback structural-borne sound control

of a flexible plate with an electromagnetic actuator: the phase lag problem, *Journal of Sound and Vibration*, **205**, 57-80

94. Blevins, R.D., 1979, *Formulas for Natural Frequency and Mode Shape*, Robert E. Krieger Publishing Company, Malabar, Florida.

95. Helical springs, The University of Tennessee at Martin, School of Engineering, http://www.utm.edu/departments/engin/lemaster/Machine%20Design/Notes%2035.pdf

96. Solecki, R. and Conant, R.J., 2003, *Advanced mechanics of materials*, Oxford University Press, New York.

Appendix A

Impedance Matrices for Distributed Parameter Isolators

As discussed in Chapter 3, various types of realistic isolator can be modelled as different idealised configurations under various types of deformation. These distributed parameter models for realistic isolator can be categorized into two types for the purpose of dynamic analysis. One type can be modelled using a second order differential equation, and is called a non-dispersive isolator, in which the wave speed is independent of frequency. The other type can be modelled using a fourth or higher order differential equation, and is called a dispersive isolator, in which the wave speed is dependent on frequency. In this appendix, the impedance matrices for these two types of distributed parameter isolator are derived.

A.1 Impedance matrix for a non-dispersive isolator

In Figure A.1, the distributed parameter isolator is modelled as a finite elastic rod under longitudinal vibration (Figure A.1(a)) or torsional vibration (Figure A.1(b)), or a beam under lateral vibration (Figure A.1(c)), respectively. The rod in Figure A.1(a, b) can be categorized as a non-dispersive isolator. The beam in Figure A.1(c) can also be categorized as a non-dispersive isolator if it is represented as a shear beam. Q_1 and Q_2 are the forces shown in Figure A.1(a) and (c), or moments shown in Figure A.1(b)

applied to each end of the isolator. $u(0)$ and $u(L)$ are displacements shown in Figure A.1(a) and (c), or angles shown in Figure A.1(b) at each end of the isolators, respectively.

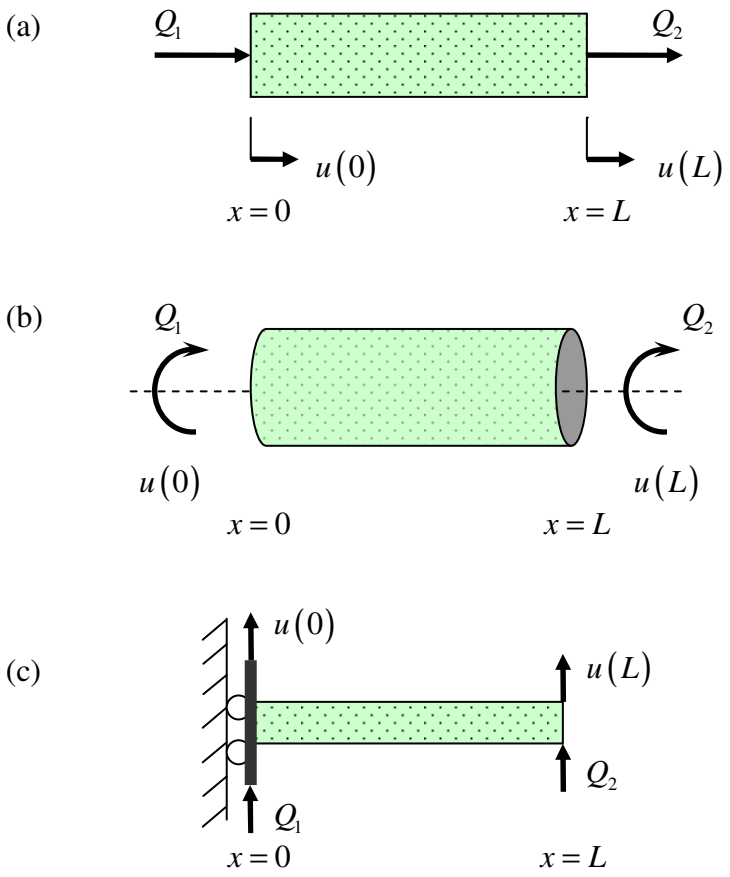

Figure A.1 *Schematic diagrams of a distributed parameter isolator undergoing (a) longitudinal, (b) torsional or (c) lateral vibration, where* Q_1 *and* Q_2 *are forces in (a) and (c), or moment in (b) applied to each end of the isolator, respectively; and* $u(0)$ *and* $u(L)$ *are displacements in (a) and (c), or angles in (b) at each end of the isolator, respectively*

The general equation of motion for the non-dispersive isolator is given by [19]

$$c_i^2 \frac{\partial^2 u(x,t)}{\partial^2 x} = \frac{\partial^2 u(x,t)}{\partial^2 t} \tag{A.1}$$

where c_i is the complex wave speed in the distributed parameter isolator. For the finite rod undergoing longitudinal vibration shown in Figure A.1(a), $c_i = c_l = \sqrt{E^*/\rho}$, where

E^* is the complex Young's modulus of elasticity and ρ is the density. For the finite rod undergoing torsional vibration shown in Figure (b) and the shear beam undergoing lateral vibration shown in Figure A.1(c), $c_i = c_s = \sqrt{G^*/\rho}$, where G^* is the complex shear modulus.

Equation (A.1) has a solution to harmonic excitation, consisting of negative going and positive going waves, which can be written as [19]

$$u(x,t) = u(x)e^{j\omega t} = \left(Ae^{jk^*x} + Be^{-jk^*x}\right)e^{j\omega t} \tag{A.2}$$

where *A* and *B* are complex wave amplitudes that depend on the boundary conditions, and *x* is the distance along the isolator. For the finite rod undergoing longitudinal vibration shown in Figure A.1(a), $k^* = k_l^* = \omega/c_l^* = \sqrt{\rho/E^*}\omega$ is the longitudinal wavenumber. For the finite rod undergoing torsional vibration shown in Figure A.1(b) and the shear beam undergoing lateral vibration shown in Figure A.1(c), $k^* = k_s^* = \omega/c_s^* = \sqrt{\rho/G^*}\omega$ is the shear wavenumber. In the following discussion, the complex harmonic ($e^{j\omega t}$) time dependence of the variables will be assumed but will be omitted for clarity.

The impedance matrix for the non-dispersive isolator can be calculated using the wave approach and the boundary conditions.

- Point impedance

The point impedances of a non-dispersive isolator at each end are equal due to symmetry, and are defined as [84]

$$Z_{11} = \left.\frac{Q_1}{\dot{u}(0)}\right|_{\dot{u}(L)=0},\ Z_{22} = \left.\frac{Q_2}{\dot{u}(L)}\right|_{\dot{u}(0)=0} \tag{A.3a,b}$$

At $x = 0$, due to Hooke's law which gives the stress-strain relationship, one has [84, 86]

$$\frac{\partial u(0)}{\partial x} = -\frac{Q_1}{\kappa} \tag{A.4}$$

where $\kappa = E^* S$ is the longitudinal rigidity for the finite rod undergoing longitudinal vibration shown in Figure A.1(a), in which S is the cross-sectional area of the isolator; $\kappa = G^* J_s$ is the torsional rigidity for the finite rod undergoing torsional vibration shown in Figure A.1(b) where J_s is the polar second moment of area of the isolator; or $\kappa = G^* S$ is the shear rigidity for the shear beam undergoing lateral vibration shown in Figure A.1(c).

At $x = L$, due to the definition of the point impedance given in equation (A.3a), one has

$$\dot{u}(L) = j\omega u(L) = 0 \tag{A.5}$$

Substituting equation (A.2) into (A.4) and (A.5) and letting $x = 0$ and $x = L$ respectively gives

$$A = -\frac{Q_1}{jk^*\kappa}\frac{1}{e^{2jk^*L}+1},\ B = \frac{Q_1}{jk^*\kappa}\frac{e^{2jk^*L}}{e^{2jk^*L}+1} \tag{A.6a,b}$$

Substituting equations (A.6a, b) into (A.2) and letting $x = 0$ gives

$$u(0) = \frac{Q_1}{jk^*\kappa}\frac{e^{2jk^*L}-1}{e^{2jk^*L}+1} = \frac{Q_1}{k^*\kappa}\tan\left(k^*L\right) \tag{A.7}$$

Differentiating equation (A.7) with respect to time and re-arranging gives

$$Z_{11} = \frac{Q_1}{\dot{u}(0)} = \frac{Q_1}{j\omega u(0)} = \frac{k^*\kappa}{j\omega\tan\left(k^*L\right)} \tag{A.8}$$

- Transfer impedance

The transfer impedances of a non-dispersive isolator at each end are equal due to reciprocity, and are defined as [84]

$$Z_{12} = \left.\frac{Q_1}{\dot{u}(L)}\right|_{\dot{u}(0)=0},\ Z_{21} = \left.\frac{Q_2}{\dot{u}(0)}\right|_{\dot{u}(L)=0} \tag{A.9a,b}$$

At $x=0$, equation (A.4) is still valid because of Hooke's law. Also due to the definition of the transfer impedance given by equation (A.9a), one has

$$\dot{u}(0)=j\omega u(0)=0 \tag{A.10}$$

Substituting (A.2) into (A.4) and (A.10) and letting $x=0$ gives

$$A=-\frac{Q_1}{2jk^*\kappa},\ B=\frac{Q_1}{2jk^*\kappa} \tag{A.11a,b}$$

Substituting (A.11a, b) into (A.2) and letting $x=L$ gives

$$u(L)=\frac{Q_1}{2jk^*\kappa}\left(e^{-jk^*L}-e^{jk^*L}\right)=-\frac{Q_1}{k^*\kappa}\sin\left(k^*L\right) \tag{A.12}$$

Differentiating equation (A.12) with respect to time and re-arranging gives

$$Z_{12}=\frac{Q_1}{\dot{u}(L)}=\frac{Q_1}{j\omega u(L)}=-\frac{k^*\kappa}{j\omega\sin(k^*L)} \tag{A.13}$$

Therefore, the impedance matrix for the non-dispersive isolator is given by

$$\mathbf{Z}=\begin{bmatrix}Z_{11} & Z_{12}\\ Z_{21} & Z_{22}\end{bmatrix}=\frac{k^*\kappa}{j\omega\sin(k^*L)}\begin{bmatrix}\cos\left(k^*L\right) & -1\\ -1 & \cos\left(k^*L\right)\end{bmatrix} \tag{A.14}$$

Substituting the appropriate k^* and κ into equation (A.14), the corresponding impedance matrix for the finite rod undergoing longitudinal vibration shown in Figure A.1(a) is given by

$$\mathbf{Z_L}=\begin{bmatrix}Z_{11} & Z_{12}\\ Z_{21} & Z_{22}\end{bmatrix}=\frac{S\sqrt{E^*\rho}}{j\sin\left(k_l^*L\right)}\begin{bmatrix}\cos\left(k_l^*L\right) & -1\\ -1 & \cos\left(k_l^*L\right)\end{bmatrix} \tag{A.15}$$

The corresponding impedance matrix for the finite rod undergoing torsional vibration shown in Figure A.1(b) is given by

$$\mathbf{Z_T}=\begin{bmatrix}Z_{11} & Z_{12}\\ Z_{21} & Z_{22}\end{bmatrix}=\frac{J_s\sqrt{G^*\rho}}{j\sin\left(k_s^*L\right)}\begin{bmatrix}\cos\left(k_s^*L\right) & -1\\ -1 & \cos\left(k_s^*L\right)\end{bmatrix} \tag{A.16}$$

And the corresponding impedance matrix for the shear beam undergoing lateral vibration shown in Figure A.1(c) is given by

$$\mathbf{Z_S}=\begin{bmatrix}Z_{11} & Z_{12}\\ Z_{21} & Z_{22}\end{bmatrix}=\frac{S\sqrt{G^*\rho}}{j\sin\left(k_s^*L\right)}\begin{bmatrix}\cos\left(k_s^*L\right) & -1\\ -1 & \cos\left(k_s^*L\right)\end{bmatrix} \tag{A.17}$$

A.2 Impedance matrix for a dispersive isolator

In Figure A.1(c), the distributed parameter isolator can be represented by an Euler-Bernoulli beam undergoing lateral vibration as an example of a dispersive isolator. One end of the isolator is sliding under external excitation. It is assumed that the other end of the isolator is excited by a force only (any moments at this end are assumed to be negligible). The equation of motion for such a dispersive isolator is given by

$$EI\frac{\partial^4 u(x,t)}{\partial^4 x}=\rho S\frac{\partial^2 u(x,t)}{\partial^2 t} \tag{A.18}$$

where I is the second moment of area about the neutral axis of the isolator. Equation (A.18) has a solution to harmonic excitation, which can be written as [19]

$$u(x,t)=u(x)e^{j\omega t}=\left(A\cosh\left(k_b^* x\right)+B\sinh\left(k_b^* x\right)+U\cos\left(k_b^* x\right)+V\sin\left(k_b^* x\right)\right)e^{j\omega t} \tag{A.19}$$

where A, B, U and V are complex wave amplitudes that depend on the boundary conditions and $k_b=\sqrt[4]{\rho S/E^* I}\sqrt{\omega}$ is the bending wavenumber. In the following discussion, the complex harmonic ($e^{j\omega t}$) time dependence of the variables will be assumed but will be again omitted for clarity. The impedance matrix for the dispersive isolator can be calculated by applying the boundary conditions.

- Point impedance Z_{11} at $x=0$

The point impedances Z_{11} at $x=0$ is defined by equation (A.3a). Due to the boundary conditions, one has, at $x=0$,

$$\frac{\partial u(0)}{\partial x}=0\ \left(\text{no rotation}\right) \tag{A.20}$$

and at $x=L$,

$$EI\frac{\partial^2 u(L)}{\partial x^2}=0\ \left(\text{no bending moment}\right) \tag{A.21}$$

Also at $x=0$, since the shear force equals to the applied force, one has

$$EI\frac{\partial^3 u(0)}{\partial x^3}=Q_1 \tag{A.22}$$

At $x = L$, due to the definition of the point impedance given by equation (A.3a), equation (A.5) is valid. Substituting equation (A.19) into (A.5) and (A.20-A.22) gives

$$A = -\frac{Q_1}{2E^* I k_b^{*3}} \frac{\sinh\left(k_b^* L\right)}{\cosh\left(k_b^* L\right)},\ U = \frac{Q_1}{2E^* I k_b^{*3}} \frac{\sin\left(k_b^* L\right)}{\cos\left(k_b^* L\right)} \tag{A.23a,b}$$

Substituting equations (A.23a, b) into (A.19) and letting $x = 0$ gives

$$u(0) = \frac{Q_1}{2E^* I k_b^{*3}} \frac{\sin\left(k_b^* L\right)\cosh\left(k_b^* L\right) - \cos\left(k_b^* L\right)\sinh\left(k_b^* L\right)}{\cos\left(k_b^* L\right)\cosh\left(k_b^* L\right)} \tag{A.24}$$

Differentiating equation (A.24) with respect to time and re-arranging gives

$$Z_{11} = \frac{Q_1}{\dot{u}(0)} = \frac{2E^* I k_b^{*3} \cos\left(k_b^* L\right)\cosh\left(k_b^* L\right)}{j\omega\left(\sin\left(k_b^* L\right)\cosh\left(k_b^* L\right) - \cos\left(k_b^* L\right)\sinh\left(k_b^* L\right)\right)} \tag{A.25}$$

- Point impedance Z_{22} at $x = L$

The point impedance Z_{22} at $x = L$ is defined by equation (A.3b). Due to the boundary conditions, equations (A.20) and (A.21) still hold. Also at $x = 0$, due to the definition of the point impedance given by equation (A.3b), equation (A.10) holds. At $x = L$, since the shear force equals to the applied force, one has

$$EI \frac{\partial^3 u(L)}{\partial x^3} = -Q_2 \tag{A.26}$$

Substituting equation (A.19) into (A.10), (A.20), (A.21), (A.26) gives

$$\begin{aligned} A = -U &= \frac{Q_2}{2E^* I k_b^{*3}} \frac{\sin\left(k_b^* L\right) + \sinh\left(k_b^* L\right)}{1 + \cos\left(k_b^* L\right)\cosh\left(k_b^* L\right)} \\ B = -V &= -\frac{Q_2}{2E^* I k_b^{*3}} \frac{\cos\left(k_b^* L\right) + \cosh\left(k_b^* L\right)}{1 + \cos\left(k_b^* L\right)\cosh\left(k_b^* L\right)} \end{aligned} \tag{A.27a,b}$$

Substituting equations (A.27a, b) into (A.19) and letting $x = L$ gives

$$u(L) = \frac{Q_2}{E^* I k_b^{*3}} \frac{\sin\left(k_b^* L\right)\cosh\left(k_b^* L\right) - \cos\left(k_b^* L\right)\sinh\left(k_b^* L\right)}{1 + \cos\left(k_b^* L\right)\cosh\left(k_b^* L\right)} \tag{A.28}$$

Differentiating equation (A.28) with respect to time and re-arranging gives

$$Z_{22} = \frac{Q_2}{\dot{u}(L)} = \frac{E^* I k_b^{*3}\left(1 + \cos\left(k_b^* L\right)\cosh\left(k_b^* L\right)\right)}{j\omega\left(\sin\left(k_b^* L\right)\cosh\left(k_b^* L\right) - \cos\left(k_b^* L\right)\sinh\left(k_b^* L\right)\right)} \tag{A.29}$$

- Transfer impedance

The transfer impedances of the dispersive isolator at each end are equal due to reciprocity, and are defined by equation (A.9). Due to the boundary conditions, equations (A.23) and (A.24) hold. At $x=0$, due to the definition of the transfer impedance given by equation (A.9a), and since the shear force equals to the applied force, equations (A.10) and (A.22) hold. Substituting equation (A.19) into (A.10) and (A.22-A.24), one can derive

$$A=-U=-\frac{Q_1}{2E^*Ik_b^{*3}}\frac{\sin\left(k_b^*L\right)+\sinh\left(k_b^*L\right)}{\cos\left(k_b^*L\right)+\cosh\left(k_b^*L\right)},\ B=-V=\frac{Q_1}{2E^*Ik_b^{*3}} \quad \text{(A.30a,b)}$$

Substituting equations (A.30a, b) into (A.19) and letting $x=L$ gives

$$u\left(L\right)=-\frac{Q_1}{E^*Ik_b^{*3}}\frac{\sin\left(k_b^*L\right)\cosh\left(k_b^*L\right)-\cos\left(k_b^*L\right)\sinh\left(k_b^*L\right)}{\cos\left(k_b^*L\right)+\cosh\left(k_b^*L\right)} \quad \text{(A.31)}$$

Differentiating equation (A.31) with respect to time and re-arranging gives

$$Z_{12}=\frac{Q_1}{\dot{u}\left(L\right)}=-\frac{E^*Ik_b^{*3}\left(\cos\left(k_b^*L\right)+\cosh\left(k_b^*L\right)\right)}{j\omega\left(\sin\left(k_b^*L\right)\cosh\left(k_b^*L\right)-\cos\left(k_b^*L\right)\sinh\left(k_b^*L\right)\right)} \quad \text{(A.32)}$$

Therefore, the impedance matrix for the dispersive isolator, if it is modelled as an Euler-Bernoulli beam undergoing lateral vibration shown in Figure A.1(c), is given by

$$\mathbf{Z_B}=\begin{bmatrix}Z_{11} & Z_{12}\\ Z_{21} & Z_{22}\end{bmatrix} \quad \text{(A.33)}$$

where

$$Z_{11}=\frac{2E^*Ik_b^{*3}\cos\left(k_b^*L\right)\cosh\left(k_b^*L\right)}{j\omega\left(\sin\left(k_b^*L\right)\cosh\left(k_b^*L\right)-\cos\left(k_b^*L\right)\sinh\left(k_b^*L\right)\right)}$$

$$Z_{22}=\frac{E^*Ik_b^{*3}\left(1+\cos\left(k_b^*L\right)\cosh\left(k_b^*L\right)\right)}{j\omega\left(\sin\left(k_b^*L\right)\cosh\left(k_b^*L\right)-\cos\left(k_b^*L\right)\sinh\left(k_b^*L\right)\right)} \quad \text{(A.34a,b,c)}$$

$$Z_{12}=Z_{21}=-\frac{E^*Ik_b^{*3}\left(\cos\left(k_b^*L\right)+\cosh\left(k_b^*L\right)\right)}{j\omega\left(\sin\left(k_b^*L\right)\cosh\left(k_b^*L\right)-\cos\left(k_b^*L\right)\sinh\left(k_b^*L\right)\right)}$$

Appendix B

Characteristics of a Helical Spring

In Chapter 3, an experiment on a helical spring was conducted to validate the characteristics of a non-dispersive isolator, because a helical spring can be modelled theoretically as an equivalent finite elastic rod under longitudinal vibration for simplicity. In this appendix, some characteristics of a helical spring, such as static stiffness and internal resonance frequencies, are derived.

B.1 Static stiffness

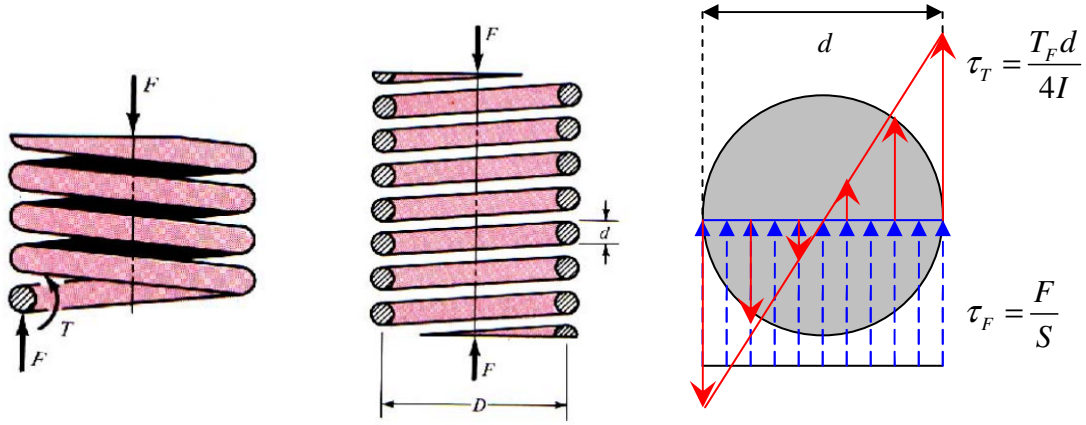

(a) (b) (c)

Figure B.1 *(a) schematic diagram of a helical spring under longitudinal excitation, (b) the cross section of the spring along its length and (c) the cross section of the spring wire, where F is the longitudinal force [95].*

The derivation of the static stiffness of a helical spring has been presented in [95]. The schematic diagram of a helical spring under longitudinal force *F* and the cross section along its length are respectively shown in Figures B.1 (a) and (b). The length, the diameter, the cross-section area and the second moment of area of the wire of the helical spring are denoted as *L*, *d*, *S*, and *I*, respectively. The mean diameter of the coil is denoted as *D*. As shown in Figure B.1 (c), the cross section of the spring wire is thus exposed to a shear force *F* and a torsion moment T_F, which is given by

$$T_F = \frac{FD}{2} \tag{B.1}$$

The stress from the shear force and the torsion moment in the helical spring are respectively given by

$$\tau_F = \frac{F}{S}, \quad \tau_T = \frac{T_F d}{4I} \tag{B.2a,b}$$

where

$$S = \frac{\pi}{4} d^2, \quad I = \frac{\pi}{64} d^4 \tag{B.3a,b}$$

Therefore, the energy generated by stress in the helical spring comes from two sources: shear force and torsion.

- Shear force strain energy

The shear force strain energy can be written as

$$U_F = \frac{1}{2} \int_{\text{vol}} \tau_F \cdot \varepsilon_F \cdot d\text{vol} \tag{B.4}$$

where

$$\varepsilon_F = \frac{\tau_F}{G} = \frac{F}{GS} \tag{B.5}$$

is the strain due to the shear force and *G* is the shear modulus. Substituting equations (B.2a) and (B.5) into (B.4), the strain energy due to the shear force is given by

$$U_F = \frac{1}{2} \int_{\text{vol}} \frac{F}{S} \cdot \frac{F}{GS} \cdot d\text{vol} = \frac{F^2}{2G} \int_L \int_S \frac{1}{S^2} dS \cdot dL = \frac{F^2 L}{2GS} \tag{B.6}$$

- Torsion strain energy

The torsion strain energy can be written as

$$U_T = \frac{1}{2}\int_{\text{vol}} \tau_T \cdot \varepsilon_T \cdot d\text{vol} \tag{B.7}$$

where

$$\varepsilon_T = \frac{\tau_T}{G} = \frac{T_F d}{4GI} \tag{B.8}$$

is the strain due to the torsion. Substituting equations (B.2b) and (B.8) into (B.7), the strain energy due to the torsion is given by

$$U_T = \frac{1}{2}\int_{\text{vol}} \frac{T_F d}{4I}\cdot\frac{T_F d}{4GI}\cdot d\text{vol} = \frac{T_F^2}{32GI^2}\int_L\int_S d^2 dS \cdot dL = \frac{T_F^2 L}{8\pi GI^2}\int_S SdS = \frac{T_F^2 L}{4GI} \tag{B.9}$$

Combining equations (B.1), (B.6) and (B.9), the total strain energy is given by

$$U_{total} = U_F + U_T = \frac{F^2 L}{2GS} + \frac{F^2 D^2 L}{16GI} \tag{B.10}$$

According to the Castigliano's theorem [96], the spring deflection due to longitudinal excitation F is given by

$$\Delta L = \frac{\partial U_{total}}{\partial F} = \frac{FL}{GS} + \frac{FD^2 L}{8GI} \tag{B.11}$$

The length of the spring wire is given by

$$L = n\pi D \tag{B.12}$$

where n is the number of active coils of the spring. Substituting equations (B.3a, b) and (B.12) into (B.11), the deflection can be written as

$$\Delta L = \frac{8nD^3 F}{Gd^4}\left(1 + \frac{d^2}{2D^2}\right) \approx \frac{8nD^3 F}{Gd^4} \tag{B.13}$$

Therefore, the static stiffness of the helical spring is given by

$$K_s = \frac{F}{\Delta L} = \frac{Gd^4}{8nD^3} \tag{B.14}$$

B.2 Internal resonances

To derive the expression for the internal resonance frequencies in a helical spring, an

analogy between a rod and a spring is assumed. The analogy works because both objects are continuously distributed elements, in that their stiffness and mass are spread uniformly throughout their interiors.

From the impedance matrix derived in Appendix A, it can be seen that the undamped natural frequencies in a fixed-fixed finite elastic rod occur when $\sin(k_l L) = 0$. Therefore, the internal resonances in the finite rod occur when

$$k_l L = n\pi \text{ (n=1, 2, 3...)} \tag{B.15}$$

Substituting the corresponding equation for the longitudinal wavenumber $k_l = \omega\sqrt{\rho/E}$ into (B.15), the internal resonance frequencies are thus given by:

$$\omega_l = \frac{n\pi}{L}\sqrt{\frac{E}{\rho}} = n\pi\sqrt{\frac{K_L}{m_i}} \text{ (in rad/s)} \tag{B.16}$$

where $K_L = ES/L$ is the static stiffness of the rod and $m_i = \rho SL$ is the mass of the rod.

By analogy, the internal resonance frequencies in a helical spring will have the same form as

$$\omega_s = n\pi\sqrt{\frac{K_s}{m_s}} \text{ (in rad/s)} \tag{B.17}$$

where K_s is the static stiffness of the helical spring given in equation (B.14) and

$$m_s = \frac{\pi^2 \rho N D d^2}{4} \tag{B.18}$$

is the mass of the helical spring.

Appendix C

Dynamic Analysis of a System Containing a Distributed Parameter Isolator

In this appendix, the equations describing the dynamics of the vibration isolation systems containing a distributed parameter isolator on a flexible base used in chapters 3, 4, and 6 are given. The input and transfer impedances of the system at the location of the equipment, the base and a point along the isolator are derived.

C.1 Impedances at the equipment and the base

Figure C.1 shows a vibration isolation system containing a distributed parameter isolator on a flexible base. The equipment, represented by its impedance Z_e is mounted on the base, represented by its impedance Z_b, through a distributed parameter isolator. The isolator is modelled as a finite elastic rod that has an impedance matrix $\mathbf{Z_L}$. The external forces f_e and f_b are applied to the equipment and the base respectively. $\dot{u}_e$ and $\dot{u}_b$ are the velocity of the equipment and the base, respectively. The dynamic behaviour of such a system can be described by

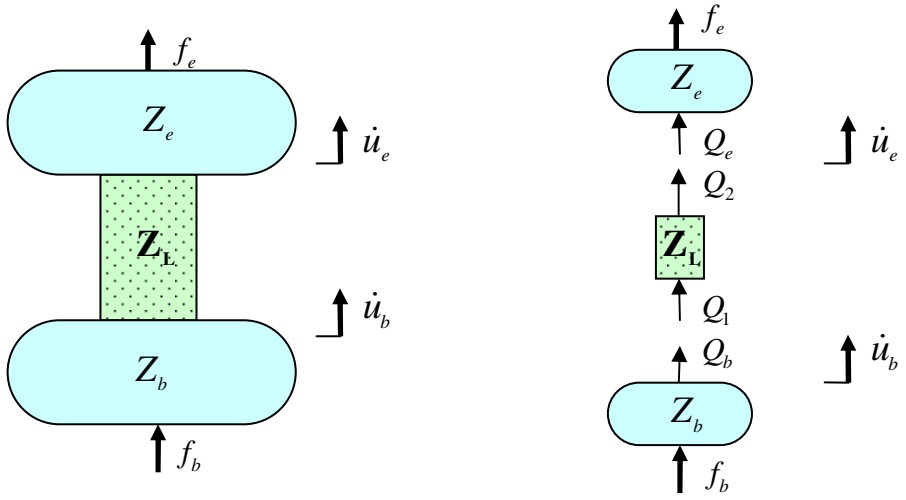

Figure C.1 *Schematic diagram of a vibration isolation system containing a distributed parameter isolator on a flexible base, where* $\dot{u}_e$ *and* $\dot{u}_b$ *are the velocity of the equipment and the base, respectively;* f_e *and* f_b *are the external forces applied to the equipment and the base, respectively;* Q_e, Q_1, Q_2 *and* Q_b *are internal forces;* Z_e *and* Z_b *are the input impedances of the equipment and the base, respectively; and* $\mathbf{Z_L}$ *is the impedance matrix for the isolator.*

$$\begin{aligned} Z_e\dot{u}_e &= f_e + Q_e = f_e - Q_2 \\ \begin{bmatrix} Q_1 \\ Q_2 \end{bmatrix} &= \mathbf{Z_L}\begin{bmatrix} \dot{u}_b \\ \dot{u}_e \end{bmatrix} = \begin{bmatrix} Z_{11} & Z_{12} \\ Z_{21} & Z_{22} \end{bmatrix}\begin{bmatrix} \dot{u}_b \\ \dot{u}_e \end{bmatrix} \\ Z_b\dot{u}_b &= f_b + Q_b = f_b - Q_1 \end{aligned} \qquad \text{(C.1a,b,c)}$$

where Q_e, Q_1, Q_2 and Q_b are internal forces. From equations (C.1a-c), the velocities of the equipment and the base are found to be

$$\begin{bmatrix} \dot{u}_e \\ \dot{u}_b \end{bmatrix} = \begin{bmatrix} Y_{ee} & Y_{eb} \\ Y_{be} & Y_{bb} \end{bmatrix}\begin{bmatrix} f_e \\ f_b \end{bmatrix} \qquad \text{(C.2)}$$

where

$$\begin{aligned} Y_{ee} &= \frac{Z_b + Z_{11}}{(Z_e + Z_{22})(Z_b + Z_{11}) - Z_{12}Z_{21}} \\ Y_{eb} = Y_{be} &= \frac{-Z_{21}}{(Z_e + Z_{22})(Z_b + Z_{11}) - Z_{12}Z_{21}} \\ Y_{bb} &= \frac{Z_e + Z_{22}}{(Z_e + Z_{22})(Z_b + Z_{11}) - Z_{12}Z_{21}} \end{aligned} \qquad \text{(C.3a,b,c)}$$

For the system shown in Figure 3.8 in Chapter 3, there is no external force applied to the equipment, i.e. $f_e = 0$, and the external force applied to the base is the primary force f, i.e. $f_b = f$. Based on the above discussion, the velocity of the equipment is thus given by

$$\dot{u}_e = Y_{eb} f \tag{C.4}$$

For the system shown in Figure 4.16 in Chapter 4, the external force applied to the equipment is the active control force f_a, i.e. $f_e = f_a$, and the external force applied to the base is the primary force f and the active control force $-f_a$, i.e. $f_b = f - f_a$. The velocity of the equipment is thus given by

$$\dot{u}_e = Y_{ee} f_a + Y_{eb}\left(f - f_a\right) = \left(Y_{ee} - Y_{eb}\right) f_a + Y_{eb} f \tag{C.5}$$

C.2 Impedances at a point along the isolator

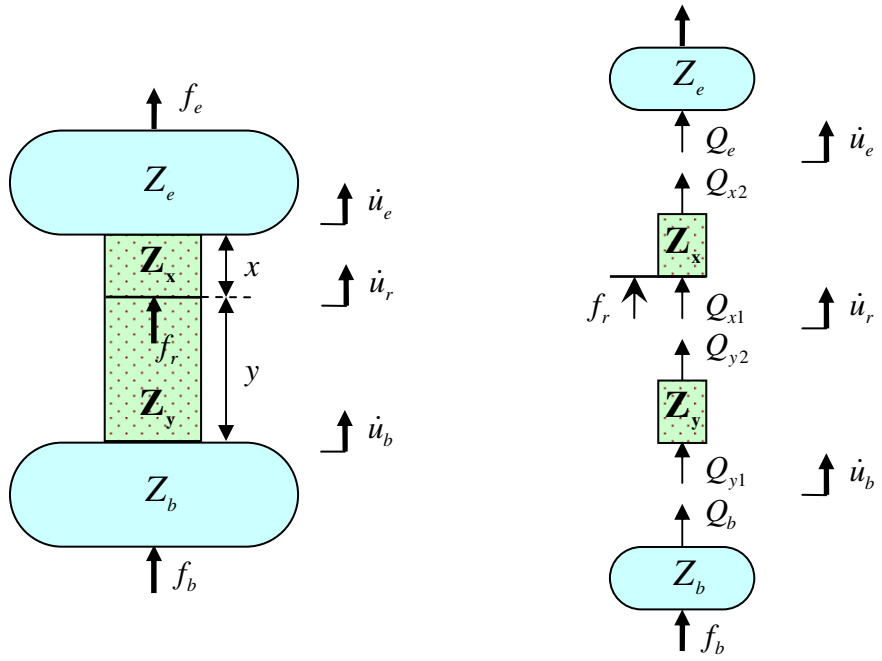

Figure C.2 *Schematic diagram of a vibration isolation system containing a distributed parameter isolator on a flexible base, where* f_r *is the external force applied at a point along the isolator;* $\mathbf{Z}_x$ *and* $\mathbf{Z}_y$ *are the impedance matrix for the upper and lower part of the isolator, respectively;* Q_{x1}, Q_{x2}, Q_{y1} *and* Q_{y2} *are internal forces; and* $\dot{u}_r$ *is the velocity of the point along the isolator.*

Figure C.2 shows a vibration isolation system containing a distributed parameter isolator on a flexible base, in which an external force f_r is applied at a point along the isolator. The external forces f_e and f_b are still applied to the equipment and base respectively. The isolator is also modelled as a finite elastic rod. The impedance matrix of the upper part of the isolator above the point where the external force applied is represented by $\mathbf{Z_x}$ and that of the lower part is represented by $\mathbf{Z_y}$. $\dot{u}_r$ is the velocity of the point along the isolator where the force f_r applied. The dynamics of such a system can be described by

$$
\begin{aligned}
&Z_e\dot{u}_e = f_e + Q_e = f_e - Q_{x2} \\
&\begin{bmatrix} Q_{x1} + f_r \\ Q_{x2} \end{bmatrix} = \mathbf{Z_x}\begin{bmatrix} \dot{u}_r \\ \dot{u}_e \end{bmatrix} = \begin{bmatrix} Z_{x11} & Z_{x12} \\ Z_{x21} & Z_{x22} \end{bmatrix}\begin{bmatrix} \dot{u}_r \\ \dot{u}_e \end{bmatrix} \\
&Q_{x1} = -Q_{y2} \\
&\begin{bmatrix} Q_{y1} \\ Q_{y2} \end{bmatrix} = \mathbf{Z_y}\begin{bmatrix} \dot{u}_b \\ \dot{u}_r \end{bmatrix} = \begin{bmatrix} Z_{y11} & Z_{y12} \\ Z_{y21} & Z_{y22} \end{bmatrix}\begin{bmatrix} \dot{u}_b \\ \dot{u}_r \end{bmatrix} \\
&Z_b\dot{u}_b = f_b + Q_b = f_b - Q_{y1}
\end{aligned}
\qquad \text{(C.6a,b,c,d,e)}
$$

where Q_e, Q_{x1}, Q_{x2}, Q_{y1}, Q_{y2} and Q_b are internal forces. From equations (C.6a-e), the velocities of the equipment, the base and the point along the isolator are given by

$$
\begin{bmatrix} \dot{u}_e \\ \dot{u}_r \\ \dot{u}_b \end{bmatrix} = \begin{bmatrix} Y_{ee} & Y_{er} & Y_{eb} \\ Y_{re} & Y_{rr} & Y_{rb} \\ Y_{be} & Y_{br} & Y_{bb} \end{bmatrix}\begin{bmatrix} f_e \\ f_r \\ f_b \end{bmatrix} \qquad \text{(C.7)}
$$

where Y_{ee}, Y_{eb}, Y_{be} and Y_{bb} are the same as those given in equations (C.3a-c), and

$$
\begin{aligned}
Y_{er} = Y_{re} &= \frac{-Z_{x21}\left(Z_b + Z_{y11}\right)\left(Z_{x11} + Z_{y22}\right)}{Z_eZ_bZ_{te}Z_{tb} - Z_{x12}Z_{x21}Z_{y12}Z_{y21}} \\
Y_{rb} = Y_{br} &= \frac{-Z_{y12}\left(Z_e + Z_{x22}\right)\left(Z_{x11} + Z_{y22}\right)}{Z_eZ_bZ_{te}Z_{tb} - Z_{x12}Z_{x21}Z_{y12}Z_{y21}} \\
Y_{rr} &= \frac{1 - Z_{x12}Y_{er} - Z_{y21}Y_{rb}}{Z_{x11} + Z_{y22}}
\end{aligned}
\qquad \text{(C.8a,b,c)}
$$

in which

$$Z_{te} = \frac{\left(Z_e + Z_{x22}\right)\left(Z_{x11} + Z_{y22}\right) - Z_{x12}Z_{y21}}{Z_e}$$
$$Z_{tb} = \frac{\left(Z_b + Z_{y11}\right)\left(Z_{x11} + Z_{y22}\right) - Z_{y12}Z_{y21}}{Z_b} \qquad \text{(C.9a,b)}$$

For the system shown in Figure 6.16 in Chapter 6, there is no external force applied to the equipment, i.e. $f_e = 0$. The external force applied to the point along the isolator is the active control force f_a, i.e. $f_r = f_a$, and the external force applied to the base is the primary force f and the active control force $-f_a$, i.e. $f_b = f - f_a$. Based on the above discussion, the velocities of the equipment and the point along the isolator are thus given by

$$\dot{u}_e = Y_{er} f_a + Y_{eb}\left(f - f_a\right) = \left(Y_{er} - Y_{eb}\right) f_a + Y_{eb} f$$
$$\dot{u}_r = Y_{rr} f_a + Y_{rb}\left(f - f_a\right) = \left(Y_{rr} - Y_{rb}\right) f_a + Y_{rb} f \qquad \text{(C.10a,b)}$$